"To strive, to seek, to find, and not to yield"

Alfred, Lord Tennyson

TABLE OF CONTENTS

Chapter 3: Modifiable Poly(*p*-Phenylene Vinylene) Copolymers Towards Functional Conjugated Materials

Chapter 4: Non-crosslinked Profluorescent PPV-based Micellar System as a Versatile Theranostics Probe

Chapter 5: Continuous Synthesis and Thermal Elimination of Sulfinyl-route Poly(*p*-Phenylene Vinylene) in Consecutive Flow Reactions

Chapter 6: Improved Mechanistic Insights into Radical Sulfinyl Precursor (MDMO)-PPV Synthesis by Combining Microflow Reactor Technology and Computer Simulations

Chapter 7: A Mild and Efficient Approach Towards Functional Macromolecules via Continuous Flow Photo-induced Diels-Alder reactions

Chapter 8: Summary and Outlook

CHAPTER 1

Introduction

1.1. HISTORY OF POLYMERS

Polymers are defined by IUPAC as 'a molecule of high relative molar mass, the structure of which essentially comprises the multiple repetition of units derived, actually or conceptually, from molecules of low relative molecular mass'.[1] The materials as we know them nowadays, entered our lives around a century ago with the discovery of the first synthetic polymer by Bakelite (poly(oxybenzylmethylenglycolanhydride)) in 1909. This formaldehyde resin was used worldwide in telephones, electronic devices (sockets, radio covers etc.) and even in aeronautics due to its good heat insulation, easy processing as well as its resistance to electricity and low conductivity. In the 1920's, Herman Staudinger was the first to develop the concept of a macromolecule: a very large molecule commonly created by some form of polymerization.[2] A turning point in the use of polymers came in the 1950's by K. Ziegler and G. Natta who discovered the use of catalysts during polymerization reactions, leading to the so called 'plastic' generation.[3;4] A variety of applications ranging from automotive, healthcare, constructions and household products soon benefited from the modern plastic industry. From that moment on polymers were integrated in our daily life and refinement towards more complex structures or specialized products with defined product properties is an ongoing process.

1.2. CLASSIFICATION OF POLYMERIZATIONS

With the integration of polymers in our daily life, a variety of polymerization mechanisms became available, with the step-growth and chain-growth polymerization mechanism as most prominent ones, Figure 1-2.[5;6] Step-growth polymerizations (e.g. polycondensation reactions) are (usually) triggered by a

catalyst, after which the monomer will grow stepwise in time. As a result, the formation of high molecular weight products is only observed at large conversions (thus at the end of the polymerization reaction). In contrast, chain-growth polymerizations (e.g. free radical polymerizations) are reactions which are triggered by the use of an initiator. Once the reaction starts, high molecular weight materials are easily reached and reactions only take place at the active site at the end of the growing chain. Under normal reaction conditions, the reaction consists of 4 stages (i) initiation, (ii) propagation (iii) chain transfer and (iv) termination. If it is possible to minimize the contribution of chain transfer as well as termination during the polymerization, a living polymerization is reached, Figure 1-1.[7]

Decomposition	I_2	$\xrightarrow{k_d}$	$2\,I^{\cdot}$
Initiation	$I^{\cdot}\ +\ M$	$\xrightarrow{k_i}$	$R_1^{\cdot}$
Propagation	$R_i^{\cdot}\ +\ M$	$\xrightarrow{k_p}$	$R_{i+1}^{\cdot}$
Chain Transfer	$R_i^{\cdot}\ +\ S$	$\xrightarrow{k_{tr}}$	$R_1^{\cdot}\ +\ P_i$
Termination	$R_i^{\cdot}\ +\ R_j^{\cdot}$	$\xrightarrow{k_t}$	$P_{i+j}\ \ or\ \ P_i + P_j$
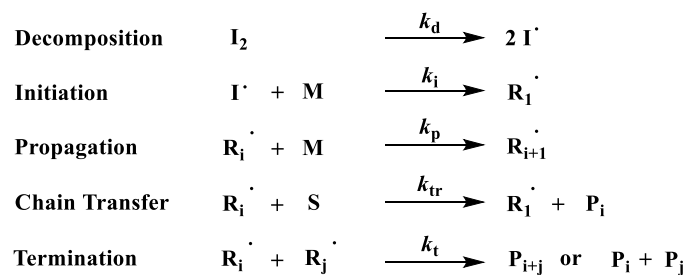
Figure 1-1: General mechanism of free radical polymerization

In living polymerizations, the number of polymer chains that are produced is equal to the number of initiator groups and the polymerization will continue until all monomer is consumed as the polymer chain end will stay active during the polymerization. This type of polymerization was labeled as 'living´ polymerization by Szwarc[8] and investigated in more detail by Flory[6] later on, leading to the following criteria for a reaction to be classified as 'living': (i) the rate of initiation must exceed the rate of propagation, (ii) no termination reactions are allowed and

(iii) a very narrow polydispersity ($Đ$ < 1.5) has to be obtained. When all criteria have been satisfied, a linear relationship between the number average molecular weight (M_n) and conversion is obtained. As a result of this development, precise design of complex polymer architectures is now possible, which was previously inaccessible.
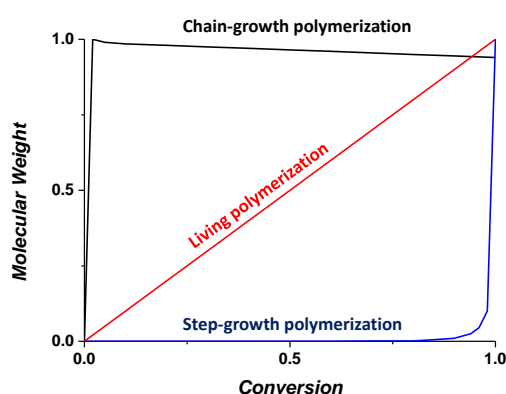
Figure 1-2: Molecular weight vs. conversion for step-growth, chain-growth and living polymerization mechanisms

1.3. DESIGN OF POLYMER ARCHITECTURES

The use of controlled / living polymerization techniques are among the most rapidly growing areas in chemistry and polymer science, with nitroxide mediated polymerization (NMP),[9-12] atom transfer radical polymerization (ATRP)[13-16] or reversible addition-fragmentation chain transfer polymerization (RAFT)[17-20] as the most prominent synthesis methods to synthesize polymers in a controllable manner. Precision design of tailor-made polymers with well-defined molecular weight and architecture can be realized. Polymers can be classified by their

composition and topology (Figure 1-3) of which only the most important ones for this work will be described in here.

Composition   **Topology**   **Self-assembly**
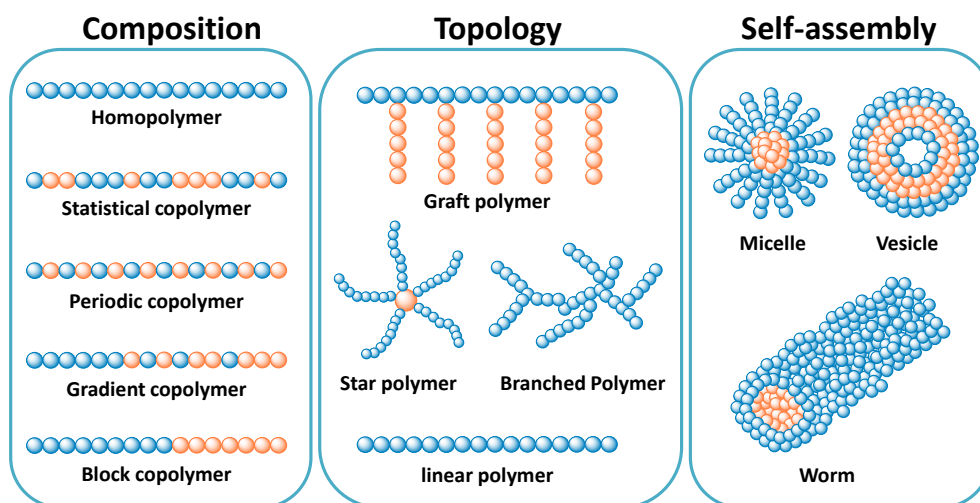
Figure 1-3: Overview of different (complex) polymer architectures

Composition means in this respect the order of the repeating units including homopolymers and statistical, -periodic, -gradient and block copolymers. In contrast to homopolymers, copolymers consist at least out of two different monomers which leads to the advantage of combining different properties in one polymer chain (viscosity, solubility and glass transition temperature). Within the range of copolymers a distinction can be made between the buildup of two separate block segments (block copolymer) or the mixture of two monomers mixed either randomly (statistical copolymer), alternating (periodic copolymer) or with a gradient (gradient copolymer). Topology on the other hand is related to the shape the various polymer structures have. A distinction can be drawn between linear, graft (comb and brushed), star or branched polymers. Graft polymers are

polymers consisting of at least two block segments that were grafted through the backbone, a technique commonly used when performing reactions on surfaces. Star-shaped polymers are formed by attaching several linear arms to a central core, which can be synthesized by using a multi-functional core leading to special properties (e.g. stimuli responsive materials). The last shape, branched polymers, is a very broad class of polymer chains consisting of at least 2 branching points, mostly seen in dendrimer synthesis. With the development of living polymerization methods, and the use of specially tailored monomers or initiators, polymers with specific architectures become readily available.

Self-assembly is the spontaneous arrangement of polymer chains into highly ordered structures by non-covalent interactions. These structures are often held together using secondary interactions that are very specific and directional (hydrogen bonding, van der Waals interactions, π-π interactions, hydrophobic and hydrophilic interactions). By using this self-assembly approach for conjugated polymers, stable and well-defined aggregates can be obtained which exhibit structural and morphological organization across multiple length scales. In this respect control could be gained over the aggregation and optoelectronic properties of the materials, leading to new applications for the use of conjugated polymers. Block copolymers are a special type of material as they can self-assemble into different structures in solution. Especially block copolymers comprising a hydrophobic and hydrophilic part can undergo self-assembly, due to their amphiphilic nature. Depending on the type of blocks, the length as well as the solvent used, formation of worms, micelles or vesicles can take place, Figure 1-3.[21]

1.4. CONJUGATED POLYMERS

Since the discovery of Heeger,[22] Mac Diarmid[23] and Shirakawa,[24] the way that conducting polymers were viewed changed and led to major advances in polymer electronics. They found that the conductivity of polyacetylene could be increased by doping the material with electron-withdrawing groups. Since then, a variety of conductive polymers have been developed of which the most prominent ones are shown in Figure 1-4.[25]

Poly(acetylene)   **Poly(fluorene)**   **Poly(thiophene)**

Poly(*p*-phenylene)   **Poly(*p*-phenylene vinylene)**   **Poly(pyrole)**
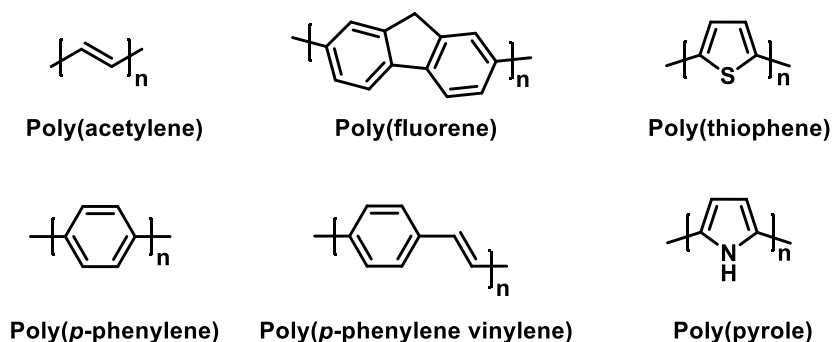
Figure 1-4: Chemical structures of some conjugated polymers

Conjugated polymers consist of alternating single (σ-bonds) and double bonds (σ-bonds and pi- bonds), with the partly delocalized and polarized pi-bonds being responsible for the transport of charges along the backbone. By injecting charge carriers (electrons and holes), conductivity in the conjugated polymer is induced, leading to multiple interesting optical as well as electronic properties, depending on the size of the band gap. Semiconducting polymers have band gaps between 0.5 eV and 4 eV depending on the molecular structure and the repeating unit of the polymer.[26]

1.4.1. Electronic properties

In order to induce conductivity, delocalized polarizable pi-electrons are needed, giving the polymer the possibility to transport charges along the backbone. In addition, injection of the charge carries (electrons and holes) by a stimuli – either externally via light / electrical or by doping the material – into to polymer should be possible, leading to transport of the charges along the conjugated backbone (interchain mobility) or between backbones of different polymer chains (intrachain hopping mechanism).[27]
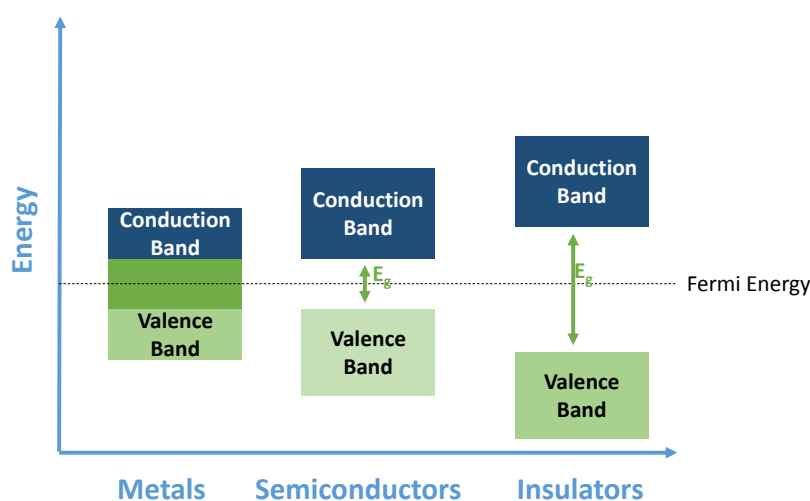
Figure 1-5: Band model for metals, semiconductors and insulators

The electrical properties of conjugated polymers are determined by the molecular orbital theory. Lower energy bonding (π) and higher energy antibonding (π^*) molecular orbitals are formed due to the overlap of adjacent atomic p_z-orbitals. Spacing many p-molecular orbitals together in a given range of energy yields more

and more bonding and anti-bonding molecular orbitals, until a virtually continuous occupied valance band and an unoccupied conducting band are generated. The energy spacing between the highest occupied molecular orbital (HOMO) and lowest unoccupied molecular orbital (LUMO) is called the band gap (E_g). A schematic representation can be seen in Figure 1-5. Depending on the type of material (metal, semiconductor, insulator) the bang gap has a different size. In addition, modification of the bandgap by side groups, steric hindrance or pi-conjugation length is possible.[28]

1.4.2. Optical properties

The energy bandgap for conjugated polymers ranges from 0.5 eV to 4.0 eV giving them both interesting electrical as well as optical properties, as this energy is directly related to the wavelength by the equation of Planck:

$$E = h\nu = \frac{hc}{\lambda}$$

In here, E is the energy, h is the Planck constant, c is the speed of light, ν is the frequency and λ is the wavelength. As a result, conjugated polymers can interact with visible light, leading to a variety of colors depending on the size of the band gap.[29] When a photon exhibits enough energy, it can be absorbed by the polymer, causing an electron to be excited from the HOMO level into the LUMO level, creating an exciton. The exciton can decay back to the ground state via a number of routes, which are depicted in Figure 1-6. If the photon emission occurs between states of the same spin (S_1 to S_0 via internal conversion (IC) in Figure 1-6), the emission of light is called fluorescence. If the spin state of the initial and

final spin state are different (T_1 to S_0 via intersystem crossing (ICS)) this process is called phosphorescence.
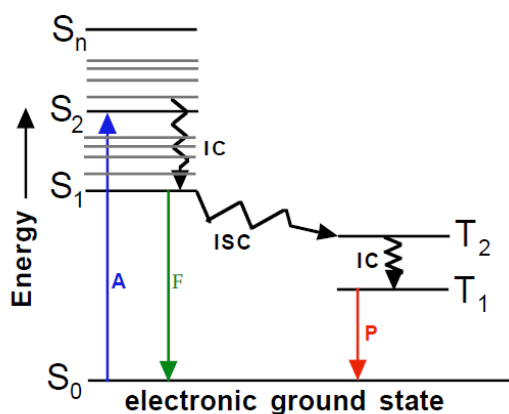
Figure 1-6: Typical Jablonksi diagram for the decay of photons in which the following abbreviations are used: absorbance (A), fluorescence (F), phosphorescence (P),

Excitation of photons from the ground state (S_0) to the excited state (S_1) is either triggered by light (photoluminescence) or by applying electrical charges (electroluminescence). Depending on the application of the materials – electronics (e.g. solar cells), biology (e.g. labeling, detectors) or optics (e.g. lamps) – the excitation of photons is triggered in a different way.[30;31] In both cases, a photon can decay back to the ground state via the processes described above.

1.4.3. Applications

Studies towards electric conductivity in conjugated polymers as we know today, began in the 70's with the discovery of poly(acetylene) by Shirakawa,[24] which was soon followed by poly(aniline) by MacDiarmid and many other conductive

polymers.[23] Throughout the 80's electric conductivity was the main research focus, which shifted towards optical properties in the early 90's. Nowadays, as more materials of higher purities have become available, conjugated polymers are applied in various semi-conductor devices like organic light emitting diodes (OLEDs),[32-35] field effect transistors (FETs)[36-39] and organic photovoltaic devices (OPVs).[40-43] More recent developments opened a variety of additional application pathways for conjugated polymers in the area of biosensors and biomedical research. The excellent fluorescent properties make them ideal candidates to replace existing bioimaging agents such as organic fluorescent markers.

1.5. POLY(*P*-PHENYLENES VINYLENES) (PPVS)

Poly(arylene-vinylene)s (PARs) were the first class of conjugated polymers where electroluminescence was observed, resulting in today's most widely studied conjugated polymer.[22-24] Within the broad range of conjugated materials, this thesis will focus on the use of poly(*p*-phenylene vinylene) (PPV) and its derivatives. PPVs are an important class of semiconducting polymer materials that display excellent optical and electrical properties and are one of the most studied conjugated polymers to date.[44;45] Throughout their history, PPVs have been used in a large variety of advanced applications, ranging from organic photovoltaic cells (OPVs),[46] organic light emitting diodes (OLEDs),[47-49] field effect transistors (FET)s[50] and biosensors.[35] Synthesis towards PARs can be divided into two different classes. The first one is the so called direct routes, in which the conjugated polymer is obtained in a single reaction step, whereas the second class refers to the 'indirect' routes. In here, a precursor method using a *p*-quinodimethane species leads to a precursor polymer, which can be thermally

converted in the conjugated polymer in a second step. In addition, ring opening metathesis polymerization (ROMP) using specialized non-precursor monomers can lead to the synthesis of PPVs as well.

1.5.1. Synthesis of PPVs via direct routes

As already mentioned above, PPV materials are accessible via step-growth (direct routes) or chain-growth (indirect or precursor route) mechanisms. Extensive work on the so called 'direct' routes – all step-growth and hence inherently non-living – has been performed over the last decades, employing Wittig,[51-53] Horner,[53;54] McMurry,[55;56] Knoevenagel,[52;57;58] and Siegrist[52;59] polycondensation reactions or the palladium catalyzed Heck,[60;61] Stille[62] and Suzuki[63] coupling reactions. The major disadvantages of these routes are the significantly lower obtained molecular weight, the low solubility of the polymers in common organic solvents, as well as their sensitivity towards reaction conditions making it very difficult to control these reactions. As a result, synthesis of complex architectures with polymers obtained from the direct routes are synthetically challenging.

1.5.2. Synthesis of PPVs via ROMP

Ring opening metathesis polymerization (ROMP) is a chain-growth polymerization process where unsaturated cyclic olefins are converted into polymeric materials. The reaction is based on olefin metathesis, a process which found its origin in the 1950s.[64-69] In here, a metal-carbene (alkylidene) complex undergoes reversible [2+2] cycloadditions with olefins, thereby completing metathesis via metallacyclobutane intermediates, Scheme 1-1.[70;71] When employing ring-strained cyclic alkenes, the olefin metathesis leads to a polymerization in which

the cyclic monomers are converted into linear polymers with unsaturated $C=C$ bonds being built into the main chain. ROMP is a widely used polymerization technique for the controlled synthesis of (complex) polymer architectures, giving access to a broad variety of interesting materials. A variety of catalysts as well as monomers is employed with the Grubbs and Schrock catalyst as well as norbornene monomers (NBE) and its derivatives being the most prominent ones.[72;73]
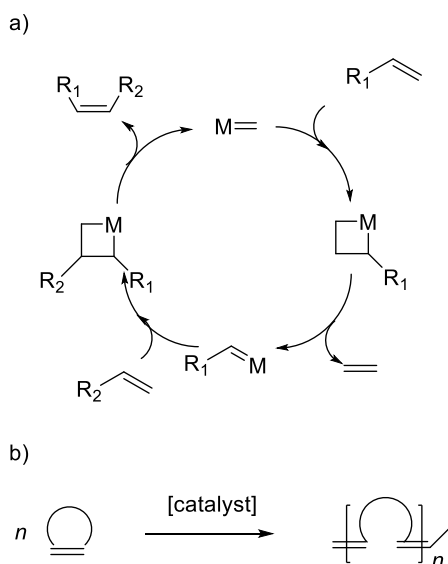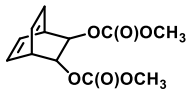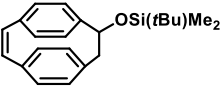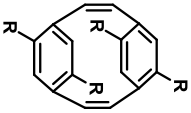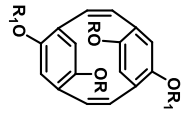
Scheme 1-1: (a) Simplified olefin metathesis mechanism and (b) conversion of cyclic alkenes to polymers in ROMP

With respect to conjugated polymers, ROMP features a significant advantage: via the olefin metathesis reaction, a vinylic bond is directly obtained in the main chain of the polymer. Hence, the pi-conjugated main-chain structure of PPV can in principle be directly made available via ROMP. However, a relatively high synthetic

effort is required to reach this goal as monomer synthesis is tedious. Yet, ROMP is inherently a living polymerization process (if transfer reactions are absent) and not only is the conjugated polymer system directly accessed by ROMP, also block copolymers and high end group functional fidelities can be directly achieved, Scheme 1-1. Research in the field led to the use of a variety of monomers either using a Schrock or Ruthenium catalyst, Table 1-1. As most of the resulting polymers were insoluble in common organic solvents, diene like monomers were used. In this way PPVs via an indirect precursor approach yielding high molecular weights (M_n) and a low dispersity ($Đ$) were synthesized.

Table 1-1: Overview of monomers used for PPV synthesis via ROMP[a]

Monomer Structure	Catalyst	M_n^{app} / g·mol^{-1}	$Đ$	Isomerism	Ref.
OC(O)OCH₃ / OC(O)OCH₃	2nd generation Schrock catalyst	46 000 / 63 000	1.23 / 1.34	Alternating *cis* and *trans*	[74]
OSi(*t*Bu)Me₂	2nd generation Schrock catalyst	n.a.	n.a	*cis*	[75]
	2nd generation rhutenium catalyst	5 000 / 25 000	1.22 / 1.21	Alternating *cis* and *trans*	[76]
	3rd generation rhutenium catalyst	10 550 / 26 210	1.30 / 1.32	Alternating *cis* and *trans*	[77]

[a] All data given in here is associated with a certain error with respect to M_n, M_w and $Đ$ values, as no precise Mark Houwink Sakurada (MKHS) parameters are available.

1.5.3. Synthesis of PPVs via indirect routes

To overcome the inherent drawbacks of step-growth polymerization the so called 'indirect' or 'precursor' quinodimethane routes were introduced, resulting in high molecular weight polymers which were relatively easy and cost effective to synthesize.[5] Precursor routes follow a chain-growth mechanism, which in principle could be employed to ultimately achieve living polymerization reaction conditions. The formation of the *p*-quinodimethane (*p*-QM) system from a sulfinyl premonomer starts with the proton abstraction by a base, which in a second step is followed by the 1,6-elimination reaction of the leaving group (L), yielding the *p*-QM.[78] Once the active monomer is formed, self-initiation of monomer dimers occurs and chain growth via propagation is observed leading to the precursor polymer when following a radical pathway. A more in-depth study into the radical mechanism is performed in chapter 6, in which experimental results are used as input for a theoretical model. The anionic pathway on the other hand is accompanied with the use of an initiator which is deprotonated by the base as well, resulting via stable anion formation in the precursor polymer. In a second step, typically at elevated temperature, elimination of the sulfinyl side groups takes place resulting in the desired conjugated polymer, (Scheme 1-2).[79;80]

This possibility for separation of the polymerization reaction from elimination is what distinguishes the sulfinyl route from most other precursor polymerization routes in which both steps occur simultaneously. The inherent division between both steps helps to increase the polymerization control (in terms the molecular weight distribution and it's accompanying molecular weight) and moreover, largely simplifies the kinetic investigation. Nowadays, research towards the mechanism behind the sulfinyl route leads to the discovery of a purely radical or

anionic route, depending on the type of base (lithium bis(trimethylsilyl)amide (LHMDS) anionic; sodium *tert*-butoxide (Na*t*BuO) radical) and solvent (THF anionic; *sec*-BuOH radical) used during the polymerization.[81]

Gilch route L = P = Cl or Br
Wessling route L = P = R$_2$S-
Xanthate route L = P = RO-C(S)-S-
Sulfinyl route L = Cl or Br; P = RS(O)-
Dithiocarbamate route L = P = R$_2$N-C(S)-S-
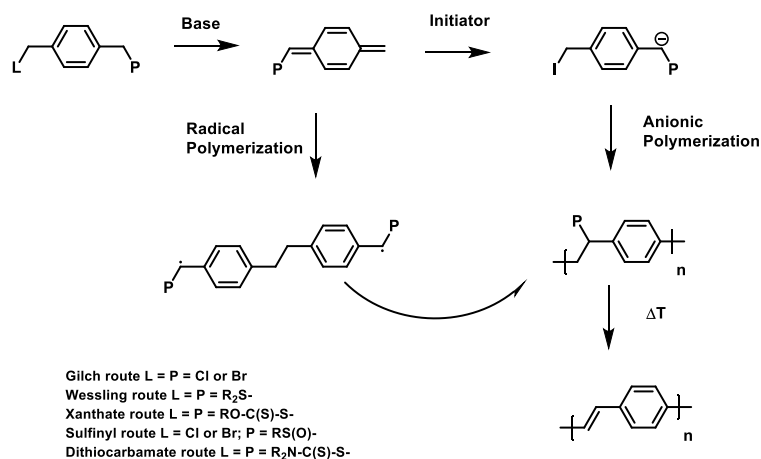
Scheme 1-2: General polymerization mechanism for the two-step synthesis of PPVs via the sulfinyl precursor route using either an anionic or radical pathway

Various 'precursor' routes were established depending on the choice of leaving group (L) and polarizer (P) attached to the premonomer. The L group is eliminated from the premonomer, the P group from the prepolymer. Symmetric monomers were employed in the Gilch,[82] Wessling,[83-85] xanthate[86;87] and dithiocarbamate (DTC)[88] route, whereas the sulfinyl[89-91] route starts from an asymmetric premonomer. In that way the polymerization and elimination process are completely decoupled, allowing full analysis and improved control over the reaction. However, care has to be taken, as complete decoupling of these processes does require carefully selected reaction conditions. In addition, low defect levels as a result of good microstructural control – mainly head to tail

attachment during the polymerization – was obtained when employing the sulfinyl route, leading to polymers with superior performance with regard to optoelectronic properties.[92;93]

The synthesis of both soluble precursor polymers as well as conjugated polymers requires the introduction of long and flexible side chains on the aromatic core.[94] The most studied p-type PPV derivatives (Figure 1-7) are poly[2-methoxy-5-(3,7-dimethyloctyloxy)-*p*-phenylene vinylene] ((MDMO)-PPV), poly[2-methoxy-5-(2-ethylhexyloxy)-*p*-phenylene vinylene] ((MEH)-PPV), poly[2,5-bis(2-ethylhexyloxy)-*p*-phenylene vinylene] ((BEH)-PPV) and poly[2-methoxy-5-(carboxypentyloxy)-*p*-phenylene vinylene] ((CPM)-PPV) of which (MDMO) -and (CPM)-PPV are the most studied ones in this thesis.

Next to the use of p-type PPV derivatives, also developments towards n-type PPV polymers developed over the last years, with poly[(2,5-dicyano)-*p*-phenylene vinylene] ((CN)-PPV) as the most studied one in our group due to its interesting optical properties.[81;95]
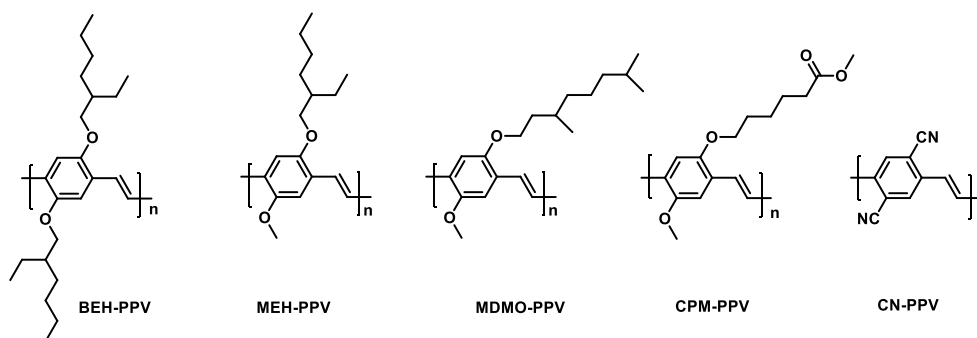
Figure 1-7: Chemical structures of most commonly used PPV structures upon the development of living / controlled polymerizations

1.5.4. Synthesis of complex PPV structures

In general, conjugated polymers are stiff materials due to their delocalized electronic structure which has limited solubility in common organic solvents. To overcome this issue, a second flexible block can be introduced leading to a variety of new morphologies and nanostructured materials (see Figure 1-3). Research towards PPV block copolymers so far was mainly focused on PPV materials synthesized via the Siegrist polycondensation method[96-100] or ROMP metathesis. Especially the latter polymerization reactions lead to the synthesis of soluble PPV materials, as most PPVs synthesized via ROMP are insoluble in common organic solvents. Block copolymers synthesized *via* this method are for instance: PPV-*b*-PNBE (poly(norbornadienes))[101-104] or PPV-*b*-PMMA (poly(methylmetacrylate)).[105] As shown, ROMP can efficiently be used to access PPVs with all features of a living polymerization. Block copolymerizations are, at least to date, limited to block extensions via ROMP – hence limiting the choice of available materials. At the same time, the accessibility of the cyclic monomers is relatively low, which probably explains why the ROMP route has – compared to other synthesis pathways – not been studied in high detail. Despite these disadvantages, the technique has high potential.
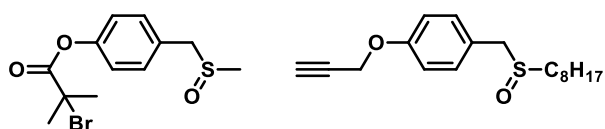
Figure 1-8: Chemical structures of functional initiators used to date in anionic sulfinyl route polymerizations

Most recent work on successful PPV block copolymers was obtained by using the anionic sulfinyl precursor route, in which a dedicated anionic initiator is used during the polymerization of the PPV. The main advantage of the anionic polymerization approach is the ability to introduce specific functionalities into the polymer alpha chain end. By doing so, a bromine group can be introduced – which is suitable for single electron transfer living radical polymerization (SET-LRP)[106-109] re-initiation – or even an alkyne suitable for direct copper-catalyzed alkyne-azide cycloaddition (CuAAC) (Figure 1-8). In this way self-assembled PPV structures e.g. PPV-*b*-P*t*BuA (poly(*tert*-butyl acrylate),[110;111] PPV-*b*-PMMA (poly(methyl methacrylate)) or PPV-*b*-PEG (poly(ethylene glycol))[112] could be obtained in an easy manner. With the successful formation of both PPV block copolymers from materials stemming from the anionic precursor route – new application domains towards PPV materials with complex architectures were opened. Thus, first the acrylate block copolymers were converted to amphiphilic structures in order to test for self-assembly behavior. Consequently, PPV-*b*-P*t*BuA was treated with trifluoroacetic acid, to yield PPV-*b*-PAA (poly(acrylic acid)) blocks. Both PPV-*b*-P*t*BuA and PPV-*b*-PEG blocks showed amphiphilic behavior and ability to self-assemble in water. Preliminary dynamic light scattering (DLS) results indicated particle formation, and provided hence a proof-of-concept for further studies into this domain, reported in this thesis.

First, advances towards controlled polymerization for the radical pathway were reported earlier as well. Generally, radical polymerizations are extremely fast reactions in which high molecular weights are easily reached with little control over the reaction. Furthermore, the biradical character of the initiating species complicates any control scheme. Since self-initiation is incompatible with a

reversible termination mechanism, transfer agents needed to be employed to reach any control over molecular weight. Only chain transfer agents (CTA) with a similarly high reactivity compared to propagation can be employed, which severely limits the choice of available agents. RAFT and macromolecular design via the interchange of xanthates (MADIX) agents were tested without any success.[113] From the list of conventional CTAs, carbon tetrabromide (CBr_4) was the most promising as it typically shows extremely high transfer rates in classical free radical polymerization (FRP). First trials towards the synthesis of PPV-*b*-PS (poly(styrene)) block copolymers showed the possibilities of the radical route, which is further exploited in this thesis.

1.6. (CLASSICAL) APPLICATIONS
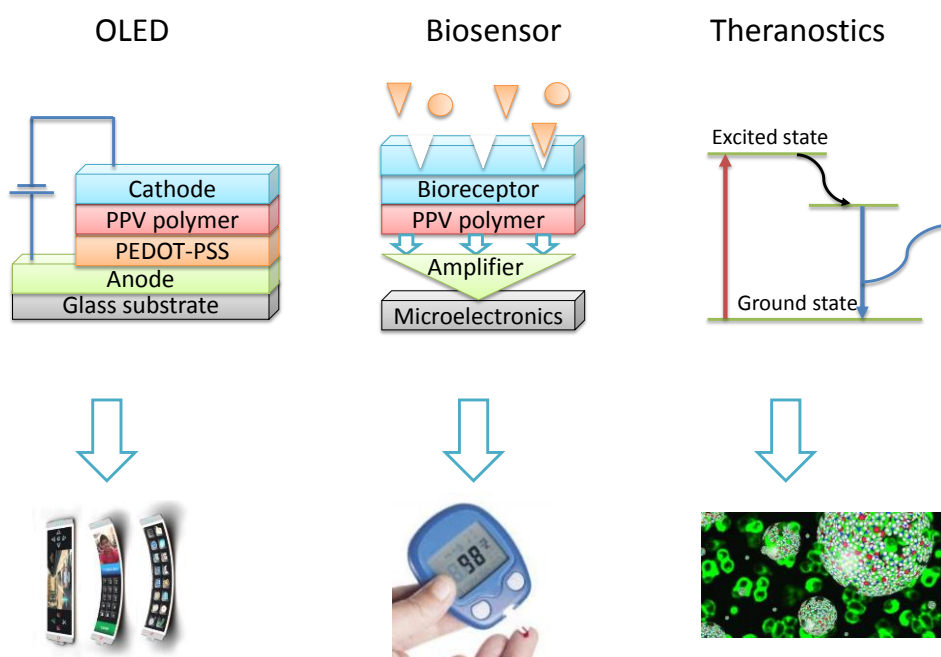
Figure 1-9: General overview of different applications of PPV polymers

Conjugated polymers nicely combine the properties of plastics (light weight, flexible and low costs) with easy processing (spin-coating, spray coating and inkjet printing for large area thin films in roll-to-roll processing) and with the electrical and optical properties of metals or semiconductors. In this way they can easily be incorporated in all kinds of devices/applications such as organic light emitting diodes (OLEDs), organic photovoltaics (OPV), field effect transistors (FETs) and in the field of theranostics (e.g. bioimaging or drug delivery) for which the main challenges are long-term stability of the materials.[114;115]

1.6.1. Organic light emitting diodes

Since the discovery of their excellent luminescence (good charge tansport and high quantum efficiency) by Burroughes and coworkers,[116] PPVs and their derivatives are one of the most studied conjugated polymers. Although high reproducibility with respect to synthesis and optical properties is displayed, PPVs have been successively replaced by other polymers in photovoltaic applications, due to their comparatively low power conversion efficiencies.[117-119] Still, PPVs are one of the most commonly used materials in OLEDs nowadays due to its low amount of defect levels. OLEDs are electrical devices where the emissive electroluminescent layer is a film of an organic compound which emits light in response to an electrical current. Under the influence of an applied electric field, the injected holes and electrons migrate to the cathode and anode respectively via a 'hopping' mechanism from one (part of the) molecule to the other. When an electron and hole are localized in the organic emissive layer (EML) on the same molecule and are spatially close, an exciton is formed (localized electron-hole pair in the excited energy state). Due to relaxation via a photo emissive mechanism, the excitons radiatively decay to the ground state by spontaneous emission

(Figure 1-9).[120] Plain-PPV has a bandgap of 2.2 eV, leading to a green-yellow emission in the spectrum. The bandgap can be tuned by introducing substituents on the aromatic core or by tuning the conjugation length of the polymers, leading to polymers with different emission colors.[121]

1.6.2. Biosensors

Biosensors are small devices specifically designed for the detection of an analyte, thereby combining biological components with a physiochemical detector of which a blood glucose device is a common practical example. Conjugated polymers have seen a tremendous increase in the use in biosensors due to their excellent optical as well as electrical properties (Figure 1-9) and were being used mostly as transducer layer in these devices. Successful tests using (MDMO)-PPV as a transducer and immobilization layer for monoclonal mouse antibodies for binding of its specific antigens[122] and non-conducting molecular imprinted polymers (MIPs) for nicotine sensing or the use of (MEH)-PPV for cholesterol sensing showed the versatility of this material.[123;124] Lately a shift towards the use of PPVs as fluorescent sensing materials is seen for e.g. measuring metal ions in living systems.[125]

1.6.3. Theranostics

Great advancements in the development of imaging tools were seen over the last decades thanks to the remarkable effort taken in understanding biological processes.[126] Extensive research towards the use of organic fluorophores are somewhat hindered due to their tendency to photo bleach. Partly solved by encapsulation, the use of these materials still leads to erroneous interpretations as well as self-quenching issues.[127;128] Hence, a shift was seen towards the use

of quantum-dots as these devices have the big advantage of showing no bleaching or leaching effect. However, the use of these materials is still under debate, as quantum dots are highly toxic materials.[129-133] The use of conjugated polymers in the bioimaging field have attracted significant interest over the last years due to their excellent optical properties and biocompatibility. Fluorescent nanoparticles synthesized from conjugated materials show excellent optical properties and no signs of cytotoxicity or photo bleaching.[134] The use of PPV materials in the field of theranostics is further explored in this thesis.

1.7. OUTLINE OF THE THESIS

The aim of the research presented in this thesis is the in-depth study towards controlled synthesis pathways of tailor-made PPVs. This thesis focusses on two components, i.e. kinetics and design. In the first part, the focus will be on the controlled synthesis of complex PPV structures in batch via the radical and anionic sulfinyl precursor route respectively, after which the use of PPVs in the field of theranostics is described. In the second part, continuous flow reactors are used as a tool to kinetically screen the polymer formation, as well as the use of this data to completely map the PPV polymerization mechanism.

In **Chapter 2**, the controlled synthesis of PPV (tri)block copolymers using atom transfer radical polymerization (ATRP) or copper-catalyzed alkyne-azide cycloaddition (CuAAC) is described. This goal was reached by using carbon tetra bromide (CBr_4) as a chain transfer agent (CTA), leading to the synthesis of PPV-*b*-P*t*BuA, PPV-*b*-PS and PPV-*b*-PEG block copolymers and PPV-*b*-P*t*BuA-*b*-PEG tri block copolymers.

Chapter 3 describes the use of the anionic sulfinyl route to synthesize random PPV copolymers. The use of different PPV monomers (MDMO, CPM and CN) allows the synthesis of water soluble materials. In addition, copolymerization parameters are determined for all investigated copolymers leading to a wide spectrum of PPV materials with varying optical properties.

Chapter 4 continues with the use of PPV block copolymers via the anionic route, however in here amphiphilic block copolymers are targeted. These materials are self-assembled and their use as bioimaging probe as well as drug carrier was

investigated. In addition, full screening of the materials with regard to cytotoxicity and cell uptake in cells was reported.

In **Chapter 5** a shift is seen towards the use of continuous flow reactors for the synthesis of PPVs via the radical sulfinyl precursor route. A full kinetic screening of the two separate steps was executed, after which the complete two-step synthesis was performed in a continuous way in the micro flow reactor, yielding high purity conjugated materials.

Chapter 6 continues with the use of flow reactors for the synthesis of the PPV precursor polymer. In here, the experimentally obtained data are used as input for a theoretical model (Predici®) to get more insight into the radical polymerization of PPVs via the sulfinyl precursor route. Investigation of different models implies that PPV synthesis follows mostly a conventional free radical polymerization mechanism that only differs with respect to its initiation mode and the biradical nature of the propagation step.

In line with previous thermal flow reactor experiments, is the thermal deprotection of maleimides in **Chapter 7**. An ESI-MS/Microreactor setup was used to screen and fully optimize the complete reaction on-line. In a next step, deprotected functional maleimides can be coupled with a functional photoenol compound, leading to the first steps of dendrimer synthesis.

In **Chapter 8**, a general summary is given (in English and Dutch) and an outlook is postulated after which in **Chapter 9**, the used materials and all characterization methods that were employed for this thesis are described.

To finalize, a **list of abbreviations** and an overview of **publications, posters** and **conference contributions** is given. Last but not least, the '**dankwoord**' is addressed to all the people that helped me, both in a scientific way as well as personal way throughout my PhD.

1.8. REFERENCES

[1] http://goldbook.iupac.org/M03667.html (April 2016)

[2] H. Staudinger, *Chem. Ber.* **1924**, *57*, 1203-1208.

[3] K. Ziegler, E. Holzkamp, H. Breil, H. Martin, *Angew. Chem. Int. Ed.* **1955**, *67*, 541−547.

[4] G. Natta, P. Pino, P. Corradini, F. Danusso, E. Mantica, G. Mazzanti, G. Moraglio, *J. Am. Chem. Soc.* **1955**, *77*, 1708−1710.

[5] G. Odian, *Principles of Polymerization,* 4th edition, Wiley International, USA, **2001**.

[6] P. J. Flory, Principles of Polymer Chemistry, 16th printing, Cornell University Press, New York, USA, **1995**.

[7] K. Matyjaszewski, T. P. Davis, *Handbook of Radical Polymerization*, John Wiley & Sons, USA, **2003**.

[8] B. J. Schwartz, *Ann. Rev. of Phys. Chem.* **2003**, *54*, 141-172.

[9] T. E. Enright, M. F. Cunningham, B. Keoshkerian, *Macromol. React. Eng*. **2010**, *4*, 186−196.

[10] K. Min, H. Gao, K. Matyjaszewski, *J. Am. Chem. Soc*. **2005**, *127*, 3825−3830.

[11] G. Delaittre, J. Nicolas, C. Lefay, M. Save, B. Charleux, *Chem. Commun*. **2005**, *5*, 614−616.

[12] C. J. Cheng, J. B. Shu, S. S. Gong, L. Shen, Y. L. Qiao, C. Q. Fu, *New J. Chem*. **2010**, *34*, 163−170.

[13] D. G. Ramirez-Wong, C. A. Posada-Velez, E. Saldivar-Guerra, J. G. Luna-Barcenas, C. Ott, U. S. Schubert, *Macromol. Symp.* **2009**, *283−284*, 120−129.

[14] J. Xia, T. Johnson, S. G. Gaynor, K. Matyjaszewski, J. M. DeSimone, *Macromolecules* **1999**, *32*, 4802−4805.

[15] L. I. Gabaston, R. A. Jackson, S. P. Armes, *Macromolecules* **1998**, *31*, 2883−2888.

[16] K. Min, K. Matyjaszewski, *Macromolecules* **2007**, *40*, 7217− 7222.

[17] G. Qi, C. W. Jones, F. J. Schork, *Macromol. Rapid Commun.* **2007**, *28*, 1010−1016.

[18] Y. W. Luo, X. G. Wang, B. G. Li, S. P. Zhu, *Macromolecules* **2011**, *44*, 221−229.

[19] M. Chenal, L. Bouteiller, J. Rieger, *J. Polym. Chem*. **2013**, *4*, 752−762.

[20] Z. Chen, X. Wang, J. Su, D. Zhuo, R. Ran, *Polym. Bull*. **2010**, *64*, 327−339.

[21] B. H. Kim, J. Y. Kim, S. O. Kim, *Soft Matter* **2013**, *9*, 2780–2786.

[22] A. Heeger, *Angew. Chem. Int. Ed.* **2001**, *40*, 2591–2611.

[23] A. MacDiarmid, *Angew. Chem. Int. Ed.* **2001**, *40*, 2581–2590.

[24] H. Shirakawa, *Angew. Chem. Int. Ed.* **2001**, *40*, 2574–2580.

[25] K. Okamoto, C. K. Luscombe, *Polym. Chem.* **2011**, *2*, 2424–2434.

[26] H. Becker, H. Speitzer, K. Ibrom, W. Kreuder, *Macromolecules* **1999**, *32*, 4925–4932.

[27] A. J. Heeger, *Synthetic Met.* **2001**, *125*, 23−42.

[28] D. F. Schriver, P. W. Atkins, C. H. Langford, *Inorganic Chemistry*, 2nd ed., Oxford University Press, Oxford, **1994**, 91.

[29] M. Rohatgi, *Fundamentals of Photochemistry*, Wiley Eastern Ltd., New Delhi, **1978**.

[30] C. S. Fischer, M. C. Baier, S. Mecking, *J. Am. Chem. Soc.* **2013**, *135*, 1148–1154.

[31] F. Schütze, B. Stempfle, C. Jüngst, D. Wöll, A. Zumbusch, S. Mecking, *Chem. Commun.* **2012**, *48*, 2104–2106.

[32] P. L. Burn, A. B. Holmes, A. Kraft, D. D. C. Bradley, A. R. Brown, R. H. Friend, R. W. Gymer, *Nature* **1992**, *356*, 47−49.

[33] J. Salbeck, *Phys. Chem.* **1996**, *100*, 1667−1677.

[34] P. May, *Phys. World* **1995**, *8*, 52−57.

[35] A. Kraft, A. C. Grimsdale, A. B. Holmes, *Angew. Chem. Int. Ed.* **1998**, *37*, 402−428.

[36] S. Roth, *One-dimensional metals*, Weinheim VCH, **1995**, 209−231.

[37] H. Sirringhaus, N. Tessler, R. H. Friend, *Science* **1998**, *280*, 1741−1744.

[38] C. D. Dimitrakopoulos, R. L. Malenfant, *Adv. Mater.* **2002**, *14*, 99−117.

[39] S. Scheinert, G. Paasch, *Phys. Status Solidi A* **2004**, *201*, 1263−1301.

[40] J. Rostalski, D. Meissner, *Sol. Energ. Mat. Sol. C.* **2000**, *61*, 87−95.

[41] J. C. Brabec, N. S. Sariciftci, J. C. Hummelen, *Adv. Funct. Mater.* **2001**, *11*, 15−26.

[42] H. Hoppe, N. S. Sariciftci, *J. Mater. Res.* **2004**, *19*, 1924−1945.

[43] H. Hoppe, M. Niggeman, C. Winder J. Kraut, R. Heisgen, A. Hinsch, D. Meissner, N. S. Sariciftci, *Adv. Funct. Mater.* **2004**, *14*, 1005−1011.

[44] A. P. Kulkarni, C. J. Tonzola, A. Babel, S. A. Jenekhe, *Chem. Mater.* **2004**, *16*, 4556−4573.

[45] D. E. Gomez, S. S. Lee, C. S. Kim Y.-L. Loo, *Mol. Org. Electron. Devices* Chapter 4, p109-152, Nova Publishers, **2010.**

[46] S. Günes, H. Neugebauer, N. S. Sariciftci, *Chem. Rev.* **2007**, *107*, 1324-1338.

[47] D. Braun, A. J. Heeger, *Appl. Phys. Lett.* **1991**, *58*, 1982-1984.

[48] A. C. Grimsdale, K. L. Chan, R. E. Martin, P. G. Jokisch, A. B. Holmes, *Chem. Rev.* **2009**, *109*, 897-1091.

[49] R. H. Friend, R. W. Gymer, A. B. Holmes, J. H. Burroughes, R. N. Marks, C. Taliani, D. D. C. Bradley, D. A. Dos Santos, J. L. Bredas, M. Lőgdlund, W. R. Salaneck, *Nature* **1999**, *397*, 121-128.

[50] G. Horrowitz, *Adv. Mater.* **1998**, *10*, 365-377.

[51] R. N. McDonald, T. W. Campbell, *J. Am. Chem. Soc.* **1960**, *82*, 4669–4671.

[52] G. Kossmehl, *J. Phys. Chem.* **1979**, *83*, 417–426.

[53] A. P. Davey, A. Drury, S. Maier, H. J. Byrne, W. J. Blau, *Synth. Met.* **1999**, *103*, 2478–2479.

[54] S. Pfeiffer, H.-H. Hörhold, *Macromol. Chem. Phys.* **1999**, *200*, 1870–1878.

[55] W. J. Feast, I. S. Millichamp, R. H. Friend, M. E. Horton, D. Phillips, S. D. D. V. Rughooputh, G. Rumbles, *Synth. Met.* **1985**, *10*, 181–191.

[56] M. Rehahn, A. D. Schlüter, *Makromol. Chem., Rapid Commun.* **1990**, *11*, 375–379.

[57] N. C. Greenham, S. C. Moratti, D. D. C. Bradley, R. H. Friend, A. B. Holmes, *Nature* **1993**, *365*, 628–630.

[58] S. C. Moratti, R. Cervini, A. B. Holmes, D. R. Baigent, R. H. Friend, N. C. Greenham, J. Grüner, P. J. Hamer, *Synth. Met.* **1995**, *71*, 2117–2120.

[59] H. Kretzschmann, H. Meier, *Tetrahedron Lett.* **1991**, *32*, 5059–5062.

[60] Z. Bao, Y. Chen, R. Cai, L. Yu, *Macromolecules* **1993**, *26*, 5281–8286.

[61] M. Pan, Z. Bao, L. Yu, *Macromolecules* **1995**, *28*, 5151–5153.

[62] F. Babudri, S. R. Cicco, G. M. Farinola, F. Naso, A. Bolognesi, W. Porzio, *Macromol. Rapid Commun.* **1996**, *17*, 905–911.

[63] F. Koch, W. Heitz, *Macromol. Chem. Phys.* **1997**, *198*, 1531–1544.

[64] H. S. Eleuterio, *J. Mol. Catal.* **1991**, *65*, 55-61.

[65] N. Calderon, *Acc. Chem. Res.* **1972**, *5*, 127-132.

[66] N. Calderon, H.-Y. Chen, K. W. Scott, *Tetrahedron letters*, **1967**, *34*, 3328-3348.

[67] J. L. Herisson, Y Chauvin, *Makromol. Chem.* **1971**, *141*, 161-176.

[68] C. P. Casey, *J. Chem. Educ.* **2006**, *83*, 192-195.

[69] M. Siaj, P. H. McBreen, *Science* **2005**, *309*, 588-590.

[70] M. B. Herbert, R. H. Grubbs, *Angew. Chem. Int. Ed.* **2015**, *54*, 5018-5024.

[71] T. M. Trnka, R. H. Grubbs, *Acc. Chem. Res.* **2001**, *34*, 18-29.

[72] R. M. Johnson, C. L. Fraser, *Macromolecules* **2004**, *37*, 2718-2727.

[73] O. Ikkala, G. ten Brinke, *Science* **2002**, *295*, 2407-2409.

[74] H. H. Fox, R. R. Schrock, R. O'Dell, *Organometallics* **1994**, *13,* 635-639*.

[75] V. P. Conticello, D. L. Gin, R. H. Grubbs, *J. Am. Chem. Soc.* **1992***, 114,* 9708-9710*.

[76] Y.-J. Miao, G. C. Bazan, *J. Am. Chem. Soc.* **1994**, *116*, 9379-9380.

[77] S. Son, A. Dodabalapur, A. J. Lovinger, M. E. Glavin*, Science* **1995***, 269,* 376-378*.

[78] L. Hermosilla, S. Catak, V. Van Speybroeck, M. Waroquier, J. Vandenbergh, F. Motmans, P. Adriaensens, L. Lutsen, T. Cleij, D. Vanderzande, *Macromolecules* **2010**, *43*, 7424–7433.

[79] E. Kesters, L. Lutsen, D. Vanderzande, J. Gelan, *Synth. Met.* **2001**, *119*, 311–312.

[80] A. J. J. M. van Breemen, A. D. J. Issaris, M. M. de Kok, M. J. A. N. Van Der Borght, P. J. Adriaensens, J. M. J. V. Gelan, D. J. M. Vanderzande, *Macromolecules* **1999**, *32*, 5728–5735.

[81] I. Cosemans, *PhD Thesis*, Universiteit Hasselt, **2013**.

[82] H. G. Gilch, W. L. Weelwright, *J. Polym. Sci. Polym. Chem. Ed.* **1966**, *4*, 1337-1349.

[83] R. A. Wessling, R. G. Zimmerman, *US Patent 3401152*, 1968.

[84] R. A. Wessling, R. G. Zimmerman, *US Patent 3401152*, 1968.

[85] F. R. Denton, A. Serker, P. M. Lathi, R. O. Garay, F. E. Karasz, *J. Polym. Sci. Part A: Polym. Chem.* **1992**, *30*, 2233-2240.

[86] E. Kesters, S. Gilissen, F. Motmans, L. Lutsen, D. Vanderzande, *Macromolecules* **2002**, *35*, 7902-7910.

[87] S. Son, A. Dodabalapur, A. J. Lovinger, M. E. Galvin, *Science* **1995**, *269*, 376-378.

[88] A. Henckens, I. Duyssens, L. Lutsen, D. Vanderzande, T. Cleij, *Polymer* **2006**, *47*, 123-131.

[89] F. Louwet, D. Vanderzande, J. Gelan, *Synth. Met.* **1995**, *69*, 509-510.

[90] A. Van Breemen, D. Vanderzande, P. Adriaensens, J. Gelan, *J. Org. Chem.* **1999**, *64*, 3106-3112.

[91] L. Lutsen, A. Van Breemen, W. Kreuder, D. Vanderzande, J. Gelan, *Helv. Chem. Acta* **2000**, *83*, 3113-3121.

[92] M. Van Der Borght, D. Vanderzande, P. Adriaensens, J. Gelan, *J. Org. Chem.* **2000**, *65*, 284-289.

[93] E. Kesters, L. Lutsen, D. Vanderzande, J. Gelan, T. P. Nguyen, P. Molinié, *Thin Solid Films,* **2002**, *403-404*, 120-125.

[94] I. Van Severen, M. Breselge, S. Fourier, P. Adriaensens, J. Manca, L. Lutsen, T. J. Cleij, D. Vanderzande, *Macromol. Chem. Phys.* **2007**, *208*, 196–206.

[95] S. Gillissen, L. Lutsen, D. Vanderzande, J. Gelan, *Synth. Met.* **2001**, *119*, 137–138.

[96] N. Sary, R. Mezzenga, C. Brochon, G. Hadziioannou, J. Ruokolainen, *Macromolecules* **2007**, *40*, 3277–3286.

[97] C. Brochon, N. Sary, R. Mezzenga, C. Ngov, F. Richard, M. May, G. Hadziioannou, *J. Appl. Polym. Sci.* **2008**, *110*, 3664–3670.

[98] C. H. Braun, B. Schöpf, C. Ngov, C. Brochon, G. Hadziioannou, E. J. W. Crossland, S. Ludwigs, *Macromol. Rapid Commun.* **2011**, *32*, 813–819.

[99] F. He, T. Gädt, M. Jones, G. D. Scholes, I. Manners, M. A. Winnik, *Macromolecules* **2009**, *42*, 7953–7960.

[100] S. Chakraborty, A. Keightley, V. Dusevich, Y. Wang, Z. Peng, *Chem. Mater.* **2010**, *22*, 3995–4006.

[101] Y.-J. Miao, G. C. Bazan, *J. Am. Chem. Soc*. **1994**, *116*, 9379-9380*.*

[102] G. C. Bazan, M. L. Renak, B. J. Sun*, Macromolecules* **1996**, *29*, 1085-1087.

[103] C.-Y. Yu, M. Horie, A.M. Spring, K. Tremel, M.L. Turner, *Macromolecules* **2010**, *42*, 222-232.

[104] M. Porz, D. Mäker, K. Brödner, U. W. F. Bunz, *Macromol. Rapid Commun.* **2013**, 34, 873-876.

[105] B. J. Lidster, J. M. Behrendt, M. L. Turner, *Chem. Commun*. **2014**, *50*, 11867-11870.

[106] V. Percec, T. Guliashvili, J. Ladislaw, A. Wistrand, A. Stjerndahl, M. Sienkowska, M. Montiero, S. Sahoo, *J. Am. Chem. Soc.* **2006**, *128*, 14156-14165.

[107] N. H. Nguyen and V. Percec, *J. Polym. Sci. Part A: Polym. Chem*. **2010**, *48*, 5109-5119.

[108] A. Anastasaki, C. Waldron, P. Wilson, R. McHale, D. M. Haddleton, *Polym. Chem.* **2013**, *4*, 2672-2675.

[109] N. H. Nguyen, B. M. Rosen, G. Ligadas and V. Percec, *Macromolecules* **2009**, *42*, 2379-2386.

[110] I. Cosemans, J. Vandenbergh, V. S. D. Voet, K. Loos, L. Lutsen, D. Vanderzande, T. Junkers, *Polymer* **2013**, *54*, 1298-1304.

[111] I. Cosemans, J. Vandenbergh, L. Lutsen, D. Vanderzande, T. Junkers, *Polym. Chem.* **2013,** *4*, 3471-3479.

[112] I. Cosemans, J. Vandenbergh, L. Lutsen, D. Vanderzande, T. Junkers, *Eur. Polym. J.* 2014, **55**, 114-122.

[113] J. Vandenbergh, I. Cosemans, L. Lutsen, D. Vanderzande, T. Junkers, *Polym. Chem.* **2012**, *3*, 1722-1725.

[114] T. A. Skotheim, J. R. Reynolds, *Handbook of conducting polymers: Conjugated polymers: processing and applications*, 3th ed; CRC Press, **2007**, Chapter 4.

[115] W.-P. Chang, W.-T. Whang, *Polymer* **1996**, *37*, 4229–4234.

[116] J. H. Burroughes, D. D. C. Bradley, A. R. Brown, R. N. Marks, K. Mackay, R. H. Friend, P. L. Burn, and A. B. Holmes *Nature* **1990**, *347*, 539-541.

[117] W. Yue, T. T. Larsen-Olsen, X. Hu, M. Shi, H. Chen, M. Hinge, P. Fojan, F. C. Krebs, D. Yu, D., *J. Mater. Chem. A 1* **2013**, 1785-1793.

[118] Y. Geng, J. Cong, K. Tajima, Q. Zeng, E. Zhou, *Polym. Chem.* **2014**, *5*, 6797-6803.

[119] K. H. Hendriks, W. Li, M. M. Wienk, R. A. J. Janssen, *J. Am. Chem. Soc*. **2014**, *136*, 12130−12136

[120] C. Adachi, T. Tsutsui, S. Saito, *Appl. Phys. Lett.* **1999**, *55*, 1489–1491.

[121] M. Van Der Borght, P. Adriaensens, D. Vanderzande, J. Gelan, *Polymer* **2000**, *41*, 2743–2753.

[122] P. Cooreman, R. Thoelen, J. Manca, M. vandeVen, V. Vermeeren, L. Michiels, M. Ameloot, P. Wagner, *Biosens. Bioelectron.* **2005**, *20*, 2151–2156.

[123] R. Thoelen, R. Vansweevelt, J. Duchateau, F. Horemans, J. D'Haen, L. Lutsen, D. Vanderzande, M. Ameloot, M. vandeVen, T. J. Cleij, P. Wagner, *Biosens. Bioelectron.* **2008**, *23*, 913–918.

[124] Z. Matharu, S. K. Arya, S. P. Singh, V. Gupta, B. C. Malhotra, *Anal. Chim. Acta* **2009**, *634*, 243–249.

[125] K. P. Carter, A. M. Young, A. E. Palmer, *Chem. Rev.* **2014**, *114*, 4564-4601.

[126] K. M. Dean, A. E. Palmer, *Nat. Chem. Biol.* **2014,** *10*, 512-523.

[127] C. Wu, B. Bull, C. Szymanski, K. Christensen, J. McNeill, *ACS Nano* **2008**, *2*, 2415-2423.

[128] L. P. Fernando, P. K. Kandel, P. C. Ackroyd, K. A. Christensen, *Anal. and Bioanal. Chem.* **2012**, *404*, 3003-3014.

[129] R. Penjweini, S. Deville, L. D'Olieslaeger, M. Berden, M. Ameloot, A. Ethirajan, *J. of Control. Rel.* **2015**, *218*, 82-93.

[130] D. Hofmann, C. Messerschmidt, M. B. Bannwarth, K. Landfester, V. Mailander, *Chem. Commun.* **2014**, *50*, 1369-1371.

[131] X. Michalet, F. F. Pinaud, L. A. Bentolila, J. M. Tsay, S. Doose, J. J. Li, G. Sundaresan, A. M. Wu, S. S. Gambhir, S. Weiss, S*cience* **2005,** *307*, 538-544.

[132] C. E. Bradburne, J. B. Delehanty, K. Boeneman Gemmill, B. C. Mei, H. Mattoussi, K. Susumu, J. B. Blanco-Canosa, P. E. Dawson, I. L Medintz, *Bioconj. Chem.* **2013**, *24*, 1570-1583.

[133] R. Alford, H. M. Simpson, J. Duberman, G. C. Hill, M. Ogawa, C. Regino, H. Kobayashi, P. L. Choyke, *Mol. Imaging* **2009**, *8*, 341.

[134] R. Ahmad Khanbeigi, T. F. Abelha, A. Woods, O. Rastoin, R. D. Harvey, M.-C. Jones, B. Forbes, A. M. Green, H. Collins, L. A. Dailey, *Biomacromolecules* **2015**, *16*, 733-742.

CHAPTER 2

Facile Synthesis of Well-Defined (MDMO)-PPV containing (Tri)Block-copolymers via Controlled Radical Polymerization and CuAAC Conjugation
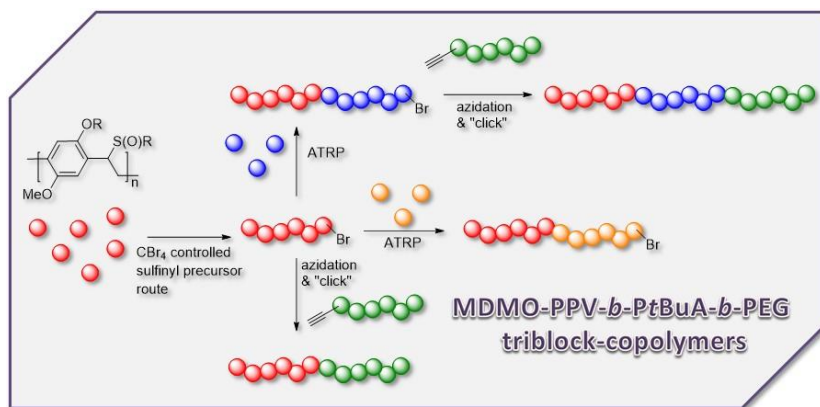
ABSTRACT

A systematic investigation into the chain transfer polymerization of the so-called radical precursor polymerization of poly(p-phenylene vinylene) (PPV) materials is presented. Polymerizations are characterized by systematic variation of chain transfer agent (CTA) concentration (CBr$_4$) and reaction temperature. For the chain transfer constant, a negative activation energy of -12.8 kJ·mol^{-1} was deduced. Good control over molecular weight is achieved for both the sulfinyl and the dithiocarbamate route (DTC). PPVs with molecular weights ranging from thousands to ten thousands g·mol^{-1} were obtained. To allow for a meaningful analysis of the CTA influence, Mark–Houwink–Kuhn–Sakurada (MHKS) parameters were determined for conjugated poly([2-methoxy-5-(3',7'-dimethyloctyloxy)]-1,4-phenylenevinylene) ((MDMO)-PPV) to $a = 0.809$ and $k = 0.00002$ mL·g^{-1}. Further, high-endgroup fidelity of the CBr$_4$-derived PPVs was proven via chain extension experiments. (MDMO)-PPV-Br was successfully used as macroinitiator in atom transfer radical polymerization (ATRP) with acrylates and styrene. In a last step, copper-catalyzed alkyne-azide cycloaddition (CuAAC) was used to synthesize block copolymer structures. Direct azidation followed by macromolecular conjugation showed only partial success, while the successive chain extension via ATRP followed by CuAAC afforded triblock copolymers of the poly(p-phenylene vinylene)-*block*-poly(*tert*-butyl acrylate)-*block*-poly(ethylene glycol) (PPV-*b*-P*t*BuA-*b*-PEG).

2.1. INTRODUCTION

Poly(*p*-phenylene vinylene)s (PPV)s are an important class of semiconducting polymer materials that display excellent optical and electrical properties and are one of the most studied conjugated polymers to date.[1-4] Throughout their history, PPVs have been used in a large variety of advanced optoelectronic applications.[5-9] Recently, our group has demonstrated how the optimized anionic pathway could be used for the synthesis of poly(*p*-phenylene vinylene)-*block*-poly(*tert*-butyl acrylate) (PPV-*b*-P*t*BuA) and poly(*p*-phenylene vinylene)-*block*-poly(ethylene glycol) (PPV-*b*-PEG).[10-12] Anionic sulfinyl precursor polymerization is a highly promising technique, yet polymerizations must be carried out under very pure conditions and the selection of monomers is limited since not all derivatives can be polymerized in a purely anionic way. Thus, further evaluation and optimization of the radical polymerization route to likewise generate complex PPV-containing precision macromolecular materials is required.
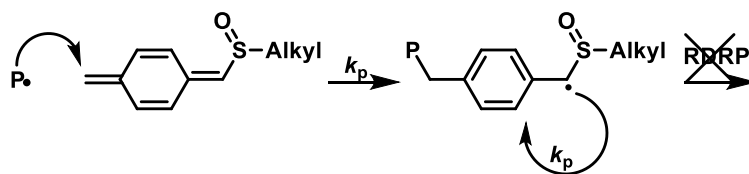
Scheme 2-1: Propagation reaction in precursor polymerization. Aromaticity is restored during propagation, which renders reversible deactivation radical polymerization

Controlling radical PPV polymerizations is not as straightforward as in standard vinyl radical polymerizations because of the *in situ* formation of the *p*-quinodimethane system and its enormous driving force to propagate, which

hinders interaction in any control equilibrium of a reversible deactivation radical polymerization (RDRP).[13-16] During propagation (associated with the kinetic rate coefficient for propagation, k_p), aromaticity of the monomer is restored (see Scheme 2-1), resulting inevitably in a competition between the propagating radicals and the control agent (a full mechanistic studies of the redical polymerization of PPVs is provided in chapter 6). Nevertheless, previous preliminary studies towards radical PPV polymerizations have shown that the use of an excess of CBr$_4$ as chain transfer agent (CTA) in combination with [2-methoxy-5-(3',7'-dimethyloctyloxy)]-1,4-phenylenevinylene (MDMO) as premonomer results in a successful molecular weight control in the polymerization and end group control of the polymers. pathway.[17-20] By transfer reactions, the resulting precursor (MDMO)–PPV contains bromine end-group functionalities which can be reactivated in a next step using atom transfer radical polymerization (ATRP) conditions. The proof of principle for block copolymer synthesis including precursor PPVs was demonstrated using styrene as monomer and Cu(I)Br/*N,N,N',N',N''*-pentamethyl diethylenetriamine (PMDETA) as metal/ligand system.[20] However, further data is required to fully understand the involved limitations and underpinning challenges since only very preliminary data was provided.

In this chapter two different aspects of the polymerization method described above are studied in more detail. First, we discuss in detail the kinetics of the process on the basis of a broad dataset generated for CBr$_4$-controlled precursor polymerization. Subsequently, we explore the synthetic potential of the technique compared to our previous study. For the kinetic study, we focus on the controlled synthesis of ((MDMO)-PPV) and 6-(2-chloromethyl-4-methoxy-5-[(octylsulfinyl) methyl]-phenoxy) hexanioc-acid methyl ester (CPM) using CBr$_4$ as CTA. Also, differences between the sulfinyl and the dithiocarbamate (DTC) precursor route

are elucidated. The range of polymer chain lengths that is accessible is thoroughly determined and activation energies for the transfer constant are derived shining light on the not yet fully resolved precursor polymerization mechanism. Secondly, the scope of the ATRP chain extension of sulfinyl precursor (MDMO)-PPV is extended by synthesizing a variety of block copolymers with styrene or *tert*-butyl acrylate to obtain well-defined PPV-*b*-PS and PPV-*b*-P*t*BuA with varying block lengths and compositions. Finally, end group modification and subsequent conjugation of the PPV-*b*-P*t*BuA block copolymers using copper-catalyzed alkyne-azide cycloaddition (CuAAC) click-chemistry results in an (comparatively) easy to purify PPV-*b*-P*t*BuA-*b*-PEG triblock copolymer—the first of their kind to the best of our knowledge.

2.2. EXPERIMENTAL SECTION

2.2.1. Monomer Synthesis

2.2.1.1. Synthesis of monomer 7 (1-chloromethyl-2-methoxy-5-(3,7-dimethyloctyloxy)-4-[(octylsulfinyl)methyl] benzene)
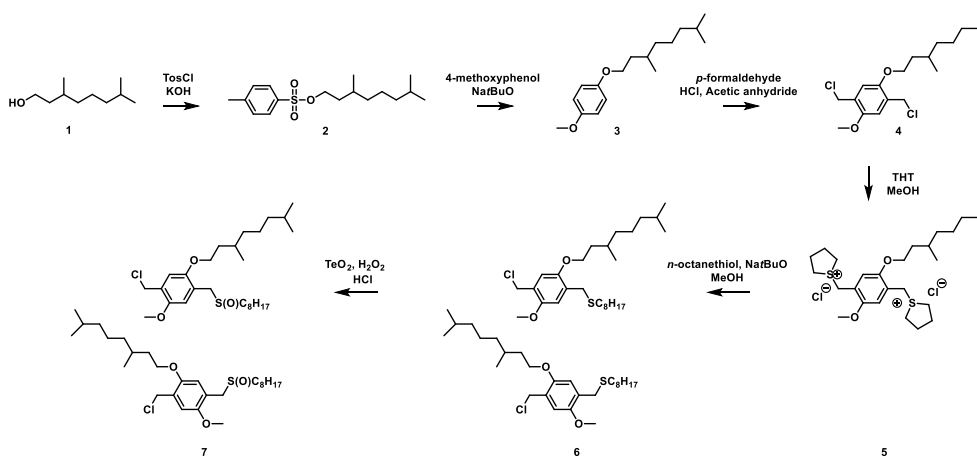
Scheme 2-2: Synthesis route for MDMO premonomer via the sulfinyl precursor route

Monomer **7** was synthesized according to known literature procedure, Scheme 2-2.[18;19]

2.2.1.2. Synthesis of monomer 13 (6-(2-chloromethyl-4-methoxy-5-[(octylsulfinyl)methyl]-phenoxy) hexanoic acid methyl ester)
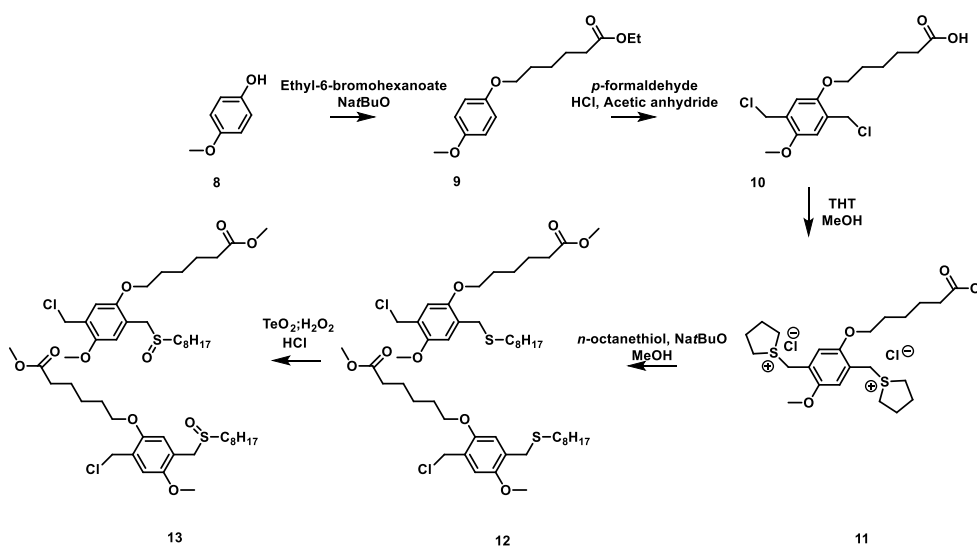
Scheme 2-3: Synthesis route for CPM premonomer via the sulfinyl precursor route

6-(4-Methoxy-phenoxy)-hexanoic acid ethyl ester (**9**) A mixture of **8** (93.5 g, 0.75 mol, 1 equiv.) and NaO*t*Bu (86.6 g, 0.90 mol, 1.2 equiv.) in EtOH (500 mL) was stirred for 1 h at room temperature under nitrogen atmosphere. A solution of ethyl-6-bromohexanoate (200 g, 0.90 mol, 1.2 equiv.) and NaI (3.4 g, 0.02 mol, 1.2 equiv.) in EtOH (200 mL) was added and the complete mixture was stirred for 4 h at reflux temperature (80 °C). The reaction was quenched with H_2O (400 mL), extracted with CH_2Cl_2 (3 × 100 mL) and the organic layer was dried over anhydrous $MgSO_4$. After filtration, evaporation of the solvent under reduced pressure gave the crude product as an orange oil. The pure product **9** was obtained by recrystallization in MeOH as white crystals, Scheme 2-3 (131.61 g, 65.70%). M_p: 30 °C. ^{1}H-NMR ($CDCl_3$): δ = 6.80 (s, 4H); 4.10 (q, J = 7.3 Hz, 2H);

3.88 (t, J = 6.4 Hz, 2H); 3.74 (s, 3H); 2.30 (t, J = 7.6 Hz, 2H); 1.74 (m, 2H); 1.68 (m, 2H); 1.47 (m, 2H); 1.23 (t, J = 7.2 Hz, 3H). ^{13}C-NMR (CDCl$_3$): δ = 173.74 (C4); 153.65 (C4); 153.13 (C4); 115.35 (CH); 114.56 (CH); 68.24 (CH$_2$); 60.24 (CH$_2$); 55.70 (CH$_3$); 34.25 (CH$_2$); 29.04 (CH$_2$); 25.65 (CH$_2$); 24.72 (CH$_2$); 14.24(CH$_3$). DIP MS (CI, m/z): 266 (M+), 221/222 (M$^+$–OEt), 143/144 (M$^+$–OPhOMe), 124/125 (M$^+$–C$_5$H$_{10}$COOEt). FT–IR (ATR): ν = 2938, 2479, 2000, 1866, 1732, 1506, 1476, 1292, 1233, 1160, 1112, 1033, 825, 742 cm^{-1}.

6-(2,5-Bis-chloromethyl-4-methoxy-phenoxy)hexanoic acid (**10**) To a stirred mixture of **9** (131.6 g, 0.49 mol, 1.0 equiv.) and p-formaldehyde (40.9 g, 1.35 mol, 2.75 equiv.), HCl (37%, 110.1 g, 3.26 mol, 6.6 equiv.) was added drop wise at 0 °C under nitrogen atmosphere. Subsequently acetic anhydride (503 g, 4.94 mol, 10 equiv.) was added drop wise, without exceeding a temperature of 70 °C. The solution was stirred at 60 °C for 3 h. After cooling down to room temperature, H$_2$O (400 mL) was added to the solution. The resulting precipitate was filtered off and redissolved in CH$_2$Cl$_2$ (200 mL). Next, the organic solution was dried over anhydrous MgSO$_4$ and filtered. Evaporation of the solvent under reduced pressure gave the crude product as a yellow oil. The pure product **10** was obtained by recrystallization in EtOAc as white crystals, Scheme 2-3 (71.7 g, 41.74%). M$_p$: 99 °C. ^{1}H-NMR (CDCl$_3$): δ = 6.90 (d, J = 3.9 Hz, 2H); 4.60 (d, J = 3.5 Hz, 4H); 3.98 (t, J = 6.2 Hz, 2H); 3.83 (s, 3H); 2.39 (t, J = 7.4 Hz, 2H); 1.82 (m, 2H); 1.72 (m, 2H); 1.56 (m, 2H). ^{13}C-NMR (CDCl$_3$): δ =171.95 (C4); 151.65 (C4); 151.13 (C4); 127.67 (C4); 127.41 (C4); 114.98 (CH); 113.90 (CH); 69.24 (CH$_2$); 61.06 (CH$_2$); 58.80 (CH$_3$); 41.93 (CH$_2$); 41.85 (CH$_2$); 34.53 (CH$_2$); 29.54 (CH$_2$); 26.14 (CH$_2$); 24.93 (CH$_2$); 21.62 (CH$_2$); 14.75 (CH$_3$). DIP MS (CI, m/z): 334 (M+), 299 (M$^+$–Cl), 263 (M$^+$–2Cl), 220/222 (M$^+$–C$_5$H$_{10}$COOH). FT–IR (ATR): ν = 2938, 2875,

1971, 1724, 1687, 1512, 1463, 1410, 1312, 1220, 1141, 1033, 875, 871, 732, 686 cm^{-1}.

6-(2,5-Bis-chloromethyl-4-methoxy-phenoxy) hexanoic acid methyl ester (**11**) To a stirred mixture of **10** (71.7 g, 0.22mol, 1.0 equiv.) in MeOH (600 mL), tetrahydrothiophene (THT) (99.8 g, 1.1 mol, 5.0 equiv.) was added. The reaction was allowed to react at 50 °C for 4 days. The solution was precipitated in cold diethyl ether (1 L) under heavy stirring and the resulting precipitate was filtered off and washed with cold diethyl ether. After drying under vacuum, the pure product **11** was obtained as a white solid, Scheme 2-3 (40.0 g; 33.85%). M$_p$: 119 °C. ^{1}H-NMR (D$_2$O): δ = 7.08 (s, 1H); 7.06 (s, 1H); 4.41 (s, 2H); 4.40 (s, 2H); 4.01 (t, J = 6.3 Hz, 2H); 3.79 (s, 3H); 3.56 (s, 3H); 3.40 (m, 8H); 2.32 (t, J = 6.3 Hz, 2H); 2.24 (m, 8H); 1.75 (m, 2H); 1.59 (m, 4H); 1.42 (m, 2H). ^{13}C-NMR (CDCl$_3$): δ = 179.43 (C4); 178.03 (C4); 152.56 (C4); 152.54 (C4); 151.89 (C4); 151.86 (C4); 120.40 (CH); 120.33 (CH); 116.78 (CH); 116.03 (CH); 69.78 (CH$_2$); 56.94 (CH$_3$); 52.75 (CH$_3$); 49.53 (CH$_2$); 45.47 (CH$_2$); 43.83 (CH$_2$); 43.77 (CH$_2$); 42.18 (CH$_2$); 34.34 (CH$_2$); 34.20 (CH$_2$); 29.08 (CH$_2$); 28.70 (CH$_2$); 25.64 (CH$_2$); 24.69 (CH$_2$). DIP MS (CI, m/z): 525 (MH$^+$), 493 (M$^+$–Cl), 401 (M$^+$–THT–Cl), 265 (M$^+$–2 THT–Cl–CH$_2$). FT–IR (ATR): ν = 3004, 2942, 2879, 2122, 1732, 1510, 1449, 1399, 1313, 1225, 1033, 909, 773, 702 cm^{-1}.

6-(5-Chloromethyl-4-methoxy-2-octylsulfanylmethyl-phenoxy)hexanoic acid methyl ester (**12**) A mixture of n-octanethiol (12.31 g, 83.9 mmol, 1.1 equiv.) and NaOtBu (8.1 g, 76.3 mmol, 1.0 equiv.) in MeOH (300 mL) was stirred at room temperature for 30 min. This mixture was added drop wise to a stirred mixture of **11** (40.0 g, 76.3 mmol, 1.0 equiv.) in MeOH (700 mL) after which it was allowed to react for 2 h at room temperature under N$_2$ atmosphere. After evaporation of the solvent

under reduced pressure, n-octane (100 mL) was added and evaporated again to remove the THT. This procedure was repeated 5 times. The residue was redissolved in CH_2Cl_2 (350 mL), extracted with a saturated NaCl-solution:H_2O (1:10) (3 × 250 mL) and the organic layer was dried over anhydrous $MgSO_4$. After filtration, evaporation of the solvent under reduced pressure gave the crude product **12** as a white solid (26.0 g, 67.5%) and used without further purification, Scheme 2-3. ^{1}H-NMR ($CDCl_3$): δ = 6.85 (m, 2H); 4.61 (s, 1H); 4.60 (s, 1H); 3.94 (m, 2H); 3.80 (m, 3H); 3.69 (d, J = 3.5 Hz, 2H); 3.65 (s, 3H); 2.45 (t, J = 6.8 Hz, 2H); 2.33 (t, J = 7.4 Hz, 2H); 1.79 (m, 2H); 1.65 (m, 2H); 1.52 (m, 2H); 1.24 (m, 12 H); 0.85 (m, 3H).

6-(5-Chloromethyl-4-methoxy-2-octylsulfinylmethyl-phenoxy)-hexanoic acid methyl ester (**13**) To a stirred mixture of **12** (26.0 g, 56.6 mmol, 1.0 equiv.) in 1,4-dioxane (350 mL), TeO_2 (1.1 g, 7.1 mmol, 1/8 equiv.) and HCl (1 M, 10 mL, 1.2 equiv.) were added. To start the reaction H_2O_2 (35%; 11.01 g 113.3 mmol, 2.0 equiv.) was added and the reaction was followed on TLC (hexane/ EtOAc; 1/1). As soon as all **12** was consumed, the reaction was quenched with a saturated Na_2SO_3-solution:H_2O (1:1; 400 mL). The solution was extracted with CH_2Cl_2 (3 × 300 mL), dried over anhydrous $MgSO_4$ and filtered. Evaporation of the solvent under reduced pressure gave the crude product as a yellow oil. The pure product **13** was obtained by column chromatography (SiO_2, hexane/EtOAc 1/1) (45.97 mmol, 21.80 g, 81.22%), Scheme 2-3. M_p: 35 °C. ^{1}H-NMR ($CDCl_3$): δ = 6.76 (s, 1H); 6.75 (s, 1H); 4.44 (s, 2H); 3.63 (d, J = 7 Hz, 4H); 3.48 (s, 3H); 3.47 (s, 3H); 2.45 (t, J = 7.4 Hz, 2H); 2.15 (t, J = 7.4 Hz, 2H); 1.65–1.45 (m, 6H); 1.32– 1.05 (m, 12H); 0.69 (t, J = 6.6 Hz, 3H). ^{13}C-NMR ($CDCl_3$): δ = 174.55 (C4); 174.42 (C4); 151.79 (C4); 151.54 (C4); 127.18 (C4); 120.43 (C4); 115.23 (CH);

113.44 (CH); 69.17 (CH_2); 56.74 (CH_3); 53.48 (CH_2); 52.03 (CH_2); 51.90 (CH_3); 41.93 (CH_2); 41.85 (CH_2); 34.34 (CH_2); 32.25 (CH_2); 29.54 (CH_2); 29.39 (CH_2); 26.16 (CH_2); 23.13 (CH_2); 14.61 (CH_3). DIP MS (CI, *m/z*): 475/477 (MH^+), 439/441 (M^+−Cl), 313/315 (M^+−S(O)C_8H_{17}), 279 (M^+−Cl−S(O)C_8H_{17}), 162/163 (S(O)C_8H_{17}). FT−IR (ATR): ν = 3003, 2942, 2881, 2409, 1732, 1545, 1510, 1447, 1400, 1313, 1220, 1165, 1104, 1034, 909, 774, 686 cm^{-1}

2.2.1.3. Synthesis of monomer 14 (2,5-bis(N,N-diethyldithiocarbamate-methyl)-1-(3,7-dimethyloctyloxy)-4-methoxybenzene)
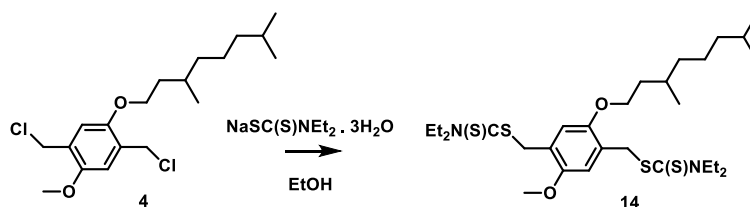
Scheme 2-4: Synthesis route for MDMO premonomer via the dithiocarbamate precursor route

Monomer **14** was synthesized according to known literature procedure, Scheme 2-4.[21]

2.2.2. Polymerization

2.2.2.1. General method for the polymerization of bromine-functionalized MDMO (P1') or CPM (P2') sulfinyl PPV
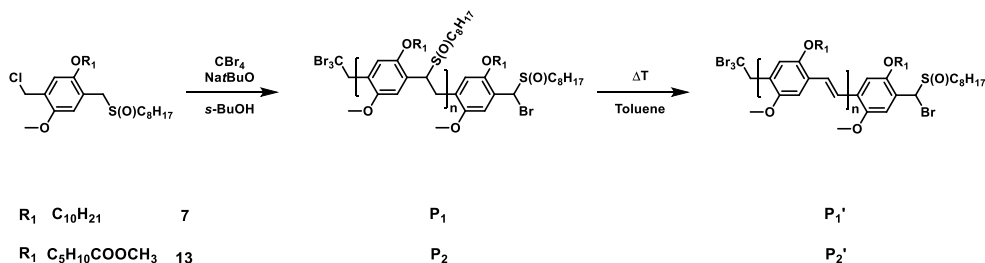
Scheme 2-5: Synthesis of (MDMO)-PPV and (CPM)-PPV via the sulfinyl precursor route using CBr$_4$ as CTA

A solution of MDMO sulfinyl premonomer **7** (1.00 g, 2.05 mmol, 1.0 equiv.) and CBr$_4$ (5.44 g, 16.4 mmol, 8.0 equiv.) in *sec*-BuOH (14.8 mL) and a solution of Na*t*BuO (0.256 g, 2.67 mmol, 1.3 equiv.) in *sec*-BuOH (16.8 mL) were degassed three times at 30 °C using nitrogen. The base solution was added in one portion to the stirred monomer solution to start the reaction. After 1 h, the reaction was quenched with HCl (1 M, 50.0 mL). After extraction with CH$_2$Cl$_2$ (3 mL × 50 mL) and evaporation, the product was dissolved in CHCl$_3$ (15 mL) and precipitated in cold methanol (100 mL). The mixture was filtered on a Teflon® filter and the polymer was collected and dried *in vacuo*. The crude product was purified via preparative recycling SEC to yield the pure polymer **P1** as a yellow viscous oil (72%), Scheme 2-5. SEC (THF): M_n^{app} = 10 100 g·mol^{-1}, Đ = 1.9. ^{1}H-NMR (CDCl$_3$): δ = 6.90–6.20 (m, 2H); 4.90–4.60 (t, 1H); 4.00–2.90 (m, 7H); 2.70–2.10 (t, 2H); 1.90–1.10 (m, 22H); 1.00–0.80 (m, 12H). ^{13}C-NMR (CDCl$_3$): δ = 151.40 (C4); 127.0 (C4); 110.50 (CH); 67.90 (CH$_2$); 59.10–55.10 (CH); 56.40 (CH$_3$); 49.70 (CH$_2$); 39.20 (CH$_2$); 37.40 (CH$_2$); 36.60 (CH$_2$); 32.10–29.10 (CH$_2$); 30.20 (CH$_2$); 27.90 (CH$_2$); 24.60 (CH$_2$); 22.60 (CH$_2$); 21.90 (CH$_3$); 19.80 (CH$_3$); 13.50 (CH$_3$). FT-IR (NaCl): 2955, 2927, 1509, 1471, 1462, 1413, 1222, 1031

cm^{-1}. Precursor PPV **P1** (200 mg) in toluene (15 mL) was degassed by purging for 15 min with nitrogen, after which the solution was heated to 110 °C and stirred for 3 h under nitrogen atmosphere. Subsequently, the reaction was cooled down to room temperature and precipitated in cold MeOH (40 mL) and filtered on a Teflon® filter. The conjugated (MDMO)–PPV polymer **P1'** was obtained as a red solid (75%), Scheme 2-5. SEC (THF): M_n^{app} = 11 500 g·mol^{-1}, Đ = 1.7. ^{1}H-NMR (CDCl$_3$): δ = 7.49 (m, 2H); 7.19 (m, 2H); 4.60–3.20 (m, 5H); 2.10–0.6 (m, 19H). ^{13}C-NMR (CDCl$_3$): δ = 151.40 (C4); 127.0 (C4); 110.50 (CH); 108.85 (CH); 67.90 (CH$_2$); 56.40 (CH$_3$); 39.20 (CH$_2$); 37.40 (CH$_2$); 36.60 (CH$_2$); 30.20 (CH$_2$); 27.90 (CH$_2$); 24.60 (CH$_2$); 22.60 (CH$_2$); 19.80 (CH$_3$). FT-IR (KBr): 2957, 2925, 2860, 1510, 1469, 1395, 1217, 1028, 872 cm^{-1}.

Synthesis of bromine-functionalized CPM sulfinyl precursor PPV **P2** was similar to synthesize the MDMO precursor PPV, Scheme 2-5. SEC (THF): M_n^{app} = 9 800 g·mol^{-1}, Đ = 1.8. ^{1}H-NMR (CDCl$_3$): δ = 7.00–6.20 (m, 2H); 4.50 (m, 2H); 4.10–3.60 (m, 6H); 3.40 (m, 2H); 2.40–1.80 (t, 4H); 1.80–1.20 (m, 18H); 0.90 (m, 3H). ^{13}C-NMR (CDCl$_3$): δ = 173.2 (C4); 151.20 (C4); 125.0 (C4); 114.50 (CH); 68.20 (CH$_2$); 61.0 (CH$_2$); 56.20 (CH$_3$); 51.90 (CH$_3$); 49.60 (CH$_2$); 33.20 (CH$_2$); 31.40 (CH$_2$); 29.10–22.80 (CH$_2$); 14.50 (CH$_3$). FT-IR (NaCl): 2929, 2856, 1728, 1506, 1463, 1409, 1212, 1032 cm^{-1}.

Synthesis of bromine-functionalized conjugated (CPM)-PPV **P2'** was similar to synthesis of the (MDMO)-PPV, Scheme 2-5. SEC (THF): M_n^{app} = 11 800 g·mol^{-1}, Đ = 1.6. ^{1}H-NMR (CDCl$_3$): δ = 7.50–7.30 (m, 2H); 7.20–6.90 (m, 2H); 4.20 (m, 2H); 3.80 (t, 3H); 3.60 (m, 2H); 2.30–0.60 (m, 6H). ^{13}C-NMR (CDCl$_3$): δ = 173.1 (C4); 153.30 (C4); 150.8 (C4); 127.2 (C4); 123.2, 110.40 (CH); 69.00 (CH$_2$); 56.10

(CH$_3$); 51.90 (CH$_3$); 49.60 (CH$_2$); 33.80 (CH$_2$); 28.60–24.70 (CH$_2$); 14.50 (CH$_3$). FT-IR (NaCl): 2934, 2866, 1728, 1505, 1205, 1034, 969 cm^{-1}.

2.2.2.2. General method for the polymerization of bromine-functionalized MDMO (P3') DTC PPV
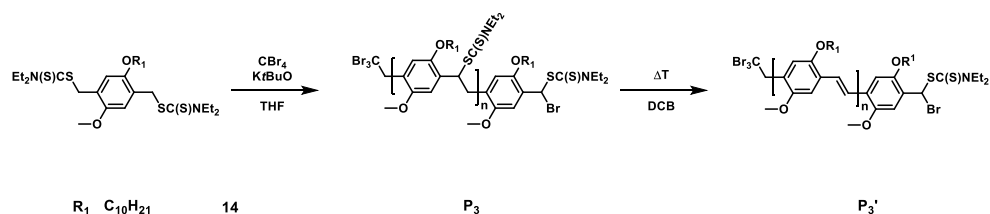
Scheme 2-6: Synthesis of (MDMO)-PPV via the DTC precursor route using CBr$_4$ as CTA

A solution of premonomer **14** in THF (0.5 g, 0.851 mmol, 1.0 equiv.) and CBr$_4$ (28.2 mg, 0.0851 mmol, 0.1 equiv.) in THF (4.23 mL) and a solution of KtBuO (0.143 g, 1.28 mmol, 1.5 equiv.) in THF (1.47 mL) were degassed three times at 35 °C using nitrogen. The base solution was added in one portion to the stirred monomer solution to start the reaction. After 1.5 h, the reaction was quenched with HCl (1 M, 50.0 mL). After extraction with CH$_2$Cl$_2$ (3 × 50 mL) and evaporation, the product was dissolved in CHCl$_3$ (15 mL) and precipitated in cold methanol (100 mL) The mixture was filtered on a Teflon® filter and the polymer **P3** was collected and dried *in vacuo* resulting in a yellow viscous oil (72%), Scheme 2-6. SEC (THF): M_n^{app} = 11 900 g·mol^{-1}, $Đ$ = 2.3. ^{1}H NMR (CDCl$_3$): δ = 6.45–6.97 (m, 2H); 5.50–5.87 (s, 1H); 3.05–4.23 (m, 11H); 1.02–1.95 (m, 16H); 0.74–1.02 (m, 9H); ^{13}C NMR (CDCl$_3$): δ = 195.76 (C4); 150.85 (C4); 127.68 (C4); 114.11 (CH); 113.09 (CH); 67.10 (CH$_2$); 56.39 (CH$_3$); 51.98 (CH$_2$); 49.08 (CH$_2$); 46.38 (CH$_2$); 39.27

(CH$_2$); 37.54 (CH$_2$); 36.60 (CH$_2$); 34.45 (CH$_2$); 29.91 (CH$_2$); 27.92 (CH$_2$); 24.67 (CH$_3$); 22.69 (CH$_3$); 22.58(CH$_3$); 19.66 (CH$_2$); 12.47 (CH$_3$); 11.55 (CH$_3$). FT-IR (NaCl): 2953, 2929, 1504, 1484, 1462, 1413, 1267, 1210, 1140, 1041 cm^{-1}.

Precursor PPV **P3** (200 mg) in dichlorobenzene (60 mL) was degassed by purging for 15 min with nitrogen, after which the solution was heated to 180 °C and stirred for 3 h under nitrogen atmosphere. Subsequently, the reaction was cooled down to room temperature and precipitated in cold MeOH (40 mL) and filtered on a Teflon® filter. The conjugated (MDMO)-PPV polymer **P3'** was obtained as a red solid (75%), Scheme 2-6. SEC (THF): M_n^{app} = 15 300 g·mol^{-1}, $Đ$ = 1.8. ^{1}H NMR (C$_2$D$_2$Cl$_4$): δ = 7.50 (2H); 7.21 (2H); 4.61–3.19 (m, 5H); 2.10–0.59 (m; 19H). ^{13}C NMR (CDCl$_3$): δ = 151.4 (C4); 127.0 (C4); 123.3 (C4); 110.5 (CH); 108.8 (CH); 67.9 (CH$_2$); 56.4 (CH$_3$); 39.2 (CH$_2$); 37.4 (CH$_2$); 36.6 (CH$_2$); 30.2 (CH$_2$); 27.9 (CH$_2$); 24.6 (CH$_3$); 22.6 (CH$_3$); 19.8 (CH$_3$). FT-IR (KBr): 2957, 2925, 2860, 1510, 1469, 1395, 1217, 1028, 872 cm^{-1}.

2.2.3. Chain Extension

2.2.3.1. Block extension using MDMO sulfinyl precursor PPV P1 as macro initiator
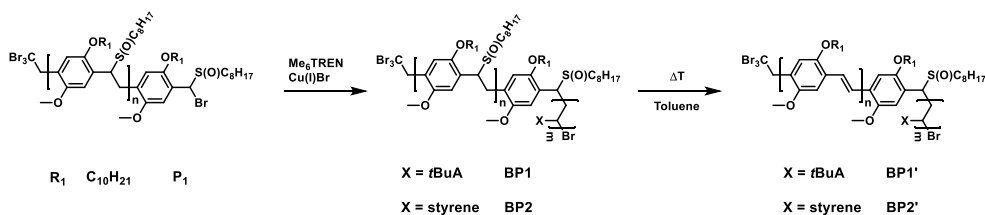
Scheme 2-7: Synthesis of (MDMO)-PPV-*b*-P*t*BuA and (MDMO)-PPV-*b*-PS block copolymers using ATRP chain extensions

For the block copolymerization with *tert*-butyl acrylate (*t*BuA), the precursor PPV **P1** – purified by recycling Gel Permeation Chromatography (GPC) – was used as macroinitator. A Schlenk tube was filled with Cu(I)Br (4.5 mg, 7.15 µmol, 1.1 equiv.), *t*BuA (75 mg, 0.580 mmol, 100 equiv.), Me$_6$TREN (tris[2-(dimethylamino)ethyl]amine, 14.3 µmol, 3.30 µL, 2.2 equiv.) and **P1** (M_n^{app} = 7 700 g·mol^{-1}, 0.1 g, 5.8 µmol, 1 equiv.) dissolved in BuOAc (1 mL). The Schlenk tube was subjected to three freeze-pump-thaw cycles and transferred into the glovebox. The reaction mixture was stirred at 75 °C, and at specified times, samples were taken. The sample mixtures were poured in an aluminum tray and precipitated in a MeOH/H$_2$O (4/1) mixture. After evaporation of the solvent, the polymer was filtered over a small alumina column to remove all copper and the solvent was evaporated. A bright yellow viscous precursor (MDMO)-PPV-*b*-P*t*BuA **BP1** polymer was obtained after filtration, Scheme 2-7. SEC (THF): M_n^{app} = 8 300–10 800 g·mol^{-1}, Đ = 2.3. (MDMO)-PPV-*b*-P*t*BuA block copolymer **BP1** (200 mg) in toluene (15 mL) was degassed by purging for 15 min with nitrogen, after which the solution was heated to 110 °C and stirred for 3 h under nitrogen atmosphere. Subsequently, the reaction was cooled down to room temperature and precipitated in cold MeOH/H$_2$O (4/1) mixture (40 mL) and filtered on a Teflon® filter. The conjugated polymer was obtained as a reddish oil **BP1'** (75%), Scheme 2-7. SEC (THF): M_n^{app} = 8 300 g·mol^{-1}, Đ = 2.1. A similar procedure was used for the thermal elimination of precursor (MDMO)-PPV-*b*-PS **BP2** into conjugated **BP2'** which also was obtained as a red solid (70%). SEC (THF): M_n^{app} = 15 300 g·mol^{-1}, Đ = 1.9.

Block extensions on **P1** were varied in the type of monomer (styrene instead of *tert*-butyl acrylate) and in number of monomer equivalents (50 and/or 100). All chain extensions were performed using the synthesis procedure described above.

However, precipitation of the precursor (MDMO)-PPV-*b*-PS **BP2** block copolymers was performed in MeOH.

2.2.3.2. Synthesis of azide functionalized precursor (MDMO)-PPV-N$_3$ Pn1
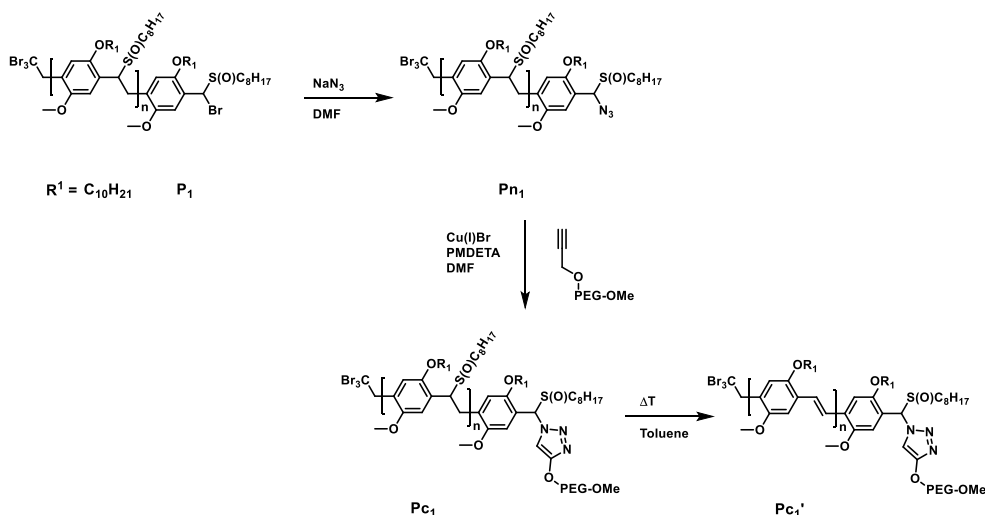
Scheme 2-8: Direct synthesis of (MDMO)-PPV-*b*-PEG block copolymer using click conditions

To a stirred solution of **P1** (M_n^{app} = 9 000 g·mol^{-1}, 0.1714 g, 1.9 μmol, 1.0 equiv.) in DMF (5 mL) sodium azide (12.9 mg, 19.0 μmol, 10 equiv.) was added. The mixture was stirred for 72 h at elevated temperature, after which cold water was added to the flask. The polymer was extracted with CHCl$_3$ (3 × 100 mL) and subsequent evaporation of the organic layer and precipitation in MeOH, resulted after filtration in the azide-functionalized precursor (MDMO)-PPV-N$_3$ **Pn1** (85%), Scheme 2-8.

2.2.3.3. Conjugation of (MDMO)-PPV-N$_3$ Pn1 using CuAAC click conditions

To a solution of **Pn1** (M_n^{app} = 9 000 g·mol^{-1}, 0.1 g, 16.7 μmol, 1.0 equiv.), PEG-alkyne (1 equiv.) and Cu(I)Br (11.9 mg, 83.0 μmol, 5.0 equiv.) in dry DMF (5 mL),

Me$_6$TREN (19.1 mg, 83.0 µmol, 5.0 equiv.) was added under nitrogen atmosphere. The reaction mixture was stirred for 72 h at room temperature. The solution was passed through a neutral alumina column in order to remove the copper salts and concentrated under reduced pressure to obtain **Pc1** as an orange viscous oil (43%), Scheme 2-8. SEC (THF): $M_p{}^{app}$ = 15,800 g·mol^{-1} $Đ$ = n.a. Precursor block copolymer **Pc1** (100 mg) in toluene (15 mL) was degassed by purging for 15 min with nitrogen, after which the solution was heated to 110 °C and stirred for 3 h under nitrogen atmosphere. Subsequently, the reaction was cooled down to room temperature and precipitated in ice cold MeOH, (40 mL) and filtered. The conjugated block-copolymer **Pc1'** was obtained as a red solid (75%), Scheme 2-8. SEC (THF): $M_p{}^{app}$ = 18 400 g·mol^{-1}, $Đ$ = n.a.

2.2.3.4. Synthesis of azide-functionalized precursor (MDMO)-PPV-*b*-P*t*BuA-N$_3$ BPn1
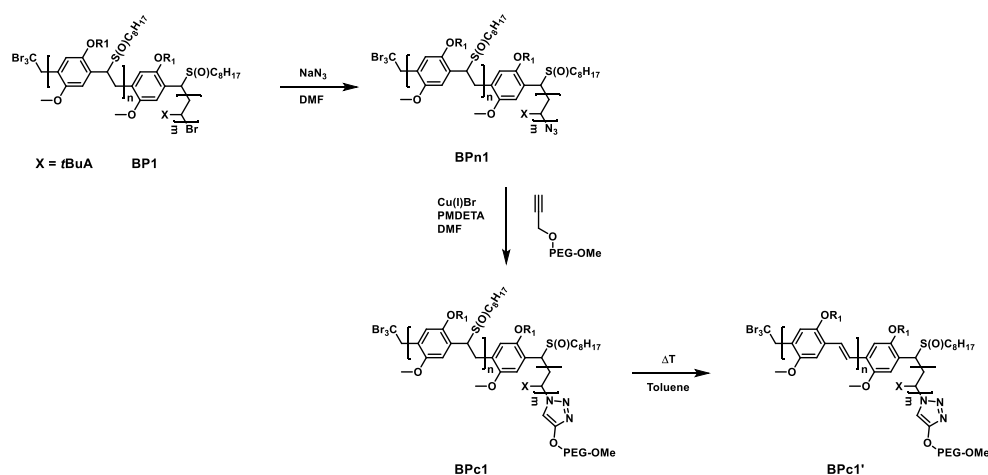
Scheme 2-9: Synthesis of PPV tri-block copolymers using click conditions

To a stirred solution of **BP1** (M_n^{app} = 6 400 g·mol^{-1}, 0.1 g, 7.8 µmol, 1.0 equiv.) in DMF (5 mL) sodium azide (5.4 mg, 78.7 µmol, 10 equiv.) was added. The mixture was stirred for 72 h at room temperature, after which cold water was added to the flask. The polymer was extracted with CHCl$_3$ (3 × 100 mL) and subsequent evaporation of the organic layer and precipitation in a MEOH/H$_2$O (4/1) mixture resulted after filtration in the azide-functionalized precursor (MDMO)-PPV-*b*-P*t*BuA-N$_3$ **BPn1**, Scheme 2-9.

2.2.3.5. Conjugation of (MDMO)-PPV-*b*-P*t*BuA-N$_3$ BPn1 using CuAAC click conditions

To a solution of **BPn1** (M_n^{app} = 6 300 g·mol^{-1}, 0.1 g, 13.7 µmol, 1.0 equiv.), PEG-alkyne (1.0 equiv.) and Cu(I)Br (9.8 mg, 68.5 µmol, 5.0 equiv.) in dry DMF (5 mL), Me$_6$TREN (15.8 mg, 68.5 µmol, 5.0 equiv.) was added under nitrogen atmosphere. The reaction mixture was stirred for 72 h at room temperature. The solution was passed through a neutral alumina column in order to remove the copper salts and concentrated under reduced pressure to obtain **BPc1** as an orange viscous oil (68%), Scheme 2-9. SEC (THF): M_n^{app} = 12 700 g·mol^{-1}, Đ = 1.5. Precursor block copolymer **BPc1** (200 mg) in toluene (15 mL) was degassed by purging for 15 min with nitrogen, after which the solution was heated to 110 °C and stirred for 3 h under nitrogen atmosphere. Subsequently, the reaction was cooled down to room temperature and precipitated in ice cold hexane (40 mL) and filtered. The conjugated triblock-copolymer **BPc1'** was obtained as a red polymer (75%), Scheme 2-9. SEC (THF): M_n^{app} = 13 400 g·mol^{-1}, Đ = 1.4.

2.3. RESULTS AND DISCUSSION

2.3.1. Control over the Radical PPV polymerization by using a CTA

A general pathway to gain control over radical polymerizations is to add control agents to the polymerization that involve the propagating radicals in reversible deactivation equilibria, leading to linear growth of chains with monomer conversion and preselection of M_n of the final polymer depending on control agent concentration. As mentioned above, achieving such reversible deactivation is not as straightforward for PPV polymerizations as for conventional radical polymerizations. During initiation (formation of a biradical) as well as during propagation of the p-quinodimethane monomers, aromaticity is restored, resulting in a very high driving force for these reactions. Therefore, initiation and propagation are extremely fast and only those control agents that allow for similarly high reactivities are able to compete. So far, no control agent from the typical RDRP methods could be identified to be effectively operational in precursor polymerizations. Only CBr_4 – a classical chain transfer agent that induces molecular weight control, but not livingness of the polymerization – had been found to be active enough to have a direct (and positive) influence on the polymer product. A good correlation between the molecular weight of conjugated (MDMO)-PPV – synthesized via the sulfinyl route – and the transfer agent concentration is reported in a previous study,[20] resulting in polymers with molecular weights ranging from a M_n of 12 000 to 25 000 g·mol^{-1} with a dispersity ($Đ$) of ~2.0.

In this study, the effect of CBr_4 on the polymerization of PPV is compared between two precursor routes, e.g., the sulfinyl and the dithiocarbamate (DTC) route. Polymerizations via the sulfinyl route show very fast reactions reaching

conversions of almost 100% in less than 5 min. As a result, the addition of high excesses of control agent is needed to obtain the desired effect. Polymerizations using the DTC route on the other hand result in slower polymerizations, and reactions only reach full conversion after 10–15 min. This indicates that good control over the DTC polymerization route using less control agent should be possible. Therefore, three different PPV premonomers were synthesized (Figure 2-1), namely the so-called MDMO sulfinyl premonomer, CPM sulfinyl premonomer and MDMO DTC premonomer. The two MDMO monomers lead equally to the formation of (MDMO)-PPV, a common conjugated material used in a multitude of applications. The CPM premonomer is used for the synthesis of a close derivative, which is interesting due to the possibility to post-functionalize the conjugated materials via trans-esterification reactions. The premonomers are polymerized using specific amounts of CBr_4 and are subsequently eliminated to result in the desired conjugated polymers that are analyzed by means of SEC, Figure 2-1. It is important to note that SEC determination of molecular weights of PPVs is not straightforward. MHKS coefficients are mostly unavailable in literature and already small differences in the PPV defect structure may have a profound effect on the hydrodynamic volume of the chains. Thus, specific MHKS parameters were determined for (MDMO)-PPV via analysis of several broad polymer distributions using viscometry and MALLS detection. Via usage of polymer samples with precisely known mass, dn/dc is directly obtained from the RI detector signal and MHKS values were fitted to the light scattering M_w data. For MDMO precursor polymer obtained via the sulfinyl route, $a = 0.67605$ and $k = 0.000142$ mL·g^{-1} and for conjugated (MDMO)-PPV $a = 0.809$ and $k = 0.00002$ mL·g^{-1} were obtained. Care has to be taken using MALLS detection, as the fluorescent properties of the materials lead to light emission interfering with the MALLS scatter signals. For that

reason, MALLS is not easily applied and can thus not be used as a routine method for molar mass determination in this case. For the determination of MHKS values, samples were measured repeatedly at different concentrations to rule out interfering effects. For (MDMO)-PPV polymers obtained from the DTC route and for the (CPM)-PPV polymer, no specific MHKS were deduced. While parameters for the conjugated polymer should in principle be independent from the polymerization route (a concept that may be debated when going into detail), and hence MHKS for sulfinyl and DTC-made (MDMO)-PPV should be identical, no absolute M_n can be given for (CPM)-PPV. Only apparent M_n^{app} are thus given for this system.
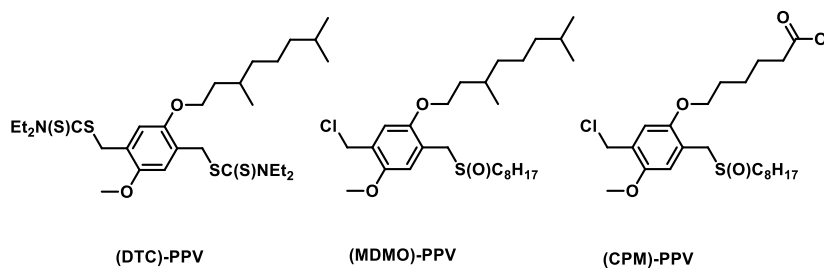
Figure 2-1: Overview of the different PPV premonomers used in this study

Table 2-1: Molecular weight data of conjugated (MDMO)-PPVs obtained from the sulfinyl (T = 30 °C using $[M]$ = 0.14 mol·L^{-1} and $[B]$ = 0.16 mol·L^{-1}) and DTC (T = 35 °C using $[M]$ = 0.20 mol·L^{-1} and $[B]$ = 0.87 mol·L^{-1}) route under varying amount of CBr$_4$

(MDMO)-PPV (DTC)			(MDMO)-PPV (sulfinyl)			(CPM)-PPV (sulfinyl)		
CTA equiv.	M_n g·mol^{-1}	Đ	CTA equiv.	M_n g·mol^{-1}	Đ	CTA equiv.	M_n^{app} g·mol^{-1}	Đ
0	98 000	2.9	0	88 900	2.6	0	82 000	2.3
0.04	54 000	3.2	0.5	31 000	2.3	0.5	20 000	3.2
0.05	49 600	3.8	1	28 400	2.5	1	14 000	1.9
0.1	30 500	3.0	2	8 900	1.8	2	6 780	2.1
0.25	11 900	2.3	4	9 800	1.8	4	6 800	2.2
0.5	2 460	2.0	8	1 000	2.0	8	6 410	2.3
0.75	2 480	1.2	12	8 700	1.6	-	-	-
0.9	1 260	1.1	14	9 900	1.7	-	-	-
1	430	1.2	16	9 600	1.6	-	-	-
8	500	1.1	20	6 700	1.5	-	-	-
-	-	-	25	8 800	1.7	-	-	-

Figure 2-2: Inverse of the degree of polymerization as a function of the CTA to monomer concentration ratio for (CPM)-PPV synthesized via the sulfinyl precursor route

Figure 2-3: SEC profile of (CPM)-PPV obtained by polymerization of the sulfinyl CPM premonomer in the presence of specified amounts of CBr$_4$ as CTA, followed by elimination of the precursor polymer into conjugated (CPM)-PPV

SEC analysis on the resulting conjugated (MDMO)-PPVs allows for chain transfer constant determination by fitting the inverse of the degree of polymerization as a function of the CTA to premonomer concentration ratio, following the well-known Mayo relation:

$$\frac{1}{DP_n} = \frac{1}{DP_n^o} + C_{tr}\frac{c_{CTA}}{c_M} \tag{1}$$

In this equation, DP_n represents the average degree of polymerization, DP_n^o the average degree of polymerization in an ideal case in absence of any transfer agent, C_{CTA} the transfer agent concentration and C_M the premonomer concentration. C_{tr} is the chain transfer constant and is defined as the ratio of the transfer rate coefficient k_{tr} over the propagation rate coefficient k_p. Thus, in case $k_p >> k_{tr}$ a C_{tr} smaller than unity will be obtained. In Figure 2-4, the Mayo plots for conjugated (MDMO)-PPV, polymerized via the sulfinyl and the DTC route using CBr$_4$ as CTA is given, while Figure 2-2 similar data for (CPM)-PPV shows. Results

clearly indicate the good molecular weight control over both polymerizations upon changing the control agent concentration (Figure 2-3). Nevertheless, compared to classical vinyl polymerizations, an immense amount of CBr_4 is needed to reach this effect. Whereas in vinyl polymerizations, few mole percent of CTA are sufficient to expect good control, several equiv. of CTA are required in both precursor monomer routes. Up to 12 equiv. of control agent are needed to decrease the molecular weight of sulfinyl (MDMO)-PPV from 100 000 to 12 000 $g \cdot mol^{-1}$. Standard (MDMO)-PPV polymerizations result in a yellow viscous oil for the precursor polymer and a red solid upon thermal elimination of the precursor to the conjugated polymer. Upon increasing amount of CBr_4, not only does the color of the conjugated (MDMO)-PPV changes from red to orange, also the physical appearance (from solid to viscous oil) changes, indicating the effect of the CTA on the chain length of the resulting (MDMO)-PPVs.
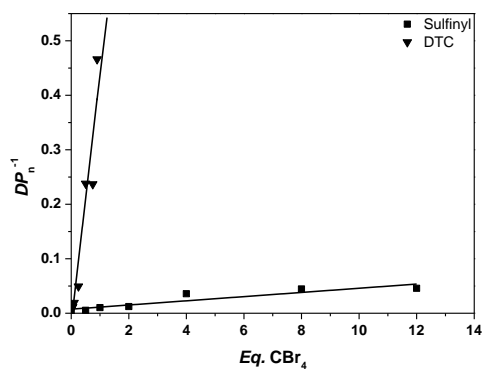
Figure 2-4: Inverse of the degree of polymerization as a function of the CTA to premonomer concentration ratio for (MDMO)-PPV synthesized via the sulfinyl and the DTC route

Interestingly, a further increase in control agent concentration above 8–12 equiv. – up to 25 equiv. was tested – does not decrease the molecular weight any further. This indicates that the chain transfer agent only controls molecular weight from a certain chain length on. For sulfinyl precursor (MDMO)-PPV, a minimum of roughly 25 repeating monomers are added to the chain before chain termination by transfer occurs. It should be noted that the precursor polymerization is not only complicated by the fact that the polymerization is rapid, but also by the fact that initiation proceeds via a biradical formation, hence requiring the transfer events to occur before chains are effectively dead.

Polymerizations of (MDMO)-PPV using the DTC precursor route show an effect of the CTA at much lower CTA concentrations. With 0.04 equiv. of CBr_4 a reduction in molecular weight is observed from 100 000 to 54 000 g·mol^{-1}, in comparison to 10-fold higher concentrations being required in the sulfinyl route to achieve the same effect. Increasing the CBr_4 content to one equiv. reduces chain growth to such a high extent that basically no polymerization is taking place anymore. This disparate chain transfer behavior is well represented in the individual transfer constants that are determined from the data. For both polymerizations in the sulfinyl route, for T = 30 °C a C_{tr} of 0.0034 is obtained in good agreement with our previous study, indicating that the small change in the side chain has no or only very little kinetic effect on the polymerization. For the DTC route polymerization, a C_{tr} of 0.46 at T = 35 °C is obtained (Figure 2-4 and Table 2-2), thus at a value much closer to conventional vinyl polymerization. This increased transfer constant indicates that either transfer to CBr_4 is favored in this route, or that propagation is significantly slower (or, in principle, a combination of the two is operational). In either way, control in the DTC route is simpler to achieve compared

to the sulfinyl route and further endeavors into controlling this type of polymerization should take the DTC route into account.

Table 2-2: Chain transfer constant for conjugated PPVs synthesized via the sulfinyl (T = 30 °C) and DTC (T = 35 °C) precursor routes

Conjugated PPVs	Chain Transfer Constant C_{tr}
(MDMO)-PPV (DTC route)	0.46
(MDMO)-PPV (sulfinyl route)	0.0038
(CPM)-PPV (sulfinyl route)	0.0034

In further investigations, a deeper look into the chain transfer kinetics of the sulfinyl route was taken. Despite the better performance of the DTC route, similarly good materials can be accessed at higher equiv. of CBr_4 in the sulfinyl route. Moreover, even though general uncertainties exist for precursor polymerizations with respect to mechanism and individual rate coefficients, the sulfinyl route is amongst the best studied precursor routes.[22-26] Further systematic kinetic investigation of this reaction type is thus highly useful and thus the reason why – in spite of the better results for the DTC route – further investigation still focuses on the sulfinyl route. To date, no reliable initiation, propagation or termination coefficients are available for any precursor polymerizations, but efforts to fill this gap have been so far mostly focused on the sulfinyl route.
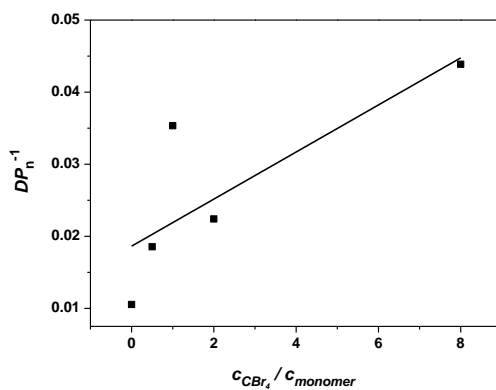
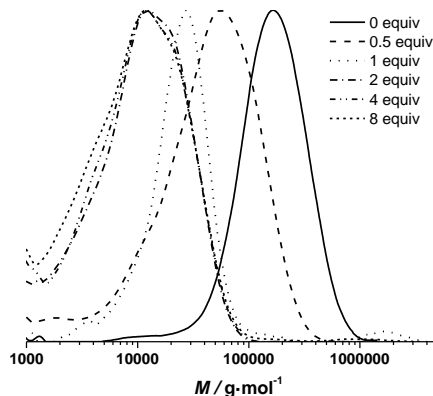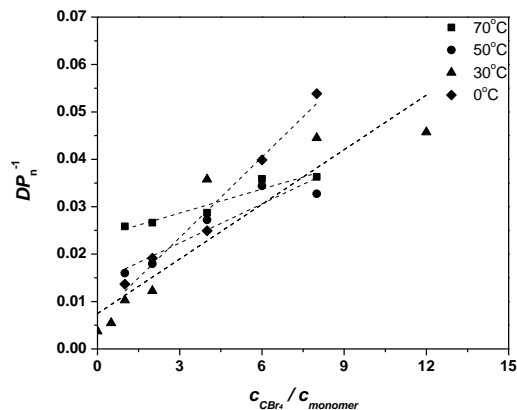Figure 2-5: Inverse of the degree of polymerization as a function of the CTA to premonomer concentration ratio for (MDMO)-PPV synthesized via the sulfinyl "precursor" route at different polymerization temperatures

Table 2-3: Chain transfer constants determined from the plots given in Figure 2-5 for conjugated (MDMO)-PPV synthesized via the sulfinyl "precursor" route at different polymerization temperatures

T	C_{tr}
0 °C	0.0056
30 °C	0.0034
50 °C	0.0028
70 °C	0.0017

A closer look towards the activation energy of chain transfer can help in understanding the otherwise rapid sulfinyl route polymerization. Polymerizations under variation of the CTA concentration were thus conducted at different temperatures and analyzed towards the conjugated (MDMO)-PPV polymer (Figure 2-5, Table 2-3). Results clearly demonstrate that upon increase in reaction temperature, a decrease in the transfer constant is followed. At the same time,

lower DP_n^o is reached with increasing temperature, indicating that also the ratio of termination, propagation and initiation changes strongly with temperature. The decreasing C_{tr} indicates that either propagation increases stronger with temperature than radical transfer, or that transfer becomes overall less effective at higher temperatures. Analysis of the Arrhenius relation for C_{tr} yields an apparent activation energy $E_A(C_{tr})$ of the coupled parameter of -12.8 kJ·mol^{-1} (Figure 2-6). The negative value is explained by the relation $E_A(C_{tr}) = E_A(k_{tr}) - E_A(k_p)$. The negative value thus indicates that the activation energy of propagation is larger than that of transfer. Under assumption that radical transfer is usually associated with activation energies in the range of 20 kJ·mol^{-1}, the conclusion can be drawn that the activation energy of propagation is in the range of 30 kJ·mol^{-1} or higher, a value that is common for radical propagation reactions.
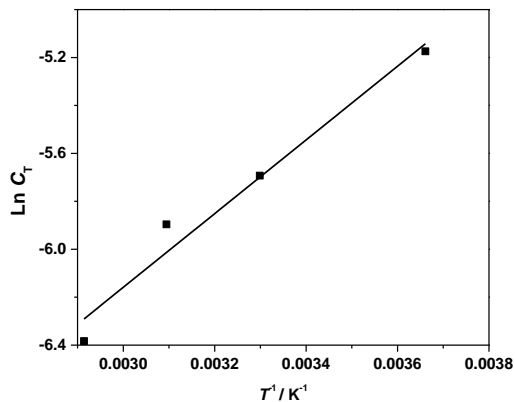
Figure 2-6: Arrhenius plot of C_{tr} obtained in the temperature range of 0 −70 °C

The above kinetic experiments nicely demonstrate the general difficulty to carry out controlled radical polymerizations to obtain PPV materials. The sulfinyl route is less susceptible to interfering transfer reactions, but allows for facile access of

chain-length controlled polymers when several equiv. of transfer agent are employed. The dithiocarbamate route is more simple to control, which is reflected by a close to 100-fold difference in the specific chain transfer constant. Determination of the activation energy of the transfer constant for the sulfinyl route shows that less control is achieved with increasing reaction temperatures due to the high activation energy of the propagation reaction. This information may seem trivial on first glance, yet for a polymerization system for which to date only very few kinetic parameters are known, this is a significant advance in knowledge. Any additional rate parameter (or at least activation energy) that becomes available will aid in future modelling studies and a paramount understanding of the polymerization. Only with such models at hand, rational selection of reaction conditions will be possible and true product control achieved.

2.3.2. Chain extension via sequential approaches (ATRP) using (MDMO)-PPV macro initiators

While the above experiments demonstrate the ability to control molecular weight, not much is yet known about the end group distribution in the polymer products. In principle, by the halogen transfer of the CTA, a bromine-end-functional polymer should be obtained with high end group fidelity. Such groups are in principle suitable to be used in post-polymerization modifications either in end group exchange reactions or in subsequent controlled polymerizations. More precisely, the bromine chain end can be used as a macro-initiator moiety for copper-mediated radical polymerization chain extensions with vinylic monomers, or can be replaced by an azide to give access to CuAAC conjugation reactions. In both ways, block

copolymers can be synthesized. As a detailed kinetic investigation on the sulfinyl route was performed in the first part, also block copolymer formation via this route are taken into account. Post-polymerization reactions concerning the DTC route will be presented in a forthcoming study.

In a first approach, atom transfer radical polymerizations (ATRP) are performed on bromine end-capped sulfinyl MDMO precursor PPV to generate block copolymers in a sequential approach, in accordance to the first experiments that we have shown before.[20] (MDMO)-PPVs (precursor level) with bromine end groups were synthesized using the sulfinyl precursor route and 8 equiv. of CBr_4 as chain transfer agent, resulting in polymers with a molecular weight of 6 900 g·mol^{-1}. The CTA needs to be thoroughly removed using preparative recycling GPC, since it can by itself act as initiator in an ATRP process. The precursor (MDMO)-PPV-Br polymer was then used for block copolymerizations. It has to be noted that chain extension is only possible on precursor polymer level (thus before elimination of the sulfinyl groups). Otherwise, interactions between the conjugated chain system and Cu(I)Br can lead to undesired oxidation reactions on one hand and defects in the polymer structure on the other hand. Reactivation of the bromine end group via ATRP reactions are carried out at 75 °C, using BuOAc as solvent and Cu(I)Br and Me_6TREN as metal/ligand system. In a first step, chain extensions with tBuA are executed. The influence of both the reaction time as well as monomer concentration is investigated. Reactions are stopped by precipitation of the polymer followed by removal of the copper on a short alumina column. Since elimination of precursor PPV starts at 75 °C, all precursor block copolymers are in a second step thermally eliminated (3 h at 110 °C) and purified, resulting in true conjugated (MDMO)-PPV-b-PtBuA block copolymers. SEC analysis is always

performed on the final conjugated block copolymers in order to allow for a meaningful comparison between different samples (the hydrodynamic volume of the PPVs change significantly from precursor to conjugated polymer, thus making comparisons of molecular weights between both states difficult).
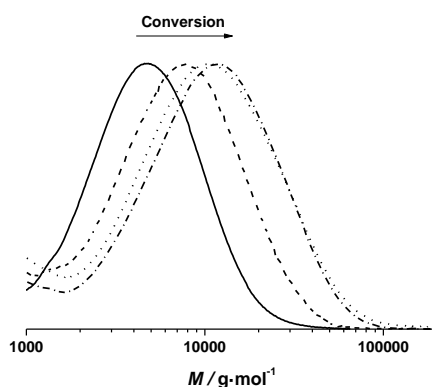
Figure 2-7: Molecular weight distributions of (MDMO)-PPV (*black line*) and (MDMO)-PPV-*b*-P*t*BuA block copolymers obtained from ATRP with 100 equiv. of monomer followed in time (*dotted lines with increasing conversion from left to right*).

Figure 2-7 depicts the molecular weight distributions of conjugated (MDMO)-PPV and the chain extended (MDMO)-PPV-*b*-P*t*BuA block copolymers, obtained during chain extension with 100 equiv. of *t*BuA relative to the precursor polymer after purification. A clear shift towards higher molecular weights upon increasing reaction times (and hence acrylate conversion) is observed. A full shift of the distributions is thereby indicative that almost all PPV chains have been reinitiated and that bromine-end group fidelity was good. Dispersity values as shown in Table 2-4 show a slight increase, which may be indicative of slow reinitiation. Furthermore, changes in the concentration of acrylate (50 and 100 equiv., Table 2-4) show a good correlation

between apparent M_n^{app} (note that only apparent values are discussed since SEC determination was carried out via polystyrene calibration) and starting monomer concentration. With a constant reaction time of 4 h, a doubling in the (apparent) block length of the polyacrylate is seen upon doubling the amount of monomer. Previous UV-Vis measurements on PPV block copolymer formation via both the anionic[11] as well as radical[20] route showed a slight influence of the non-conjugated block on the λ_{max} values of the conjugated system, by detecting a small blue shift in the spectra. Similar shifts are expected for the current block copolymers synthesized in here and no additional measurements were performed as the practical consequences with regards to fluorescence are overall expected to be small.

Table 2-4: Apparent average molecular weights of (MDMO)-PPV-*b*-P*t*BuA block copolymers from ATRP chain extensions using different equiv. of monomer

(MDMO)-PPV homopolymer and block copolymers	M_n^{app} g·mol^{-1}	M_w^{app} g·mol^{-1}	Đ
(MDMO)-PPV	6 900	9 970	1.4
(MDMO)-PPV-*b*-P*t*BuA (50 equiv. *t*BuA)	8 200	12 900	1.6
(MDMO)-PPV-*b*-P*t*BuA (100 equiv. *t*BuA)	9 200	16 600	1.8

The above observations are mostly qualitative, thus additional quantitative investigations into the ATRP chain extension were also undertaken. ATRPs were conducted with both *t*BuA and styrene and monomer conversion was followed gravimetrically. If reactions were well controlled, not only shifts in the molecular weight as indicated above should be expected, but also first order kinetics for monomer consumption (to test for constant radical concentration). For both styrene and the acrylate, linear first order plots are observed with only small deviations from the linear behavior in the initial time regime, Figure 2-8. The

acrylate polymerizes in the first 30 min of the polymerization significantly faster than styrene and only after that period, similar reaction rates are observed for the following reaction, leading to a small error in onset of the reaction.
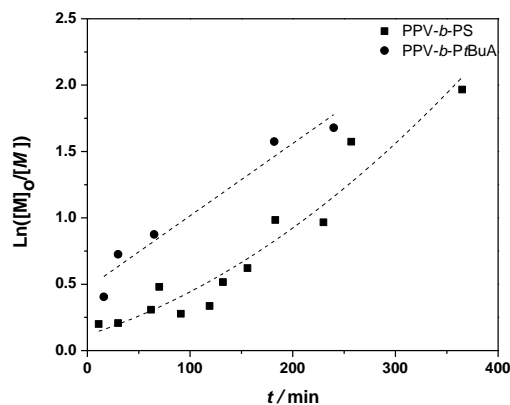
Figure 2-8: Semi-logarithmic first order kinetic plot of (MDMO)-PPV-*b*-P*t*BuA and (MDMO)-PPV-*b*-PS block copolymerizations via ATRP. Samples were taken over a time period of 6 hr
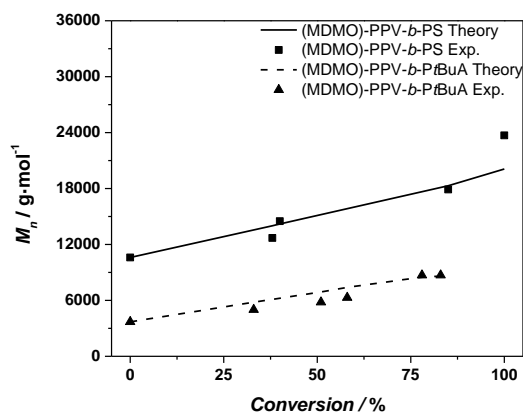
Figure 2-9: The dependence of the molecular weight M_n upon the conversion for the (MDMO)-PPV-*b*-P*t*BuA and (MDMO)-PPV-*b*-PS block copolymers. Markers represent experimental M_n values, the lines theoretical M_n

Figure 2-9 depicts for the same polymerizations the evolution of number-average molecular weight as a function of conversion, nicely demonstrating the good correlation of experimental with theoretical molecular weights. Note that the different offsets of M_n in Figure 2-6 stem from different PPV precursor polymers being used in the reactions. Thus, it may be concluded that the combination of the radical CBr$_4$ sulfinyl precursor PPV route and ATRP chain extension technique allows for the synthesis of a variety of PPV containing block copolymers of different sizes, functionalities and properties in an easy fashion.

2.3.3. Conjugation of PPV block copolymers using CuAAC conditions

Sequential approaches towards successful block copolymerization (e.g., ATRP or SET-LRP) restrict the choice of the second block to vinyl-type monomers that are able to undergo (controlled) radical polymerization. Thus, the development of a modular approach allowing any combination of building blocks is also highly attractive. Therefore, copper-catalyzed alkyne-azide cycloaddition (CuAAC) is employed for the synthesis of PPV block copolymers. As a first attempt, (MDMO)-PPV-*b*-PEG block copolymers were targeted using such a modular approach. Therefore, bromine endcapped precursor sulfinyl (MDMO)-PPV was first functionalized at elevated temperatures with an azide group, using an excess amount of sodium azide (10 equiv. to polymer) in DMF. In a second step, the obtained precursor (MDMO)-PPV-azide is then clicked to a PEG-alkyne using standard CuAAC reaction conditions. Reactions are carried out at 25 °C, using DMF as solvent and Cu(I)Br and PMDETA as catalyst. Both precursors PPV and PEG were added in equimolar amounts to avoid excesses of homopolymer being

left after reaction. The reaction mixture was allowed to stir for an extended time (up to three days) after which copper was removed from the product mixture by passing the solution over a short alumina column. In a second step, all precursor block copolymers are eliminated, resulting in conjugated (MDMO)-PPV-*b*-PEG block copolymer. Results regarding molecular weight and dispersity for the starting (MDMO)-PPV homopolymer and the resulting (MDMO)-PPV-*b*-PEG block copolymer can be found in Table 2-5 and molecular weight profiles are plotted in Figure 2-10.

As can be seen from the molecular weight distributions in Figure 2-10, a bimodal SEC profile is obtained after reaction, representing a mixture of two separate distributions — (MDMO)-PPV homopolymer — and the block copolymer (MDMO)-PPV-*b*-PEG, indicating a partly successful ligation. Comparison of the starting materials M_p indicated that the click reaction by itself was successful, but that pure PPV remained – whether due to reaction inefficiencies or due to insufficient functionalization of the homopolymer. Closer inspection and repetitions of the CuAAC reaction leads to the conclusion that the partial success (no improvement is seen even after three days' reaction time under varying conditions) is due to solubility issues. As mentioned before, the azide functionalized (MDMO)-PPV does not dissolve well in DMF, which can make the azide partially inaccessible for reaction. Purification of the (MDMO)-PPV-*b*-PEG block copolymer from the homopolymer leftovers is far from trivial. Residual PEG can relatively easily be removed by washing the mixture with water, residual (MDMO)-PPV can only be removed by preparative recycling SEC, as was done before.[10]

Table 2-5: Molecular weights and *Đ* for the homopolymers and conjugated (MDMO)-PPV-*b*-PEG block copolymer

(MDMO)-PPV homo-and diblock copolymer	M_n^{app} g·mol^{-1}	M_w^{app} g·mol^{-1}	M_p^{app} g·mol^{-1}	*Đ*
(MDMO)-PPV-N$_3$	7 800	12 400	8 300	1.6
PEG-alkyne	6 400	6 600	7 300	1.1
(MDMO)-PPV-*b*-PEG	-	-	18 400	-
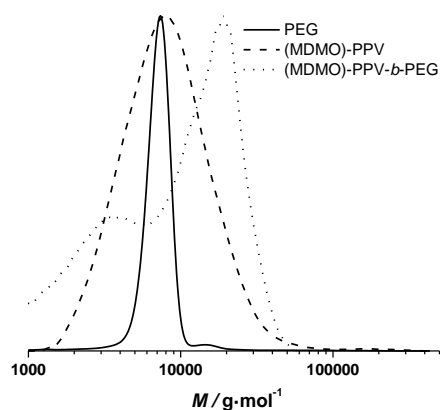
Figure 2-10: SEC profile for the direct coupling of alkyne-functionalized PEG to azide functionalized eliminated (MDMO)-PPV using click conditions without purification of the homopolymer leftovers. Reaction was performed under ambient conditions over a time period of 3 days

As solubility of the polymers may play a significant role in the somewhat hindered click reaction, synthesis of triblock copolymers from successive chain transfer polymerization, ATRP chain extension with an acrylate and CuAAC conjugation was tested, yielding material with the desired structure (MDMO)-PPV-*b*-P*t*BuA-*b*-PEG. (MDMO)-PPV-*b*-P*t*BuA-Br polymers as discussed above were modified with NaN$_3$ to obtain azide-functional material. The generally better solubility of the

acrylate block and the higher chain flexibility of the second block should aid in the click reaction and improve the system. Furthermore, P*t*BuA can at a later stage be eliminated to yield poly(acrylic acid) blocks and thus give access to pH-responsive triblock copolymer structures. The CuAAC reaction with PEG-alkyne was then again allowed to react for three days under the same conditions of the diblock CuAAC conjugation reaction, after which the reaction is stopped by precipitation of the resulting triblock copolymers in ice-cold hexane followed by removal of the copper on a short alumina column. After thermal elimination of the material and precipitation, an orange colored conjugated (MDMO)-PPV-*b*-P*t*BuA-*b*-PEG was obtained. Molecular weight distributions of the individual homo-, di- and resulting tri-block copolymers as well as corresponding molecular weights are presented in Figure 2-11 and Table 2-6. The CuAAC conjugation shows in this case good success.
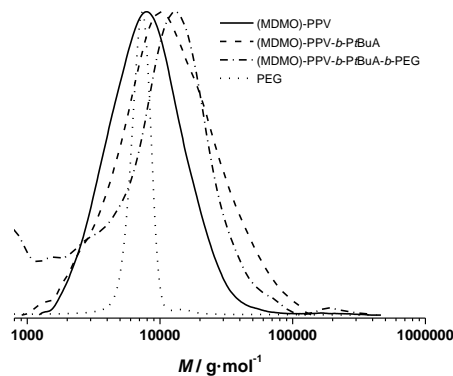
Figure 2-11: Molecular weight distributions of the clicked (MDMO)-PPV-*b*-P*t*BuA-*b*-PEG triblock copolymer and its precursors. Reaction was performed under ambient conditions over a time period of 3 days

Table 2-6: Average molecular weights and *Đ* for the (MDMO)-PPV-*b*-P*t*BuA-*b*-PEG triblock copolymers and its precursors

(MDMO)-PPV di-and triblock copolymers	$M_n{}^{app}$ g·mol^{-1}	$M_w{}^{app}$ g·mol^{-1}	$M_p{}^{app}$ g·mol^{-1}	*Đ*
(MDMO)-PPV	6 100	9 300	8 000	1.5
(MDMO)-PPV-*b*-P*t*BuA	7 300	11 800	10 500	1.6
PEG-alkyne	6 400	6 600	6 500	1.1
(MDMO)-PPV-*b*-P*t*BuA-*b*-PEG	-	-	19 200	-

The ATRP chain extension yields similar good results as in the case described above. The CuAAC reaction proceeds well. The triblock copolymer product distribution still shows some material at the lower molecular weight side of the distribution, which could not be removed by precipitation or washing. Thus, no average molecular weights could be determined and again only M_p is discussed The (MDMO)-PPV-*b*-P*t*BuA copolymer has a peak molecular weight of 10 500 g·mol^{-1}. The PEG-alkyne block has a molecular weight of 6 500 g·mol^{-1}. In the sum, the triblock structure features a M_p of 19 200 g·mol^{-1}, which can be regarded as a good match – taking into account that no calibration exists for these materials and large variations in the MHKS parameters of the chains must be expected with each consecutive chain extension.

2.4. CONCLUSIONS

The concept of controlling the precursor polymerization of PPV via the use of a CBr$_4$ chain transfer agent has been studied in detail. Control over molecular weight is achieved by using several equiv. of CTA compared to precursor monomer. Systematic kinetic investigations confirmed that better chain length control is achieved when polymerizations are carried out at lower temperatures. Via determination of the activation energy of the coupled parameter C_{tr} (-12.8 kJ·mol^{-1}), important information on the propagation reaction could be gathered, which will aid in future modelling studies that aim at the final elucidation of the to-date only partially understood PPV polymerization mechanism. Interestingly, easier control is achieved in the precursor polymerization, when the dithiocarbamate polymerization route is employed compared to the sulfinyl route, hinting at large differences in radical stability and propagation tendency between the two types of monomers.

PPVs with number average molecular weights between 10 000 and 100 000 g·mol^{-1} are obtained by varying the amount of CTA, allowing large scale synthesis of these polymers in a wide range of molecular weights. In addition to good control over chain length, high chain-end fidelity could be demonstrated. Employment of the PPV-Br species that are obtained from the chain transfer polymerization as macro-initiators in copper-mediated radical polymerizations allowed for the facile synthesis of several diblock copolymer structures via the ATRP route. Concomitantly, also the *click*-type conjugation of PPV was investigated. Direct substitution of the terminal bromine at the PPV chain end followed by CuAAC conjugation with an alkyne-functionalized PEG yielded only partial success. Significant improvement of the CuAAC was seen when the PPVs were first chain

extended with *tert*-butyl acrylate to make the terminal bromine/azide functionality more accessible. In this way, (MDMO)-PPV-*b*-P*t*BuA-*b*-PEG was obtained successfully, giving rise to high precision multiblock organic semiconductor materials.

The CTA-based synthesis procedure thus allows for relatively easy – and most importantly – scalable synthesis of well-controlled PPV materials, a task that is otherwise very hard to achieve. Chain length control and especially the ability to form more complex macromolecular structures in both sequential and modular design approaches allows to build in PPV segments into virtually any existing polymer architecture. This advancement in field opens a variety of possibilities for PPVs outside the classical application domain of organic electronics.

2.5. REFERENCES

[1] S. Günes, H. Neugebauer, N. S. Sariciftci, *Chem. Rev*. **2007**, *107*, 1324–1338.

[2] A. P. Kulkarni, C. J. Tonzola, A. Babel, S. A. Jenekhe, *Chem. Mater*. **2004**, *16*, 4556–4573.

[3] E. D. Gomez, S. S. Lee, C. S. Kim, Y.-L. Loo, *Molecular Organic Electronics Devices*. Nova Science Publishers: Hauppauge, New York, NY, USA, **2010**; Chapter 4, pp. 109–152.

[4] G. Horowitz, *Adv. Matter* **1998**, *10*, 365–377.

[5] D. Braun, A. J. Heeger, *Appl. Phys. Lett.* **1991**, 58, 1982-1984.

[6] A. C. Grimsdale, K. L. Chan, R. E. Martin, P. G. Jokisch, A. B. Holmes, *Chem. Rev.* **2009**, 109, 897-1091.

[7] R. H. Friend, R. W. Gymer, A. B. Holmes, J. H. Burroughes, R. N. Marks, C. Taliani, D. D. C. Bradley, D. A. Dos Santos, J. L. Bredas, M. Lőgdlund, W. R. Salaneck, *Nature* **1999**, 397, 121-128.

[8] P. Cooreman, R. Thoelen, J. Manca, M. VandeVen, V. Vermeeren, L. Michiels, M. Ameloot, P. Wagner, *Biosens. Bioelectron*. **2005**, *20*, 2151–2156.

[9] Z. Matharu, S. K. Arya, S. P. Singh, V. Gupta, B. C. Malhotra, *Anal. Chim. Acta* **2009**, *634*, 243–249.

[10] I. Cosemans, J. Vandenbergh, V. S. D. Voet, K. Loos, L. Lutsen, D. Vanderzande, T. Junkers, *Polymer* **2013**, *54*, 1298-1304.

[11] I. Cosemans, J. Vandenbergh, V. S. D. Voet, K. Loos, L. Lutsen, D. Vanderzande, T. Junkers, *Polym. Chem.* **2013**, *4*, 3471-3479.

[12] I. Cosemans, J. Vandenbergh, V. S. D. Voet, K. Loos, L. Lutsen, D. Vanderzande, T. Junkers, *Eur. Polym. J.* **2014**, *55*, 114-122.

[13] A. Issaris, D. Vanderzande, J. Gelan, *Polymer* **1997**, *38*, 2571–2574.

[14] L. Hontis, V. Vrindts, L. Lutsen, D. Vanderzande, J. Gelan, *Polymer* **2001**, *42*, 5793–5796.

[15] L. Hontis, V. Vrindts, L. Lutsen, D. Vanderzande, *Macromolecules* **2003**, *36*, 3035–3044.

[16] J. Wiesecke, M. Rehanh, *Angew. Chem. Int. Ed*. **2003**, *42*, 567–570.

[17] Odian, G. *Principles of Polymerization*, 3rd ed.; John Wiley & Sons, Inc.: Hoboken, NY, USA, **1991**; p. 243.

[18] A. Issaris, *Ph.D. Thesis*, Limburgs Universitair Centrum, Hasselt and Diepenbeek, Belgium, **1997**.

[19] L. Hontis, *Ph.D. Thesis*, Limburgs Universitair Centrum, Hasselt and Diepenbeek, Belgium, **2002**.

[20] J. Vandenbergh, I. Cosemans, L. Lutsen, D. Vanderzande, T. Junkers, *Polym. Chem*. **2012**, *3*, 1722–1725.

[21] J. Vandenbergh, *PhD Thesis*, Hasselt University, Belgium, **2011**.

[22] F. Louwet, D. Vanderzande, J. Gelan, J. Mullens, *Macromolecules* **1995**, *28*, 1330–1331.

[23] F. Louwet, D. Vanderzande, J. Gelan, *Synth. Met*. **1995**, *69*, 509–510.

[24] A. Issaris, D. Vanderzande, P. Adriaensens, J. Gelan, *Macromolecules* **1998**, *31*, 4426–4431.

[25] A. Van Breemen, D. Vanderzande, P. Adriaensens, J. Gelan, *J. Org. Chem*. **1999**, *64*, 3106–3112.

[26] L. Lutsen, A. Van Breemen, W. Kreuder, D. Vanderzande, J. Gelan, *Helv. Chem. Acta* **2000**, *83*, 3113–3121.

[27] B. M. Rosen, V. Percec, *Chem. Rev*. **2009**, *109*, 5069–5119.

CHAPTER 3
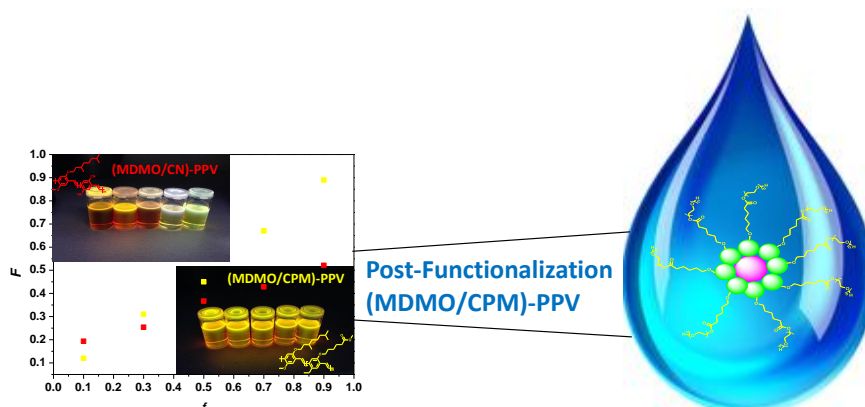
Modifiable Poly(*p*-Phenylene Vinylene) Copolymers Towards Functional Conjugated Materials

ABSTRACT

The copolymerization behavior of poly[2-methoxy-5-(3,7-dimethyloctyloxy)-p-phenylene vinylene] (MDMO-PPV) with poly[2-methoxy-5-(carboxypentyloxy)-p-phenylene vinylene] (CPM-PPV) and poly[2,5-dicyano-p-phenylene vinylene] (CN-PPV) in the anionic sulfinyl precursor route is studied and copolymerization parameters are determined. (MDMO/CPM)-PPV shows similar reactivity ratios for both monomers – $r_1 = 0.74 \pm 0.09$ and $r_2 = 0.90 \pm 0.10$ – when reactions were performed to almost full conversion (> 90 %). Kinetics of (MDMO/CN)-PPV on the other hand clearly indicate the preference to fully enrich the copolymer with MDMO as $r_1 = 0.65 \pm 0.16$ and $r_2 = 0.015 \pm 0.02$. Although deviations from the ideal behavior are observed for (MDMO/CN)-PPV, already a small amount of CN leads to significant difference in absorption and emission of the material, allowing to tune the color of the material. Further, post polymerization modification via transesterification of the CPM groups with poly(ethylene glycol) (PEG) or propargyl alcohol via the DCC/DMAP procedure leads to a versatile way of synthesizing a variety of (water soluble) PPV copolymers, without affecting the optical properties of the PPV materials. All reactions are carried out on the anionic polymerization pathway of the sulfinyl route, hence allowing to incorporate these polarity and wavelength tunable PPVs into more complex structures.

3.1. INTRODUCTION

Conjugated polymers have in the last two decades been a very active field of research, both in synthesis and in application of such materials. A broad variety of (semi) conducting polymer materials has to date been developed.[1-3] Due to their excellent optoelectronic characteristics, conjugated materials established a fortified position in electronic devices.[4-8] While many other conjugated polymers are likely also suitable for biomedical application, PPVs feature the additional advantage that tailor-made, high precision polymers are with this type of polymer accessible.[9] High structural and functional control is indispensable for controlled interaction with biological processes. Also, specifically end group functionalities are important to form block copolymer structures or to couple polymers to biomaterials – e.g. proteins or bio receptors.[10] So far, in almost all approaches to synthesize such advanced PPV-containing materials, no modification of the PPV backbone itself was performed, and the added functionality always stemmed from the non-conjugated polymer block, e.g. *tert*-butyl acrylate (*t*BuA) and methyl acrylate (MA)[11] or polyethylene glycol (PEG).[12] Ideally, a truly universal platform towards functional complex PPV materials would also allow to modify the conjugated part, with the aim for example solubility and/or the absorption/emission behavior. In principle, such aim can be achieved via post-functionalization approaches, or by copolymerization of different premonomers. First successful trials towards such a platform was already demonstrated in a proof of concept study by Duchateau *et al*,[13] in which a copolymer of poly[2-methoxy-5-(3,7-dimethyloctyloxy)-*p*-phenylene vinylene] ((MDMO)-PPV) and poly[2-methoxy-5-(carboxypentyloxy)-*p*-phenylene vinylene] ((CPM)-PPV) was

synthesized via the (non-controlled) radical precursor route in a 9 : 1 monomer ratio (Figure 3-1).
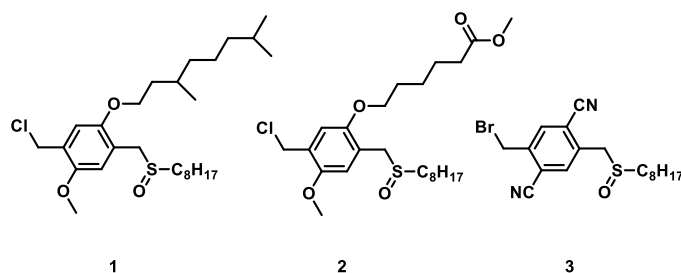
Figure 3-1: Chemical structure of MDMO-premonomer **1**, CPM-premonomer **2** and CN-premonomer **3**

The ester side chain in the (CPM)-PPV was then thereby available for transesterification reactions, and a variety of functional groups (e.g. vinyl, acrylates, initiator groups) could be built in in this manner. Since only a minority of 10% of ester side chains were present in the polymer, the (MDMO/CPM)-PPV copolymer remained soluble in common organic solvents like THF, $CHCl_3$ and CH_2Cl_2. In addition, a radical pathway was followed, leading to uncontrolled polymerization of the copolymers and high molecular weight materials with broad dispersities. Typically number average molecular weights (M_n) of 10^5 Da with a dispersity (Đ) of > 2.5 were obtained. Hence, while demonstrating efficiently how a broad variety of chemical functionalities could be introduced into the conjugated polymers, these materials were not yet ready for advanced applications, where also the ability for chain extension or water solubility would play a role (i.e. in biological systems).[14]

In here, we built on the method of Duchateau *et al.* and combine their approach with the superior controlled polymerization approaches developed in the meantime. Also, a closer look at copolymerization parameters has been taken to enable good predictability over copolymer contents. An in-depth study on the copolymerization behavior of (MDMO)-PPV with (CPM)-PPV is therefore provided. In a next step functionalization of the ester side chain via post polymerization reactions are demonstrated to induce water-solubility of the PPV segments. In addition, also (MDMO/CN)-PPV copolymers are targeted (where (CN)-PPV represents a n-type electron-deficient monomer), to provide tenability of the optical properties of the materials.

3.2. EXPERIMENTAL SECTION

3.2.1. Monomer Synthesis

3.2.1.1. Synthesis of monomer (1-(Chloromethyl)-5-((3,7-dimethyloctyl)oxy) -2-methoxy-4-((octylsulfinyl)methyl)benzene) (1) and monomer 6-(5-chloromethyl-4-methoxy-2-octylsulfinylmethyl phenoxy) hexanoic acid methyl ester (2)

Synthesis of monomer **1** and **2** was performed as already described in Chapter 2.

3.2.1.2. Synthesis of 1-bromomethyl-2,5-dicyano-4-[(octylsulfinyl) methyl]benzene (8)
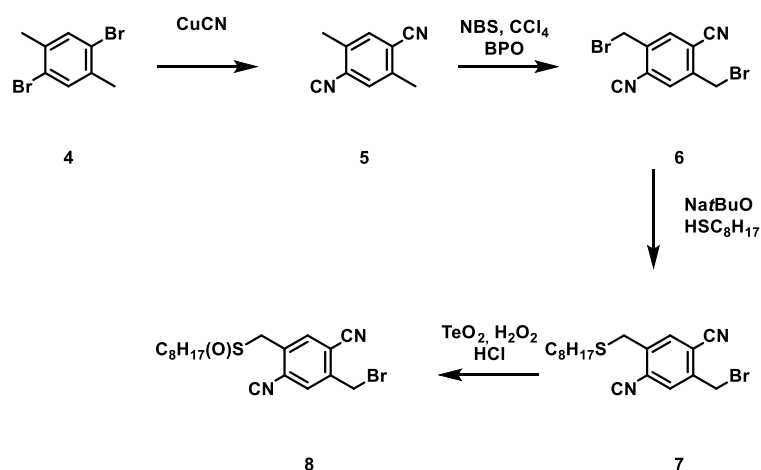
Scheme 3-1: Synthesis of 1-bromomethyl-2,5-dicyano-4-[(octylsulfinyl)methyl] benzene **8** (Cyano (CN) premonomer)

Compound **5** was synthesized by means of a substitution reaction with CuCN on **4**.[15;16] Crude product **5** could be purified via recrystallization in ethanol to obtain white needle-like crystals. After radical bromination of **5**, using NBS combined

with dibenzolyperoxide (BPO) as an initiator in CCl_4 as the solvent, compound **6** was reached and isolated as white crystals after crystallization from CCl_4 when cooling down the reaction mixture after filtration (to remove succinimide).[17] The last two steps of the synthesis were performed as described before for all other sulfinyl monomers.[18] Crude **8** was purified by means of two recrystallizations in EtOAc/petroleum ether (1/1) and obtained as white fluffy crystals (27.1%), Scheme 3-1.^{1}H-NMR ($CDCl_3$, 300MHz): δ (ppm) 7.94 (1H, s), 7.91 (1H, s), 4.61 (2H, s), 4.20 (2H, dd), 2.45 (2H, m), 1.26-1.57 (12H), 0.86 (3H, t). MS (EI, m/z, rel. int. (%)): 397 ([M]$^+$, 96), 317 ([M- Br]$^+$, 20). FT-IR (KBr): ν (cm^{-1}) 3034, 2918, 2852, 2225, 1741, 1496, 1469, 1417, 1297, 1215, 1188, 1021, 925, 721, 627.

3.2.2. Synthesis of anionic initiator
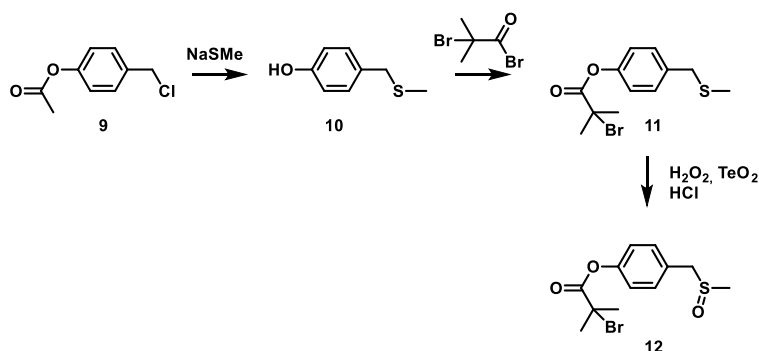
Scheme 3-2: Synthesis of functionalized anionic initiator **12**

To a mixture of NaSMe (21% in H_2O, 4.33 g, 12.97 mmol, 1 equiv.) in EtOH (8 mL), **9** (2.28 g, 12.36 mmol, 1 equiv.) was added while stirring and further stirred for 1 h at reflux temperature (80 °C). A solution of KOH (1.38 g, 24.72 mmol, 2 equiv.) in H_2O (50 mL) was added and again stirred for 1h at room temperature.

The solution was acidified with HCl (2M) to a pH~2. The solution was extracted with diethyl ether (3 x 100 mL) and the organic layer was dried over anhydrous MgSO$_4$. After filtration, evaporation of the solvent under reduced pressure gave the crude product as an orange oil. The pure product **10** was obtained by column chromatography (SiO$_2$, eluent CH$_2$Cl$_2$) as a colorless oil, Scheme 3-2 (1.04 g, 54.5 %). ^{1}H-NMR (CDCl$_3$): δ = 7.15 (d, J = 8.2 Hz, 2H); 6.76 (d, J = 8.5 Hz, 2H); 5.28 (s, 1H); 3.60 (s, 2H); 1.97 (s, 3H). ^{13}C-NMR (CDCl$_3$): δ = 150.3 (C4); 136.9 (C4) ; 130.7 (CH); 115.9 (C4); 38.3 (CH$_2$); 15.5 (CH$_3$).

2-bromo-2-methylpropanoylbromide (8.77 mmol, 1 mL) was added drop wise to a stirred mixture of **10** (1.04 g, 6.74 mmol, 1 equiv.), CH$_2$Cl$_2$ (50 mL) and pyridine (1 mL, 13.49 mmol, 1 equiv.) at 0 °C. The solution was stirred overnight at room temperature. The reaction was quenched with water (50 mL), extracted with CH$_2$Cl$_2$ (3 x 100 mL), dried over anhydrous MgSO$_4$ and filtered. Evaporation of the solvent under reduced pressure gave the crude product **11** as a yellow oil (2.51 g) and the product was used without further purification (Scheme 3-2). ^{1}H-NMR (CDCl$_3$): δ = 7.32 (d, J = 8.6 Hz, 2H); 7.06 (d, J = 8.6 Hz, 2H); 2.05 (s, 6H); 1.98 (s, 5H). ^{13}C-NMR (CDCl$_3$): δ = 170.2 (C4); 149.6 (C4); 136.2 (C4); 129.9 (CH); 121.0 (CH); 55.2 (C4); 37.5 (CH$_2$); 30.6 (CH3); 14.9 (CH3).

To a stirred mixture of **11** (2.51 g, 8.31 mmol, 1 equiv.) in 1,4-dioxane (50 mL), TeO$_2$ (0.26 g, 1.66 mmol, 1/8 equiv.) and HCl (2M, 0.40 mL) were added. To start the reaction H$_2$O$_2$ (35%; 1.42 mL, 16.62 mmol, 2 equiv.) was added. The reaction was followed on TLC (CHCl$_3$/petroleum ether; 6/4). As soon as all **11** was consumed, the reaction was quenched with a saturated NaCl-solution: H$_2$O (1:1; 50 mL). The solution was extracted with CH$_2$Cl$_2$ (3 x 100 mL), dried over

anhydrous $MgSO_4$ and filtered. Evaporation of the solvent under reduced pressure gave the crude product as a yellow oil. The pure product **12** was obtained by crystallization in hexane/EtOAc (3/1; 3 mL/1 g product) as white crystals, Scheme 3-2. (1.23 g, 31.23 %). Mp: 79 °C. ^{1}H-NMR (CDCl$_3$): δ = 7.33 (d, J = 8.2 Hz, 2H); 7.16 (d, J = 8.6 Hz, 2H); 2.46 (s, 2H); 2.05 (s, 6H). ^{13}C-NMR (CDCl$_3$): δ = 162.7 (C4); 143.5 (C4) ; 123.8 (CH); 120.2 (C4); 114.3 (CH); 51.9 (CH2); 47.8 (C4); 29.8 (CH3); 23.2 (CH3). DIP MS (CI, m/z): 319/321 (MH$^+$), 255/257 (M$^+$-S(O)Me). FT-IR (NaCl): ν (cm^{-1}) = 3005, 2977, 2925, 1751, 1504, 1464, 1267, 1210, 1035.

3.2.3. Anionic Polymerization
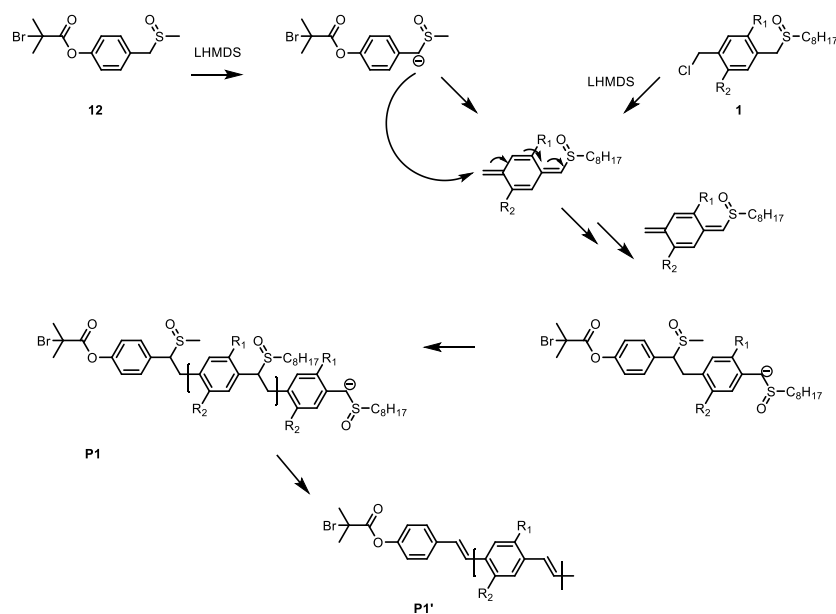
Scheme 3-3: General mechanism for the polymerization of PPVs via the anionic pathway using MDMO premonomer **1**

All glassware was dried overnight in a drying oven at 110 °C and flame-dried under vacuum. Monomer **1** (MDMO premonomer; 0.119 g, 0.25 mmol, 1 equiv.) (flushed 3 times with N_2 and vacuum) was dissolved in dry THF (4.67 mL) under N_2 atmosphere at 0°C. While stirring under N_2 atmosphere, LHMDS (1M in THF; 0.33 mL, 0.33 mmol, 1.3 equiv.) was added to start the reaction. After 15 minutes the reaction was quenched with HCl (37%; 0.2 mL) and the solution was poured into H_2O (10 mL). After extraction with CH_2Cl_2 (3 x 50 mL) and evaporation, the product was isolated as a bright yellow sticky oil. To eliminate the precursor polymer, toluene (10 mL) was added to **P1** and stirred for 3hrs under N_2 atmosphere at reflux temperature (110 °C). When cooled down to room temperature, the product was precipitated in cold MeOH (40 mL) and filtered on a Teflon® filter. The polymer **P1'** was obtained as a red powder. Procedure is similar for synthesis of polymer **2** (CPM premonomer) and **3** (CN premonomer).

Synthesis of (MDMO/CPM)- and (MDMO/CN)-PPV copolymers is performed following a similar procedure, enabling the presence of both monomers at the start of the polymerization using $[M]_t = 0.05$ M. Variations in time, temperature and concentration during the polymerization are individually checked keeping all other parameters constant.

3.2.4. Hydrolysis of (MDMO/CPM)-PPV

A solution of eliminated polymer **P2'** (0.06 g, 0.19 mmol ester functionalities) and dioxane (20 mL) was heated to reflux temperature after which a solution of KO*t*Bu (0.22 g, 1.94 mmol) in water (1 mL) was added at reflux temperature. After stirring at reflux temperature for 4 h, CH_2Cl_2 (150 mL) was added to the reaction mixture and extracted with 1M HCl-solution (100 mL). The organic layer was

evaporated under reduced pressure giving eliminated polymer **aP2'**. The resulting red copolymer was dried at room temperature under reduced pressure, Scheme 3-4. FT-IR (ATR): ν (cm^{-1}) 3502, 2960, 2930, 2857, 1733, 1500, 1460, 1413, 1383, 1356, 1258, 1205, 1094, 1030, 968, 860, 800.
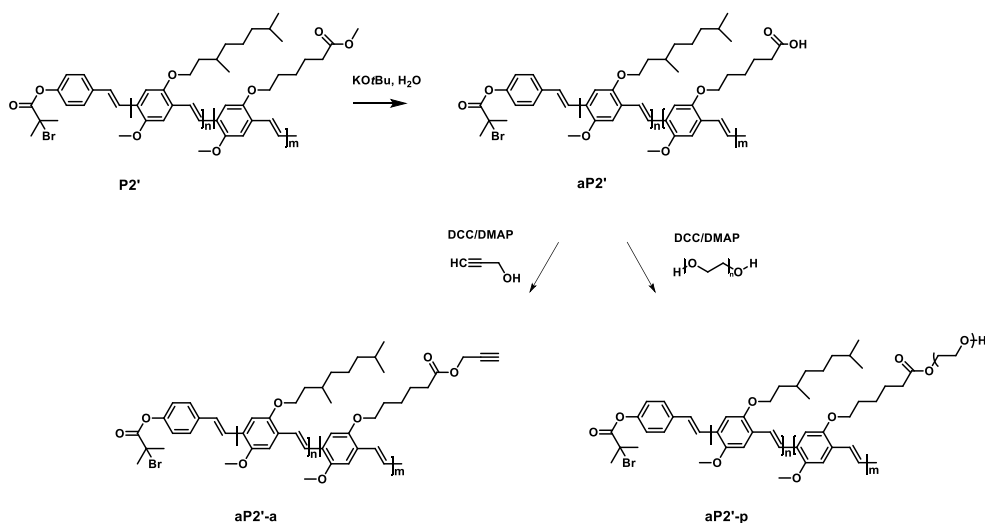
Scheme 3-4: General reaction scheme for the post-polymerization reactions of (MDMO/CPM)-PPV via the DCC/DMAP procedure, leading to an alkyne **aP2'–a** or polyethylene glycol (PEG) **aP2'–p** functionality in the side chain

3.2.5. Allyl ester of (MDMO/CPM)–PPV

(MDMO/CPM)-PPV **aP2'** (0.05 g, 0.16 mmol carboxylic acid functionalities) was dissolved in dry CH$_2$Cl$_2$ (12 mL) and cooled down to 0 °C. The alcohol-functionalized reagent, *i.e.* propargyl alcohol (11.4 µL, 0.19 mmol) and N,N'-dicyclohexylcarbodiimide (DCC) (0.04 g, 0.19 mmol) were added. Subsequently 4-N,N'-dimethylamino)pyridine (DMAP) (0.002 g, 0.19 mmol) in dry CH$_2$Cl$_2$ was added drop wise over a period of 15 minutes under N$_2$ atmosphere. The reaction

was allowed to proceed for 1 h at 0 °C and for an additional 24 h at room temperature after which the solution was precipitated drop wise in cold MeOH (200 mL). The resulting red copolymer was filtered off, washed with cold MeOH and dried at room temperature under reduced pressure, yielding a red fibrous polymer **aP2'–a** (63 %). SEC (THF) M_n^{app} = 11 400 g·mol^{-1}; Đ = 1.59. FT-IR (NaCl, cm^{-1}): ν (cm^{-1}) 3059, 2954, 2926, 2868, 1738, 1651, 1505, 1464, 1414, 1384, 1353, 1259, 1158, 1092, 1037, 968, 859. Depending on the MDMO : CPM ratio a different solvent was used to enable correct solubility of the starting PPV product. Copolymers containing a CPM content < 70 mole % were still soluble in common organic solvents like CH_2Cl_2, $CHCl_3$ or THF. 70 mole % or higher CPM contents were soluble in DMSO, DMF and water after hydrolysis of the ester side chain, Scheme 3-4.

3.2.6. Polyethylene glycol functionalized (MDMO/CPM)–PPV.

Copolymer **aP2'-p** was prepared following the DCC/DMAP procedure as described for copolymer **aP2'-a** using polyethylene glycol (PEG) (M_n = 2 000 g·mol^{-1} and M_n of 5 000 g·mol^{-1} respectively) (0.013g, 0.0065 mmol) as the functionalized reagent, yielding a red solid **aP2'-p** (87%), Scheme 3-4. SEC (THF) M_n^{app} = 5 600 g·mol^{-1}; Đ = 1.55. FT-IR (NaCl, cm^{-1}): ν (cm^{-1}) 3486, 2974, 2868, 1606, 1461, 1376, 1285, 1101, 1102, 956, 791, 758.

3.3. RESULTS AND DISCUSSION

3.3.1. Copolymerization of MDMO with CPM monomer

Over the past years a variety of PPV monomers have been applied to the sulfinyl precursor synthesis route. 1-chloromethyl-2-methoxy-5-(3,7-dimethyloctyloxy)-4-[(octylsulfinyl)methyl] benzene **1** (MDMO) is thereby one of the most commonly used PPV monomers. Full mechanistic studies towards its polymerization mechanism have been reported previously, and the radical as well as the anionic polymerization modes of these monomers are today well understood with respect to their potential, but also their specific limitations. Molecular weight of polymers from anionic polymerization is tunable via the initiator concentration, and well endgroup-functionalized polymers are usually obtained. Yet, the anion chain end is less stable compared to classical anionic polymerization and no isolation of the macroanion is feasible, also leading to homo- and block copolymer mixtures after sequential monomer addition.[12,13] The main drawback of this monomer and its accompanying polymer is the inability to functionalize the material in any way. As a result, an ester functionalized monomer – 6-(5-chloromethyl-4-methoxy-2-octylsulfinyl methyl phenoxy) hexanoic acid methyl ester **2** (CPM) – was developed, enabling functionalization reactions at both monomer as well as polymer level. In order to maintain 'standard' PPV characteristics as obtained when polymerizing pure (MDMO)-PPV – e.g. good microstructure and excellent optical properties – copolymers containing (MDMO)-PPV are synthesized using (CPM)-PPV as co-monomer (Figure 3-1).

To study the copolymerization of the two monomers in greater detail and to provide data that in the future can be used to predict copolymer compositions, a

variety of (MDMO/CPM)-PPV copolymers were synthesized under variation of the CPM premonomer feed with molar ratios between 0 % and 100 %. Thermal elimination towards conjugated PPV copolymers is performed in the second step, to enable full analysis of the conjugated copolymer products. Via this, the copolymerization behavior of (MDMO)-PPV with (CPM)-PPV is fully analyzed and copolymerization parameters are determined. For this aim, anionic polymerization reaction conditions are employed – which requires THF as solvent and LHMDS as base – and polymerizations were performed at 0 °C for 1 minute using a bromine-functionalized initiator. Previous studies clearly indicated the living behavior of the polymerization when using dedicated anionic initiators. This knowledge was extended to the monomers used in this research (Figure 3-2).
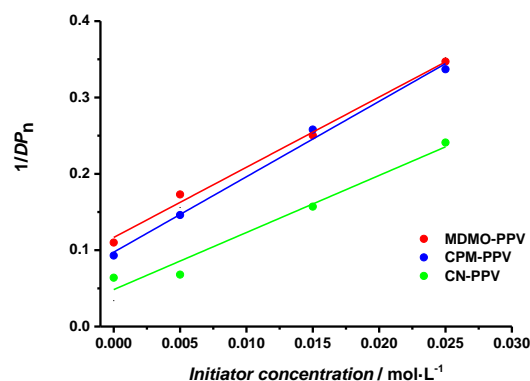
Figure 3-2: Inverse of degree of polymerization (precursor polymer) versus the initiator concentration for the anionic polymerization of different premonomers

Ideally, low conversions (< 5%) are needed to determine the copolymerization parameters. In this case, however, even very short reaction times (< 1 min)

results in almost full conversion (> 90%) due to the very fast reaction kinetics even at low temperatures (- 78 °C). Thus, care has to be taken upon the determination of the copolymer parameters due to the unavoidable composition drift in the feed ratios occurring during the reaction. The results presented are thus integrated copolymerization parameters rather than true kinetic parameter ratios. Nevertheless, as premature stopping of these polymerizations is almost impossible, the herein presented data is of high practical value. Still, so far no research towards the copolymerization kinetics in PPV systems had been performed, hence any kinetic knowledge is of great value for future synthesis of complex functional molecular structures in any way.

Table 3-1: Results of eliminated (MDMO/CPM)-PPV copolymers based on the mol % of CPM build in in the polymer chain

[CPM] : [MDMO]	M_n g·mol^{-1}	M_w g·mol^{-1}	Đ	F_{CPM} %	λ_{max_abs} nm	λ_{max_em} nm
0 : 100	8 900	13 800	1.5	0	495	585
10 : 90	9 000	11 100	1.2	11	496	584
30 : 70	7 500	10 200	1.3	23	495	584
50 : 50	7 300	9 900	1.3	56	496	584
70 : 30	6 800	8 400	1.2	67	497	583
90 : 10	7 100	8 800	1.2	88	496	584
100 : 0	7 500	12 900	1.4	100	495	583
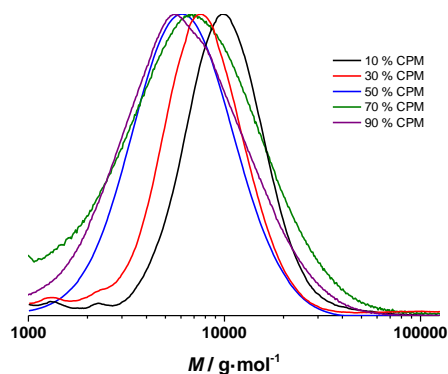
Figure 3-3: SEC chromatogram of (MDMO/CPM)-PPV copolymer upon varying the amount of (CPM)-PPV built in

The results from the copolymerizations are summarized in Table 3-1. SEC analysis of the obtained conjugated copolymers (Figure 3-3) indicate successful polymer formation with good livingness, reaching molecular weights (M_n) between 6 000 g·mol^{-1} and 9 000 g·mol^{-1} and low dispersity ($Đ$) values (< 1.5). It must be noted that all data given in Table 3-1 is associated with a certain error with respect to M_n, M_w and $Đ$ value, as no precise Mark Houwink (MKHS) parameters for the different copolymers were available and analysis was based on homo-MDMO-PPV parameters. Unfortunately end group analysis via ^{1}H NMR is not easily feasible for the determination of molecular weights with the present initiator used. As the chemical structure of both MDMO as well as CPM are similar no large deviation is, however expected when using SEC to determine molecular weights. This statement can be confirmed by further analyzing all copolymers on their optical properties. UV-Vis and fluorescent results indicate the expected absorption at approximately 500 nm and emission at 584 nm respectively, values similar to the ones obtained when pure conjugated MDMO-PPV was synthesized. Full

conjugation was confirmed by ^{1}H NMR results as well, due to the clear absence of the sulfinyl peak at 2.55 ppm. The built in content of CPM-PPV obviously does not seem to influence the optical properties of the resulting copolymers, as is also visually observed when shining UV light on the different products dissolved in chloroform, see Figure 3-6 below. In addition, FT-IR results show the characteristic *C=O* vibration band at 1736 cm^{-1} when CPM-PPV is built in, even in small quantities (10%) all indicating the successful copolymerization of MDMO-PPV with CPM-PPV.

As a last step, the actual copolymer content of (CPM)-PPV is determined via ^{1}H NMR, in which the signals at 0.99 ppm are assigned to the *CHCH$_3$* groups of the (MDMO)-PPV part of the copolymer. The triplet occurring at 2.35 ppm in the ^{1}H NMR spectra originates from the *CH$_2$COOCH$_3$* in the ester part of the (CPM)-PPV copolymer. Based on these two signals, the actual ratio of [CPM] : [MDMO] can be determined, leading to a fairly good resemblance between the theoretical and experimental built in of CPM co-monomer (Table 3-1). Upon the copolymerization of 10 % to 90 % of CPM co-monomer, an actual copolymer content of 11 % to 88% is obtained and thus copolymer compositions are in good agreement with the feed-ratio, indicating close to ideal copolymerization. With these actual feed-ratio values, the reactivity ratios (r_1 and r_2) can be determined in which

$$r_1 = \frac{k_{p,MDMO-MDMO}}{k_{p,MDMO-Co}} \; and \; r_2 = \frac{k_{p,Co-Co}}{k_{p,Co-MDMO}} \tag{1}$$

$k_{p,MDMO-MDMO}$ and $k_{p,Co-Co}$ denote the homopropagation rate coefficients and $k_{p,MDMO-Co}$ and $k_{p,Co-MDMO}$ denote the crosspropagation rate coefficients, with the

abbreviation *Co* referring to the co-monomer used, CPM in this specific case. As denoted, very high conversions are easily reached when following the anionic precursor route. The monomer feed (f_{Co} and f_{MDMO}) and copolymer composition (F_{Co}) were used to calculate the actual r_1 and r_2 values (terminal model) by fitting the Mayo-Lewis equation (2) to the data, see Figure 3-4.

$$F_{CPM} = \frac{r_2 f_{Co}^2 + f_{Co} f_{MDMO}}{r_2 f_{Co}^2 + 2 f_{Co} f_{MDMO} + r_1 f_{MDMO}^2} \tag{2}$$

Ideally, a straight line in the Mayo-Lewis plot is obtained when both monomers possess identical reactivity toward both propagating species. A slight non-linear behavior is obtained, though, with a reactivity ratio for MDMO of $r_1 = 0.74 \pm 0.08$ and for CPM of $r_2 = 0.90 \pm 0.09$, respectively. This represents only a small deviation from ideal polymerization, which is within expectations taking into account that both monomers are of very similar chemical nature.

Figure 3-4: Polymer composition as a function of co-monomer feed composition for copolymerizing (CPM)-PPV with (MDMO)-PPV

3.3.2. Copolymerization of MDMO with CN monomer

More interesting – from the viewpoint of obtainable physical characteristics and copolymerization kinetics – is to study a copolymerization pair in which the generated anions are substantially different in their anion stabilization. Therefore, also the copolymerization of MDMO monomer with 1-bromomethyl-2,5-dicyano-4-[(octylsulfinyl)methyl] benzene **3** ((CN)-monomer) was investigated. (CN)-monomer contains two electron withdrawing cyano groups attached to the phenyl core, leading to more n-type semiconductor properties and very different optical properties of the polymer as compared to the use of (MDMO)- or (CPM)-PPV polymers. To date, the polymerization of (CN)-monomer is only superficially studied and no information on its ability to polymerize in the anionic sulfinyl precursor route is given, let alone its ability to copolymerize with the more conventional sulfinyl route monomers. Therefore, (CN)-monomer is used as co-monomer and polymerized with (MDMO)-monomer, leading to statistical (MDMO/CN)-PPV copolymers. As for the MDMO/CPM pair, a variety of (MDMO/CN)-PPV copolymers were synthesized via the anionic sulfinyl precursor route with feed ratios between 0% and 100%. Despite the limited kinetic information available for (CN)-PPV, the monomers are believed to behave relatively similar to (MDMO)-monomer, at least with respect to the polymerization mechanism. Hence, similar reaction conditions as used for the (MDMO/CPM)-PPV polymerizations were employed – polymerization in THF using LHMDS as base at 0 °C for 1 minute – using a bromine-functionalized initiator, as given in Table 3-2 and Figure 3-5.

Table 3-2: Results of eliminated (MDMO/CN)-PPV copolymers based on the mol % of CN build in in the polymer chain

[CN] : [MDMO]	M_n^{app} g·mol^{-1}	M_w^{app} g·mol^{-1}	Đ	F_{CN} %	λ_{max_abs} nm	λ_{max_em} nm
0 : 100	10 500	14 200	1.4	0	489	586
10 : 90	11 400	19 800	1.7	17	472	551
30 : 70	8 300	15 700	1.6	26	471	551
50 : 50	3 800	7 400	1.9	37	425	551
70 : 30	3 600	5 700	1.6	47	403	552
90 : 10	4 500	8 100	1.8	52	401	552
100 : 0	2 200	4 400	2.0	100	400	552
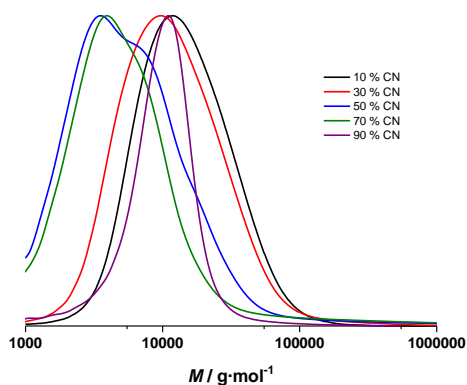
Figure 3-5: SEC chromatogram of (MDMO/CN)-PPV copolymer upon varying the amount of (CN)-PPV built in

SEC analysis of the resulting copolymers (Figure 3-5) again indicate that this assumption was correct, as successful polymer formation is observed, reaching molecular weights between 3 800 g·mol^{-1} and 11 000 g·mol^{-1} and somewhat

higher dispersity (< 2.0) indicating a slightly decreased control over the polymerization. This behavior was generally already observed in previous research upon polymerizing (CN)-PPV as homopolymer.[19] In addition, a comparison of the molecular weights and its accompanying dispersities between SEC and MALLS measurements, indicates the over estimation of the SEC, as dispersities obtained via MALLS measurements all show values below 1.5, underpinning the living behavior of PPV monomers via the anionic sulfinyl route using dedicated anionic initiators.[13] Further UV-Vis and fluorescent results indicate the considerable influence of the inclusion of the (CN)-monomer, see Figure 3-6. Upon 10 % (CN)-monomer feed, a decrease in absorption from 489 nm to 472 nm is seen. A further increase in (CN)-monomer feed up to 90 % results in absorption values of 400 nm with an accompanying emission of 551 nm. These values directly demonstrate the influence of even a small percentage of (CN) monomer on the final optical properties of the (MDMO/CN)-PPV copolymer. This can easily be visualized when shining UV light on the different materials – again Figure 3-6– in which the color changes from red / orange to yellow / green with increasing CN content. Such variation in color is of high significance, especially when considering the use of such copolymers in bioimaging, since the absorption and emission wavelength can be tuned in this way in an easy and very accessible manner. It should be noted that the low molecular weights may in principle indicate that chains have not reached full conjugation length, yet the clear trend in absorption and emission peak wavelengths indicate that the length reached is most likely sufficient.
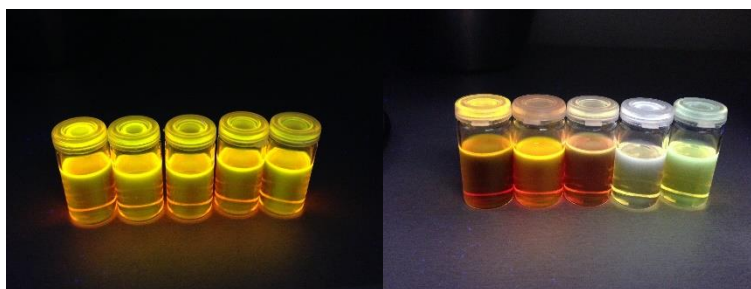
Figure 3-6: Copolymers dissolved in chloroform as observed under UV radiation (λ = 365 nm); *left*: (MDMO/CPM)-PPV with increasing (CPM)-content from left to right. *right*: (MDMO/CN)-PPV with increasing (CN)-content from left to right

All analysis results as displayed in Table 3-2 indicate the successful built-in of cyano groups into the (MDMO/CN)-PPV copolymer. Again, copolymerization parameters for the monomer pair were determined by ^{1}H NMR analysis of the copolymer content. Assigning different proton signals to both polymers is challenging in this case, as CN-PPV is only associated with aromatic proton shifts, which in turn are also present in the MDMO premonomer. Thus, the integration of the *OCH$_3$* protons signal of the MDMO part at 3.9 ppm was fixed at three protons, after which the aromatic signals were integrated accordingly. For these aromatic signals, it was assumed that in total 2 protons are originating from (MDMO)-PPV, leaving the remaining signals left for the (CN)-PPV part. Although a small error is made in this way upon interpretation of the aromatic signals, the error is similar to all copolymers synthesized enabling comparison of the products.
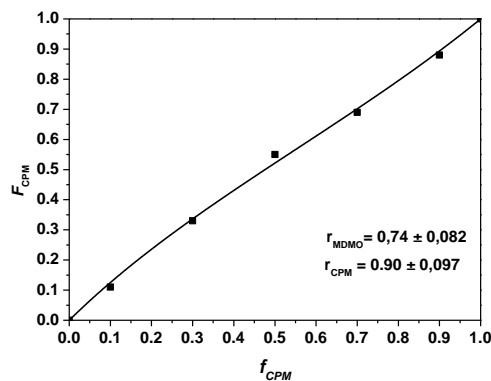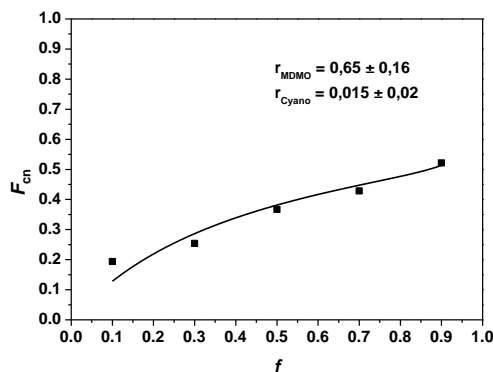
Figure 3-7: Polymer composition as a function of co-monomer feed composition for copolymerizing (CN)-PPV with (MDMO)-PPV

Results indicate a significant deviation from ideal behavior as for a 50 : 50 ratio of [CN] : [MDMO] only 37 % of CN is built in. Upon increasing the (CN)-content even more deviation from ideal behavior is seen, leading to a maximum built-in of 52 % of (CN)-groups. With these actual feed-ratio values, the reactivity ratios (r_1 and r_2) can be determined according to formula (1). As explained already for (MDMO/CPM)-PPV, the values for r_1 and r_2 will be affected to the unavoidable composition drift. Reactivity ratios for MDMO of $r_1 = 0.65 \pm 0.16$ and for CN of $r_2 = 0.015 \pm 0.02$, respectively, were obtained, showing a clear tendency for (MDMO)-monomer to propagate while (CN)-monomer termini are relatively unreactive towards the (CN)-monomer, leading to enrichment of the copolymer with (MDMO)-PPV (Figure 3-7). Only upon depletion of (MDMO)-monomer, (CN)-monomer is copolymerized and one can expect that at low overall monomer conversion an even smaller fraction of (CN)-monomer will be found than is indicated by the high-conversion data discussed herein. Still, as indicated above,

this relatively small amount of (CN)-PPV in the copolymer is enough to change the optical properties significantly.

3.3.3. Post-functionalization of Copolymers

The fundamental kinetic study described above helps tremendously to predict the outcome of the copolymerizations. As (MDMO/CPM) shows almost ideal behavior, it can be expected that the (CPM/CN) pair will not show much deviation from the (MDMO/CN) mixtures. In the following, a focus is now set at the ability to post-functionalize (CPM)-PPV copolymers. A prerequisite to use PPV polymers for example for bioimaging is the ability to function in an aqueous environment, which current PPV synthesis methods do not support. Previously, (MDMO/CPM)-PPV with a 9 : 1 feed ratio of MDMO to CPM had been synthesized and was functionalized via transesterification. Based on these preliminary results and in combination with newly obtained kinetic data – this approach was now extended towards different MDMO : CPM ratios. As in the kinetic studies, (MDMO/CPM)-PPV copolymer synthesis was performed via the anionic precursor route using a bromine-initiator to control the reaction, after which the polymers undergo thermal elimination leading to conjugated copolymers, see Figure 3-8 (**P2'**).
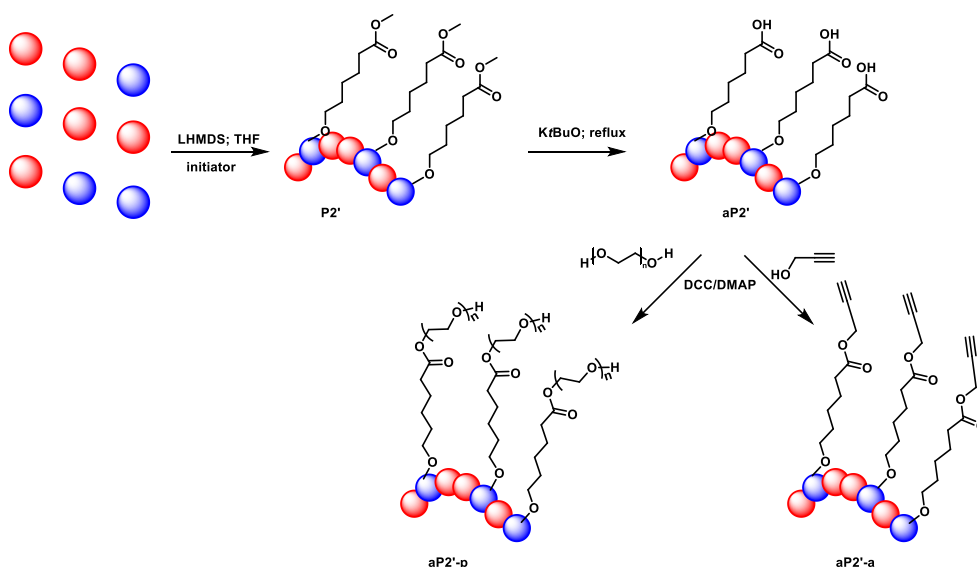
Figure 3-8: Schematic overview of the anionic polymerization of (MDMO/CPM)-PPV copolymers (**P2'**) and the accompanying post-functionalization reactions using the DCC/DMAP procedure leading to a PEG (**aP2'-p**) or alkyne (**aP2'-a**) functionality in the side chain

This approach yields polymers that are in principle available for further chain extension in SET-LRP reactions, as we had demonstrated before.[11;12] The (CPM)-monomer feed ratios were carefully chosen, to result in the 5 [MDMO] : [CPM] copolymer composition ratios as given in Table 3-3. Without any further change of the copolymers, all materials obtained were hydrophobic and only soluble in apolar media. To increase polarity, the ester side chains of the CPM units were hydrolyzed to carboxylic acid functionalities (**aP2'**), followed by esterification with hydroxyl-terminated poly(ethylene glycol) (PEG) in an optimized DCC/DMAP procedure – to obtain a PEG-graft copolymers (**aP2'-p**). Ideally, water soluble (MDMO/CPM)-PPV copolymers could in this way be synthesized. PEG with a molecular weight of 2 000 g·mol^{-1} (PEG-2000) and 5 000 g·mol^{-1} (PEG-5000) was

attached to the copolymers, to verify the influence of the chain length on the solubility of the materials. Results regarding molecular weight, dispersity and absorption of the different starting and functionalized copolymers can be found in Table 3-3.

Table 3-3: Results of PEG-functionalized eliminated (MDMO/CPM)-PPV copolymers using either a PEG chain with M_n = 2 000 g·mol^{-1} (PEG-2000) or M_n = 5 000 g·mol^{-1} (PEG-5000)

Functionality Side chain	[CPM] : [MDMO]	$M_n{}^{app}$ g·mol^{-1}	$M_w{}^{app}$ g·mol^{-1}	Đ	λ_{max_abs} nm	Solubility
Ester		7 300	9 900	1.35	496	CHCl$_3$, toluene
PEG-2000	11 : 89	5 600	8 800	1.55	479	CHCl$_3$, toluene
PEG-5000		4 400	7 200	1.60	477	CHCl$_3$, toluene
Ester		8 200	10 600	1.30	495	CHCl$_3$, toluene
PEG-2000	23 : 77	6 500	10 500	1.62	477	THF
PEG-5000		5 800	8 900	1.53	475	THF
Ester		9 000	11 400	1.22	496	CHCl$_3$, toluene
PEG-2000	56 : 44	7 800	12 300	1.70	476	THF, DMF, DMSO
PEG-5000		6 900	13 400	1.90	476	THF, DMF, DMSO
Ester		6 900	8 500	1.25	497	CHCl$_3$, toluene
PEG-2000	67 : 33	n.a.	n.a.	n.a.	473	Water, DMSO, DMF
PEG-5000		n.a.	n.a.	n.a.	472	Water, DMSO, DMF
Ester		7 000	8 700	1.23	495	CHCl$_3$, toluene
PEG-2000	88 : 12	n.a.	n.a.	n.a.	471	Water, DMSO, DMF
PEG-5000		n.a.	n.a.	n.a.	471	Water, DMSO, DMF

It is evident from Table 3-3 that the polarity of the obtained polymers increases with attachment of the PEG chains, and obviously also with the original (CPM)-PPV content. The higher the number of ester groups in the polymer, the more PEG can be grafted, resulting in polymers with the highest original CPM content to become water soluble. Yet, apparent number average molecular weights for the functionalized copolymers (up to 50 mole % CPM content) are lower than the starting copolymers. These differences occur because of shifts in hydrodynamic volumes (synthesis with stiff PPV backbone and flexible PEG side chains) and measurements towards polystyrene standards with (MDMO)-PPV MKHS-parameters, which necessarily gives erroneous results. Typical molecular weights for the conjugated materials of 7 300 g·mol^{-1} with $Đ = 1.35$ show a M_n of 5 600 g·mol^{-1} with $Đ = 1.55$ or 4 400 g·mol^{-1} with $Đ = 1.60$ when grafting either PEG-2000 or PEG-5000 to the backbone. The PEG chains are expected to wrap tightly around the PPV backbone, resulting in less interaction between the different chain segments of the same chain (PPV vs. PEG) and hence reduced hydrodynamic volume. As a result, lower molecular weights are observed with a general decrease of roughly 15 % in apparent molecular weight for all copolymers. This behavior is even more pronounced when longer PEG chains (PEG-5000) are attached to the side chain. In addition, higher dispersities are obtained upon post functionalization with PEG, which is even more visible when higher (CPM)-contents – and thus higher PEG content – was realized. It should be further noted that no weight analysis could be performed on the hydrolyzed (CPM)-PPV copolymers, as the residual materials were only soluble in water, and hence not suitable for conventional SEC analysis. Solubility of the materials in non-aqueous solution is thus indicative of successful PEG grafting, despite the apparent lowering of the average molecular weights.

To further verify successful grafting, UV-Vis, FT-IR and ^{1}H NMR analysis was performed on all materials, with results being collated in Table 3-3 and Figure 3-9 (only [MDMO] : [CPM] of 30 : 70 was taken into account). UV Vis results clearly indicate a small shift in maximum wavelength upon attaching PEG to the side chain from the typical 497 nm to 473 nm and 472 nm when attaching a PEG-2000 or PEG-5000 respectively. This indicates that not only is it possible to synthesize water soluble PPVs in this manner, but also all optical PPV characteristics – absorption and emission – are still intact.
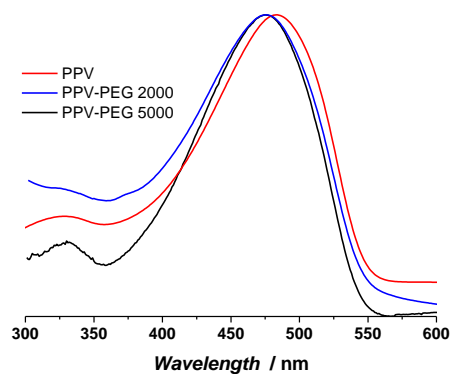
Figure 3-9: UV-VIS spectra for (MDMO/CPM)-PPV (*red line*) functionalized with a PEG-2000 (blue line) or PEG-5000 (*black line*)

FT-IR and ^{1}H NMR results on the other hand did not proof the presence of the PEG chains, due to an overlap between the signals of the CPM co-monomer with the PEG signals in both analysis techniques. Since further proof was required, grafting of propargyl alcohol to the copolymers was carried out instead of PEG attachment, in order to obtain an alkyne functionality in the side chain (**aP2'–a**) that is clearly distinguishable from the backbone peaks – and which is concomitantly also useful

as clickable groups for further synthesis approaches. Propargyl alcohol grafting was performed under similar reaction conditions as used for the PEG functionalization. Results regarding molecular weight, dispersity and absorbance of the different starting and functionalized copolymers can be found in Table 3-4 and Figure 3-10.

Table 3-4: Results of the alkyne-functionalized eliminated (MDMO/CPM)-PPV copolymers using a theoretical [CPM] : [MDMO] ratio of 70 : 30 and 90 : 10

Functionality Side chain	[CPM] : [MDMO]	M_n^{app} g·mol⁻¹	M_w^{app} g·mol⁻¹	Đ	λ_{max_abs} nm
Ester		13 600	22 700	1.7	497
Propargyl alcohol	67 : 33	11 200	17 800	1.6	481
Ester		12 100	23 200	1.9	495
Propargyl alcohol	88 : 12	10 400	19 900	1.9	478

Results displayed in Table 3-4 clearly show the same trends with respect to molecular weight as described above. Lower molecular weights are observed when the copolymers are functionalized with propargyl alcohol. Dispersity values on the other hand are in the same range. In addition, UV-Vis results show a small blue shift in the maximum absorbance upon functionalization of the copolymers. Again, this is only a minor shift and thus the conjugation of PPV materials is almost not affected. FT-IR and ^{1}H NMR analysis on the other hand do show the presence of the alkyne functionality in the materials after functionalization. FT-IR results clearly display the appearance of the $C{\equiv}N$ stretch vibration around 2260 cm⁻¹ and

the -$C{\equiv}C$-H bend vibration around 688 cm^{-1} in combination with the disappearance of the O-H stretch vibration around 3400 cm^{-1}.
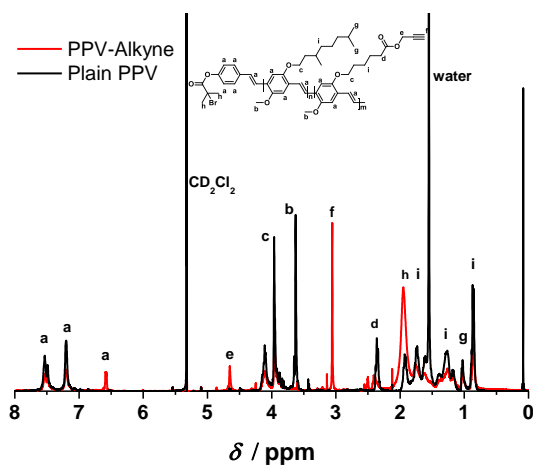
Figure 3-10: ^{1}H NMR results on (MDMO/CPM)-PPV(*red line*) functionalized with propargyl alcohol (*black line*)

In addition, ^{1}H NMR shows the appearance of the -$C{\equiv}C$-H proton at 4.6 ppm and the $-CH_2$-$C{\equiv}C$- protons at 3.1 ppm, Figure 3-10. These alkyne signals were compared with the -CH_2-$C(O)O$- signal of ester side chain, leading to an average post functionalization with propargyl alcohol of 77 %. Similar values were obtained when either a ratio of [MDMO] : [CPM] of 30 : 70 or 10 : 90 for the (MDMO/CPM)-PPV copolymer were used.

3.4. CONCLUSION

A general method for synthesizing well-defined and functional PPV copolymers to be used in an biological environment was developed. (MDMO/CPM)-PPV and (MDMO/CN)-PPV copolymers were synthesized via the anionic sulfinyl route, thereby enabling control – with respect to molecular weight – over the synthesis via the addition of an anionic initiator. In order to reach precision design of different PPV copolymers, a better understanding of its underlying copolymerization kinetics was needed. An in-depth study on the copolymerization behavior of (MDMO)-PPV with (CPM)-PPV was performed by synthesizing (MDMO/CPM)-PPV copolymers with a varying feed of CPM co-monomer (0 mol % to 100 mol %). Results on the copolymer – SEC, UV-VIS and fluorescence – indicate similar characteristics for the different copolymers synthesized. By fitting the Mayo-Lewis equation to the copolymer composition data, similar reactivity ratio's for both monomers are obtained – $r_1 = 0.74 \pm 0.08$ and $r_2 = 0.90 \pm 0.09$ – for reactions performed up to almost full conversion (> 90 %). In addition, also (MDMO/CN)-PPV copolymers were targeted, as materials with different (optical) properties can be obtained when cyano-groups are built-in in the phenyl core. A significant influence on the absorption spectra of the materials was observed, especially upon increasing CN content. PPV copolymers with different color and absorption profile are in this way available in a facile manner. A closer look into (MDMO/CN)-PPV showed completely different reaction kinetics, with $r_1 = 0.65 \pm 0.16$ and $r_2 = 0.015 \pm 0.02$.

In a next step functionalization of the ester side chain via post polymerization procedures led to the synthesis of materials with fine-tunable polarity, by grafting PEG chains to the PPV backbones, without affecting the conjugation length of the

PPV materials. Under retention of the essential optoelectronic characteristics of the PPV, up to 77 % of the functionalized side groups in the polymer could be trans esterified and water soluble (MDMO)-PPV became accessible.

Thus, the anionic sulfinyl precursor route – to date proven to be an efficient tool for the synthesis of complex polymers containing PPV segments – was shown to be also highly suitable to synthesize polymers with tunable polarity. By knowledge of the detailed copolymerization kinetics, the exact content of polar groups can be pre-determined, and also the absorption and emission behavior of the PPVs can be altered on purpose. The combination of these three aspects – controllability of the polymerization, tunability of the optical spectra, and adjustability of polarity opens new avenues in use of PPV materials in a biomedical context, with respect to bioimaging, drug delivery or other applications.

3.5. REFERENCES

[1] A. J. Berresheim, M. Müller and K. Müllen, *Chem. Rev*. **1999**, *99*, 1747-1786.

[2] J. Roncali, *Chem. Rev*. **1992**, *92*, 711-738.

[3] U. Scherf and E. J. W. List, *Adv. Mater*. 2002, *14*, 477-487.

[4] D. Braun, A. J. Heeger, *Appl. Phys. Lett.* **1991**, *58*, 1982-1982.

[5] R. H. Friend, R. W. Gymer, A. B. Holmes, J. H. Burroughes, R. N. Marks, C. Taliani, D. D. C Bradley, D. A. Dos Santos, J. L. Bredas, M. Lőgdlund, W. R. Salaneck, *Nature* **1999**, *397*, 121-128.

[6] S. Günes, H. Neugebauer, N. S. Sariciftci, *Chem. Rev.* **2007**, *107*, 1324-1338.

[7] G. Horrowitz, *Adv. Mater.* **1998**, *10*, 365-377.

[8] A. C. Grimsdale, K. L. Chan, R. E. Martin, P. G. Jokisch, A. B. Holmes, *Chem. Rev.* **2009**, *109*, 897-1091.

[9] J. H. Burroughes, D. D. C Bradley, A. R. Brown, R. N. Marks, R. H. Friend, A. B. Holmes, *Nature* **1990**, *347*, 539-541.

[10] J. Wiesecke, M. Rehanh, *Angew. Chem. Int. Ed.* **2003**, *42*, 567-570.

[11] I. Cosemans, J. Vandenbergh, L. Lutsen, D. Vanderzande, T. Junkers, *Polym. Chem.* **2013**, *4*, 3471-3479.

[12] I. Cosemans, J. Vandenbergh, L. Lutsen, D. Vanderzande, T. Junkers, *Eur. Polym. J.* **2014**, *55*, 114-122.

[13] J. Duchateau, L. Lutsen, W. Guedens, T. C. Cleij, D. Vanderzande, *Polym. Chem*, **2010**, *1*, 1313-1322.

[14] M. Peters, N. Zaquen, L. D'Olieslager, H. Bové, D. Vanderzande, N. Hellings, T. Junkers, A. Ethirajan, *Biomacromolecules*, **2016**, submitted.

[15] L. Friedman, H. Shechter, *J. Org. Chem.* **1961**, *26*, 2522-2524.

[16] G. P. Ellis, T. M. Romney-Alexander, *Chem. Rev.* **1987**, *87*, 779-794.

[17] R. K. McCoy, F. E. Karasz, *Chem. Mater.* **1991**, *3*, 941-947.

[18] I. Cosemans, J. Wouters, T. Cleij, L. Lutsen, W. Maes, T. Junkers, D. Vanderzande, *Macromol. Rapid Commun.* **2012**, *33*, 742-752.

[19] J. Sun, L. P. Sanow, S.-S. Sun, C. Zhang, *Macromolecules* **2013**, *46*, 4247-4254.

CHAPTER 4

Non-crosslinked Profluorescent PPV-based Micellar System as a Versatile Theranostics Probe
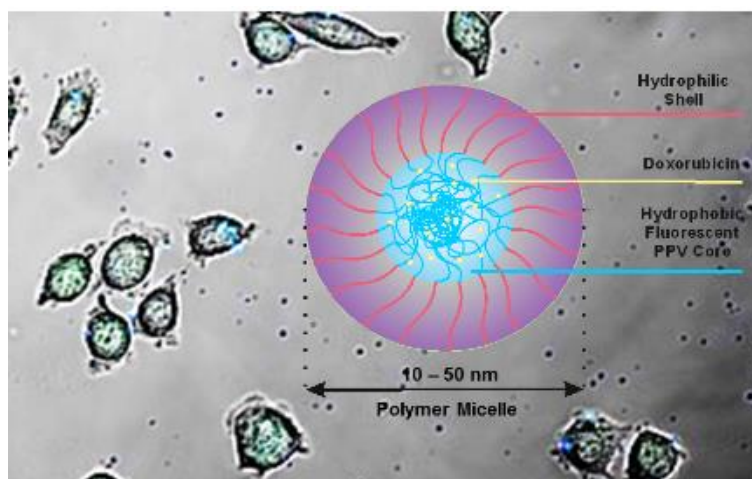
N. Zaquen, H. Lu,[*] T. Chang,[*] R. Mamdooh,[*] L. Lutsen, D. Vanderzande, M. Stenzel,[*] T. Junkers, *Chem. Sci.* **2016**, submitted.

[*]Collaboration with the University of New South Wales, Sydney (Australia)

ABSTRACT

Micelles are commonly used for drug delivery purposes. However, their long-term fate is often unknown since common fluorescent labels that allow monitoring the movement of micelles using fluorescent microscopy are subject to photo-bleaching. Other labels such as quantum dots require the use of metals and are therefore mainly used for scientific purposes. Here, we present a metal-free non-toxic non-bleaching fluorescent micelle that can address these shortcomings. A simple, yet versatile profluorescent micellar system – built from amphiphilic poly(*p*-phenylene vinylene) (PPV) block copolymers – for use in drug delivery applications is introduced. Polymer micelles made from PPV material – fluorescent as block copolymer but non-fluorescent when assembled – show excellent stability for up to 1 year and are successfully loaded with anti-cancer drugs (curcumin or doxorubicin) without requiring introduction of physical or chemical crosslinks. The micelles are taken up efficiently by the cells, which triggers disassembly, releasing the encapsulated material. Disassembly of the micelles and drug release is conveniently monitored as fluorescence of the single polymer chains appear

4.1. INTRODUCTION

Synthesis and characterization towards conjugated polymers has seen significant improvement over the last years, leading to a variety of complex polymer materials of different chemical nature and architecture.[1] The most significant area of their application is organic electronics[2-4] – due to their usually excellent optoelectronic characteristics – with poly(*p*-phenylene vinylene)s (PPV)s as one of the best studied type of material.[5] Although mostly replaced nowadays by other polymers in the field of organic electronics,[6] PPVs show still excellent fluorescent properties, high reproducibility and non-toxic behavior, making them ideal candidates for bioimaging and drug delivery applications.[7]

Over the years, many synthesis routes were developed towards tailor-made PPVs, with the so-called sulfinyl precursor route as one of the most versatile pathways to obtain conjugated PPVs in a two-step mechanism.[8] Upon carefully chosen reaction conditions, a fully anionic (and hence living) mechanism can be accessed with the sulfinyl route.[9] Combined with the use of dual initiator approaches, well-defined PPV block copolymers of various types can be synthesized. The *alpha*-end group of the initiator is easily functionalized, and the combination with single electron transfer living radical polymerization (SET-LRP)[10] chain extensions has proven to be a very promising synthesis pathway.[11] Depending on the chemical structure of the co-monomers, amphiphilic block copolymers that form micellar structures may be obtained. Micellar systems based on non-fluorescent polymers are widely used for example for drug delivery applications, in which the addition of a fluorophore is needed to enable visualization by high-contrast fluorescent imaging.[12] Nowadays, either fluorescent dyes – which show signs of bleaching – or the use of imaging agents such as toxic quantum dots are needed to monitor

the micelles, yet conjugated polymers are surprisingly to date not directly used for this purpose.[13] Still, little is known about the fate of the micelles over a longer period of time, as well as their pathway and disassembly mechanism in the cells. In addition, many micellar systems self-assemble spontaneously, yet do not show very high stability with payload encapsulation, hence requiring physical crosslinking of one block segment in order to create a drug carrier.[14] These crosslinks must then be opened upon an exogenous trigger to open the micelles and to release the payload. An intrinsically metal-free profluorescent stable micellar system would hence be highly favorable to combine the excellent properties of polymeric micelles for drug delivery, while the drug carrier can be monitored over an extended period of time without requiring complex core-shell particles to protect the potentially toxic payload.

In this study, profluorescent non-crosslinked micelles are synthesized based on amphiphilic PPV block copolymers, which spontaneously decompose and release their payload after cell uptake. As the micelles are composed of conjugated polymers, no additional fluorophores are needed to enable cell uptake or drug release visualization. Also, the conjugated segments allow to form highly stable micelles via pi-stacking,[15] removing the need to introduce chemical crosslinks. To realize this, amphiphilic PPV block copolymers were synthesized using SET-LRP using either ethylene glycol methyl ether methacrylate (EGMA), *2*-hydroxyethyl acrylate (HEA) or *2*-hydroxypropyl methacrylate (HPMA) as co-monomer, to yield PPV-*b*-PEGMA, PPV-*b*-PHEA or PPV-*b*-PHPMA block copolymers respectively. Next, polymer micelles are generated of which the morphological and optical properties are investigated. In addition, micelles were loaded with curcumin or doxorubicin as model drugs and tested towards stability, morphology, optical properties and drug release.

4.2. EXPERIMENTAL SECTION

4.2.1. Synthesis of monomer (MDMO) and anionic initiator

Synthesis of both was performed as already described in Chapter 2 and 3.

4.2.2. Anionic Polymerization

Synthesis of precursor polymer and conjugated polymer **P1'** was performed as described in Chapter 3.

4.2.3. Synthesis of PPV-*b*-PEGMA block copolymer BP1' via SET-LRP
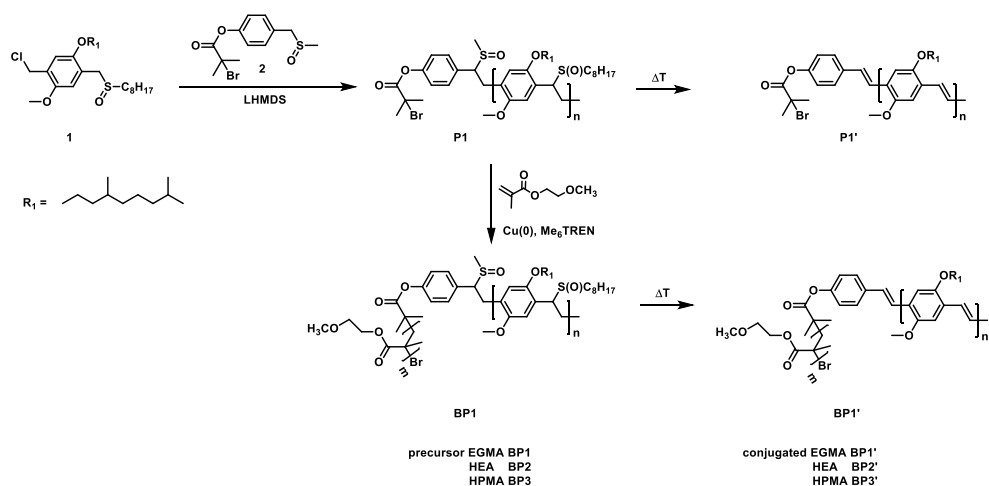
Scheme 4-1: Synthesis of (MDMO)-PPV block copolymers using EGMA, HEA or HPMA as monomer and SET-LRP reaction conditions. General reaction scheme of the synthesis of PPV-*b*-PEGMA is shown

For the block copolymer synthesis with ethylene glycol methyl ether methacrylate (EGMA) the non-purified precursor polymer **P1** was used. A Schlenk tube was filled with tris[2-(dimethylamino) ethyl]amine (Me$_6$TREN; 5.3 µL, 19.8 µmol, 1

equiv.), EGMA (0.128 g, 0.89 mmol, 45 equiv.) and **P1** (M_n = 5 100 g·mol^{-1}, 0.1 g, 19.8 µmol, 1 equiv.) dissolved in DMF (1 mL). The Schlenk tube was subjected to five freeze pump thaw cycles, after which it was transferred into the glove box. Cu(0) (1.26 mg, 19.8 µmol, 1 equiv.) was added to the Schlenk tube to start the reaction. The mixture was stirred for 4 h at room temperature, after which the content was poured into an aluminum tray to evaporate the solvent. The polymer **BP1** was filtered over a column of basic alumina to remove all copper and subsequently all solvent was evaporated. In order to obtain the conjugated block copolymer **BP1'**, precursor polymer BP1 was eliminated as described in Chapter 3. **BP1'** was isolated as a red / orange viscous solution after precipitation in MeOH / H_2O (4/1) mixture and filtration, Scheme 4-1. SEC (DMAc): M_n^{app} = 9 500 g·mol^{-1}, M_w^{app} = 12 400, $Đ$ = 1.3. ATR FT-IR: 2955 (m), 2927 (m), 2365 (m), 1677 (s), 1559 (s), 1479 (s), 1301 (m), 1215 (m), 1097 (s), 1042 (s), 747 (m), 672 (m), 629 (m), 544 (m) cm^{-1}. UV-Vis (CHCl$_3$): $\lambda_{max,abs}$ = 418 nm. Fluorescence (CHCl$_3$) = $\lambda_{max,em}$ = 506 nm.

4.2.4. Synthesis of PPV-*b*-PHEA BP2' and PPV-*b*-PHPMA BP3' via SET-LRP

The synthesis was similar to synthesizing (MDMO)-PPV-*b*-PEGMA, however, a reaction time of 2 hrs was used, Scheme 4-1, structure **BP2'**. SEC (DMAc): M_n^{app} = 16 100 g·mol^{-1}, M_w^{app} = 22 900, $Đ$ = 1.4. ATR FT-IR: 3397 (sh), 2945 (m), 2476 (m), 2349 (m), 1717 (s), 1441 (s), 1392 (s), 1253 (m), 1162 (m), 1064 (s), 1021 (s), 893 (m), 838 (m), 774 (m), 624 (m), 516 (m) cm^{-1}. UV-Vis (DMF): $\lambda_{max,abs}$ = 438 nm. Fluorescence (DMF) = $\lambda_{max,em}$ = 512 nm. The synthesis was similar to (MDMO)-PPV-*b*-PEGMA, however, a reaction time of 3 days was used in

combination with $CuCl_2$ (11.6 mg, 87 µmol, 1 equiv. Scheme 4-1, structure **BP3'**. SEC (DMAc): M_n^{app} = 5 100 g·mol^{-1}, M_w^{app} = 6 100, Đ = 1.2. ATR FT-IR: 3305 (sh), 2983 (m), 2854 (m), 2355 (m), 1726 (s), 1656 (s), 1602 (s), 1441 (s), 1409 (s), 1376 (s), 1333 (m), 1210 (m), 1124 (m), 1032 (s), 903 (m), 823 (m), 646 (m), 559 (m) cm^{-1}. UV-Vis (DMF): $\lambda_{max,abs}$ = 466nm. Fluorescence (DMF) = $\lambda_{max,em}$ = 546 nm.

4.2.5. Self-assembly of PPV block copolymers

2 mg of block copolymer was dissolved in 0.4 mL of DMF. The solution was placed on a stir plate with a high stirring rate at room temperature. Deionized water (3.6 mL) was added dropwise to the solution with a flow rate of 0.2 mL·h^{-1}, leading to a total polymer concentration of 0.5 mg·mL^{-1}. Afterwards the solution was placed in a dialysis membrane with pore size M_w < 3 500 g·mol^{-1} and dialyzed against deionized water for 48 hrs.

4.2.6. Encapsulation of material into PPV micelles

2 mg of block copolymer and 1 mL of stock solution (concentration = 1 mg·mL^{-1} in DMF) of the encapsulated material (Nile Red, Curcumin or Doxorubicin) was dissolved in in 0.4 mL of DMF. The solution was placed on a stir plate with a high stirring rate at room temperature. Deionized water (3.6 mL) was added dropwise to the solution with a flow rate of 0.2 mL·h^{-1}, leading to a total polymer concentration of 0.4 mg·mL^{-1}. Afterwards the solution was placed in a dialysis membrane with pore size M_w < 3 500 g·mol^{-1} and dialyzed against deionized water for 48 hrs.

4.3. RESULTS AND DISCUSSION

4.3.1. Block copolymer synthesis

In order to synthesize amphiphilic PPV block copolymers, first anionic initiator **2** and monomer **1** were synthesized, as described in Chapter 3. Next, PPV block copolymers were synthesized by chain extending precursor (MDMO)-PPV using SET-LRP reaction conditions – wheter SET-LRP or supplemental activator and reducing agent (SARA) ATRP is used is not studied in here – leading to amphiphilic block copolymers with either ethylene glycol methyl ether methacrylate (EGMA), *2*-hydroxyethyl acrylate (HEA) or *2*-hydroxypropyl methacrylate (HPMA) as counter block. A complete overview of all analysis results is given in Table 4-1, while only the individual results of PPV-*b*-PEGMA block copolymer are shown below (see Appendices for all analysis spectra of PPV-*b*-PHEA and PPV-*b*-PHPMA).

Table 4-1: Overview of different PPV block copolymers synthesized and their characteristics

	$M_n{}^{app}$	$M_w{}^{app}$	$Đ$	$λ_{max\_abs}$	$λ_{max\_em}$	$φF$
	$g·mol^{-1}$	$g·mol^{-1}$		nm	nm	%
PPV	-	-	-	494	584	26.48
PPV-*b*-PEGMA	9 500	12 400	1.3	418	506	20.56
PPV-*b*-PHEA	16 100	22 900	1.4	438	512	19.46
PPV-*b*-PHPMA	5 100	6 100	1.2	466	546	21.19
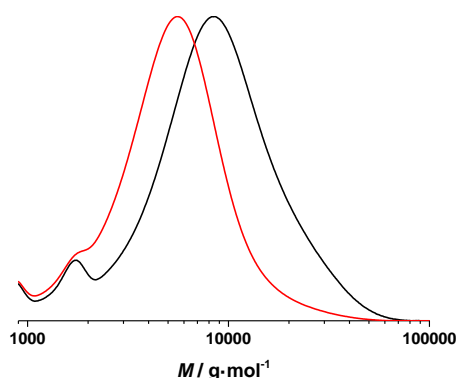
Figure 4-1: SEC profile (RI detection, DMAc) of (MDMO)-PPV **P1'** (**red**) and PPV-*b*-PEGMA **BP1'** (**black**)
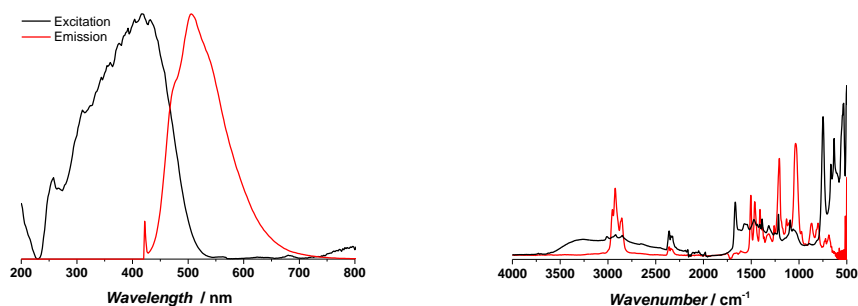
Figure 4-2: (*left*) UV-Vis (**black**) and fluorescence spectra (**red**) of PPV-*b*-PEGMA block copolymers **BP1'**. Measurements are performed in DMF as solvent, using an absorption wavelength of 418 nm; (*right*) ATR-FT-IR of (MDMO)-PPV **P1'** (**red**) and PPV-*b*-PEGMA **BP1'** (**black**)

Clear shifts towards higher molecular weights are observed for all block copolymers (Figures 4-1, S4-1 and S4-3), as well as the appearance of the *C=O* vibration band of the acrylic monomers around 1700 cm^{-1} (Figures 4-2, S4-2 and S4-4) in the infrared spectra. In addition, a blue shift in λ_{max} in the UV-Vis and the fluorescence emission spectrum is observed after block copolymerization, indicating the quenching effect of the second block on the photo physical

properties of the PPV block (Figures 4-2, S4-2 and S4-4). Although partly quenched, the absorbance / emission wavelengths are still within the range of most commonly used fluorescent dyes. Reasonable values for the quantum yields are obtained for the different PPV block copolymers and the typical PPV characteristics are mostly retained (Table 4-1).
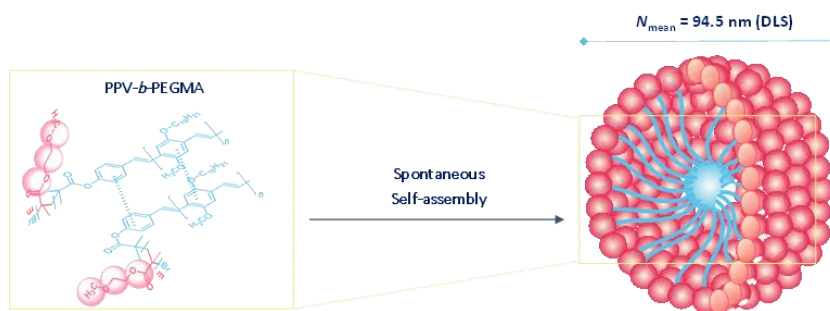
Figure 4-3: Spontaneous self-assembly of the amphiphilic block copolymers in water leads to the process of micelle formation, in which the hydrophobic PPV is situated at the core of the micelle (**blue**) and the hydrophilic PEGMA at the outside (**pink**)

4.3.2. Self-assembly of micelles

Block copolymers were self-assembled in DMF/water followed by dialysis, leading to micelle formation as shown in Figure 4-3. Size distributions of the formed micelles were analyzed by means of dynamic light scattering (DLS) (Table 4-2) With increasing hydrophobicity, an increasing particle diameter (or more specifically the hydrodynamic volume) and dispersity ($Đ$) is observed, leading to micelles with an average size between 94 and 160 nm respectively. The speed of water addition during micellization was investigated for the PPV-*b*-PEGMA block copolymers and a small increase in size as well as $Đ$ is seen upon increasing flow rate (0.1 mL·h^{-1} vs. 0.2 mL·h^{-1}).

Table 4-2: Overview of different PPV micelles synthesized and their characteristics

Solid content	Addition speed	DLS nm				TEM nm	λ_{max} [1] nm		Zeta potential
$mg \cdot mL^{-1}$	$mL \cdot h^{-1}$	I_{mean}	V_{mean}	N_{mean}	PDI	D_{50}	Abs	Em	mV
PPV-b-PEGMA									
0	0	0	0	0	0	0	418	506	0
0.5	0.2	119.3	109.2	94.5	0.197	22 ± 2	361	464	-28.9
0.5	0.1	127.8	108.6	82.6	0.096	11 ± 3	361	470	-33.0
PPV-b-PHEA									
0	0	0	0	0	0	0	438	512	0
0.5	0.2	183.5	182.5	156.7	0.337	30 ± 15	389	491	-35.7
PPV-b-PHPMA									
0	0	0	0	0	0	0	466	512	0
0.5	0.2	346.4	341.7	158.3	0.363	50 ± 5	421	495	-38.7

[1] measurements are performed in DMF as solvent
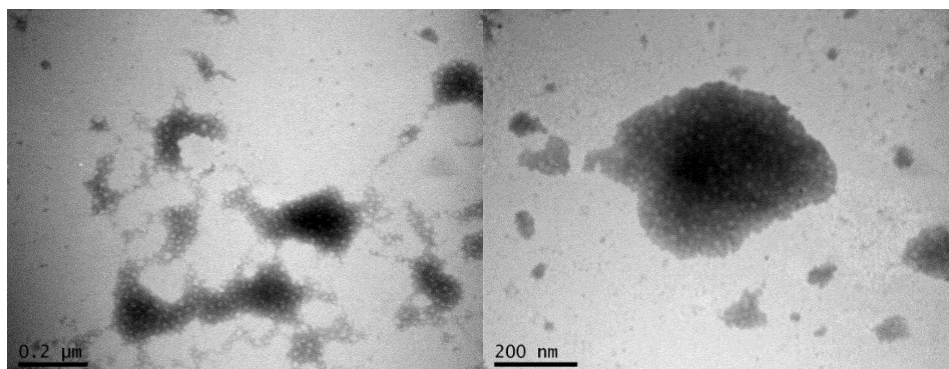
Figure 4-4: TEM images of micelles prepared from PPV-*b*-PEGMA block copolymer using a flow rate of 0.2 mL·h^{-1} (*left*) or 0.1 mL·h^{-1} (*right*) upon the preparation of the micelles, scale bar 200 nm, phosphotungstic acid staining

Next, the size and morphology of the micelles was also studied via transmission electron microscopy (TEM) (Figure 4-4 and S4-5). Average diameters measured by TEM are as expected smaller than those obtained by DLS, due to the aggregation of the micelles in water and to hydrodynamic effects, especially with the extremely hydrophilic PHEA or PHPMA polymers. Micelles with a size between 11 nm (PPV-*b*-PEGMA) and 50 nm (PPV-*b*-PHPMA) are obtained. As mentioned above, micelles lose their characteristic fluorescence due to the pi stacking of the PPV chains.
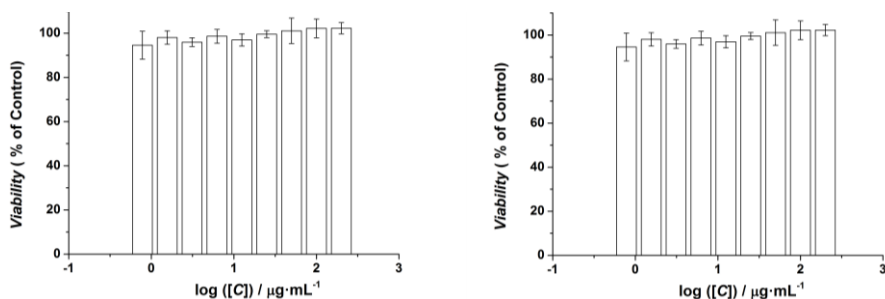
Figure 4-5: Cytotoxicity analysis (SRB) for PPV-*b*-PEGMA micelles using AsPC-1 cells and an incubation time of 72 h, using a flow rate of 0.2 mL·h^{-1} (*left*) or 0.1 mL·h^{-1} (*right*) upon the preparation of the micelles

In the next step, all micelles formed were subjected to a cytotoxicity study (SRB or WST-1 assay). The proliferation of human pancreatic cancer cell line AsPC-1 upon contact with the micelles was investigated at different concentrations over a period of 72 h (Figure 4-5 and S4-6). Even at high concentrations of 250 µg·ml^{-1}, the PPV-*b*-PEGMA micelles showed no sign of significant cytotoxicity as compared to cells exposed to normal growth conditions. Similar results were obtained for PPV-*b*-PHEA micelles, however PPV-*b*-PHPMA micelles did show slight toxicity, leading to an IC 50 value of 0.599 µM. The latter is most likely related to insufficient purification of the copper residuals after block copolymer synthesis rather than due to the HPMA block, as both PPV as well as HPMA separately display no toxicity.
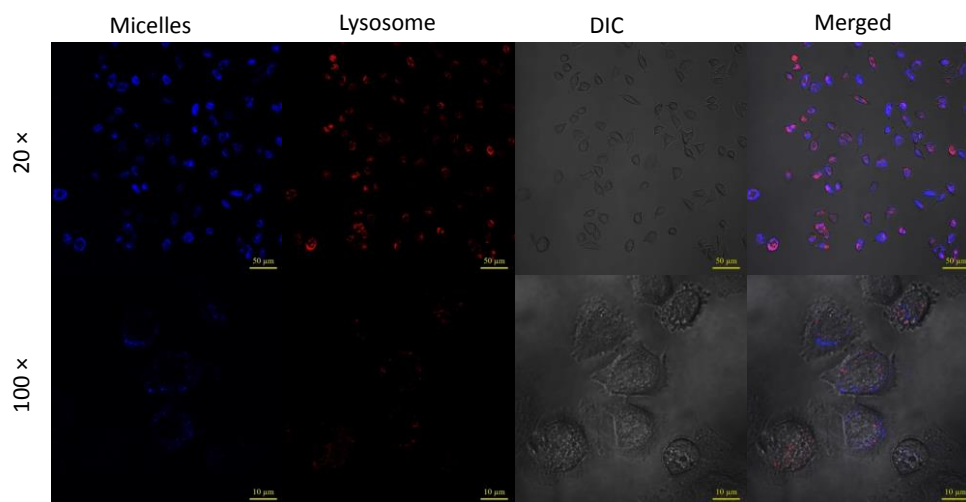
Figure 4-6: Cellular uptake of PPV-*b*-PEGMA micelles (prepared at a flow rate of 0.2 mL·h^{-1}) measured by confocal fluorescence microscopy using AsPC-1 cells incubated for 72 h and an additional 2 h for the micelles, scale bar 50 μm

Figure 4-7: Cellular uptake of PPV-*b*-PEGMA micelles (prepared at a flow rate of 0.1 mL·h^{-1}) measured by laser scanning confocal microscopy using AsPC-1 cells incubated for 72 h and an additional 2 h for the micelles, scale bar 50 μm

Yet, all three micellar systems were subjected to cell uptake studies. AsPC-1 cell lines were incubated for 72 h, after which the micelles were loaded into the cells and incubated for 2 h. Although the fluorescence of the micelles was quenched in water, upon cell uptake into the cytosols the micelles became visible again and the amount of micelles taken up by the cells is directly linked to the appearing fluorescence intensity. This actually means that for the first time, a profluorescent system is created which allows visualization of the fate of the micelles over a longer period of time, as well as their pathway and disassembly mechanism in the cells. Consequently, accumulation of the material in the body over time can easily be followed, as compared to currently used metal-containing systems. Fluorescence is also seen overlapping with the lysosomes, indicating that micelles entered the lysosomes after endocytosis. The larger PPV-*b*-PEGMA micelles show an easier and better uptake as compared to the smaller ones, which is in line with previous studies, indicating best cell uptake by particles with a size of 40 – 50 nm.[16] (Figure 4-6 and 4-7). PPV-*b*-PHEA and PPV-*b*-PHPMA micelles are in a similar size range and thus should show similar uptake as the large PPV-*b*-PEGMA micelles (Figure S4-7 and S4-8). The slower uptake of these micelles might be related to the design – hydrophobic / hydrophilic part – of the block copolymer[17] Yet, fluorescent polymer is present in all cases indicating the uptake and subsequent break down of the micelles in the cells.
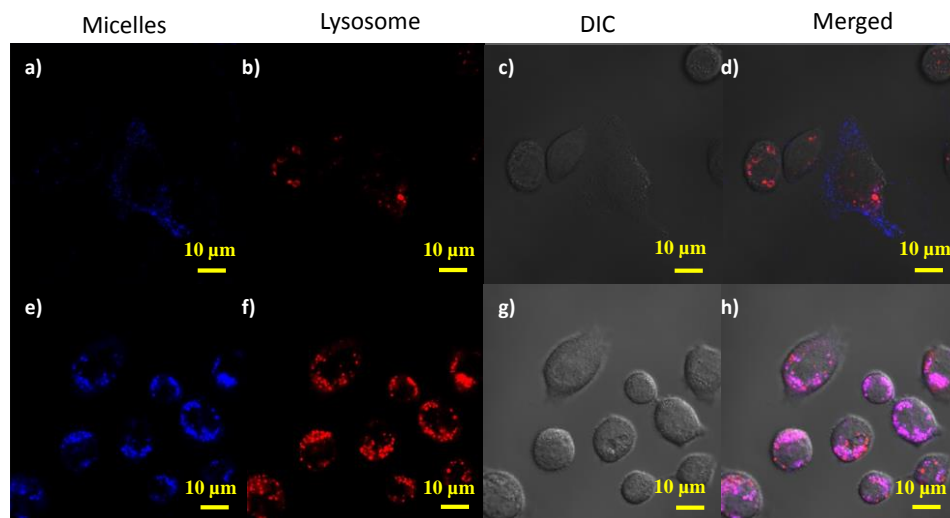
Figure 4-8: Cellular uptake observed by laser scanning confocal microscopy. Images of the PPV-*b*-PEGMA micelles (**blue**) in pure water using AsPC-1 cell lines, LysoTracker Red DND-99 (**red**) is added to stain the lysosomes upon an incubation of 2 h (**a-d**) or 18 h (**e-h**) of the micelles after loading

PPV-*b*-PEGMA micelles were subjected to additional cellular uptake tests in which the incubation time was extended from 2 h to 18 h and a colored lysotracker (LysoTracker Red DND-99) was used to counterstain the lysosomes (Figure 4-8; A CellLight® lysosome-GFP was also used to stain the lysosomes, the results were shown in Figure 4-9). After incubation with micelles for 18 h, more micelles were internalized into the cells – 18.7 % after 18 h as compared to 10.7 % for an incubation time of 2 h – and a full transport of the micelles from the endosomes into the lysosomes is seen (Figure 4-9). The higher fluorescence intensity over time indicates that more micelles were taken up and disassembled within the cell. Even after 18 h most of the micelles are still present in the lysosomes, showing living stable cells. A slight increase in the size of the fluorescence as compared to the size of the lysosomes is indicating that some micelles or block copolymers are

released from the lysosomes. Various trials to mimic cell conditions on lab scale – surrounding the micelles in an (acidified) PBS solution for up to 24 h – did not lead to the desired disassembly and hence fluorescence signal as observed when the micelles are taken up by the cell.

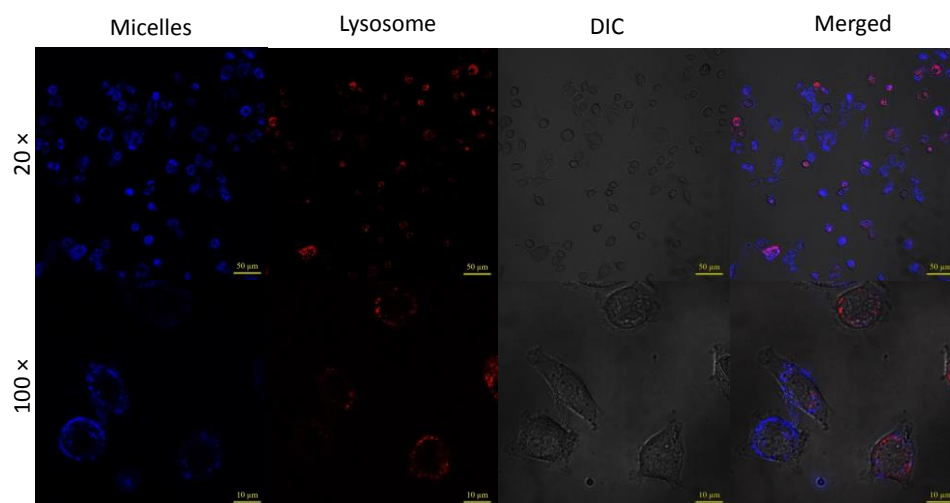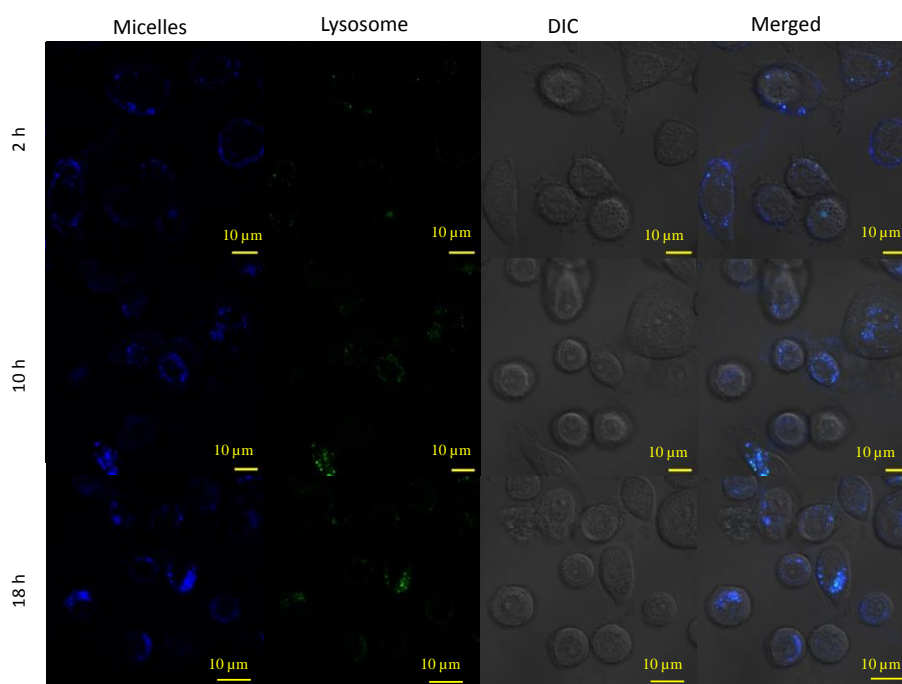Figure 4-9: Cellular uptake of PPV-b-PEGMA micelles (prepared at a flow rate of 0.2 mL·h^{-1}) measured by laser scanning confocal microscopy using AsPC-1 cells incubated for 72 h and an additional 2, 10 or 18 h for the micelles using cell light$^{\circledR}$ lysosome-GFP, scale bar 10 µm

Table 4-3: Overview of different PPV micelles and their loading (Nile Red (NR), Curcumin (Cur) or Doxorubicin (Dox)) synthesized and their characteristics

Encapsulation		DLS nm			PDI	TEM nm	λ_{max}[1] nm		Zeta potential	η
	mg	I_{mean}	V_{mean}	N_{mean}		D_{50}	Abs	Em	mV	%
PPV-b-PEGMA		119.3	109.2	94.5	0,197	22±2.0	357	466	-28.9	0
NR	0.5	300.7	450.4	116	0.335	n.a.	543	650	-37.3	28.9
Cur	0.5	672.4	812.3	109.4	0.485	30±2.5	428	538	-43.2	27.8
Dox	0.5	260.5	262.2	259.2	0.943	30±2.5	480	593	-35.6	9.1
PPV-b-PHEA		183.5	182.5	156.7	0.337	30±1.5	389	491	-25.3	0
NR	0.5	148.5	149.1	147.5	1	n.a.	543	625	-32.9	36.3
Cur	0.5	163.3	163.9	161.4	0.985	n.a.	428	525	-28.0	28.4
Dox	0.5	399.3	404.9	390.7	0.765	n.a.	480	575	-27.9	14.9
PPV-b-PHPMA		364.4	341.7	128.3	0.363	50±5	421	495	-38.7	0
NR	0.5	120.5	120.7	119.4	1	n.a.	543	650	-32.8	25.5
Cur	0.5	71.38	71.31	70.26	0.874	n.a.	428	515	-22.4	11.1
Dox	0.5	700.3	714.3	699.4	0.743	n.a.	480	575	-1.58	10.1

[1] measurements are performed in DMF as solvent

4.3.3. Encapsulation of Micelles

After the general non-toxicity of the micelles (and their block copolymers) was proven and their long term fate over 18 h in the cells were shown the next step was to test the micelles for release of a payload within the cells (note that the at this stage the exact entry mechanism and reason for micelle breakdown is not fully clear, but irrespective for the herein described application). Therefore, the different PPV micelles were successfully loaded (in-situ) with a fluorescent drug (Curcumin (Cur) or Doxorubicin (Dox)) allowing both the monitoring of the drug carrier as well as release and disassembly at a later stage (Table 4-3).
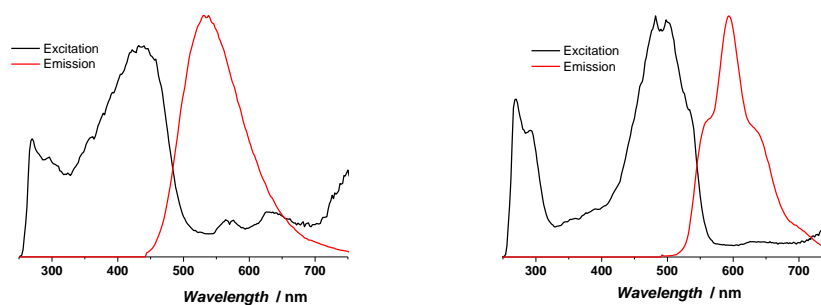
Figure 4-10: UV-Vis (**black**) and fluorescence spectra (**red**) of PPV-b-PEGMA micelles loaded with Curcurmin (*left*) or Doxorubicin (*right*). Measurements are performed in DMF as solvent using an absorption wavelength of 428 nm or 480 nm respectively

UV-Vis and fluorescent analysis indicate the successful loading of the materials in the different PPV micelles (Figure 4-10, S4-9 and S4-10). An increase in particle size by DLS measurements – up to a factor of 5 – as well as a difference in zeta potential is observed after loading (Table 4-3). Loading of the PPV-*b*-PEGMA micelles was studied in more detail. Drug release studies on loaded PPV-*b*-PEGMA micelles performed via UV-Vis indicate the expected release of the different payloads within the first hour (Figure 4-11).
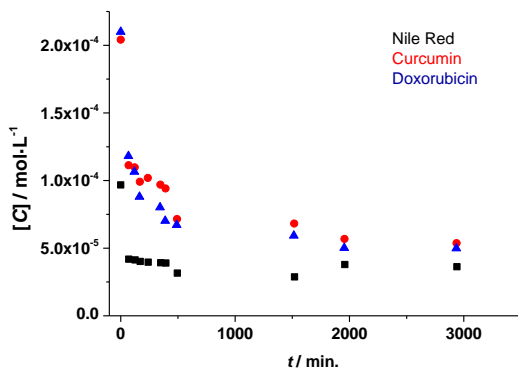
Figure 4-11: Release of loaded dye (Nile Red, **black**) or drugs (Curcumin (**red**) or Doxorubicin (**blue**)) using PPV-*b*-PEGMA micelles (prepared a flow rate of 0.2 mL·h^{-1}) as measured by UV-Vis in DMF as solvent
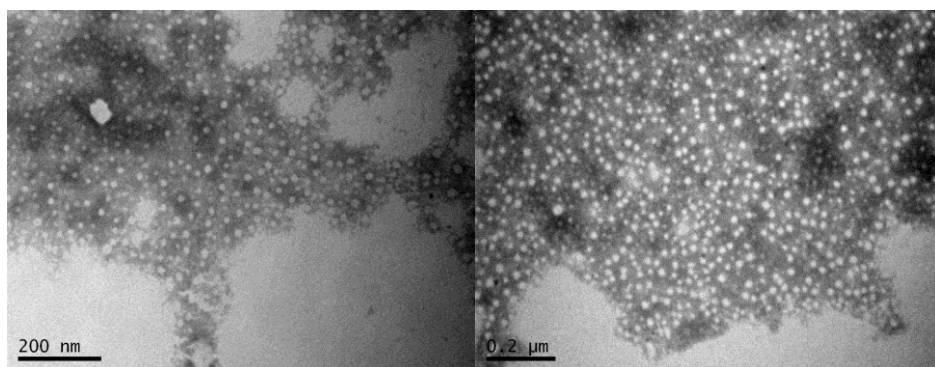
Figure 4-12: TEM images of micelles prepared from PPV-*b*-PEGMA block copolymer using a flow rate of 0.2 mL·h^{-1} upon the preparation of the micelles. Micelles loaded with Curcumin (*left*) and Doxorubicin (*right*), scale bar 200 nm, phosphotungstic acid staining

Even when dissolved in DMF and excited at both the PPV-*b*-PEGMA as well as Dox wavelength, both materials become visible in the fluorescence spectra, confirming the successful loading of the material. Next, size and morphology was confirmed

by TEM measurements (Figure 4-12). Spherical micelles with increased particle size from 22 nm to 30 nm were obtained when using Cur or Dox as payload.

Although non-toxic by nature, once loaded with Cur or Dox, the micelles show the expected toxicity with a IC 50 value of 1.18 µM or 1.51 µM respectively (Figure 4-13) and indicate the successful loading of drug into the PPV-*b*-PEGMA micelles. As a last step, cell uptake by means of confocal microscopy on the Dox loaded micelles was performed. Incubation of the micelles for 2 h (using AsPC-1 cell lines incubated for 72 h before micelle loading) shows a clear uptake of the loaded micelles in the cell and subsequent release of the payload is confirmed by confocal microscopy results (Figure 4-14).
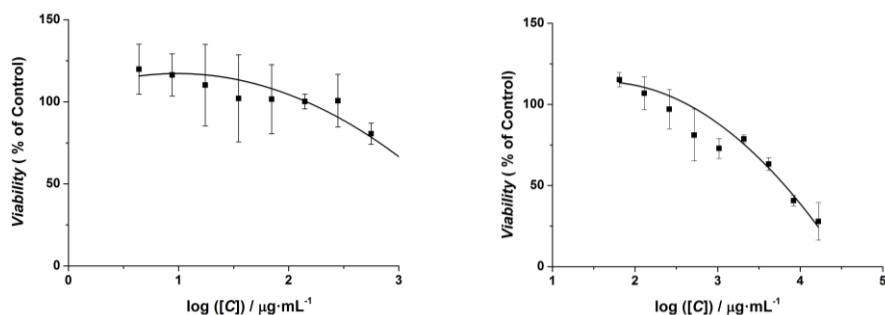
Figure 4-13: Cytotoxicity analysis (WST-1) for PPV-*b*-PEGMA micelles using AsPC-1 cells and an incubation time of 72 h. Micelles are loaded with Curcumin (*left*) and show an IC 50 value of 1.18 μM or loaded with Doxorubicin (*right*) and show an IC 50 value of 1.51 μM
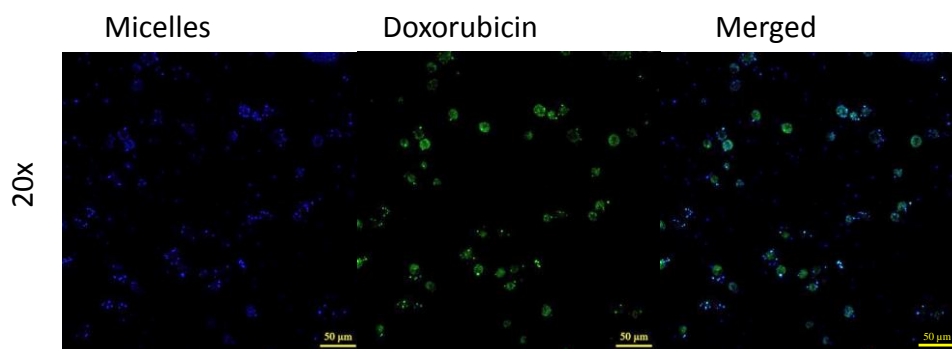
Figure 4-14: Cellular uptake of PPV-*b*-PEGMA micelles (*blue*) loaded with Doxorubicin (*green*), measured by confocal fluorescence microscopy using AsPC-1 cells. Green area partially separated from the blue dots indicates that Dox was released from the micelles. Micellar incubation time was 2 h. scale bar 50 μm

The micelles are able to internalize into the lysosomes and spontaneously release the drug upon cell uptake, without the need for an exogenous trigger. After 2 h of incubation, some of the cells are starting to decompose, clearly confirming the release of the toxic Dox into the cells. A new micellar system without the use of crosslinks to stabilize the micelles, a trigger to break them down or to release the payload has been developed, opening new possibilities for the use of conjugated polymers in biomedical applications.

4.4. CONCLUSIONS

In conclusion, a unique profluorescent non-crosslinked nanosized micellar system to be used for drug delivery applications has been synthesized. The fate of the micelles, as well as their transport, disassembly and payload release in the cell can directly be visualized for the first time by high-contrast fluorescent imaging methods. In addition, an easy way to load the micelles – and their subsequent release without the use of a trigger – indicates the versatility of these materials. As a result, a novel pathway for an intrinsically fluorescent stable micellar system of highly added value for targeting concomitant bioimaging and drug delivery has been developed. Current work on the uptake and disassembly mechanism of the micelles into the cells is ongoing in our laboratories and will be reported in due course.

4.5. APPENDICES
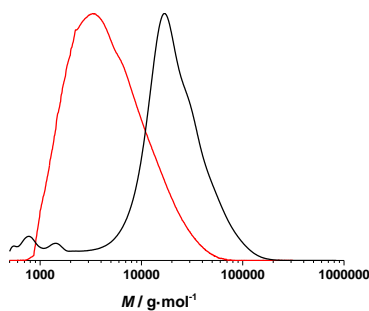
Figure S4-1: SEC profile (RI detection, DMAc) of (MDMO)-PPV **P1'** (**red**) and
PPV-*b*-PHEA **BP2'** (**black**)
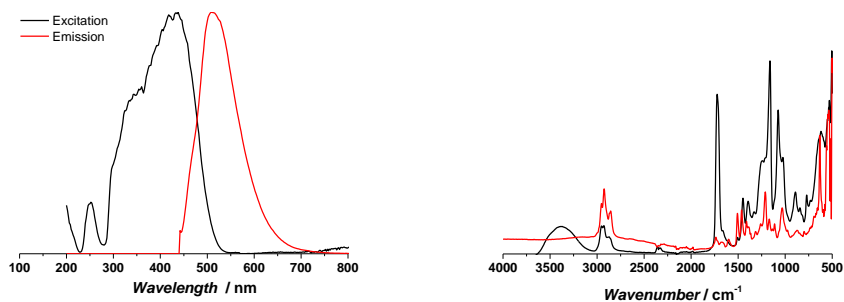
Figure S4-2: (l*eft*) UV-Vis (**black**) and fluorescence spectra (**red**) of PPV-*b*-PHEA
block copolymer **BP2'**. Measurements are performed in DMF as solvent, using an
absorption wavelength of 438 nm; (*right*) ATR-FT-IR of (MDMO)-PPV P1' (**red**)
and PPV-*b*-PHEA **BP2'** (**black**)
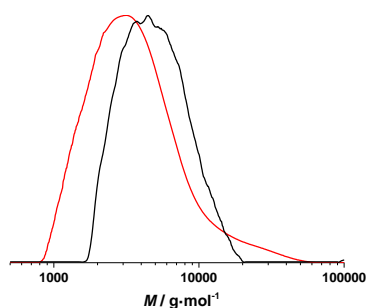
Figure S4-3: SEC profile (RI detection, DMAc) of (MDMO)-PPV **P1'** (**red**) and PPV-*b*-PHPMA **BP3'** (**black**)
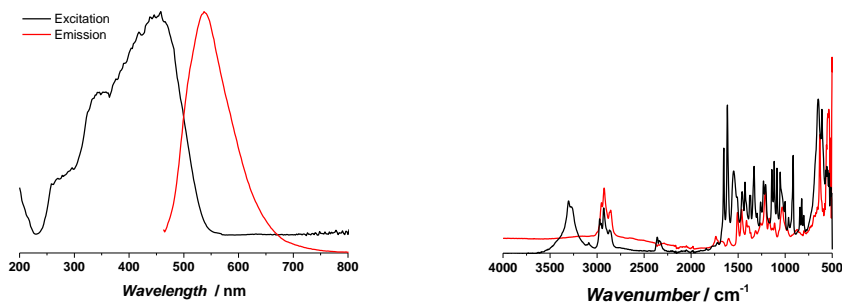
Figure S4-4: (*left*) UV-Vis (**black**) and fluorescence spectra (**red**) of PPV-*b*-PHPMA block copolymer **BP3'**. Measurements are performed in DMF as solvent, using an absorption wavelength of 466 nm; (*right*) ATR-FT-IR of (MDMO)-PPV P1' (**red**) and PPV-*b*-PHPMA **BP3**' (**black**)
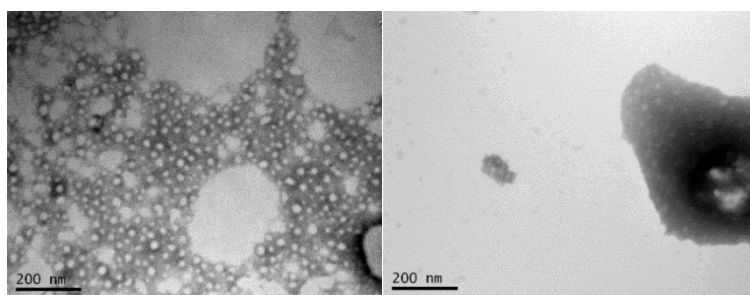
Figure S4-5: TEM image of micelles prepared from (*left*) PPV-*b*-PHEA or (*right*) PPV-*b*-PHPMA block copolymer upon the preparation of the micelles, scale bar 200 nm, phosphotungstic acid staining
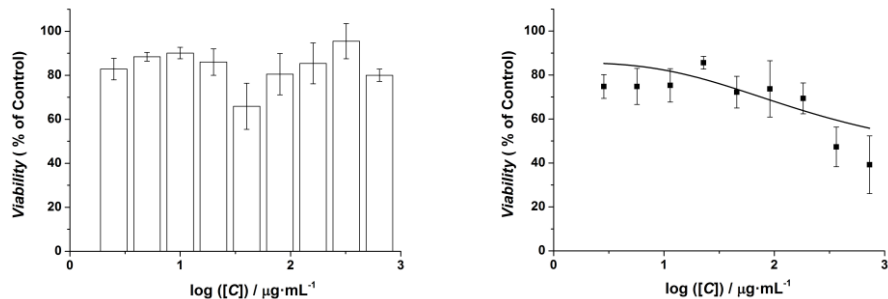
Figure S4-6: Cytotoxicity analysis (WST-1) for (*left*) PPV-*b*-PHEA and (*right*) PPV-*b*-PHPMA micelles using AsPC-1 cells and an incubation time of 72 h. PPV-*b*-PHPMA micelles show an IC_{50} value of 0.599 µM
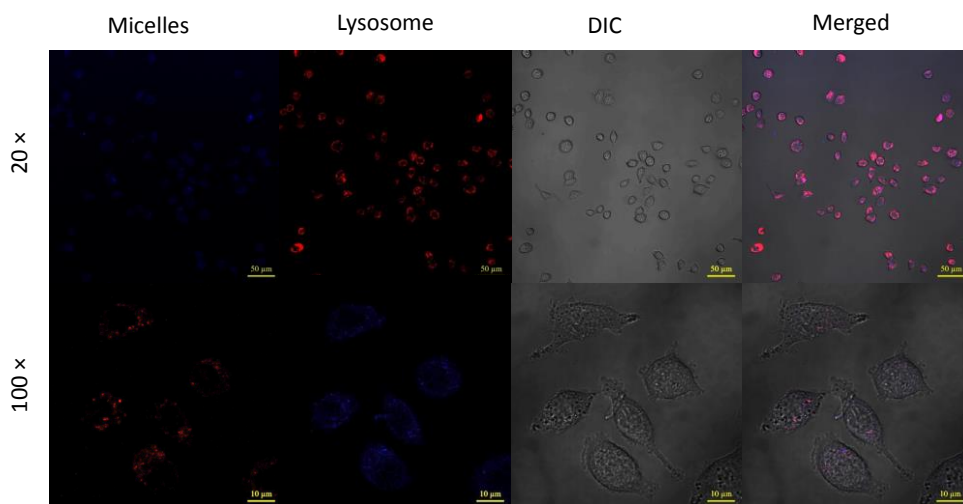
Figure S4-7: Cellular uptake of PPV-*b*-PHEA micelles measured by confocal fluorescence microscopy using AsPC-1 cells incubated for 72 h and an additional 2 h for the micelles, scale bar 50 µm
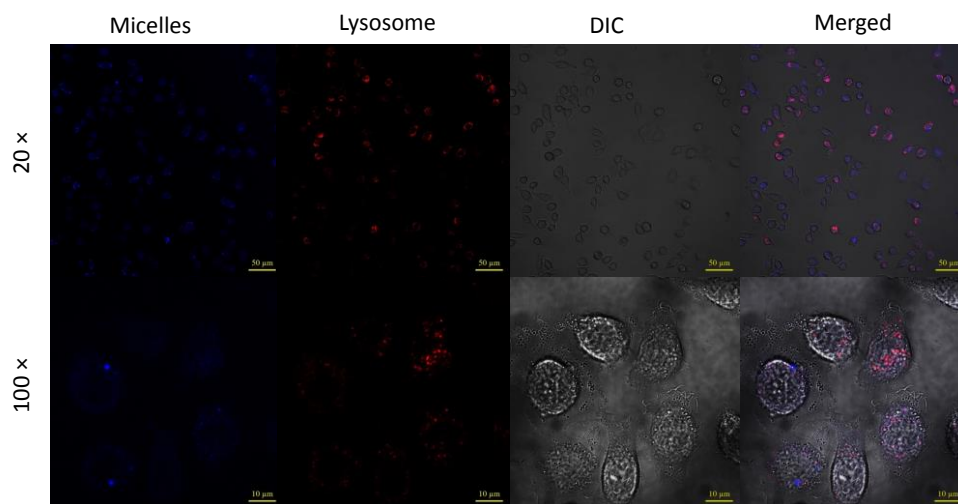
Figure S4-8: Cellular uptake of PPV-*b*-PHPMA micelles measured by confocal fluorescence microscopy using AsPC-1 cells incubated for 72 h and an additional 2 h for the micelles, scale bar 50 μm
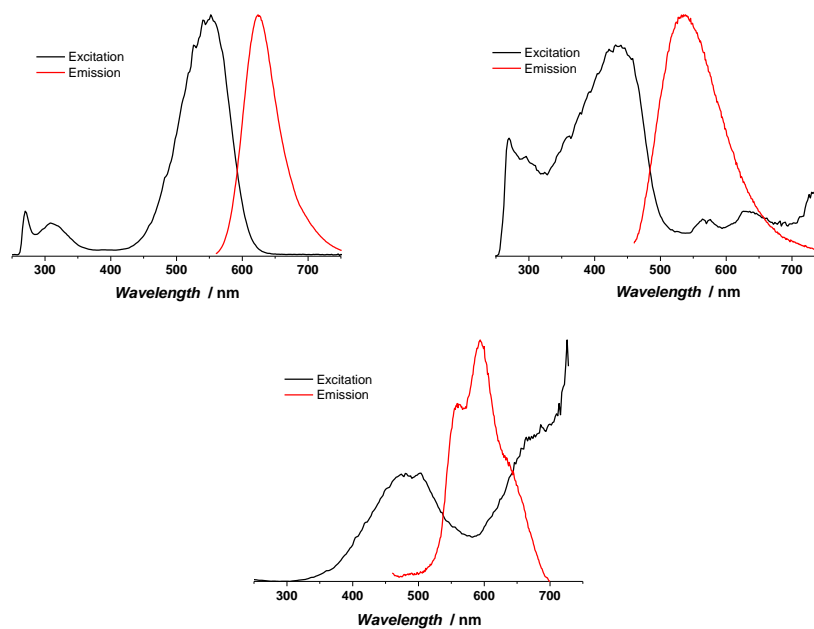
Figure S4-9: UV-Vis (**black**) and fluorescence spectra (**red**) of PPV-b-PHEA micelles loaded with Nile Red (*top left*) Curcumin (*top right*) or Doxorubicin (*bottom*). Measurements are performed in DMF as solvent using an absorption wavelength of 543 nm, 428 nm or 480 nm respectively
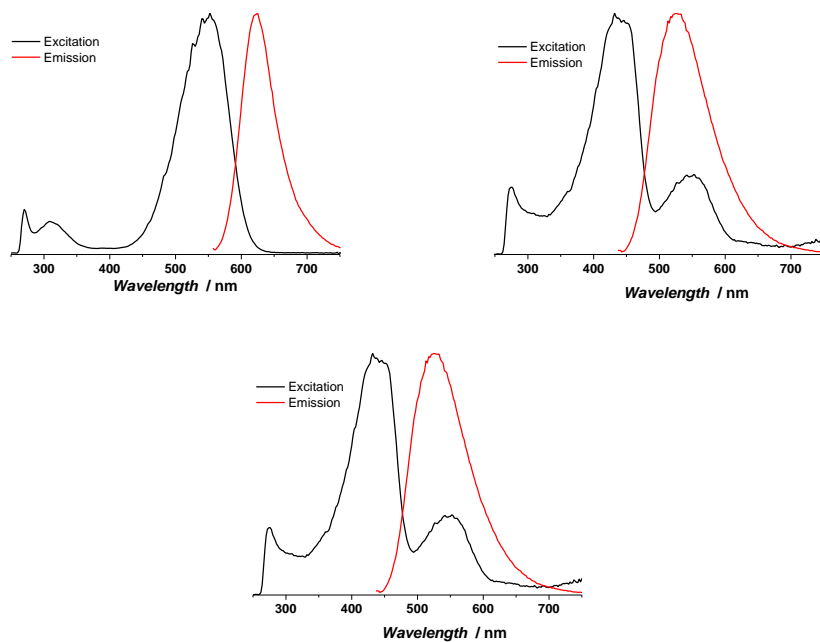
Figure S4-10: UV-Vis (**black**) and fluorescence spectra (**red**) of PPV-b-PHPMA micelles loaded with Nile Red (*top left*) Curcumin (*top right*) or Doxorubicin (*bottom*). Measurements are performed in DMF as solvent using an absorption wavelength of 543 nm, 428 nm or 480 nm respectively

4.6. REFERENCES

[1] D. Letian, L. Yongsheng, H. Ziruo, L. Gang, Y. Yang, *Chem. Rev.* **2015**, *115*, 12633-12665; b) M. J. Robb, D. Montarnal, N. D. Eisenmenger, S.-Y. Ku, M. L. Chabinyc, C. J. Hawker, *Macromolecules* **2013**, *46*, 6431-6438.

[2] D. Braun, A. J. Heeger, *Appl. Phys. Lett.* **1991**, *58*, 1982-1984; b) A. C. Grimsdale, K. Leok Chan, R. E. Martin, P. G. Jokisz, A. B. Holmes, *Chem. Rev*. **2009**, *109*, 897-1091; c) R. H. Friend, R. W. Gymer, A. B. Holmes, J. H. Burroughes, R. N. Marks, C. Taliani, D. D. C. Bradley, D. A. Dos Santos, J. L. Bredas, M. Lőgdlund, W. R. Salaneck, W. R. *Nature* **1999**, *397*, 121−128.

[3] G. Horowitz, *Adv. Mater.* **1998**, *10*, 365−377.

[4] S. Gűnes, H. Neugebauer, N. S. Sariciftci, *Chem. Rev.* **2007**, *107*, 1324−1338.

[5] J. H. Burroughes, D. D. C Bradley, A. R. Brown, R. N. Marks, R. H. Friend, A. B. Holmes, K. Mackay, P. L. Burns, *Nature* **1990**, *347*, 539−541; b) A. P. Kulkarni, C. J. Tonzola, A. Babel, S. A. Jenekhe, *Chem. Mater.* **2004**, *16*, 4556−4573; c) D. E. Gomez, S. S. Lee, C. S. Kim, Y.-L. Loo, *Mol. Org. Electron. Devices* **2010**, 109−152.

[6] W. Yue, T. T. Larsen-Olsen, X. Hu, M. Shi, H. Chen, M. Hinge, P. Fojan, F. C. Krebs, D. Yu, *J. Mater. Chem. A* **2013**, *1*, 1785-1793; b)   Y. Geng, J. Cong, K. Tajima, C. Zeng, E. Zhou, *Polym. Chem.* **2014**, *5*, 6797-6803.

[7] a) D. Dini, *Chem. of Mater.* **2005**, *17*, 1933-1945; b)   B. J. Schwartz, *Ann. Rev. of Phys. Chem.* **2003**, *54*, 141-172; c) A. J. Heeger, *Chem. Soc. Rev.* **2010**, *39*, 2354-2371.

[8] a) T. Junkers, J. Vandenbergh, P. Adriaensens, L. Lutsen, D. Vanderzande, *Polym. Chem*. **2012**, *3*, 275-285; b)   A. Van Breemen, A. Issaris, M. de Kok, M.

van Der Borght, P. Adriaensens, J. Gelan, D. Vanderzande, *Macromolecules* **1999**, *32*, 5728-5735; c) E. Kesters, S. Gilissen, F. Motmans, L. Lutsen, D. Vanderzande, *Macromolecules* **2002**, *35*, 7902-7910.

[9] N. Zaquen, L. Lutsen, D. Vanderzande, T. Junkers, *Polym. Chem.* **2016**, *7*, 1355-1367.

[10] a) V. Percec, T. Guliashvili, J. Ladislaw, A. Wistrand, A. Stjerndahl, M. Sienkowska, M. Montiero, S. Sahoo, *J. Am. Chem. Soc*. **2006**, *128*, 14156-14165; b) N. H. Nguyen, V. Percec, *J. Polym. Sci., Part A: Polym. Chem*. **2010**, *48*, 5109-5119; c) N. H. Nguyen, B. M. Rosen, G. Ligadas, V. Percec, *Macromolecules* **2009**, *42*, 2379-2386; d) A. Anastasaki, C. Waldron, P. Wilson, R. McHale, D. M. Haddleton, *Polym. Chem*. **2013**, *4*, 2672-2675.

[11] a) I. Cosemans, J. Vandenbergh, V. S. D. Voet, K. Loos, L. Lutsen, D. Vanderzande, T. Junkers, *Polymer* **2013**,*54*, 1298-1304; b) I. Cosemans, J. Vandenbergh, L. Lutsen, D. Vanderzande, T. Junkers, *Polym. Chem*. **2013**, *4*, 3471-3479.

[12] a) F. Su, R. Alam, Q. Mei, Y. Tian, D. R.Meldrum, *Plosone* **2011**, *9*, 24425; b) H. Tan, Y. Zhang, M. Wang, Z. Zhang, X. Zhang, A. M. Yong, S.Y. Wong, A.Y. Chang, Z.-K. Chen, X. Lu, M. Coolani, J. Wang, *Biomaterials* **2012**, *33*, 237-246; c) Y. Tian, W.-C. Wu, C.-Y. Chen, T. Strovas, Y. Li, Y. Jin, F. Su, R. Meldrum, A. K.-Y. Jen, *J. Mater. Chem.* **2010**, *20*, 1728-1736.

[13] a) W.-C. Wu, H.-H. Chang, *Coll and Polym. Sci.* **2015**, *293*, 453-462; b) H. Wang, H. H. Wang, V. S. Urban, K. C. Littrell, P. Thiyagarajn, L. Yu, *J. Am. Chem. Soc.* **2000**, *122*, 6855-6861; c) Y. Jung, R. J. Hickley, S.-J. Park, *Langmuir* **2010**, *26*, 7540-7543; d) W.-C. Wu, C.-Y. Cheng, W.-Y. Lee, W.-C. Chen, *Polymer* **2015**, *65*, A1-A16.

[14] a) Y. Xu, F. Meng, R. Cheng, Z. Zhong, *Macromol. Biosci.* **2009**, *9*, 1254-1261; b) J. Yue, R. Wang, S. Liu, S. Wu, Z. Xie, Y. Huang, X. Jing, *Soft Matter* **2012**, *8*, 7426-7435.

[15] a) Y. Zhao, F. Sakai, L. Su, Y. Lui, K. Wei, G. Chen, M Jiang, *Adv. Mater.* **2013**, 25, 5215-5226; T. K. Paira, A. Saha, S. Banerjee, T. Das, P. Das, N. R. Jana, T. K. Mandal, *Macromol. Biosci.* **2014**, 14, 929-935.

[16] W. Jiang, B.Y.S. Kim, J. T. Rutka, W.C.W Chan, *Nature Nanotech.* **2008**, *3*, 145-150.

[17] T. Chang, M. S. Lord, B. Bergmann, A. Macmillan, M. H. Stenzel, *J. Mater. Chem. B* **2014**, *2*, 2883-2891.

CHAPTER 5

Continuous Synthesis and Thermal Elimination of Sulfinyl-Route Poly(*p*-Phenylene Vinylene) in Consecutive Flow Reactions
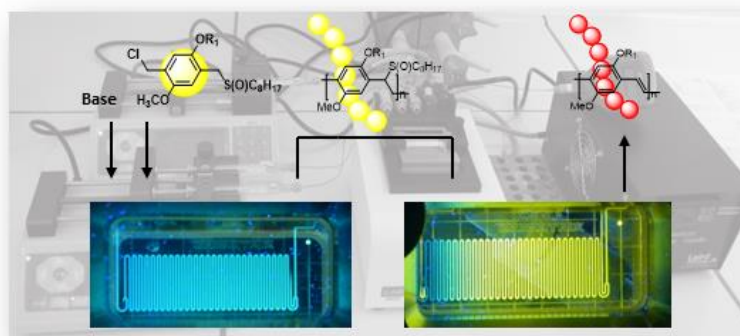
ABSTRACT

Continuous synthesis of multistep polymerizations at micro scale is made available by coupling two microstructured chip reactors in a single reactor setup. Conjugated poly([2-methoxy-5-(3',7'-dimethyloctyloxy)]-1,4-phenylenevinylene) ((MDMO)-PPV) is synthesized via the radical sulfinyl precursor route. Reactions are carried out in separate reactors and optimization of the second step – elimination of the polymer – can be effectively carried out at temperatures between 180 °C and 195 °C, allowing for full polymer conversion within 5-20 min and formation of conjugated materials with maximum absorption wavelengths λ_{max} of up to 500 nm. Combination of both processes in a single coupled reactor setup allows for total monomer-to-conjugated-(MDMO)-PPV conversions in the range of 40 % within a total residence time of 8.2 min, while retaining its pristine optical properties. Polymer characteristics are comparatively good and the reduction in yield (due to the lower initial monomer concentrations) is compensated by the much shorter reaction times required in the flow process.

5.1. INTRODUCTION

In previous chapters, batch polymerizations following either the radical (chapter 2) or anionic (chapter 3 and 4) pathway, led to the two step synthesis of conjugated PPV polymers via the sulfinyl precursor route. Polymerizations are relatively fast and proceed usually in less than 15 min for the radical route. Currently, a major drawback in batch-wise operations is the difficulty to control the exothermic behavior of the polymerization reaction, which limits the scale at which these reactions can be carried out since an increase in batch size is often accompanied with a loss of the superior polymer properties. This key issue can be overcome by utilizing continuous microreactor technology (MRT).[1-9] MRT has frequently shown to be an efficient and attractive alternative for advanced polymer reactions compared to classical batch reactions.[3-11] The small volume of a microreactor – in comparison to the size of its reactor channels (< 1 mm) – leads to a high surface-to-volume ratio, which assures an excellent heat transfer.[4,7-11] This way, almost ideal isothermal reaction conditions can be reached throughout the whole reactor leading to less side reactions, higher product yields – and most importantly for polymer reactions – a better definition of the polymeric material. In addition, temperature regimes above the boiling point of the solvent can be easily maintained by working under elevated pressures (20 bar).[1,8] Combined with rapid mixing, reactions can be significantly accelerated, allowing for better kinetics and shorter reaction times as compared to batch processes.[4,8] The transfer of batch protocols to microflow thus requires re-optimization of reaction temperatures, residence times and reagent concentrations.[12-14] After process optimization, uniform product distributions are obtained since microreactors offer very stable and highly reproducible reaction

conditions. In addition, significant product volumes can be produced by employing extended reaction run times or by upscaling to larger or parallel reactor set-ups.[1,4]

In here, the direct synthesis of conjugated PPV materials is targeted in microfluidic reactors. Therefore, the elimination process of sulfinyl precursor polymer in microflow reactors is studied, from which poly([2-methoxy-5-(3',7'-dimethyloctyloxy)]-1,4-phenylenevinylene]) ((MDMO)-PPV), a well-studied conjugated material, is obtained. Optimization of the elimination in flow is described. In a second step, the elimination is then combined with the sulfinyl precursor route radical polymerization in flow (optimization of the radical sulfinyl polymerization from MDMO precursor monomer into MDMO-precursor PPV was reported elsewhere).[9,12] Two glass-chip reactors are coupled to perform both stages of the (MDMO)-PPV synthesis in one step without requirement to isolate the intermediate. In this way, the excellent sulfinyl precursor route and its thermal elimination step is combined with the advantages of MRT, yielding a continuous process for the synthesis of well-defined conjugated PPV materials in a simple and easily scalable manner.

5.2. EXPERIMENTAL SECTION

5.2.1. Microreactor set-up for polymerization (P1) or elimination (P1') of (MDMO)-PPV

Microreactions are performed in the Labtrix® Start R2.2 system (Chemtrix BV, NL) fitted with a glass microreactor (3227, reactor volume 19.5 μL) containing an SOR-2 static micromixer, Figure 5-1. The system is maintained at 20 bar of back pressure by means of a preset ultralow dead-volume (6 μL) back pressure regulator (Upchurch Scientific). Reactant solutions are introduced into the reactor through three 1 mL gastight syringes (SGE). The pumps are capable of delivering three solutions at flow rates between 0.1 and 40 μL·min^{-1}. The flow rates are controlled via two syringes pumps (Chemyx). The reactor is controlled by a temperature controller MTTC1410 (Melcor Thermal Solutions, temperature range -15 °C to 195 °C).
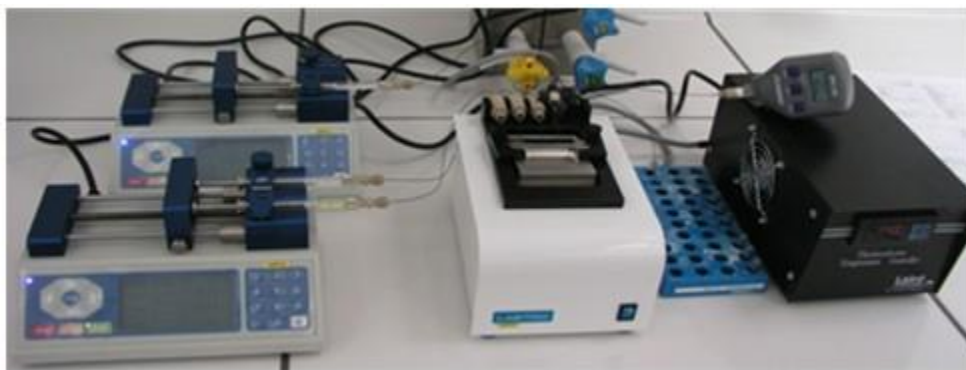
Figure 5-1: Microreactor setup for production of (MDMO)-PPV under optimized flow conditions

5.2.2. Flow reactor coupling

A scheme of the reactor setup is given in Scheme 5-1. The reagent solutions (premonomer and base solutions) are directly injected via syringe pumps (**A**) into the first microreactor (3223, reactor volume 10 μL, **D**) to perform the polymerization reaction (Scheme 5-2). The reaction temperature is controlled by a temperature controller (**C**) and is set via a reactor heating unit block (**B**). An in-line manometer connected via a Micro Tee Splitter (Upchurch Scientific, dead volume 29 nL) (**E**) is placed after the first reactor to monitor the pressure over the second reactor, thereby detecting eventual blockages at a premature stadium. The use of a check valve (**F**) (Upchurch Scientific, dead volume 7.4 μL) at the entrance of the second reactor prevents solvent or product back-flow from the second to the first reactor. The dead volume between the reactors is kept at minimum volume to avoid reactions during transfer between the two reactors. Addition of a second solvent via a syringe pump (**G**) enables the thermal elimination reaction in the second reactor (3227, reactor volume 19.5 μL, **J**). At this point, a dilution factor can be chosen to obtain certain concentrations in the microreactor, by systematically varying the flow rate of the syringe pumps (**G**). As a result, a doubling in flow rate in the second reactor as compared to the first is employed, leading to shorter residence times in the second reactor at equal volume. Thus, higher reactor volumes for reactor 2 are chosen to permit use of longer residence times. The temperature is controlled by a separate temperature controller (**I**) and a reactor heating unit block (**H**). Via an in-line back pressure regulator (BPR) (**K**) (20 bar) the reaction mixture exits the microflow reactor and is collected in glass vials. The BPR is placed after the second reactor to enable reactions above the boiling temperature of the solvent, creating an overpressure

thereby preventing oxygen inclusion into the system and increasing the flow stability in general. The BPR has a significant dead volume (compared to the reactor volume), yet due to the much lower temperature in the BPR, no further reaction must be expected in this dead volume part. Tubings used in this set up are made from polyether ether ketone (PEEK) (1/32″ O.D. and 90 μm I.D.). The dead volume in between the first and second microreactor is 7.7 μL and between the exit of the second microreactor exit and the collection vial is 7.6 μL, resulting in a total dead volume of 15.3 μL of the complete set up. The corresponding dead time that correlates with the dead volume results in a total dead time of 1.53 min.
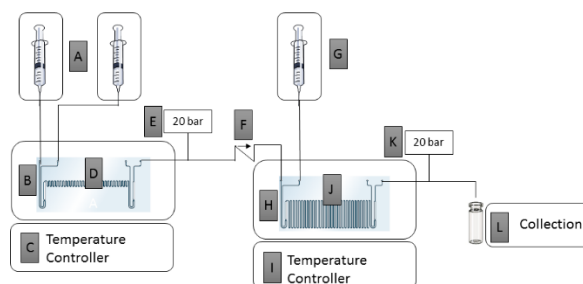
Scheme 5-1: Schematic overview of the PPV precursor polymerization (**P1**) and thermal elimination (**P1'**) in continuous flow (micro)reactors

5.2.3. General method for the polymerization of (MDMO)–PPV

$R_1 = C_{10}H_{21}$
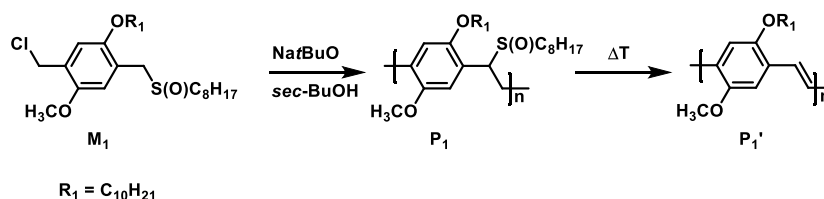
Scheme 5-2: Synthesis of conjugated (MDMO)-PPV via the sulfinyl precursor route

A solution of MDMO sulfinyl premonomer (15.8 mg, 32 µmol, 1 equiv.) in *sec*-BuOH (1 mL) and a solution of sodium *tert*-butoxide (Na*t*BuO; 3.2 mg, 32 µmol, 1 equiv.) in *sec*-BuOH (1 mL) were added to separate Schlenk tubes and subjected to three freeze pump thaw cycles and subsequently inserted into the glovebox. The Schlenk tubes were opened and two 1 mL syringes were filled with the different mixtures, after which the syringes were connected to the Labtrix® system and subsequently pumped into the microreactor (3223, reactor volume 10 μL). Several reaction times as well as reaction temperatures were screened by collecting samples in small vials containing hydroquinone and 1M HCl to deactivate the radicals and base respectively, resulting in the crude product **P1** as a yellow viscous oil (49 %), Scheme 5-2. SEC (THF): M$_n$ = 30 600 g.mol^{-1}, Đ = 2.2. ^{1}H-NMR (CDCl$_3$): δ = 6.90 – 6.20 (m, 2H); 4.90 – 4.60 (t, 1H); 4.00 – 2.90 (m, 7H); 2.70 – 2.10 (t, 2H); 1.90 – 1.10 (m, 22H) ; 1.00 – 0.80 (m, 12H). ^{13}C-NMR (CDCl$_3$): δ = 151.40 (C4); 127.0 (C4); 110.50 (CH); 67.90 (CH$_2$); 59.10 – 55.10 (CH); 56.40 (CH$_3$); 49.70 (CH$_2$); 39.20 (CH$_2$); 37.40 (CH$_2$); 36.60 (CH$_2$); 32.10 – 29.10 (CH$_2$); 30.20 (CH$_2$); 27.90 (CH$_2$); 24.60 (CH$_2$); 22.60 (CH$_2$); 21.90 (CH$_3$); 19.80 (CH$_3$); 13.50 (CH$_3$). FT-IR (NaCl): 2955, 2927, 1509, 1471, 1462, 1413, 1222, 1031 cm^{-1}

5.2.4. General method for the elimination of (MDMO)-PPV

Precursor PPV (9.4 mg) in toluene (1 mL) was added to a Schlenk tube and subjected to three freeze pump thaw cycles and subsequently inserted into the glovebox. The Schlenk tube was opened and a 1 mL syringe was filled with precursor polymer solution, after which the syringe was connected to the Labtrix® system and subsequently pumped into the microreactor (3227, reactor volume 19.5 μL). Several reaction times as well as reaction temperatures were screened

by collecting samples in small vials filled with methanol, leading to a red precipitate. The precipice was dried under vacuum to yield the conjugated polymer as a red powder (98 %). SEC (THF): M_n = 35 800 g.mol^{-1}, $Đ$ = 2.4. ^{1}H-NMR (CDCl$_3$): δ = 7.49 (m, 2H); 7.19 (m, 2H); 4.60 – 3.20 (m, 5H); 2.10 – 0.6 (m, 19H). ^{13}C-NMR (CDCl$_3$): δ = 151.40 (C4); 127.0 (C4); 110.50 (CH); 108.85 (CH); 67.90 (CH$_2$); 56.40 (CH$_3$); 39.20 (CH$_2$); 37.40 (CH$_2$); 36.60 (CH$_2$); 30.20 (CH$_2$); 27.90 (CH$_2$); 24.60 (CH$_2$); 22.60 (CH$_2$); 19.80 (CH$_3$). FT-IR (KBr): 2957, 2925, 2860, 1510, 1469, 1395, 1217, 1028, 872 cm^{-1}.

5.3. RESULTS AND DISCUSSION

5.3.1. Synthesis of Conjugated PPVs in two separate steps

As mentioned above, the batch synthesis of (MDMO)-PPV via the radical sulfinyl precursor route is a two-step process. Reaction kinetics of the polymerization are difficult to follow due to the fast initiation and propagation of radicals, hence the formation of the polymer can only be followed spectroscopically (UV-Vis). The elimination, however, is easily followed visually due to the formation of the pi-conjugated system. During elimination, the color changes from yellow (precursor polymer) to red (conjugated polymer). For batch reactions both steps have been extensively optimized, though always for stand-alone reactions. Optimization of the precursor (MDMO)-PPV polymerization in flow leads to the conclusion that maximum conversion is reached using a $[M]_t$ of 1.625 x 10^{-2} mol·L^{-1} at 50 °C and 10 minutes of polymerization time (Figure 5-2). Maximum conversions around 45 % are somewhat lower than in batch synthesis, but this can be accounted to the decreased monomer concentration. Batch polymerization of the same solution leads to similar yields as observed in flow. Wong and coworkers[9] were able to reach up to 70 % conversion for the Gilch precursor route in a different flow system, making use of five times higher monomer concentration. As a downside, however, long reaction times of 30 min were required and severe problems regarding reactor blockages were reported. Upon increasing reaction temperature, elimination of the precursor polymer into its conjugated form will start to appear, which should be avoided during polymerization to maintain a good stability and conformity of the polymerization. A decrease in reaction temperature leads to generally slower reactions as well as to more random kinetic data. In the polymerization itself, the initial monomer concentration plays a crucial role. Higher

monomer concentration and as a consequence also polymer concentrations, in combination with a number-average molecular weight (M_n) of 50 000 g·mol^{-1} and the higher viscosity *sec*-BuOH, hinders continuous polymerization in flow. Yet, with the above mentioned parameters well-defined polymers with neat molecular weights are obtained. Final conversions are somewhat lower than in the corresponding batch processes (~60%), but still within range of a satisfactory process keeping the general difficulties of PPV polymerization in mind. Details on this protocol will be discussed in a forthcoming study alongside extensive kinetic modelling to elucidate the exact reaction mechanism and to determine kinetic rate coefficients that underpin the polymerization.[15]
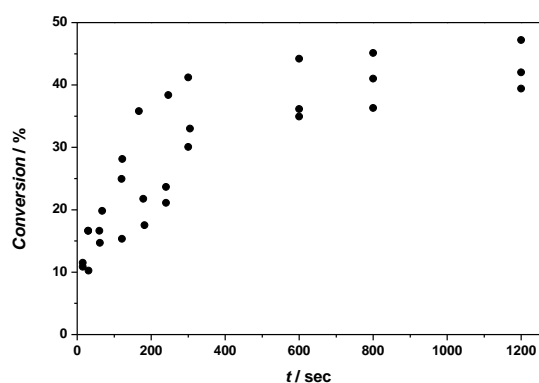
Figure 5-2: Conversion of precursor (MDMO)-PPV synthesized at 50 °C in flow using a $[M]_t$ of 1.625 x 10^{-2} mol·L^{-1}. The reaction is performed 3 times for reproducibility

Standard batch elimination reactions of the precursor polymer take 3 h at 110 °C to reach full conversion. Higher temperatures are only difficult to realize in batch due to the limitations stemming from the choice of solvent. Microreactors allow

for easy screening of reaction temperatures and reaction times and an assessment of the elimination reaction in a broader range of conditions is easily achievable. For testing flow eliminations, (MDMO)-PPV was synthesized in batch ($[M]_i$ = 0.14 mol·L^{-1} in *sec*-BuOH) and Na*t*BuO as base ($[B]_i$ = 0.16 mol·L^{-1} in *sec*-BuOH). To ensure full conversion, the reaction was allowed to react for 1 h at 30 °C, after which precipitation in cold methanol results in the purified yellow precursor polymer. Next, the precursor (MDMO)-PPV was dissolved in toluene ($[P]_i$ = 3.25 x 10^{-2} mol·L^{-1}) and injected into the flow reactor via a glass syringe. The eliminated product was collected and directly precipitated in methanol upon exiting the flow reactor. Due to the dimensions of the flow reactor and limitations in the flow rate, the residence time was limited to 20 minutes and temperature was screened between 110 °C and 195 °C.

Table 5-1: Precursor polymer conversion into conjugated chains as determined by ^{1}H NMR and maximum absorption wavelengths λ_{max} as obtained by UV-Vis results offer conjugated (MDMO)-PPV synthesized under different various reaction conditions in the continuous flow (colored numbers indicate best results).

| Time | Conversion[a] | | | | λ_{max} | | | |
| min | % | | | | nm | | | |
	110°C	150°C	180 °C	195 °C	110°C	150°C	180 °C	195 °C
20	n.a.	93	**97**	n.a.	370	497	**500**	n.a.
10	n.a.	92	97	99	373	495	493	487
5	n.a.	92	93	<u>99</u>	372	495	488	**493**
4	n.a.	92	92	98	n.a.	494	487	491
3,03	n.a.	91	n.a.	n.a.	n.a.	492	n.a.	n.a.
2	n.a.	89	94	96	n.a.	485	480	487
1	n.a.	88	91	93	n.a.	461	494	491
0,5	n.a.	87	91	94	n.a.	442	491	492

[a] conversions were determined by ^{1}H NMR measurements

Progress of the elimination reactions is traced via two different methods. Via ^{1}H-NMR, the conversion of the elimination reactions is followed by observation of the loss of the sulfinyl-group typical signals in the spectrum. The sulfinyl signal (2.65 ppm) is compared to the *OCH₃* group attached to the phenyl ring (3.91 ppm) of which one example of the ^{1}H NMR spectrum of (partly) eliminated PPV is shown in Figure 5-3.
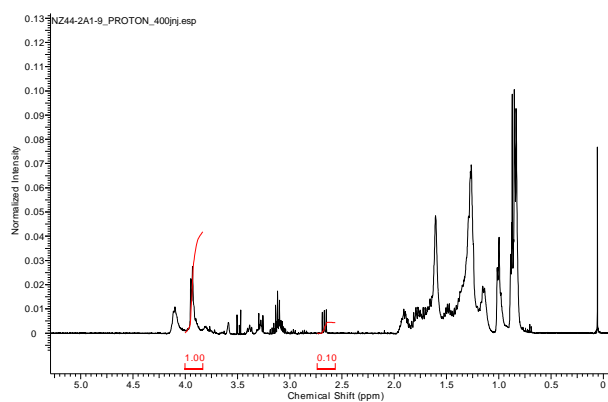
Figure 5-3: Zoom into ^{1}H NMR spectrum of (partly) eliminated PPV used for quantifying the elimination step from precursor PPV to conjugated PPV

Generally, this method is highly reliable. Nevertheless, a second technique was used to assess the quality of the formed (MDMO)-PPV. If defects occur in the conjugated system, the maximum absorption wavelength of the material is shifted towards lower wavelengths. Thus, this characteristic wavelength can also be used to monitor the progress of the elimination (build-up of the conjugated system) as well as for detection of side-reactions that might disturb conjugation (reduction of wavelength) For a high-quality (MDMO)-PPV as typically obtained by the sulfinyl precursor route, maximum absorption (λ_{max}) should be observed close to 500 nm.
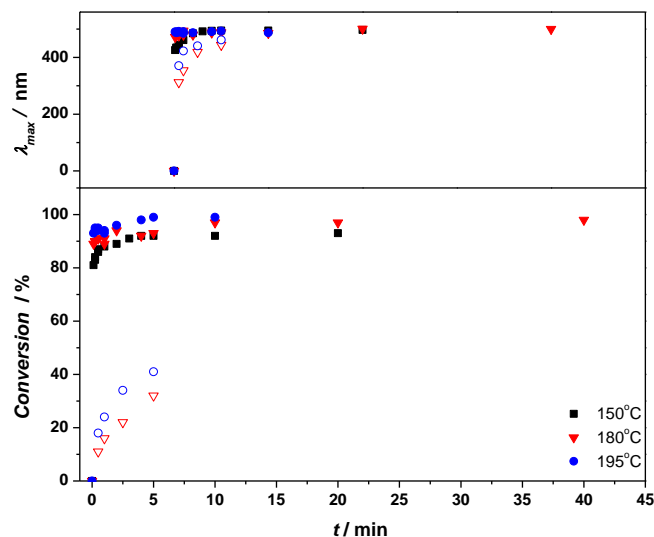
Figure 5-4: Visualization of data given in Table 5-1 for the flow elimination of precursor polymer to obtain conjugated (MDMO)-PPV. Closed symbols display the results as obtained when performing solely the elimination step. Open symbols display the results of the complete two step reaction when two reactors are coupled together

UV-Vis and ^{1}H NMR measurements (Table 5-1 and Figure 5-4) reveal that all polymers synthesized at 110 ˚C did not reach full conversion within 20 minutes, as could also be directly observed by the lack of color change in the reaction. λ_{max} values indicate an insufficient maximum red shift from 300 nm to 420 nm. Upon increasing temperature, UV-Vis as well as ^{1}H NMR results confirm successful conversion of the precursor PPV into the conjugated (MDMO)-PPV. At 150 °C, a maximum conversion of 93 % is achieved after 20 minutes of residence time, while raising the temperature even further to 180 °C clearly indicates full conversion up to almost 100 % elimination after a residence time of 20 minutes. The obtained λ_{max} value of 500 nm is in line with measurements found in literature

for standard (MDMO)-PPV. A further increase in temperature to 195 °C decreases the required reaction time to even 5 minutes, however, a minimal blue shift towards 493 nm is observed for the product, indicating an onset of degradation of the polymer.[16] Progress of the reaction is easily followed by shining UV-light (365 nm) onto the reactor (Figure 5-5), allowing a visual observation of the progress of the elimination reaction. In the initial stage, no to little fluorescence is seen but with increasing length (and thus residence time) of the microchannel, increasing intensity of the fluorescence can be observed – directly indicating the success of the elimination reaction. In principle, 2D-spectrophotometric analysis of the reactant distribution in the reactor channel would allow for instantaneous determination of the full reaction kinetics.
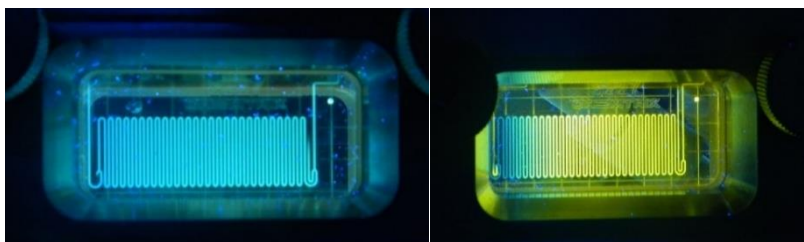
Figure 5-5: Microflow polymerization for precursor (MDMO)-PPV synthesis as observed under UV radiation (λ = 365 nm); *left:* polymerization into precursor polymer at 30 °C, *right;* elimination into conjugated polymer at elevated temperatures

The above experiments are – like the precursor polymer synthesis in flow – performed at rather low polymer concentrations. An increase in concentration would have a rather small effect on the rate of elimination, yet, it can lead to blockages in the reactor due to precipitation of (MDMO)-PPV and the formation of salts. The polymer concentration was thus chosen accordingly to allow for stable

operation of the reactor. Regardless, closer inspection of the above screening of reaction conditions shows that operation of the flow reactor between 180 °C and 195 °C with a residence time of maximum 10 minutes results in conjugated (MDMO)-PPV with good product quality. Overall, (MDMO)-PPV can be synthesized in two separate steps in flow already with good success. While for both reaction steps reduced concentrations in monomer and polymer, respectively, must be applied to avoid viscosity issues, significant acceleration of the reaction can be reached. The precursor polymer synthesis is optimized for reaction times of 10 minutes – compared to 1 to 1.5 h in batch. The elimination reaction is accelerated from 3 h in the typical batch procedure to merely 5-10 minutes in flow. Thus, the gain in reaction rate counteracts the reduction in concentration, allowing the synthesis of (MDMO)-PPV in good overall yields. For an increase of initial monomer concentration, and thus increase in overall conversion, the obstacle of reactor fouling must be overcome. A scale up from reactors with μm channel widths to close to mm has in the past already proven to be beneficial when used for reactions containing salt formation.[17] Upscaling of the herein described process would thus directly also lead to an even better yield/time relation.

5.3.2. Synthesis of conjugated PPVs in a coupled flow reactor set-up

In the above described separate flow reactions, still isolation of material at the precursor polymer stage is required (as in the batch process). A direct combination of both steps into one coupled flow reactor setup is preferable since in such reactor system no material is lost in the isolation step – and obviously because a one-step process is significantly simpler in operation. The general difficulty here is to allow the successful coupling of two reactor chips. Reaction combination within

one chip is not feasible since very different reaction temperatures need to be applied for polymerization and elimination, respectively. Also, the choice of solvent is crucial. For the polymerization reaction, generally *sec*-BuOH is favored while elimination is best carried out in less polar solvents such as toluene. Since a complete solvent change is not easily reached, dilution of the reaction mixture in the second step was tested. To test the coupling precursor monomer and base were both dissolved individually in *sec*-BuOH ($[M]_t$ = 3.25 x 10^{-2} mol·L^{-1}) and subsequently injected into the first reactor. Addition of further *sec*-BuOH (1 μL·min^{-1}) via the quencher line at the end of the reactor residence unit is required to prevent clogging at the reactor outlet. The outlet of the first reactor is directly – via a check valve connection – inserted into the second reactor. This reaction mixture is diluted with toluene in a 1:1 v/v% ratio, resulting in a total polymer concentration $[P]_i$ of 1.625 x 10^{-2} mol·L^{-1}. It has to be added that the third entrance in the first reactor – *sec*-BuOH with a flow rate of 1 μL·min^{-1} – further decreases $[M]_t$ within the second reactor. For reactions performed at longer residence times (>10 minutes), this can lead to a decrease of up to 20% in $[M]_t$ in the second reactor. As in this study the residence time in the first reactor is limited to 5 minutes, this effect is neglected. Elimination reactions in the second reactor are screened at optimized temperature (180, 187 and 195 °C) thereby varying the residence time between 3.2 and 0.5 min. in the second reactor. Under these conditions, thermal elimination of the precursor (MDMO)-PPV takes place and precipitation of the product after exit from the second reactor in methanol results in the desired conjugated (MDMO)-PPV product (up to 42 % total conversion and λ_{max} of close to 500 nm).

Table 5-2 summarizes the results of the one-step two-reactor flow synthesis of (MDMO)-PPV under variation of the individual reactor residence times. Again UV-Vis and ^{1}H NMR are used to monitor the success of the reactions. Conversions are given individually for the elimination (step 2) as well as for the overall process (step 1+2, thus conversion of monomer into conjugated (MDMO)-PPV). Additionally, average molecular weights of the residual (MDMO)-PPV is given. Polymerizations are in all cases carried out at 50 °C, while eliminations are performed at 180 °C, 187 °C and 195 °C, respectively. All reactions result in synthesis of conjugated (MDMO)-PPV. Maximum conversion (of the elimination) of almost 100 %, a λ_{max} value close to the theoretical value of 500 nm and a M_n in the range of 10 000 - 30 000 g·mol^{-1} indicate that the complete reaction pathway from precursor PPV to conjugated PPV in a combined microflow system is successful when residence times and temperatures are chosen accordingly.

Table 5-2: ^{1}H NMR and UV-Vis results for conjugated (MDMO)-PPV synthesized under different reaction conditions in a coupled continuous microflow reactor using a $[M]_t$ of 1.625×10^{-2} mol·L^{-1}

Residence Time / min		Conversion[a] %		M_n g·mol^{-1}	Đ	λ_{max} nm	Conversion[a] %		M_n g·mol^{-1}	Đ	λ_{max} nm	Conversion[a] %		M_n g·mol^{-1}	Đ	λ_{max} nm
R1	R2	Step 1+2	Step 2	Reactor 1: 50 °C / Reactor 2: 180 °C			Step 1+2	Step 2	Reactor 1: 50 °C / Reactor 2: 187 °C			Step 1+2	Step 2	Reactor 1: 50 °C / Reactor 2: 195 °C		
5	3.2	32	93	17 100	2.7	487	38	96	18 500	2.3	495	41	99	9 700	2.7	489
		33	95	16 100	2.5	489						42	99	11 600	2.4	489
2.5	2	22	92	17 300	2.7	481	25	95	24 600	2.2	494	34	97	18 000	2.4	488
		24	94	18 900	2.5	487						35	98	17 000	2.5	491
1	1	16	89	19 800	2.9	480	19	92	30 500	1.9	496	24	95	18 000	3.2	484
		17	88	12 200	2.2	486						26	97	21 800	2.0	490
0.5	0.5	11	90	22 800	3.0	476	14	92	37 600	2.0	495	18	95	29 100	1.9	487
		18	92	28 200	2.5	484						21	97	31 800	2.2	491

[a] conversions are determined via ^{1}H NMR measurements

As was already concluded for the elimination step, reactions performed at 195 °C show an onset in degradation of the polymer. M_n generally decreases with increasing reaction time (and thus monomer conversion) in reactor 1. This can be explained by the reduction in propagation rate upon consumption of the monomer. At the same time, at comparable high conversions, also a decrease in M_n with increasing temperature is observed, which can only be explained by chain scission events taking place at 195 °C. Thus, even though monomer conversion and elimination efficiency is slightly better at 195 °C, the result for 5 min/3.2 min residence time with the second stage reaction at 187 °C is regarded as most optimal outcome. Molecular weights are still not yet significantly altered compared to 180 °C reaction temperature, yet good λ_{max} is reached with overall satisfying conversions.

Variations in reaction time and temperature demonstrate that the reaction time for the polymerization reaction inside the first reactor is the limiting factor to reach high overall yields. Yet, in the discussion of overall yields, it should be noted that herein a one-step procedure is compared with a two-step batch process. Yields of polymerization in batch are often higher, yet usually material is lost during precipitation and product isolation, making a lower yield in the combined flow process more valuable. Short residence time in the first reactor results in low overall conversions as not all monomer is consumed in the polymerization before thermal elimination is started upon reaching the second reactor stage. By choosing longer residence times in the first reactor, overall yields can be increased. Interestingly, at shorter residence times in the first reactor, not only lower monomer conversions are observed, but also significantly lower molecular

masses are obtained – which indicates the influence of oligomer formation upon decreasing monomer concentration.

Regardless, it should be noted that determination of molecular weights of PPV materials are associated with significant difficulties in SEC calibration and numbers given are thus only indicative. Despite the somewhat reduced M_n for the results obtained at 195 °C, longer residence times are additionally beneficial due to the in such case lower flow rates in the first stage, giving access to increased residence times in the second reactor. This allows giving the elimination more time. As could already be seen from Figure 5-2, maximum conversion of the first polymerization step is limited to 45 %. The total conversion that is reached for the reaction at 50 °C /195 °C and 5 min / 3.2 min residence time of 42 % can thus be regarded as very close to the theoretically possible conversion for the coupled process. As mentioned above, reactions performed at 187 °C show a slight decrease in conversion (38 %), but a representative M_n and λ_{max} value of 18 500 g·mol^{-1} and 495 nm respectively as compared to results for the 195 °C reaction – M_n of 9 700 g·mol^{-1} and λ_{max} of 489 nm. Hence, reactions performed at 50 °C /187 °C and 5 min / 3.2 min residence time therefore demonstrates concomitantly that elimination could take place sufficiently despite the presence of some *sec*-BuOH in the reaction mixture, allowing for the synthesis of high-quality (MDMO)-PPV as is typically obtained by the sulfinyl precursor route.

5.4. CONCLUSIONS

A general method for the continuous synthesis of the multistep sulfinyl-route (MDMO)-PPV polymerizations is made available by coupling two flow microreactors. Conjugated polymer is in this way obtained directly from monomer, which is under batch conditions not easily reached for this type of polymerization. Polymerization takes place at 50 °C and reaches a maximum conversion of 45 % within 10 minutes (for an initial monomer concentration of $[M]_i = 3.25 \times 10^{-2}$ mol·L^{-1}). The elimination step is also optimized for flow conditions and full conversion is reached within 20 minutes residence time at 180 °C. Conjugated polymer with a characteristic λ_{max} of 500 nm is obtained, indicating good microstructural control over the reaction. A further increase in temperature to 195 °C decreases the required reaction time to even 5 minutes, however, a minimal blue shift towards 489 nm is observed for the product due to the onset of polymer degradation as well as onset of chain scission, limiting the molecular weights accessible. Both reactions can be combined in a coupled microreactor setup and (MDMO)-PPV synthesis is demonstrated in a one-step procedure, reaching a total monomer-to-conjugated (MDMO)-PPV conversion of 38 % for a reaction at 50/187 °C and 5/3.2 min residence time, respectively. The successful coupling of two reactors solves not only a significant obstacle in the upscaling of conjugated polymer synthesis via continuous flow methods, but also marks a significant step in the evolution of polymer reaction design in microstructured flow reactors in general.

5.5. REFERENCES

[1] J. Vandenbergh, T. de Moraes Ogawa, T. Junkers, *J. of Polym. Sci. Part A: Polym. Chem.* **2013**, *51*, 2366-2374.

[2] N.-T. Nguyen, Z.J. Wu, *Micromech. Microeng.* **2005**, *15*, R1.

[3] G. Jas, A. Kirschning, *Chem. Eur. J.* **2003**, *9*, 5708-5723.

[4] K. Geyer, J. D. C. Codée, P. H. Seeberger, *Chem. Eur. J.* **2006**, *12*, 8434-8442.

[5] V. Hessel, A. Renken, J. Schouten, J. Yoshida, *Micro Process Engineering*: *A Comprehensive Handbook;* Wiley-VCH: Weinheim, **2009**.

[6] N. Kockmann, O. Brand, G. K. Feder, *Micro Process Engineering*, Wiley-VCH: Weinheim, **2006**.

[7] D. Wilms, J. Klos, H. Frey, *Macrom. Chem. and Phys.* **2008**, *209*, 343-356.

[8] K. Jähnisch, V. Hessel, H. Löwe, M. Baerns, *Angew. Chem. Int. Ed.* **2004**, *43*, 406-446.

[9] H. Seyler, D. J. Jones, A. B. Holmes, W. W. H. Wong, *Chem. Commun*. **2012**, *48*, 1598-1600.

[10] C. Wiles, P. Watts, *European J. of Org. Chem.* **2008**, 1655-1671.

[11] P. D. I. Fletcher, S. J. Haswell, E. Pombo-Villar, B. H. Warrington, P. Watts, S. Y. F. Wong, X. Zhang, *Tetrahedron* **2002**, *58*, 4735-4757.

[12] J. Vandenbergh, T. Junkers, *Polym. Chem.* **2012**, *3*, 2739-2742

[13] J. J. Haven, J. Vandenbergh, T. Junkers, *Chem. Commun.* **2015**, *51*, 4611-4614.

[14] C. Tonhauser, A. Natalello, H. Löwe, H. Frey, *Macromolecules* **2012**, 45, 9551-9570.

[15] N. Zaquen, P. H. M. Van Steenberge, D. R. D'Hooge, M.-F. Reyniers, G. B. Marin, J. Vandenbergh, L. Lutsen, D. Vanderzande, T. Junkers, *Macromolecules* **2015**, *48*, 8294-8306.

[16] E. Kesters, S. Gilissen, F. Motmans, L. Lutsen, D. Vanderzande, *Macromolecules* **2002**, *35*, 7902– 7910.

[17] J. Vandenbergh, T. Tura, E. Baeten, T. Junkers, *Polym. Chem.* **2014**, 52, 1263-1274.

CHAPTER 6

Improved Mechanistic Insights into Radical Sulfinyl Precursor (MDMO)-PPV Synthesis by Combining Microflow Reactor Technology and Computer Simulations
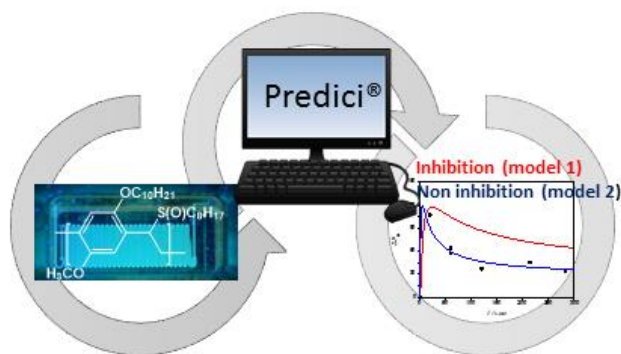
N. Zaquen, P. H. M. Van Steenberge, D. R. D'Hooge, M.-F. Reyniers, G. B. Marin, J. Vandenbergh, L. Lutsen, D. Vanderzande, T. Junkers, *Macromolecules* **2015**, *48*, 8294-8306.

ABSTRACT

A kinetic model using Predici® is developed and applied to obtain an improved mechanistic understanding of the radical sulfinyl precursor polymerization route for poly([2-methoxy-5-(3'-7'-dimethyloctyloxy-4-((octylsulfinyl)methyl))]-1,4-phenylene vinylene) ((MDMO)-PPV) synthesis. In this route, the premonomer – 1-(chloromethyl)-5-((3,7-dimethyloctyl)oxy)-2-methoxy-4-((octylsulfinyl) methyl)benzene (MDMO) – is subjected to a base induced elimination reaction using NatBuO as base and sec-BuOH as solvent. Microreactors are used to ensure rapid mixing of reaction components and sharp quenching at precisely determined time points. Systematic kinetic data that follow the very fast precursor polymerizations with reaction time have in this way become available for the first time. Via the applied kinetic model, the presence of a chain transfer reaction is unambiguously confirmed and kinetic rate coefficients have been deduced, which fall within the typical expectations of radical chain reactions. Two models were further compared, one including chain reinitiation (non-inhibition model) and one excluding reinitiation (inhibition model) of the by chain transfer-generated radical species. Investigation of trend lines suggest a preference for the reinitiation model, thereby implying that (MDMO)-PPV synthesis follows mostly a conventional free radical polymerization mechanism that only differs with respect to its initiation mode and the biradical nature of the propagation step.

6.1. INTRODUCTION

Despite the recent advances in the controlled synthesis of PPVs, there are considerable uncertainties about the underpinning mechanism and the rate of the individual reaction steps. Several kinetic studies concerning not only the sulfinyl[1-3] but also the Gilch[4] and the dithiocarbamate[5-7] routes provided already more insight into the mechanistic details of the polymerization. However, comprehensive kinetic modeling studies for the precursor routes towards PPVs are still scarce.[8-11] The latest work on kinetic modeling of sulfinyl precursor PPV synthesis by Van Steenberge *et al.,*[11] which is a follow up on the work of Hermosilla *et al.,*[8] is based on Monte Carlo and Predici® kinetic calculations. At that time, only little experimental data, typically at final monomer conversion, was available that could be reasonably described by a kinetic model ignoring radical recombination and cyclization. Recent more dedicated size exclusion chromatography (SEC) and electrospray ionization mass spectrometry (ESI-MS) measurements, however, do indicate the significant occurrence of these reactions.[12] A revision of the so far used kinetic models is thus clearly required.

Retrieval of accurate data during PPV synthesis is though difficult due to the high reaction rate and the inherent self-initiation that occurs even at low reaction temperatures (< 0 °C). Yet, much better models and mechanistic insights could be obtained by the consideration of time dependent experimental data taken at different polymerization temperatures and initial concentrations. Recently, microreactors were shown to provide excellent synthesis conditions as well as being excellent tools for kinetic screening.[13-15] A high control over reaction conditions is established in microreactors, allowing often for the stable production

of higher yields and a lower byproduct formation compared to conventional batch processes.[16-18] In addition, under microflow conditions a better reproducibility, a fast and efficient screening of reaction conditions and an easy scale-up production from mg to kg scale is possible.[19] As an additional advantage – of very high value with respect to PPV polymerization – microreactors can also be used to conveniently perform reactions with very short reactions times (minute scale) as the impact of mixing effects is minimized, in contrast to comparable batch reactions. Hence, kinetic data for poly([2-methoxy-5-(3'-7'-dimethyloctyloxy-4-((octylsulfinyl)methyl))]-1,4-phenylene vinylene) ((MDMO)-PPV) synthesis could be gathered for short reactions times, which would in comparable batch reactions not be possible.

Herein, we focus on the improved mechanistic understanding of PPV synthesis via the radical sulfinyl precursor route. First, the synthesis of (MDMO)-PPV is experimentally optimized under microflow conditions. Different reaction temperatures, initial pre-monomer concentrations and reaction times are screened, yielding a broad range of systematic kinetic data. In a second step, a Predici® model is designed based on these time dependent experimental data, placing special emphasis on the trend line prediction of yield, number degree of polymerization (DP_n) and dispersity ($Đ$) of the precursor polymer. Modeling results are compared to experimental data, in this way giving access to individual rate coefficients and to a more refined mechanistic model, including transfer reactions.

6.2. EXPERIMENTAL SECTION

6.2.1. General method for the polymerization of (MDMO)-PPV

(MDMO)-PPV was synthesized as described in chapter 2 (synthesis of the monomer) and chapter 5 (polymerization in a continuous flow reactor).

6.2.2. Description of the kinetic model

A free radical polymerization (FRP) reaction scheme is assumed as a basis for the kinetic modeling study (Scheme 6-1). PPV polymerizations, however, differ from standard FRP for vinylic monomers as the monomer – *p*-quinodimethane – is formed *in situ* from premonomer, after which this species spontaneously polymerizes via a self-initiation mechanism by forming a biradical species (see Scheme 6-1, reactions I and II).[20] Polymerization of the latter results in the so-called precursor polymer, which can be converted to the conjugated polymer in an additional step via either a thermal treatment or base induced elimination. Polymerization and elimination can be considered as independent reactions and elimination must, hence, not be accounted for in the polymerization model, at least under well-defined conditions. On the other hand, the anionic attack of deprotonated solvent to a quinodimethane monomer could still occur (Reaction VIIb in Scheme 6-1). Yet, due to the presence of a protic solvent in the present work, such anionic chain reaction is immediately stopped, as shown in the reaction scheme and in agreement with earlier kinetic studies.[21]

(I) Monomer formation and self initiation

(II) Chain-Initiation

(III) Propagation

(IV) Radical Recombination

(V) Elimination and formation of conjugated polymers

(VI) Side reactions: Transfer reaction and chain reinitiation

(VII) Side reactions: Intramolecular termination and base induced product.
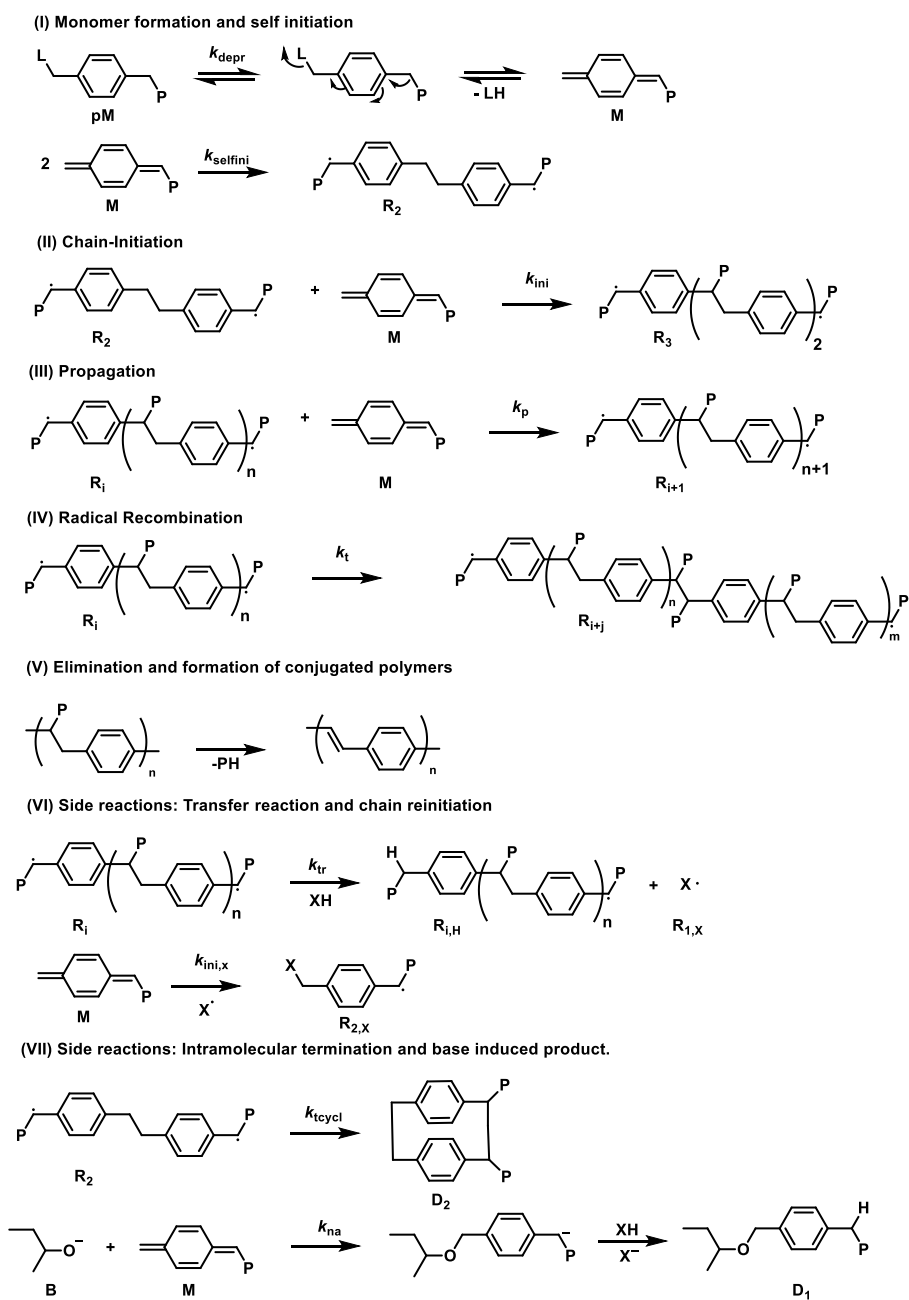
Scheme 6-1: Main reactions for the synthesis of PPV precursor polymer as used in the Predici® model and subsequent polarizer elimination; defects not explicitly shown

Termination is assumed to occur via bimolecular combination. Due to the formation of biradical species, however, this reaction leads only to a reduction of the radical concentration, but not to the formation of dead polymer chains as termination products are inherently still biradicals (see Scheme 6-1, reaction IV). On the other hand, polymer chains do not grow to "infinite" length (typically DP_n of 100), indicating the presence of a chain stopping event. One such reaction, intramolecular radical combination, *i.e.* cyclization, has been confirmed before, at least for short chain biradicals.[22] When analyzing crude product mixtures, significant amounts of paracyclophanes are found, which stem from such cyclization reaction. Whether such reaction also occurs at longer chain lengths is unclear but appears still reasonable taking into account the diluted conditions. Nevertheless, as quantitative data are not available for cyclization, paracyclophane formation was only accounted for with biradicals of length 2.

Another potential side reaction that can stop chain growth is radical transfer, which can transform a growing biradical into a growing chain with only one propagating end. Such species would then behave accordingly to classical macroradicals in FRP. The nature of the transfer reaction is however, not precisely known and only anticipated, since the chains cannot inevitably grow to "infinite" length and based on time dependent experimental data presented in this work (see further). As a placeholder, transfer to solvent (*sec*-BuOH; reaction VIa in Scheme 6-1) is assumed in the kinetic model as this is one of the most feasible transfer mechanisms, taking into account the high solvent concentration. Placeholder means in this respect that different transfer reactions might as well be occurring (e.g. transfer to polymer), but that all these effects are for the lack of better knowledge lumped into the transfer to solvent reaction in order to not overcomplicate the model. The impact of such transfer reaction may, however,

not be underestimated. To date, all kinetic models and proposals for reaction mechanisms did not take any type of transfer into account. At first sight driving forces for radical propagation are very high due to restoration of aromaticity of the quinodimethanes, putting a question mark on transfer. Yet, previous studies involving classical chain transfer agents demonstrate that transfer reactions can occur in PPV polymerization.[23]

It must also be noted that with the presence of a chain transfer event the question arises in how far a re-initiation of the polymerization can be assumed, starting from the fragment generated in the transfer. It can be expected that each formed radical will have difficulties to compete with the rapid self-initiation mechanism of the quinodimethanes, yet especially with respect to chain defects, information of chains stemming from a re-initiated fragment is of highest importance. In the following, two kinetic models are thus considered, which differ in whether chain re-initiation by the small radical fragments stemming from chain transfer reactions (X·) can be excluded (**model 1; inhibiton model**) or included (**model 2; non-inhibition model**).

Accurate rate coefficients for the above described reactions are scarce and limited to experimental work as published by *Hermosilla* et al.[8] A value of 14.62 ± 0.4 L·mol^{-1}·s^{-1} for the deprotonation coefficient (k_{depr}) was proposed after the use of stop-flow UV-VIS measurements at 25 °C. The remaining unknown parameters were initially taken from the simplified model of *Van Steenberge* et al.[11] In the further development, a broad range of values for the individual rate coefficients was screened, thereby putting special emphasis on the reaction observables M_n, Đ and polymer yield. Values and trend lines of the individual models were compared to experimental results as obtained by using microflow reactors.

6.2.3. Predici® model

Simulations have been carried out with Predici® (CIT) version. 7.1.0 on an Intel i7 CPU running at 2.40 GHz. For all simulations, a Predici® model comprising the following reaction steps and respective rate coefficients has been used:

Monomer Formation

(1)	$pM + B \rightarrow M$	k_{depr}
(2)	$M + M \rightarrow R_2$	$k_{selfini}$
(3)	$B + M \rightarrow D_1 + \cdots$	k_{na}

Chain Initiation

(4)	$R_2 + M \rightarrow R_3$	k_{ini}
(5)	$R_{1,X} + M \rightarrow R_{2,X}$	$k_{ini,x}$

Propagation

(5)	$R_i + M \rightarrow R_{i+1}$	$2k_p$
(6)	$R_{i,H} + M \rightarrow R_{i+1,H}$	k_p
(7)	$R_{i,X} + M \rightarrow R_{i+1,X}$	k_p

Transfer reactions

(8)	$R_i + X \rightarrow R_{i,H} + R_{1,X}$	$2k_{tr}$
(9)	$R_{i,H} + X \rightarrow P_{i,H} + R_{1,X}$	k_{tr}
(10)	$R_{i,X} + X \rightarrow P_{i,X} + R_{1,X}$	k_{tr}

Termination

$$(11) \qquad R_2 \rightarrow D_2 \qquad\qquad\qquad\qquad k_\text{tcycl}$$

$$(12) \qquad R_i + R_j \rightarrow R_{i+j} \qquad\qquad\qquad 4k_\text{t}$$

$$(13) \qquad R_{i,H} + R_j \rightarrow R_{i+j,H} \qquad\qquad 2k_\text{t}$$

$$(14) \qquad R_{i,X} + R_j \rightarrow R_{i+j,X} \qquad\qquad 2k_\text{t}$$

$$(15) \qquad R_{i,H} + R_{j,H} \rightarrow P_{i+j,H,term} \qquad k_\text{t}$$

$$(16) \qquad R_{i,H} + R_{j,X} \rightarrow P_{i+j,X,term} \qquad k_\text{t}$$

$$(17) \qquad R_{i,X} + R_{j,X} \rightarrow P_{i+j,XX,term} \qquad k_\text{t}$$
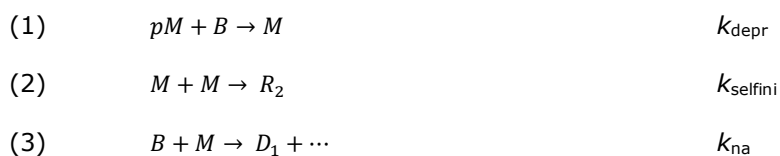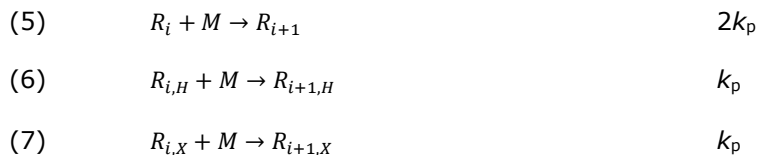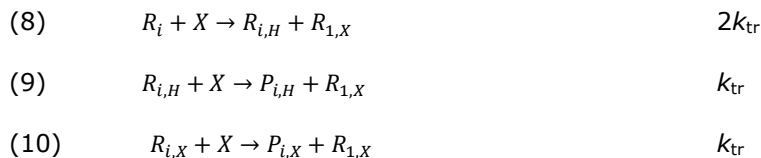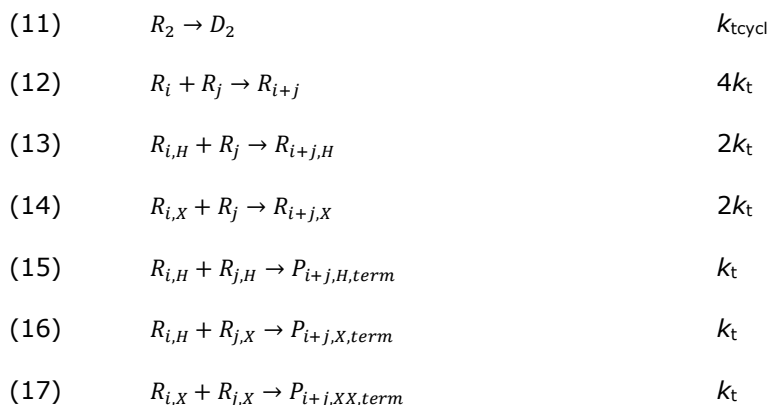
The above model describes the kinetics of the synthesis of (MDMO)-PPV via a radical sulfinyl pathway. A few assumptions and simplifications had to be made in order to arrive at a model that can be used on a practical level:

- Two models are designed in which chain reinitiation can either be excluded (**model 1**, inhibition model) or included (**model 2** non-inhibition model). As a placeholder, transfer to solvent (*sec*-BuOH) is assumed in the model, denoted as species X. Species X is defined as *sec*-BuOH with an initial starting concentration of 10.5 M (ρ = 0.808 g·cm^{-3} and M_n = 74.12 g·mol^{-1}). In general, species X could be seen as an additional (unknown) compound, susceptible to possible chain transfer.
- ESI-MS results indicate the presence of cyclic side products (dimers, trimers, tetramers and paracyclophane). As it is currently impossible to differentiate between these products quantitatively, all these reactions are placed together in one reaction in the model.

- Previous modelling work of *Van Steenberge* et. al.[11] assumed the presence of a base induced product as well. Although not observed experimentally via ESI-MS, this reaction step is still considered in the model to verify its influence.

- Termination occurs via bimolecular combination. Due to the formation of biradical species, however, this reaction leads only to a reduction of overall radical concentrations, but not to dead polymer chains as termination products remain inherently biradicals. Still, polymer chains do not grow to infinite length indicating the presence of an unknown chain stopping event. As a result a radical transfer reaction is implemented in the model as well.

Using the above reaction steps and rate coefficients as described above, simulations varying the individual kinetic parameters are monitored and compared to the experimental results obtained using MRT.

A differentiation between the different models needs to be made. Model 1 represents a model in which the X-species stemming from chain transfer is inactive. Model 2 represents the model where the same species can reinitiate polymerization.

6.3. RESULTS AND DISCUSSION

6.3.1. Experimental optimization of precursor (MDMO)-PPV synthesis in a microreactor

As mentioned above, the batch synthesis of (MDMO)-PPV via the radical sulfinyl precursor route has been optimized intensively.[16] Standard batch polymerization protocols take between a few minutes to one hour at 30 °C to reach maximum polymer yield. Due to the fast self-initiation and propagation of radicals, batch kinetics are, however, extremely difficult to follow. In addition, at higher temperatures premature elimination of the precursor polymer might occur, further complicating any kinetic investigation. In order to gain insights into an ongoing polymerization, two conditions must be fulfilled: (*i*) reactions must be very well-defined in their start point as monomer formation already occurs on the timescale of mixing the base into the premonomer solution; and (*ii*) reactions need to be efficiently quenched at very defined and sharp reaction times to prevent further self-initiation of the quinodimethane moieties. Quenching can in principle be achieved by addition of an acid (to stop monomer formation) and by addition of a radical scavenger (e.g. 2,2,6,6-tetramethylpiperidin-1-oxyl (TEMPO)) to stop chain growth of any (bi)radical still present. Microreactors – next to their very stable reaction conditions and advantages for upscaling of chemical reactions – offer – when designed accordingly – very rapid mixing of reaction components. At the same time, very short reaction times can be easily accessed by adjusting reactor residence times, since increasing flow rates result in decreasing reaction times. With certain glass chip microreactors or with specialized micromixers, mixing of two solutions can be achieved on a millisecond timescale and, hence, be carried out faster than the polymerization itself. Consequently, the herein used

kinetic data were obtained from the following microflow conditions (Table 6-1). Premonomer solutions and base solutions in *sec*-BuOH with $[\text{pre}M]_i$ = 0.0325 mol·L^{-1} and $[B]_i$ = 0.0325 mol·L^{-1} are inserted into the flow reactor using two syringe pumps. The precursor polymer is collected and directly precipitated in a mixture of hydroquinone / 1 M HCl upon exiting the flow reactor, to quench the radicals and base, respectively. After collection, the samples are dried under vacuum and analyzed to obtain molecular weight and dispersity data by means of SEC.

Obtaining premonomer conversion data is more difficult, since all premonomer is likely to be consumed during quenching, even if polymerizations were prematurely stopped. As relatively high molecular weight polymers are synthesized, signals in ^{1}H NMR are overlapping, hindering the allocation of specific protons to the signals in the spectrum. Due to the presence of side products, also other classical conversion determination methods fail or yield very unreliable data. Thus, the collected crude product mixture containing precursor polymer, unreacted (pre)monomer, base and all quench products – have to be collected for analysis. Precursor polymers are fortunately associated with a characteristic UV absorption at 364 nm.[8] UV-Vis measurements are in consequence performed on the crude mixtures, allowing the determination of the absolute concentration of polymer. From this polymer yields are calculated by comparison with the molar amount of premonomer injected to the flow reactor during the collection time of the sample. It is important to note that this procedure provides the polymer yield based on the initial molar amount of premonomer rather than premonomer conversion. Nevertheless, to the best of our knowledge this is the first time that comparable data have become available.

Table 6-1: Experimental screening results of the synthesis of (MDMO)-PPV via the radical sulfinyl precursor route, using a microreactor with $[\text{pre}M]_i = 0.0325$ mol·L^{-1} and $[B]_i = 0.0325$ mol·L^{-1} upon varying temperature and reaction time; all isothermal conditions and reactions are performed in triplicate

Reaction Temperature °C	Reaction Time min	M_n g·mol^{-1}	DP_n	Đ	Polymer yield %
30	5	14 500 ± 2900	29	2.4	47 ± 7.0
30	4	26 100 ± 5200	52	1.8	43 ± 6.3
30	3	24 000 ± 4800	48	2.1	32 ± 4.9
30	2	31 000 ± 2100	62	1.9	26 ± 3.9
30	1	28 500 ± 5700	56	2.1	19 ± 2.8
30	0.5	24 100 ± 4800	48	2.2	14 ± 2.1
30	0.25	n.a.	n.a.	n.a.	n.a.
50	20	16 300 ± 3300	33	1.9	44 ± 6.6
50	13.3	18 400 ± 3700	37	2.1	44 ± 6.6
50	10	20 600 ± 4100	41	2.1	42 ± 6.3
50	5	24 600 ± 4900	49	2.0	40 ± 6.0
50	4	38 400 ± 7700	77	2.0	38 ± 5.6
50	3	44 500 ± 8900	89	1.9	35 ± 5.3
50	2	38 300 ± 7700	77	2.0	29 ± 4.3
50	1	45 500 ± 9000	91	1.9	19 ± 2.8
50	0.5	53 300 ± 10700	107	1.9	17 ± 2.5
50	0.25	52 300 ± 10500	105	1.8	10 ± 1.5
70	3	29 600 ± 5900	59	2.5	n.a.
70	2	37 100 ± 7400	62	2.1	n.a.
70	1	33 300 ± 6600	67	2.1	n.a.
70	0.5	33 500 ± 6700	67	1.9	n.a.
70	0.25	28 900 ± 5800	58	1.9	n.a.

Due to side reactions such as cyclization of small biradicals, the polymer yields can be significantly lower than the premonomer conversions. As a direct result of the dimensions of the flow reactor and limitations of the flow rate, the accessible residence time is limited to 20 minutes. Reaction temperatures between 30 °C and 70 °C were screened to discern trends in polymerization with increasing temperature (Table 6-1).

An important factor to keep in mind when using the flow reactor is its sensitivity towards viscosity fluctuations, which could lead to erroneous results and blockages of the reactor channel. As a result, optimization of $[\text{pre}M]_i$ and $[B]_i$ for microreactor technology (MRT) is inevitable. First trials by mimicking typical batch concentrations – $[M]_{total} = 6.5 \times 10^{-2}$ mol·L^{-1} – failed due to blockages in the reactor stemming from salt formation in combination with the occurrence of high viscosities. Reproducible results are however obtained when applying dilutions up to $[M]_{total} = 1.625 \times 10^{-2}$ mol·L^{-1}. This concentration was thus used as standard concentration throughout the whole study, resulting in $[\text{pre}M]_i = 0.0325$ mol·L^{-1} and $[B]_i = 0.0325$ mol·L^{-1} when equal injection volumes are considered. Important to note here is that polymer yields are lowered upon dilutions in batch, even after longer reaction times, a phenomenon that is to date unexplained for PPV polymerizations, but which might be related to unimolecular paracyclophane formation. Regardless, the lower yields are inevitable and will be subjected to a thorough discussion in the following.

Special care has to be taken when analyzing the polymers synthesized at 70 °C, since premature elimination of the precursor polymer occurs already on the time-scale of the polymerization. As a result, a mixture of precursor as well as conjugated PPV is obtained, which has a profound effect on the UV-absorption

characteristics. Also, eliminated PPV has very different hydrodynamic volumes compared to the precursor, making the SEC analysis much more complicated. This effect is spectroscopically visualized on lab-scale by shining UV-light (365 nm) onto the microreactor, allowing nicely the follow-up of the polymerization (blue) and elimination reaction (yellow), Figure 5-5. As a result, correct analysis of polymers obtained at 70 °C is impossible, and consequently only the low temperature data were used for modeling.
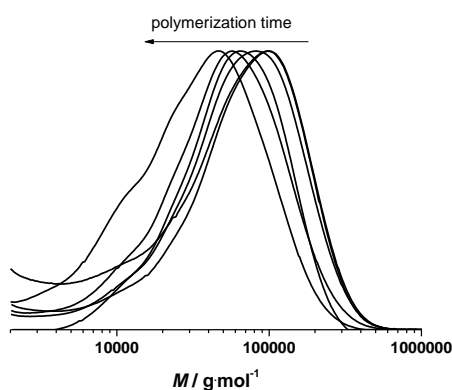
Figure 6-1: Molecular weight distributions for precursor (MDMO)-PPV synthesized at 50 °C with increasing reaction time, resulting in a decrease in overall DP_n (initial conditions: Table 6-1)

SEC (Figure 6-1 and 6-3) and UV-VIS (Figure 6-2) measurements confirm the successful polymerization of (MDMO)-PPV under the diluted flow conditions. The molecular weight distributions in Figure 6-1 are shifted clearly towards lower molecular weights with increasing reaction time. This can be explained by the progressive formation of low molecular weight side products as well as the lower availability of monomer with time. A similar trend is qualitatively seen in batch reactions as well.[20-22] M_n values ranging from 12 700 g·mol^{-1} to 28 000 g· mol^{-1}

and a *Đ* of ~2.5 are obtained when polymerizations are performed at 30 °C in which residence times are varied between 15 sec and 20 min. This is in contrast to the generally higher M_n and lower dispersities for reactions performed at 50 °C (15 700 g·mol^{-1} to 53 600 g·mol^{-1} and dispersities of ~2.0, Figure 6-3). Differences between the data at 30 °C and 50 °C can be related to increasing propagation and transfer rates at higher temperatures. For completeness it is reminded here that the data obtained from batch commonly show considerably larger scatter than the data obtained from flow.
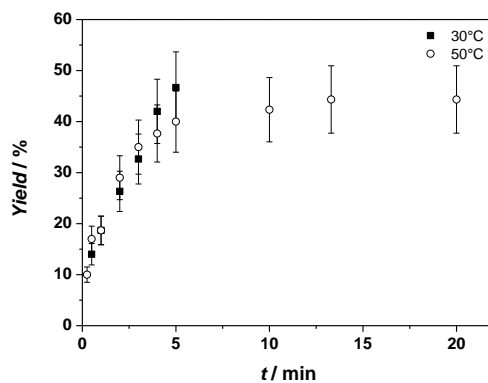
Figure 6-2: Polymer yield as function of time, based on integrating UV-Vis absorption of precursor polymer at 365 nm. Measurements are performed in duplicate of the precursor PPVs synthesized in flow (initial conditions: Table 6-1)
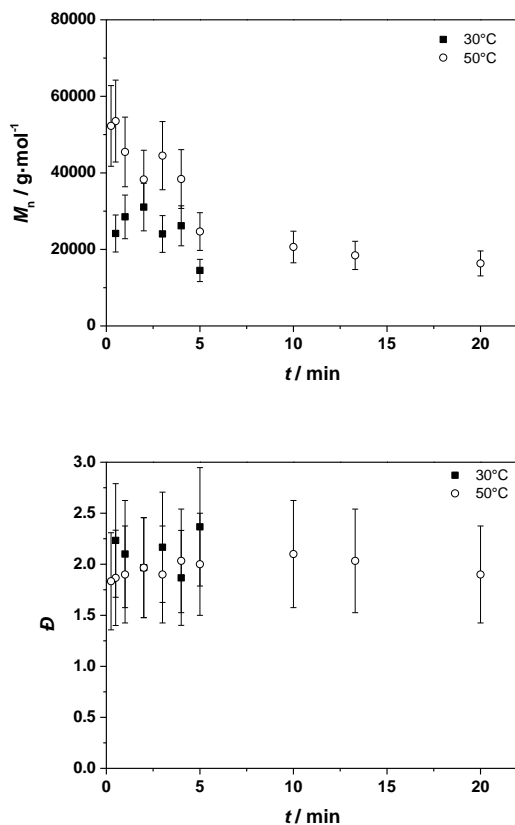
Figure 6-3: Number average molecular weight (*top*) and dispersity (*bottom*) upon varying the reaction temperature as a function of time (initial conditions: Table 6-1)

UV-Vis allowed to trace the polymer yield of the precursor polymer at different temperatures as a function of time, as shown in Figure 6-2. Interestingly, at short residence times, similar yields are obtained for both reaction temperatures, whereas an increase in polymerization time results in somewhat higher yields for the polymers synthesized at 30 °C. This could be an indication that side reactions play a lesser role for reactions performed at lower temperatures. Interestingly,

batch experiments showed similar trends, which was considered to be not of significant interest at that time.[6]

Overall, MRT is found to be a powerful tool for screening reaction conditions, gathering relatively accurate kinetic data using only small amounts of material. So far a comparable dataset does not exist, due to the above described difficulties, therefore resulting in a very significant scattering of data. In any way, the information that has become herein available through the use of flow conditions can be used in a next step to build and validate a comprehensive kinetic model using the software program Predici®. Via kinetic modeling not only mechanistic questions can be investigated, but also specific rate coefficients can be assessed. In this way, a much refined picture of sulfinyl precursor polymerization becomes available, which can in future endeavors be employed to model even more advanced PPV polymerizations (e.g. implementation of RAFT, copolymerization, and functional groups) as well.

6.3.2. Modeling of experimental data in a microreactor

As described above, MRT proves to be a powerful tool to easily screen different reaction conditions under well-defined conditions for FRP of PPVs. The decrease in M_n and increase in polymer yield upon increasing reaction time, and the decrease in polymer yield upon dilution was conveniently followed at different reaction temperatures. In addition, the expected decrease in yield upon diluting the reaction conditions is observed in MRT as well. The next step is to build a realistic kinetic model which captures the above described typical PPV behavior. Importantly, in this model transfer is taken into account for the first time, based on the observed experimental trends. As only a basic knowledge of the different

reaction steps is known (Scheme 6-1), two models are designed in which chain reinitiation can either be excluded (**model 1**, inhibition model) or needs to be included (**model 2**, non-inhibition model). Chain reinitiation means that the X· fragment that is produced when a propagating species undergoes chain transfer (Scheme 6-1, reaction VI) can start a new chain. In other words, the model describes either a situation in which transfer may lead to inhibition of the polymerization (X· being unable to reinitiate) or in which the transfer behavior is more in line with classical FRP. By comparison of model 1 and model 2, the role of transfer and inhibition will thus be elucidated.

6.3.2.1. Initial rate coefficients

Since the rate coefficient for the premonomer elimination reaction (k_{depr}) is from literature only known at 25 °C and knowledge on quinodimethane formation is crucial for the modeling main focus was put on the 30 °C data, assuming that no significant difference in k_{depr} exists between 25 °C and 30 °C. Reaction times up to 5 minutes were also considered to guarantee a complete reaction (Table 6-1). An overview of the rate coefficients used as starting point for the model at 30 °C is shown in Table 6-2. In here, the different rate coefficients from the reactions as displayed in Scheme 6-1 are shown together with the range used for screening, aiming at the determination of improved rate coefficients that merely allow a qualitative description of the polymerization characteristics. Knowledge on rate coefficients for the above described reactions are scarce and very limited, explaining this qualitative aim.

Table 6-2: Rate coefficients used as initial input parameters and their screening range in the Predici® models[8;11]

Reaction	Rate coefficient[a]	k (30 °C) $L \cdot mol^{-1} \cdot s^{-1}$	Screening range $L \cdot mol^{-1} \cdot s^{-1}$
Monomer formation	k_{depr}	1.4×10^1	n.a.
	$k_{selfini}$	2.0×10^2	$2.0 \times 10^{-2} - 2.0 \times 10^2$
	k_{na}	2.3×10^0	$2.3 \times 10^0 - 9.4 \times 10^0$
Chain Initiation	k_{ini}	2.0×10^0	$2.0 \times 10^0 - 2.0 \times 10^6$
	$k_{ini,x}$	2.0×10^0	$2.0 \times 10^0 - 2.0 \times 10^{6b}$
Propagation	k_p	1.0×10^2	$1.0 \times 10^1 - 1.0 \times 10^5$
Chain Transfer	k_{tr}	5.0×10^{-1}	$5.0 \times 10^{-3} - 5.0 \times 10^{-1}$
Termination	k_{tcycl}	2.0×10^3	$2.0 \times 10^{-3} - 2.0 \times 10^3$
by recombination	k_t	1.0×10^7	$1.0 \times 10^7 - 1.0 \times 10^9$

[a] defined per reactive center; [b] zero value for model 1

The only parameter that is known with satisfying accuracy is k_{depr} = 14.62 ± 0.36 $L \cdot mol^{-1} \cdot s^{-1}$ for the premonomer formation, see Hermosilla *et al.*[8] As explained above, two side reactions are considered: (*i*) paracyclophane formation and (*ii*) anionic base attack. The initial value for the rate coefficient of the nucleophilic addition product (k_{na}) was taken from the work of Van Steenberge *et al.* and set to 2.3×10^0 $L \cdot mol^{-1} \cdot s^{-1}$. Paracyclophane formation is captured by the cyclization rate coefficient (k_{tcycl}). Work by *Errede* et al[24] indicated a minimum value of 1.0 $\times 10^{-1}$ s^{-1} for this coefficient, which is based on 1% of paracyclophane production. Since the paracyclophane yield is significantly higher than 1%,[12] the value of k_{tcycl} is most likely higher and chosen arbitrarily to be 2.0×10^3 s^{-1}. Initial values for the rate coefficients of self-initiation ($k_{selfini}$), chain initiation (k_{ini}), propagation

(k_p) and termination (k_t) are derived from previous work.[11] As seen in Scheme 6-1, initial chain initiation and propagation are very similar and thus k_{ini} should not differ too much from k_p. Therefore a value in the same order of magnitude for both coefficients is expected, resulting in a starting value for k_{ini} of 2.0×10^0 L·mol^{-1}·s^{-1}. Finding a reasonable starting value for the self-initiation coefficient ($k_{selfini}$) is much more difficult, as it is almost impossible to isolate the p-QM product. The only indication on this value is obtained from work of *Rehahn.*[6] High driving forces can be anticipated for the reaction, due to the rapid polymerization observed, indicating a high value of 2.0×10^2 L·mol^{-1}·s^{-1} for this coefficient. The value for k_p and k_t were set higher as reported previously,[11] as in here termination reactions are taken into account as well, resulting in values of 1.0×10^2 L·mol^{-1}·s^{-1} and 1×10^7 L·mol^{-1}·s^{-1} for k_p and k_t respectively. This leaves the rate coefficient for the transfer reaction (k_{tr}) and the accompanying reinitiation of the chain ($k_{ini,x}$) as the only two yet undefined parameters. In model 2 (non-inhibition), the value for the latter one was set initially similar to k_{ini} as it was assumed for simplicity that both initiation reactions behave similarly. As for the k_{tr} value, this is the most critical parameter in the model as it determines the formation of end-groups and marks the chain breaking event. Initially, a very arbitrary number was chosen with $k_{tr} = 5.0 \times 10^{-1}$ L·mol^{-1}·s^{-1} as basically no information on this reaction is to date available.

While these initial parameters are in many aspects only crude assessments, they allow for reasonable modeling of the sulfinyl polymerization route as preliminary simulations quickly testified. Variations on each single coefficient using the range as described above (Table 6-2) will allow an evaluation of the validity of model 1 (inhibition model) and model 2 (non-inhibition model) by comparing the

observables $Đ$, yield and DP_n. A systematic variation of the values for all rate coefficients was performed for both models to discern trends and sensitivities of the different reactions towards the modeling outcome (see Appendices). After each individual optimization, the obtained value was used to continue the optimization process, leading in the end to a more coherent mechanistic picture capturing the optimization of all rate coefficients, at least in a qualitative manner as indicated above. Care has to be taken when comparing experimentally obtained DP_n and $Đ$ results, as SEC measurements are accompanied with a certain error in molecular weigth values (up to 15 %). As a result, only trendlines will be targeted for both observables and less attention will be paid to obtaining exact numbers.

In here, model optimizations based on the experimental DP_n, $Đ$ and yield are summarized. It should be emphasized that not all observables are sensitive towards the reaction coefficients as described in Scheme 6-1. Dispersity and yield will be more sensitively affected towards side reacions as well as transfer reactions in the model (Scheme 6-1, reactions VI and VII) and will be less prone to variations in k_{depr} and $k_{selfini}$ and, hence, towards the actual biradical formation. This is in contrast to DP_n, which directly takes into account the formation as well as the growth of the biradical into a polymer chain, leaving k_{depr}, $k_{selfini}$ and k_p (including k_{ini} as this value is set according to k_p) as well as k_t and k_{tr} as the most crucial parameters (Scheme 6-1, reaction I, II and III, IV and VI). In the following, a sensitivity analysis is first given for the influence of the rate coefficients on the three observables. Next, the optimized parameters for model 1 and 2 are discussed first per observable and then together, allowing an overall qualitative comparison of both models.

6.3.2.2. Effect of variations in rate coefficients on DP_n

Experimental DP_n results indicate that molecular weight distributions are shifted towards lower molecular weights with increasing reaction time, which can be explained by progressive formation of low molecular weight side products as well as lower availability of monomer with time. Both models follow similar trend lines. As is clear from the results as displayed in Figures S6-5, S6-6, 6-4, variations in k_p, k_t and k_{tr} have the most profound effect on the DP_n trend line. This is within expectations, as a faster chain growth directly leads to formation of longer polymer chains. When k_p in the range of 1.0×10^4 L·mol^{-1}·s^{-1} is used, the high initial DP_n at the beginning of the polymerization is represented well. Further, k_t has a strong influence. At first glance it seems unexpected that termination plays an important role in the growth of the polymer chain. In a conventional FRP, the instantaneous DP_n is related to the ratio of k_p to k_t. In the PPV polymerization, however, termination is not per se a chain stopping event due to the biradical reaction (only in combination with transfer it becomes also a chain stopping event). As a result, the k_t value plays an important role in the FRP of PPVs in here as well. Screening k_t between 1.0×10^7 L·mol^{-1}·s^{-1} and 1.0×10^9 L·mol^{-1}·s^{-1} has a tremendous effect, resulting in an optimized value of $k_t = 1.0 \times 10^7$ L·mol^{-1}·s^{-1} for both models. Yet, k_p and k_t should be seen as a mutual pair of parameters. Lower k_p values might be applicable if k_t is likewise decreased. A value of 1.0×10^7 L·mol^{-1}·s^{-1} for the termination rate coefficient is, however, already at the lower end of expectations for a radical polymerization. All MRT reactions were performed under high dilution, implying a limited effect of diffusional limitations and thus a relatively high termination rate coefficient. As expected, k_{tr} has the biggest influence on the simulated DP_n. For example, the results for a screening within the range of 5.0×10^{-3} L·mol^{-1}·s^{-1} to 5.0×10^{-1} L·mol^{-1}·s^{-1} (other

parameters as in Table 6-2) are depicted in Figure 6-4 (bottom). A most suited value of 1.4 x 10^{-2} L·mol^{-1}·s^{-1} is obtained as a result of this model tuning based on a single response (red line in Figure S6-4 (bottom)).
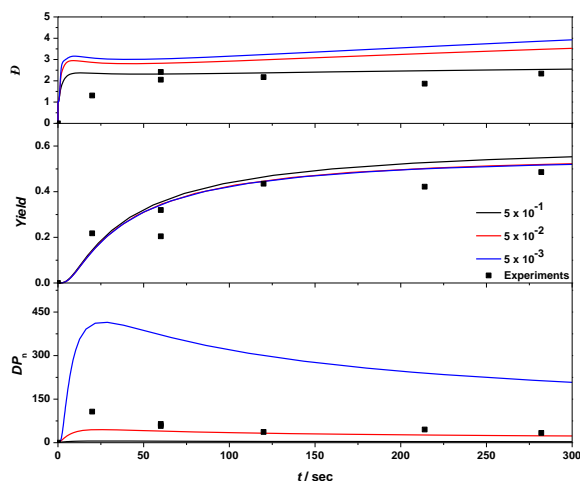
Figure 6-4: Effect of chain transfer rate coefficient (k_{tr}) on number average chain length, polymer yield and dispersity profile; initial conditions: 30 °C; [pre$M$]$_i$ = 0.0325 mol·L^{-1} and [B]$_i$ = 0.0325 mol·L^{-1}

Although the above defined parameters nicely describe the end-level of the curve, the steep increase in the beginning of the polymerization can only be described correctly for varying also k_{depr}, $k_{selfini}$ and to some extent k_{ini} ($k_{ini,x}$). The value of k_{depr} was optimized at 1.4 x 10^1 L·mol^{-1}·s^{-1} in agreement with literature, which perfectly resembles the correct description of DP_n for model 2 (Figure 6-5 bottom (blue line); Table 6-3 optimized parameters). This in contrast to model 1 where a lower k_{depr} value (1.4 x 10^0 L·mol^{-1}·s^{-1}) is needed to realize a correct qualitative description (also Figure 6-5 bottom (red line)). The difference in k_{depr} arises from the fact that in model 2 also chain reinitiation reactions are included, leading to

more active radicals that consume the in-situ formed quinodimethane moieties. Since model 2 yields k_{depr} in very good agreement to the literature value, this can be seen as a strong indication for the presence of chain reinitiation reactions. Optimized values for k_{ini} and $k_{ini,x}$ lead to similar values as for k_p (2.0 x 10⁴ L·mol⁻¹·s⁻¹). This leads to the general conclusion that based on variations of all coefficients a preference towards model 2 is observed if only the DP_n data are considered.

6.3.2.3. Effect of variations in rate coefficients on Đ

The dispersity or the broadness of a molecular weight distribution is found to be mainly affected by the transfer and propagation reactivity. Variations in the coefficients concerning side reactions (k_{na} and k_{tcycl}) have in contrast no effect on the curvature, start or end position of the dispersity as these reactions simply remove initiating species but do not influence the chain growth by itself. These reactions simply remove initiating species but do not influence the chain growth by itself. Varying k_{tr} on the other hand shows an effect on the curvature and end value of Đ. Also here, screening within a range of 5.0 x 10⁻³ L·mol⁻¹·s⁻¹ to 5.0 x 10⁻¹ L·mol⁻¹·s⁻¹ was performed, where a higher transfer reactivity resembles experimental conditions best, see Figure 6-4 (*top*). This is again a strong indication that transfer does take place and must be accounted for in the kinetic model. As expected, $k_{selfini}$, $k_{ini,x}$ and k_t do not show a major influence on the dispersity. The value for k_{depr} was kept as before in agreement with literature data at least for model 2, which leaves the initiation and propagation coefficient as the last two variables. Importantly, changes in k_{ini} and k_p are of major influence on not only the curvature but also the final value of the dispersity.

While the results concerning DP_n resemble model 2 conditions best, as explained above, the dispersity results show a clear tendency towards the use of model 1, see Figure 6-5 (*top*; red line), as dispersity is overestimated by model 2 (parameters: Table 6-3). This does, however, not automatically indicate that chain reiniation does not take place. More refined reaction parameters might be able to match the dispersity data better, and within the qualitative scope of this study also model 2 might be regarded as a good representation, especially keeping in mind that parameter optimization of model 2 matches the k_{depr} value reported in literature and leads to a better description of the DP_n data, as discussed above.
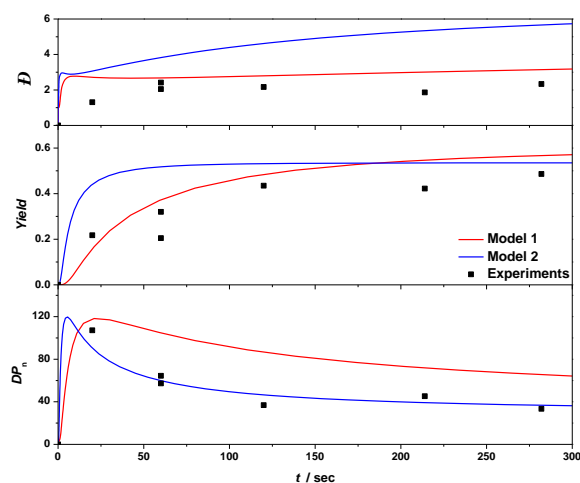
Figure 6-5: Comparison of number average chain length, polymer yield and dispersity of model 1, model 2 and experimental results (Table 6-1); initial conditions: 30 °C; [pre$M$]$_i$ = 0.0325 mol·L^{-1} and [B]$_i$ = 0.0325 mol·L^{-1}; optimized rate coefficients (see Table 6-3)

6.3.2.4. Effect of variations in rate coefficients on the polymer yield

As a last measurable response, polymer yield is modeled and compared to MRT experimental results, see again Figure 6-5 (model 1 (red line) *vs* model 2 (blue line); parameters: Table 6-3). Monomer consumption is directly proportional to the propagation and initiation rates and limited by the given side reactions. The exact curvature of the yield vs time plot is complex and not easily described by modeling, yet the final maximum conversion can be directly related to the side reactions, as side products are not UV active and are, hence, not accounted for in the yield determination.

Both models show an increase in polymer yield upon increasing polymerization time, reaching a plateau with a yield of ~50%, similar to the MRT experimental results. As expected, a decrease in k_{tcycl} leads to an increase in polymer yield, leading to more high molecular weight polymers and to almost similar values for the optimum rate coefficient for both models. For k_{na}, no significant effect on the observables within reasonable limits of the rate parameters is obtained, which is in good agreement with experimental evidence as no anionic polymerization product is observed. No differentiation is made between polymer formation via a biradical or chain reinitiation, thus k_{tr} or $k_{ini,x}$ varying in the range as specified above has no influence on the total polymer yield.

Finally, this leads to a value of 5.0 x 10^{-2} L·mol^{-1}·s^{-1} and 2.0 x 10^4 L·mol^{-1}·s^{-1} for the transfer and reinitiation coefficient, respectively, as best concomitant description for number average chain length, dispersity and yield. Formation of the biradical is a direct result of the already fixed k_{depr} value as well as the self-initiation coefficient. Increasing the value of the latter displays a similar effect for both models, as higher $k_{selfini}$ values seem to level off the polymer yield. Next, polymer growth takes place, based on the variation in k_p (and thus k_{ini}) and k_t

values. Both models do show a small influence on variations in the k_p value. Contrary to classical FRP but in line with the present model, k_t does not influence the yield at all. It can be concluded that based on polymer yield no clear distinction can be made between model 1 and 2 as both yield reasonable qualitative results. Yet, due to the fact that a reduced k_{depr} is employed for model 1 (see above) a preference towards model 2 can still be given.

Table 6-3: Optimized rate coefficients for model 1 and model 2, aiming at a qualitative description of the data in Figure S6-3

Reaction	Rate coefficient[a]	Model 1	Model 2
		k (30 °C) / L·mol^{-1}·s^{-1}	
Monomer formation	k_{depr}	1.4×10^0	1.4×10^1
	$k_{selfini}$	2.0×10^1	2.0×10^1
	k_{na}	2.3×10^{-1}	9.2×10^0
Chain initiation / Inhibition	k_{ini}	2.0×10^4	2.0×10^4
	$k_{ini,x}$	0	2.0×10^4
Propagation	k_p	1.0×10^4	1.0×10^4
Transfer reaction	k_{tr}	5.0×10^{-2}	5.0×10^{-2}
Termination by recombination	k_{tcycl}	2.0×10^1	2.0×10^1
	k_t	1.0×10^7	1.0×10^7

[a]defined per reactive center

6.3.2.5. Overall comparison

The optimized rate coefficients as discussed above are given in Table 6-3 with the joint modeling results based on these parameters provided in Figure 6-5. While the coefficients derived are certainly still associated with considerable error margins, their order of magnitudes should already at this stage be well represented. In any way, presence of a chain transfer reaction (as this is included in both models) can be confirmed, adding this reaction to the mechanistic scheme of the precursor route PPV polymerizations. It can be further concluded that the polymer yield data are described in a reasonable qualitative manner by both models. Model 1 is better for the description of the dispersity data, whereas model 2 is better for the description of the DP_n data with its k_{depr} value in agreement with literature data, favoring the occurrence of chain reinitiation upon chain transfer.

To further verify the general robustness of the PPV model, both models 1 and 2, are subjected to an additional test to see if the models are also capable of a correct prediction towards other reaction conditions. Sulfinyl precursor polymerization are characterized by the trend that upon dilution of the reaction mixture a decrease in final polymer yield is obtained. Experiments show a decrease in conversion from 75 % to 33 %, respectively, when diluting the premonomer by a factor of 10 ($[preM]_{total} = 6.5 \times 10^{-2}$ M at $T = 30$ °C – to a dilution of $[preM]_{total} = 6.5 \times 10^{-3}$ M at $T = 30$ °C).
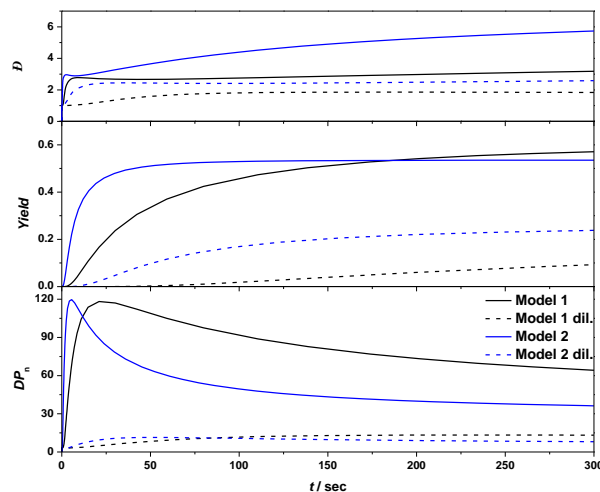
Figure 6-6: Simulation results for number average chain length, polymer yield, dispersity for both models employed upon variation of the premonomer concentration in the model (dilution of factor 10). For all cases, the optimized values as given in Table 6-3 are applied; initial conditions: $[preM]_{total}$ = 6.5×10^{-2} M at $T = 30$ °C (Table 6-1) – to a dilution of $[preM]_{total} = 6.5 \times 10^{-3}$ M at $T = 30$ °C (base concentration also diluted)

Figure 6-6 shows the simulated effect that dilution has on the observables DP_n, $Đ$ and yield, using the optimized reaction coefficients as displayed in Table 6-3. Results on polymer yield verify the expected drop upon dilution of the initial premonomer and base concentration. A plateau is reached after a reaction time of only 5 minutes, resulting in maximum yields of 9 % and 24 % for model 1 and model 2, respectively. Comparison to experimental values – 33 % under similar reaction conditions – again indicates that model 2 is more able to represent the polymerization kinetics. Similar trends for both models are observed when considering DP_n. A final length of 10 units (equal to a M_n of ~5 000 g·mol^{-1}) is

predicted under the diluted conditions, which is similar to the experimental data. Values for experimentally obtained M_n values range between 3 000 g·mol^{-1} and 9 500 g·mol^{-1}. As a last parameter, also dispersity was considered leading to similar trends with both models reaching a plateau. The small difference in the actual Đ value – 1.9 for model 1 vs. 2.3 for model 2 – under diluted conditions is not significant enough to differentiate between the models.

The simulation of the diluted reaction conditions again confirms the relevance of chain transfer and thus give even more indication for the validity of model 2. Regardless, the models as used in here are conveniently verified as they demonstrate their predictive character. Again, one must be careful with the exact coefficients given in Table 6-3, as they rather indicate orders of magnitude rather than precise values. Yet, this situation can be regarded already as a significant improvement compared to all previous model suggestions and model 2 may serve from here on as a basis for much a more refined description of (MDMO)-PPV precursor polymer synthesis.

6.4. CONCLUSIONS

For the first time, reliable and systematic time dependent data has been obtained for different reaction times, temperatures and initial concentrations for the synthesis of (MDMO)-PPV precursor polymer via the so-called sulfinyl route, using microreactor technology. The polymerization follows a radical polymerization pathway, which differs at first sight significantly from conventional radical polymerization and which exact mechanism was to date not in-depth known.

While the focus of the presented work was put on the mechanistic and kinetic understanding of this specific polymerization technique, it is also a good example on how microreactor technology can be effectively used not only for synthetic purposes but also for in-depth kinetic studies. Comparable data allowing mechanistic analysis, especially for PPV synthesis, were not available before and would without microreactors also in future be largely inaccessible.

Experimental screening showed that a sufficiently low polymerization temperature allows to separate the synthesis step of the precursor polymer from the subsequent elimination step, a key prerequisite for kinetic analysis.

Experimental UV-Vis data that give access to polymer yield indicate the presence of side reactions such as cyclization and nucleophilic addition. Experimental SEC data indicate the presence of chain transfer reactions, as confirmed by a kinetic model in which reinitiation takes place (non-inhibition model) and in which it can be ignored (inhibition model). Thus, the presence and importance of radical chain transfer events in precursor polymerizations to obtain PPV materials has been confirmed for the first time. Since the optimized model parameters for a model with reinitiation have a higher physical relevance next to an acceptable trend line prediction of the evolution of the number average chain length, the dispersity,

and polymer yield, a preference is given to the non-inhibition model for future kinetic modeling studies.

It can hence be concluded that radical precursor polymerization, despite all its differences to conventional free radical polymerization – mostly due to a different initiation mode and the biradical character of the growing chains – follows largely the same driving forces as observed for most radical reactions. All kinetic rate coefficients fall with their order of magnitude in the expected range for typical radical chain reactions. On the one hand, the herein studied polymerization reactions relate to a complex and unusual kinetic system whereas on the other hand they are in very good agreement with the general trends in free radical polymerization – a satisfying result which may in hindsight appear obvious, but that has been debated for a long time.

6.5. APPENDICES
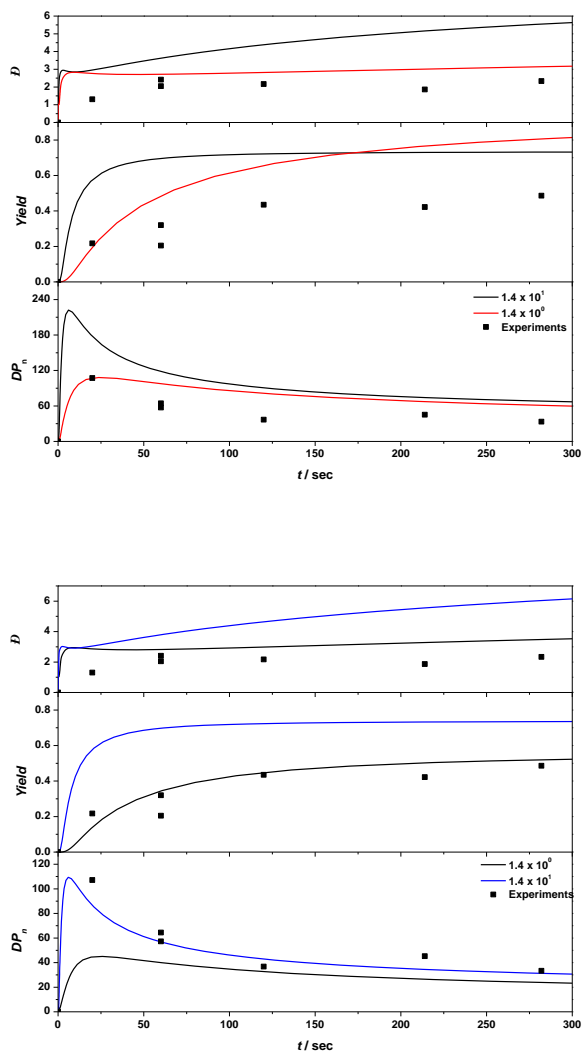
Figure S6-1: Influence on DP_n, $Đ$ and yield upon varying the k_{depr} value for model 1 (*top*) and model 2 (*bottom*)
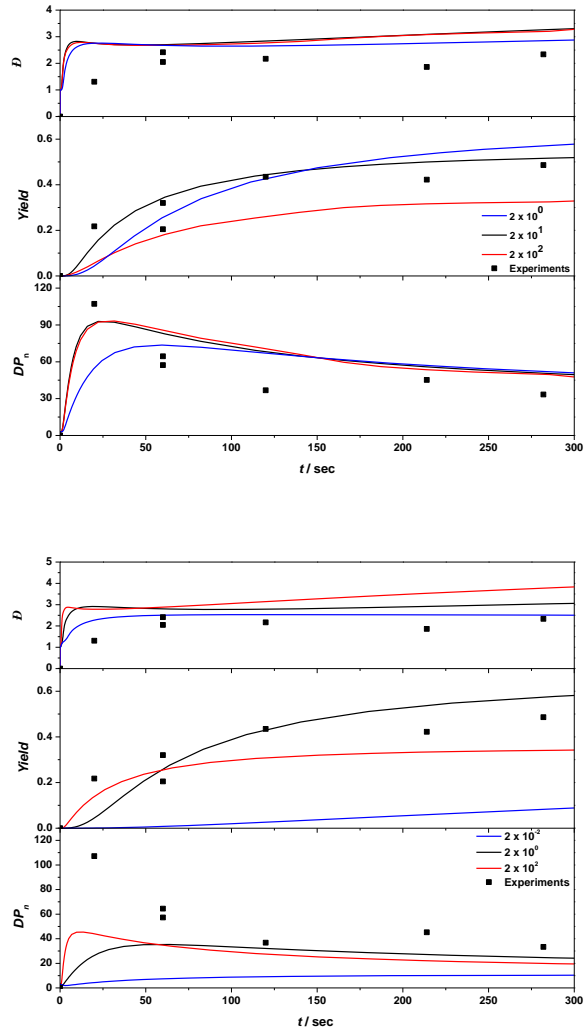
Figure S6-2: Influence on DP_n, $Đ$ and yield upon varying the $k_{selfini}$ value for model 1 (*top*) and model 2 (*bottom*)
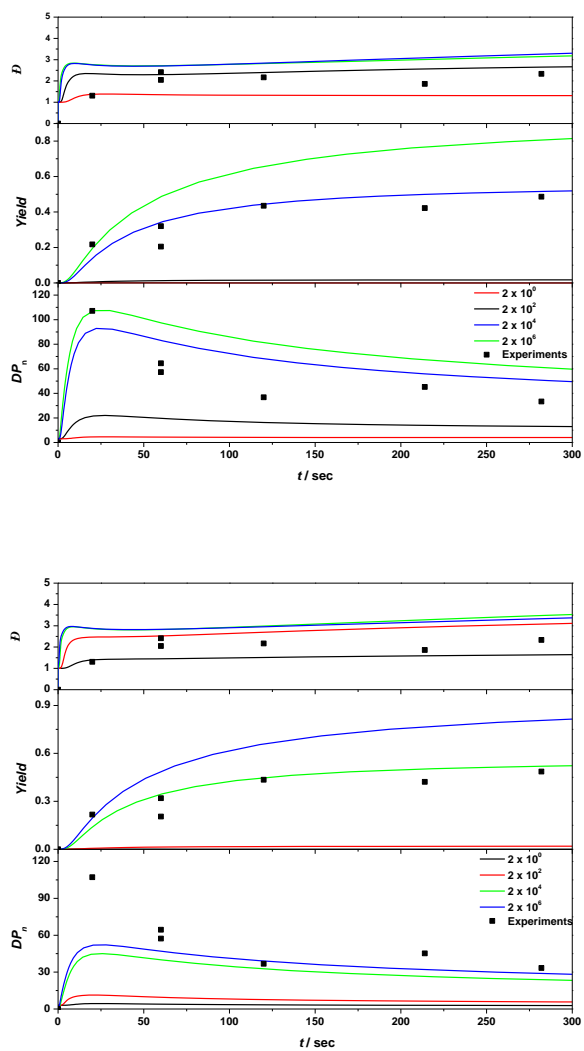
Figure S6-3: Influence on DP_n, $Đ$ and yield upon varying the k_{ini} value for model 1 (*top*) and model 2 (*bottom*)
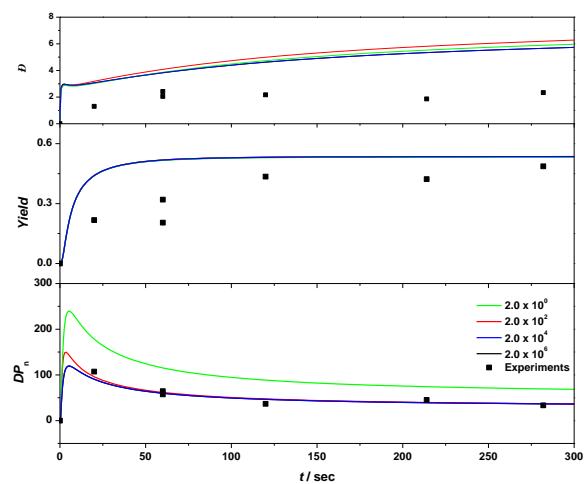
Figure S6-4: Influence on DP_n, $Đ$ and yield upon varying the $k_{ini,x}$ value for model 2; in model 1 always zero value, hence, no additional plot
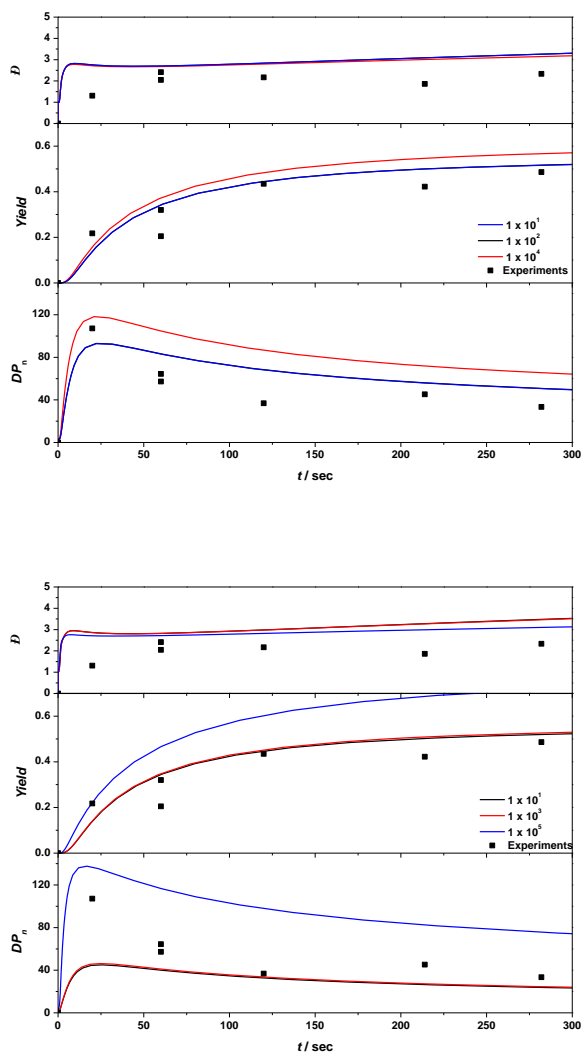
Figure S6-5: Influence on DP_n, $Đ$ and yield upon varying the k_p value for model 1 (*top*) and model 2 (*bottom*)
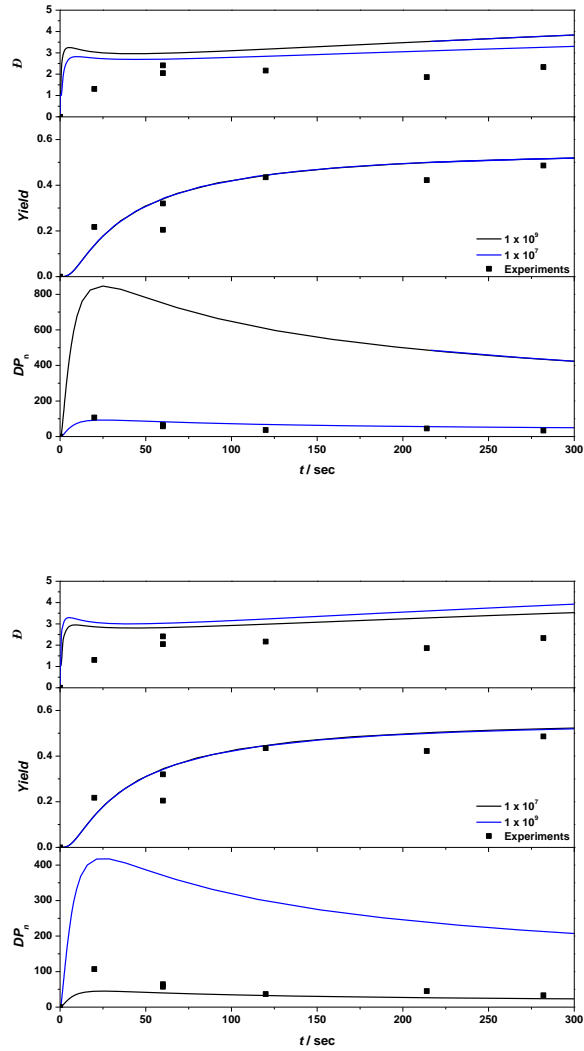
Figure S6-6: Influence on DP_n, $Đ$ and yield upon varying the k_t value for model 1 (*top*) and model 2 (*bottom*)
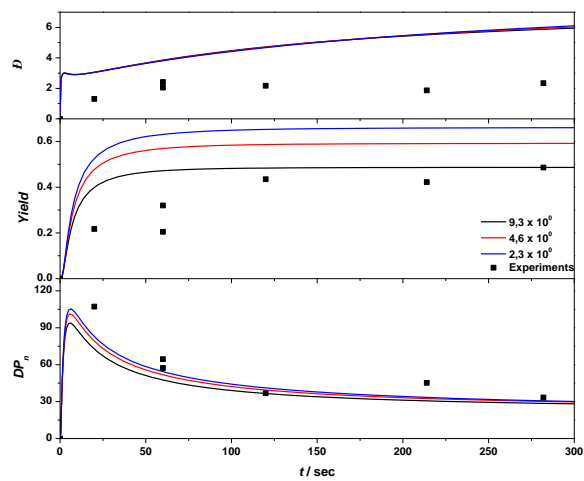
Figure S6-7: Influence on DP_n, $Đ$ and yield upon varying the k_{na} value for model 2
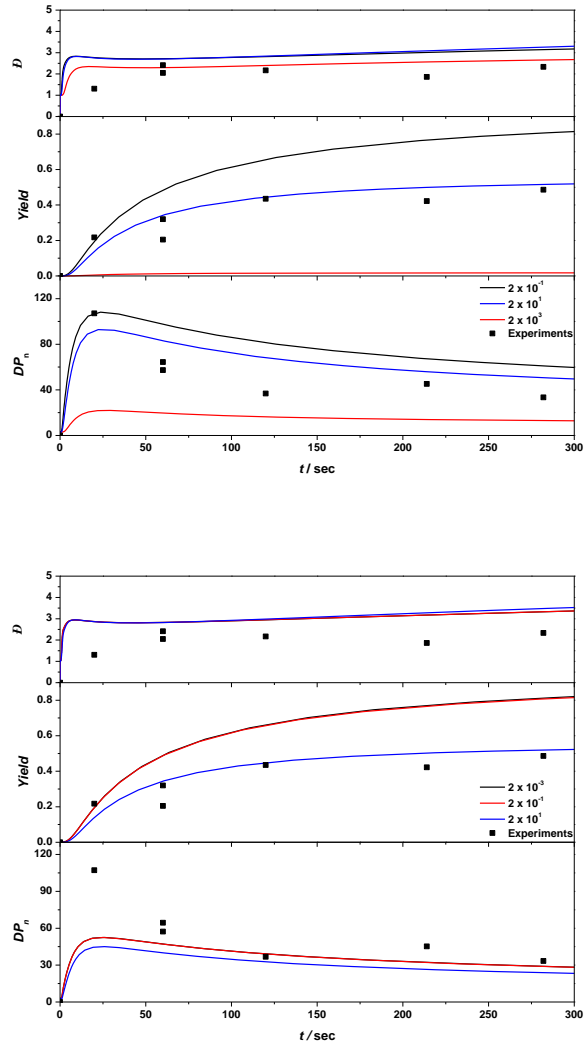
Figure S6-8: Influence on DP_n, Đ and yield upon varying the k_{tcycl} value for model 1 (*top*) and model 2 (*bottom*)

6.6. REFERENCES

[1] E. Kesters, S. Gilissen, F. Motmans, L. Lutsen, D. Vanderzande, *Macromolecules* **2002**, *35*, 7902– 7910.

[2] F. Louwet, D. Vanderzande, J. Gelan, J. Mullens, *Macromolecules* **1995**, *28*, 1330–1331.

[3] A. Issaris, D. Vanderzande, P. Adriaensens, J. Gelan, *Macromolecules* **1998**, *31*, 4426–4431.

[4] H. G. Gilch, W. L. Wheelwright, *J. Polym. Sci. Part A-1* **1966,** *4*, 1337- 1349.

[5] T. Schwalm, M. Rehahn, *Macromol. Rapid Commun.* **2007**, *28*, 188-193.

[6] T. Schwalm, M. Rehahn, *Macromol. Rapid Commun.* **2008**, *29*, 207-213.

[7] P. Van Steenberge, J. Vandenbergh, D. R. D'Hooge, M.-F. Reyniers, P. Adriaensens, L. Lutsen, D. Vanderzande, G. B. Marin, *Macromol. Theory Simul.* **2013**, *22*, 246-255.

[8] L. Hermosilla, S. Catak, V. Van Speybroek, M. Waroquier, J. Vandenbergh, F. Motmans, P. Adriaensens, L. Lutsen, T. Cleij, D. Vanderzande, *Macromolecules* **2010**, *43*, 7424-7433.

[9] R. R. Cho, Y. K. Kim, M. S. Han, *Macromolecules* **1998**, *31*, 5218-5223.

[10] C. Yin, C.-Z. Yang, *Synth. Met.* **2001**, *118*, 75-79.

[11] P. Van Steenberge, J. Vandenbergh, D. R. D'Hooge, M.-F. Reyniers, P. Adriaensens, L. Lutsen, D. Vanderzande, G.B. Marin, *Macromolecules* **2011**, *44*, 8716-8726.

[12] J. Vandenbergh, *PhD Thesis*, Hasselt University, **2011**.

[13] G. Jas, A. Kirschning, *Chem. Eur. J.* **2003**, *9*, 5708-5723.

[14] V. Hessel, A. Renken, J. Schouten, J. Yoshida, *Micro Process Engineering*: *A Comprehensive Handbook;* Wiley-VCH: Weinheim, **2009**.

[15] J. Greener, E. Tumarkin, M. Debono, A. P. Dicks, E. Kumacheva, *Lab Chip* **2012**, *12*, 696-701.

[16] K. Jähnisch, V. Hessel, H. Löwe, M. Baerns, *Angew. Chem. Int. Ed.* **2004**, *43*, 406-446.

[17] J. Vandenbergh, T. de Moraes Ogawa, T. Junkers, *J. of Polym. Sci. Part A: Polym. Chem.* **2013**, *51*, 2366-2374.

[18] D. Wilms, J. Klos, H. Frey, *Macromol. Chem. and Phys.* **2008**, *209*, 343-356.

[19] N. Zaquen, E. Baeten, J. Vandenbergh, L. Lutsen, D. Vanderzande, T. Junkers, *Chem. Eng. & Tech.* **2015**, *38*, 1749-1757.

[20] J. D. Nikolić, S. Wouters, J. Romanova, A. Shimizu, B. Champagne, T. Junkers, D. Vanderzande, D. Van Neck, M. Waroquier, V. Van Speybroeck, S. Catak, *Chem. Eur. J.* **2015**, *21*, 19176-19185.

[21] T. Junkers, J. Vandenbergh, P. Adriaensens, L. Lutsen, D. Vanderzande, *Polym. Chem*. **2012**, *3*, 275-285.

[22] J. Wiesecke, M. Rehanh, *Angew. Chem. Int. Ed.* **2003**, *42*, 567-570.

[23] N. Zaquen, J. Vandenberg, L. Lutsen, D. Vanderzande, M. Scheinder, T. Junkers, *Polymers* **2015**, *7*, 418-452

[24] L. A. Errede, R. S. Gregorian, J. M. Hoyt, *J. Am. Chem. Soc.* **1960**, *82*, 5218-5223.

CHAPTER 7

A Mild and Efficient Approach towards Functional Macromolecules via Continuous Flow Photo-induced Diels-Alder Reactions
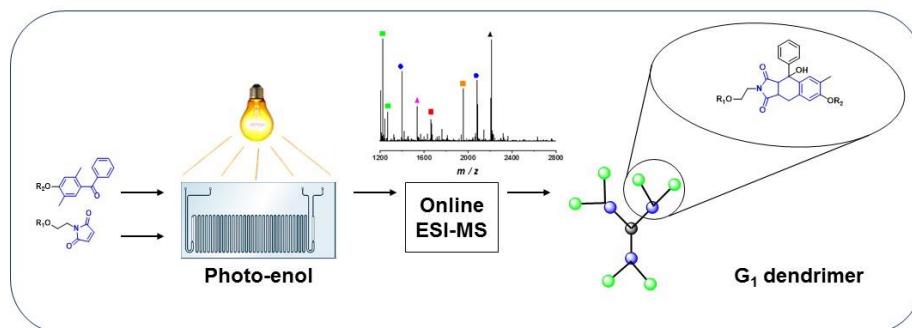
* Collaboration with Karlsruhe Institute of Technology, Karlsruhe (Germany)

ABSTRACT

Continuous flow systems have become a standard tool for the synthesis of a variety of (multi)block copolymers via thermally as well as light-induced polymerizations, e.g. reversible addition-fragmentation chain-transfer (RAFT) or atom transfer radical polymerization (ATRP). In here, the deprotection of maleimides (MIs) in flow was explored, after which the UV-induced photo-enol reaction in microfluidic reactors was targeted. A trifunctional 'core' with dienophile functionality and a bifunctional 'arm' with photo-enol functionality were conjugated utilizing a compact fluorescent lamp (wavelength (λ_{max}) = 365 nm), leading to a first generation dendrimer species. Although the deprotection of the furan protected MIs is highly successful, dendrimer synthesis in flow was accompanied with incomplete conversions. Hence, only preliminary results are presented for the photo-enol reactions in continuous flow systems.

7.1. INTRODUCTION

As a starting point of the second part of the thesis, the use of continuous flow reactors was implemented for the synthesis of poly(*p*-phenylene vinylene)s (PPV)s. Both the precursor formation as well as elimination reactions were screened separately, after which the coupling of two micro flow reactors enabled the continuous synthesis of conjugated PPVs. Special interest was placed at the elimination reaction, as thermally induced reactions greatly benefit from the use of flow reactions over batch reactions. Isothermal reaction conditions combined with almost ideal radial mixing as well as the benefit of working under pressure, greatly reduced the polymerization time for the elimination reaction of PPVs from 3 h in batch to less than 5 min in flow. As a continuation on this success – and to prove that the use of flow reactors for thermally induced reactions indeed enhances - the deprotection of maleimides (MIs) in micro flow reactors was tested. Once deprotected, the resulting dienophile can readily react with the active specie – *o*-quinodimethane – via a photo-induced Diels Alder (DA) reaction, enabling the synthesis of complex functional structures, Scheme 7-1.
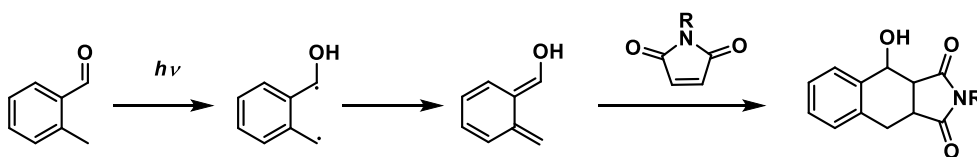
Scheme 7.1: Photo-induced Diels-Alder reaction via an *o*-quinodimethane

The popularity of photo DA reactions can be attributed to the special features of these reactions like (*i*) high yields are readily obtained and no byproducts are formed, thus work up of these reactions is relatively simple, (*ii*) robust reactions as they are tolerant towards a variety of chemical solvents.[1-5] The molecules are

excited by absorption of a photon, leading to a triplet state of a highly reactive diene, called *o*-quinodimethane (Scheme 7-1). The diene adds immediately to a present dienophile in a [4+2] DA cycloaddition – thereby regenerating the aromatic structure – leading to a fast and efficient pathway towards macromolecular structures.[6-9] Similar mechanism – regeneration of aromaticity – is observed during the *in situ* formation of the PPV monomer as described in previous chapters.

Although photo-enol conjugation is easily reached, batch synthesis is accompanied with upscaling issues, making it challenging to obtain large amounts of functional polymers.[10-12] This key issue can be overcome by using continuous microreactor technology (MRT). Over the last years MRT has proven to be an attractive and efficient tool for the synthesis of complex architectures. The high surface-to-volume ratio and the almost ideal mixing behavior leads to nearly isothermal reaction conditions, the suppression of side reactions and an increase in product yield. In addition, upscaling from mg to kg scale is enhanced as well.[13-18] Stable and reproducible synthesis protocols are obtained, allowing the production of a significant amount of functional polymers.

In here, the deprotection of a trifunctional trisuccinate 'core' with dienophile functionality in microflow was studied on-line by using the ESI-MS/Microreactor set-up.[19] Optimization is performed by screening different reaction times as well as temperatures. In addition, a trapping agent (tetracyanoethylene) is added to speed up the reaction and reach full conversion of the reaction at elevated temperatures. In a next step, a photo-enol reaction between the deprotected 'core' and a bifunctional 'arm' using a compact fluorescent lamp (wavelength (λ_{max}) = 365 nm) is screened on-line as well. Preliminary results will be shown in

this chapter and it will be revealed that, by means of ESI-MS experiments, no 100% efficiency could be reached so far for the photo-enol reaction.

7.2. EXPERIMENTAL SECTION

7.2.1. Microreactor set-up for de deprotection (2) and photo-enol (4) reaction

A similar flow reactor set-up as described in chapter 5, paragraph 5.2.1 is used for the photo-enol reaction.

7.2.2. ESI-MS/Microreactor Coupling
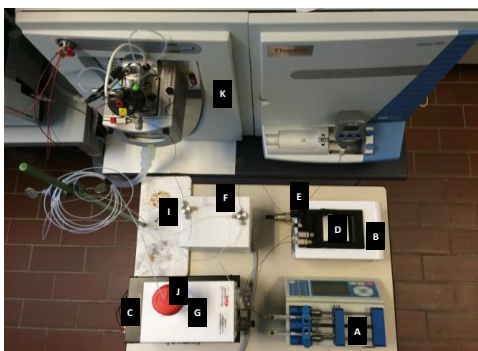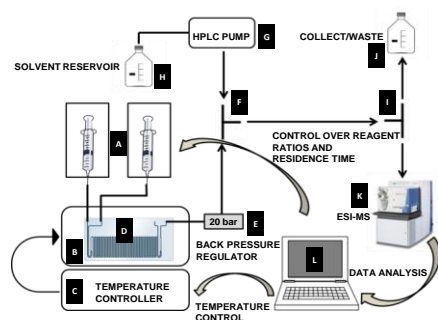
Scheme 7-2: Representation of a flow chart of the on-line set-up (*left*) and photo of the set-up (*right*)

Full details of the ESI-MS /Microreactor set-up can be found in literature.[19] Reactions take place in a conventional microreactor chip (**D**). When the microreactor is operated under true synthesis conditions, a reaction mixture is obtained at the reactor outlet that is unsuitable for MS analysis due to a mismatch in sample concentration, solvent, absence of doping agents and flow rate. These issues can, however, be conveniently overcome by a strong dilution of the reactor flow mixture (**F**) with suitable doped ESI solvent mixtures (**H**) followed by a flow T-splitter (**I**) to meet the requirements of the ESI-MS nozzle (**K**). Dilution also

serves thereby as an effective solvent change next to the decrease in sample concentration down to the micromolar range. One of the many advantages of such a setup is the high flexibility in terms of concentrations and reaction conditions that can be investigated. A wide concentration window in the microreactor can be accessed; higher flow rates of increased sample concentration can be dynamically compensated by adjusting the dilution factor (Scheme 7-2). In here case, a 2 mL·min^{-1} dilution flow, variable reaction flow rate and 5 μL/min fixed split flow was used, resulting in a dead time of at least 2.00 min.

7.2.3. Monomer Synthesis

7.2.3.1. Synthesis of monomer 1 (*O,O',O''*-(benzene-1,3,5-triyltris (methylene)) tris(2-(1,3-dioxo-1,3,3a,4,7,7a-hexahydro-2*H*-4,7-epoxy isoindol-2-yl)ethyl) trisuccinate)
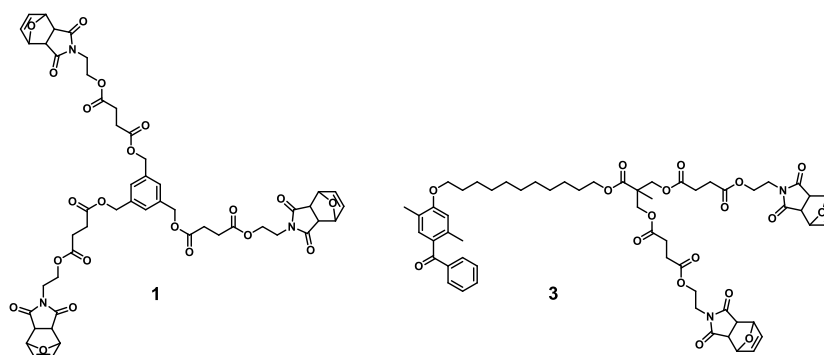
Scheme 7-3: Chemical structure of trisuccinate core **1** and disuccinate arm **3**

The trisuccinate core **1** was provided by Karlsruhe Institute of Techolnogy (Scheme 7-3). SEC (THF): M_n^{app} = 629 g·mol^{-1}, Đ = 1.0. ^{1}H-NMR (CDCl$_3$): δ = 7.25 (s, 3H); 6.48 (s, 6H); 5.23 (s, 6H); 5.10 (s, 6H); 4.23-4.21 (t, 6H); 3.73-3.70 (t, 6H); 2.84 (s, 6H); 2.67-2.57 (m, 12H). ^{13}C-NMR (CDCl$_3$): δ = 176.03

(C4); 171.97 (C4); (C4); 136.53 (C4); 127.51 (CH$_2$); 80.08 (CH); 65.89 (CH$_2$); 60.82 (CH$_2$); 47.44 (CH); 37.75 (CH$_2$); 28.88 (CH$_2$). GC-MS (EI, m/z): 838 [MH$^+$], 597 [M$^+$ - C$_{10}$H$_{11}$NO$_6$], 242 [M$^+$ - C$_{29}$H$_{29}$N$_2$O$_{12}$].

7.2.3.2. Synthesis of monomer 3 (*O,O'*-(2-(((11-(4-benzoyl-2,5-dimethyl phenoxy)undecyl)oxy)carbonyl)-2-methylpropane-1,3-diyl) *bis* (2-(1,3-dioxo-1,3,3a,4,7,7a-hexahydro-2*H*-4,7-epoxyisoindol-2-yl) ethyl) disuccinate)

The disuccinate arm **3** was provided by Karlsruhe Institute of Technology (Scheme 7-3). SEC (THF): M_n^{app} = 703 g·mol^{-1}, Đ = 1.0. ^{1}H-NMR (CDCl$_3$): δ = 7.74-7.40 (m, 5H); 7.13 (s, 2H); 6.49 (d, 4H); 5.23 (s, 4H); 4.23-3.70 (m, 16H); 2.85 (s, 4H); 2.59-2.51 (m, 8H); 2.35 (s, 3H); 2.14 (s, 3H); 1.84-1.76 (m, 4H); 1.61-1.19 (m, 17H). ^{13}C-NMR (CDCl$_3$): δ = 198.00 (C4); 176.04 (C4); 172.64 (C4); 171.64 (C4); 159.00 (C4); 138.97 (C4); 137.84 (C4);136.52 (CH); 132.55 (CH$_2$); 129.98 (CH$_2$); 128.20 (C4); 123.18 (C4); 113.35 (CH$_2$); 80.89 (CH); 68.00 (CH$_2$); 65.47 (CH$_2$); 65.35 (CH$_2$); 60.84 (CH$_2$); 47.45 (CH); 46.15 (C4); 37.37 (CH$_2$); 29.51-25.79 (CH$_2$); 15.70 (CH$_3$). GC-MS (EI, m/z): 960 [M$^+$ - C$_8$H$_8$O$_2$], 379 [M$^+$ - C$_{25}$H$_{26}$N$_2$O$_{14}$].

7.2.4. Removal of the furan protective groups from the maleimides compound
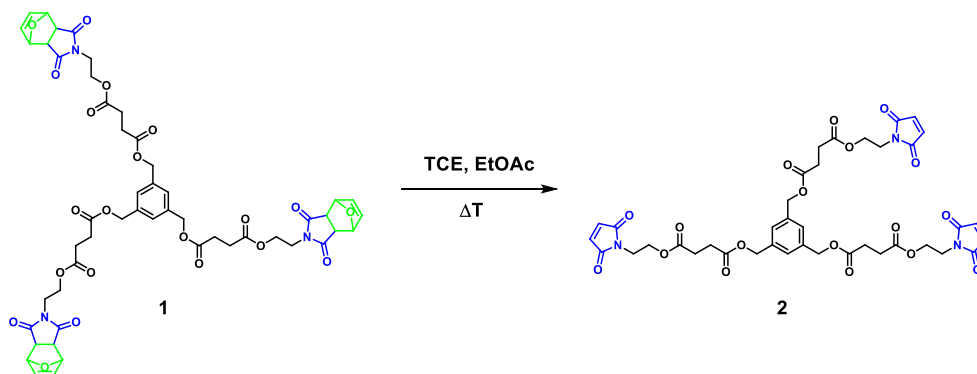
Scheme 7-4: General reaction scheme for the deprotection of compound **1** in flow

Compound **1** (100 mg, 9.6×10^{-5} mol, 1.0 equiv.) and tetracyanoethylene (TCE trapping agent; 60 mg, 4.8×10^{-4} mol, 5.0 equiv.) in EtOAc (1 mL) were added to a Schlenk tube, subjected to 3 freeze pump thaw cycles to remove the residual oxygen and subsequently inserted into the glovebox. The Schlenk tube was opened and a 1 mL gas tight syringe was filled with the reagents, after which the gas tight syringe was connected to the Labtrix® system and subsequently pumped into the microreactor (3227, reactor volume 19.5 μL). Both microreactor residence time as well as temperature were screened by collecting samples in small vials, resulting in the crude product **2** as a yellow viscous oil (99 % for reactions at 175 °C for 5 min), Scheme 7-4. SEC (THF): M_n^{app} = 564 g·mol^{-1}, $Đ$ = 1.0. ^{1}H-NMR (CDCl$_3$): δ = 7.26 (s, 3H); 6.70 (s, 6H); 4.24-4.22 (t, 6H); 4.00–2.90 (s, 6H); 3.78-3.76 (t, 6H); 2.68-2.59 (m, 12H). ^{13}C-NMR (CDCl$_3$): δ = 171.93 (C4); 170.42 (C4); 136.64 (C4); 134.20 (CH$_2$); 127.53 (CH$_2$); 65.90 (CH$_2$); 67.13

(CH$_2$); 36.78 (CH$_2$); 28.84 (CH$_2$). GC-MS (EI, *m/z*): 838 [MH$^+$], 597 [M$^+$ - C$_{10}$H$_{11}$NO$_6$], 242 [M$^+$ - C$_{29}$H$_{29}$N$_2$O$_{12}$].

7.2.5. Photo-enol coupling reaction
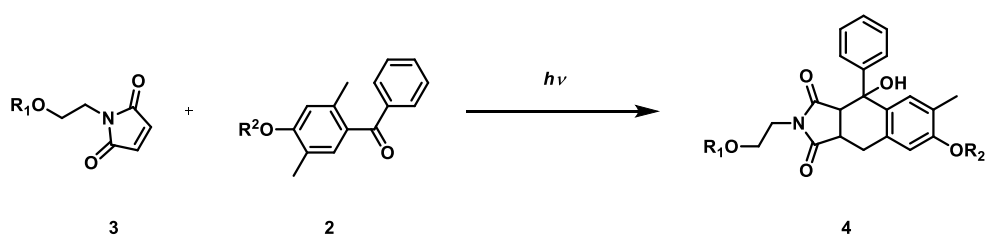
Scheme 7-5: Photo-enol reaction using deprotected core **2** with protected arm **3**

Compound **2** (5 mg, 5.81 x10^{-6} mol, 1.0 equiv.) and compound **3** (19 mg, 1.74 × 10^{-5} mol, 3.0 equiv.) in EtOAc (1 mL) were added to a Schlenk tube, subjected to 3 freeze pump thaw cycles to remove the residual oxygen and subsequently inserted into the glovebox. The Schlenk tubes were opened and two 1 mL gas tight syringes were filled with the reagents, after which the gas tight syringes were connected to the Labtrix$^®$ system and subsequently pumped into the microreactor (3227, reactor volume 19.5 μL). The glass chip reactor was illuminated with a fluorescent UV-lamp (λ_{max} = 365 nm) enabling light induced reaction conditions. Microreactor residence time, reagent concentration, equivalents as well as light intensity were screened by collecting reaction samples in small vials, resulting in the crude product **4** as a yellow viscous oil (99 %), Scheme 7-5).

7.3. RESULTS AND DISCUSSION

7.3.1. Removal of the furan protective endgroups from the maleimides compound (1) via ESI-MS/MRT coupling

In the current work, the well-known photo-enol reaction is tested for advanced solvent based synthesis in continuous flow reactors, ultimately leading to an easy, efficient and scalable way of synthesizing functional materials. In here, a trifunctional 'core' **1** with a triple dienophile functionality and a bifunctional 'arm' **3** with a photo-enol functionality were conjugated utilizing a compact fluorescent lamp (wavelength (λ_{max}) = 365 nm), leading to a first generation dendrimer species. Prior to optimizing flow reaction conditions for the conjugation reaction the furan protective groups were removed from the core molecule **1** to yield the reactive enone moiety (MIs). In order to visualize the complete deprotection, the optimization of the furan removal was performed in a flow set up via on-line ESI-MS coupling. A Labtrix® reactor set-up was used combined with a 3227 chip reactor (volume = 19.5 μL) to enable a full time range for screening. Deprotection in batch typically takes place at 110 °C using toluene as solvent, leading to full conversions in 15 h. Molecule **1** was dissolved in toluene – using a total concentration of $[M]_t$ = 91.4 mmol·L^{-1} – and the reaction was screened on-line using ESI-MS by varying microreactor residence time and temperature in a micro flow set-up.

Table 7-1: ESI-MS analysis results of the stepwise deprotection of the core, based on the ESI-MS results displayed in Figure 7-1

Structure description	m/z
Fully protected core **2** (Na$^+$)	1064.292
Deprotection 1x (Na$^+$)	996.262
Deprotection 2x (Na$^+$)	928.232
Fully deprotected core (Na$^+$)	860.210
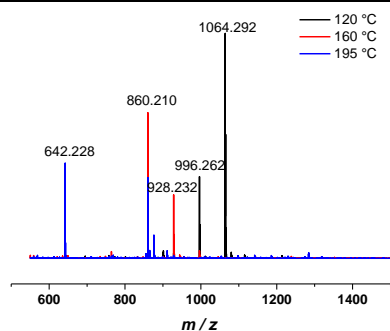
Figure 7-1: Zoom into the ESI-MS spectrum of the product obtained after deprotection of the core at different reaction temperatures after 2 min microreactor residence time in the micro flow reactor

Figure 7-1 and Table 7-1 demonstrate the power of the on-line ESI-MS reaction screening in the furan end group removal of the core molecule **2** (m/z of furan = 68.06). The trifunctional core contains three protective furan groups, which need complete removal before the photo-enol reaction can take place. The reaction was screened at different temperatures – in the range from 120 °C to 195 °C – with a microreactor residence time of 2 min. Although unexpected at first glance, results clearly show that deprotection of the trifunctional molecule is a stepwise process in which the furans are removed one by one. As a result, four peaks could be

monitored in the ESI-MS screening which can be appointed to either a fully protected core (m/z = 1064.292), 1x deprotection of the core (m/z = 996.262), 2x deprotection of the core (m/z = 928.232) or a complete deprotected core (m/z = 860.210). An additional peak at m/z = 642.228 showed up at high reaction temperatures (T= 195 °C) which can be attributed to the breakage of the ester bond [$C_6H_6NO_3$] and thus partial decomposition of the material.
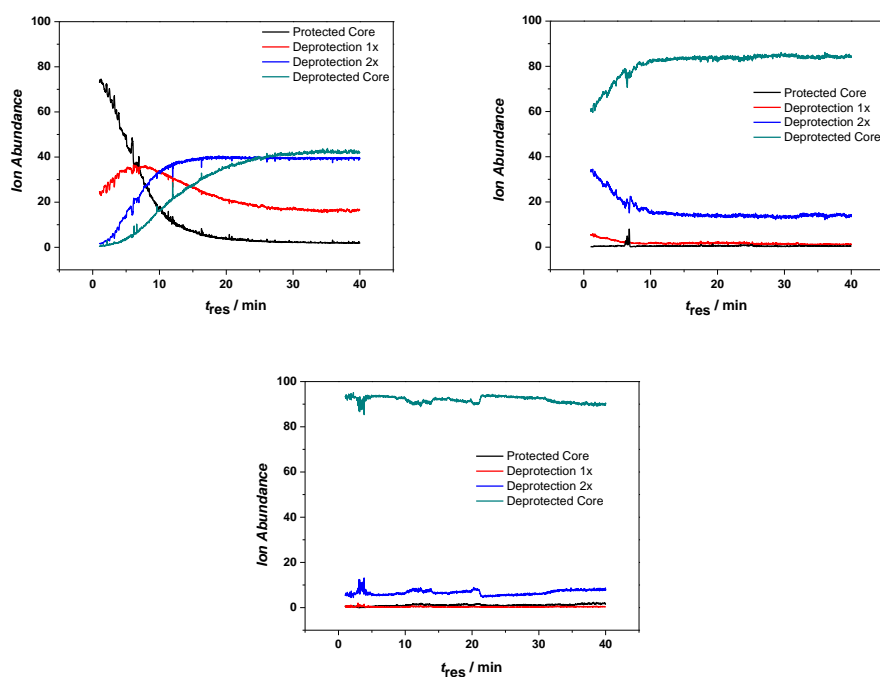
Figure 7-2: Furan removal as a function of residence time in the photo-enol polymerization at 120 °C (*top left*), 160 °C (*top right*) and 195 °C (*bottom*) in the micro flow reactor. Conversion from premonomer (protected core **1**) to monomer (deprotected core **2**) is shown

In addition, peak intensities – as observed in Figure 7-1 – were analyzed relative to each other, which can be plotted as a function of the residence time leading to an ideal microreactor residence time and temperature for the deprotection of the trifunctional core.[19] The ESI-MS peak intensities were measured every 1.33 seconds for all peaks for a time period of 40 min, allowing to obtain 1 800 data points for each temperature, see Figure 7-2. Although deprotection of the core takes place at 120 °C, a maximum conversion of only 42 % was reached. A large part of the molecule is only partly deprotected – 1x or 2x – even after 40 minutes microreactor residence time. Upon increasing the reaction temperature to 165 °C, results significantly improved as a conversion of 80 % was reached within 10 minutes. Both starting products as well as 1x deprotected core have completely reacted within 5 minutes of microreactor residence time, however still a large part of 2x deprotected core is present. Best results are obtained when deprotection takes place at 195 °C, leading to maximum conversions of 95 % within less than 1 minute of microreactor residence time.

Despite the very fast reaction kinetics at 195 °C, also decomposition of the molecules takes place, as shown in Figure 7-1. Hence, a trapping agent (TA; tetracyanoethylene (TCE)) was added to speed up the reaction and reach full conversion at elevated temperatures (< 195 °C). Due to solubility issues of the TA in toluene, the solvent was switched to ethyl acetate (EtOAc). The protected core and TA (5 equiv. relative to the core) were dissolved in EtOAc and injected via 1 gas tight syringe into the flow reactor. Results obtained without the use of trapping agent – and for temperatures of 160 °C or higher – showed no increase in yield upon increasing microreactor residence time after 10 minutes. In addition, maximum conversion was reached when reactions were performed at 195 °C,

however, also decomposition of the product took place. Hence, the use of a TA for furan removal at 120 °C, 165 °C, 175 °C and 195 °C was screened on-line for a time frame of 10 min, Figure 7-3.
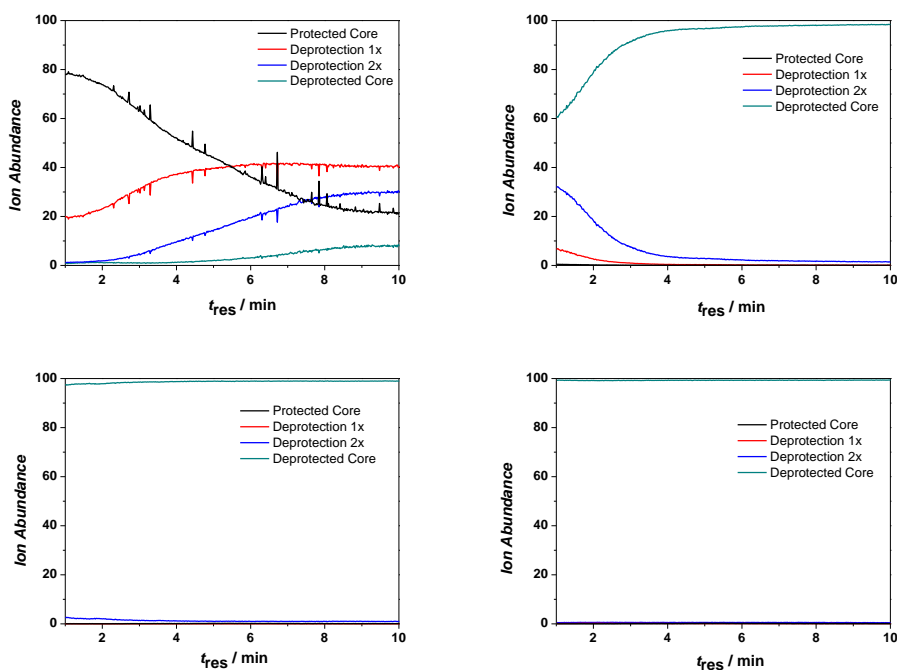
Figure 7-3: Furan removal as a function of residence time in the photo-enol polymerization at 120 °C (*top left*), 160 °C (*top right*) 175 °C (*bottom left*) and 195 °C (*bottom right*) in the micro flow reactor using tetracyanoethylene as trapping agent

The results immediately indicate the profound effect of the TA on the maximum conversion obtained for each temperature. Reaction temperatures of 160 °C or higher are sufficient to easily reach full conversion (> 98 %) within 10 minutes reaction time. Even better results were obtained when the temperature was

increased to 175 °C. In less than 5 minutes full conversion was reached and the core molecule was fully deprotected. In addition, no decomposition of the material was detected in the ESI-MS spectrum, leading to optimized flow conditions for the furan removal of the core, Figure 7-4.
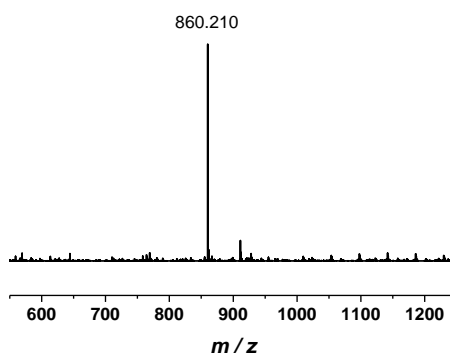
Figure 7-4: ESI-MS spectrum of the product obtained after deprotection of the core at 175 °C after 5 minutes of microreactor residence time in the micro flow reactor using TCE as TA

As depicted in the beginning of the chapter, full conversion of the furan removal in batch takes 15 h at 110 °C, while a similar reaction can be formed in continuous flow systems in just 5 minutes at 175 °C (a temperature not possible to use in batch due to the boiling point of toluene). By using the on-line ESI-MS/Microreactor coupling, visualization of the complete deprotection of the trifunctional furan protected core is possible. In addition, optimized reaction conditions were obtained, leading to a fast and efficient way of deprotecting functionalized materials.

7.3.2. Photo-enol reaction via ESI-MS/MRT coupling

In here, a trifunctional 'core' **2** with triple dienophile functionality and a bifunctional 'arm' **3** with photo-enol functionality are conjugated using a compact fluorescent lamp (wavelength (λ_{max}) = 365 nm), leading to a first generation dendrimer species. In order to screen flow reaction conditions for the conjugation reaction, the core molecule was successfully deprotected in flow, as described in section 7.3.1. Next, kinetics of the conjugation reaction leading to the first generation dendrimer synthesis via photo-enol reactions was studied via on-line ESI-MS/Microreactor coupling. A Labtrix® reactor set-up was used combined with a 3227 chip reactor (volume = 19.5 μL) to enable a wide time range for screening. Both starting compounds (**2** and **3**) were separately dissolved in EtOAc – using a total concentration of the reaction mixture of $[M]_t$ = 29.1 mmol·L^{-1} – and injected into the flow reactor at room temperature. Kinetic screening of the reaction with respect to microreactor residence time and light intensity was enabled, together with the on-line monitoring of the conjugation reaction leading to product formation (Scheme 7-5).
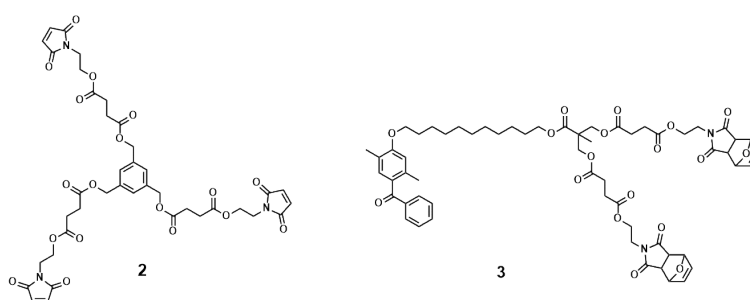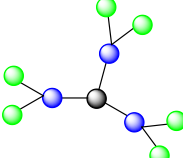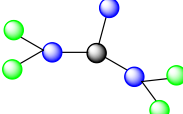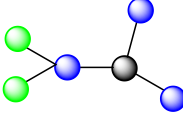
Figure 7-5: Chemical structure of the two starting components; trisuccinate core **2** and disuccinate arm **3**

The reaction was screened at different light intensities (18.5 mW/cm^2 to 64.7 mW/cm^2) for a microreactor residence time between 1 and 10 minutes. Full photo-enol conjugation would lead to macromolecule **4**, a reaction between the trisuccinate core **2** with three disuccinate arms **3** and a total mass in ESI-MS of m/z = 4143.600 for a positively single sodium charged species. Unfortunately, this peak is out of range for ESI-MS detection (the detection range is between m/z = 200 to 4000). However, double (m/z = 2084.311) and triple charged (m/z = 1397.200) product peaks are clearly visible in the ESI-MS spectrum, hence the ESI-MS spectrum of the on-line conjugation reaction using a microreactor residence time of 1 minute and a light intensity of 36 mW/cm^2 was fully analyzed on all observable peaks. To enable full completion of the reaction a small excess of the arm (0.1 equiv. per functionality of the core) was added. Due to the higher ionization of the arm in the ESI-MS screening, the intensity of this peak was much higher as compared to other peaks and thus it was chosen to only display ESI-MS results above the m/z value of the excess arm (m/z = 1117.452) for clarification. Results are displayed in Figure 7-6 and accompanying ESI-MS analysis is shown in Table 7-2.

Table 7-2: Comparison between measured and calculated values for different dendrimer structures found in the ESI-MS spectrum as shown in Figure 7-6

Peak No	Structure description	Schematics of structure [a]	Peak in spectrum m/z	Peak calculated m/z
5	MS^2 peak of m/z = 1205 (single Na^+)	-	1225.510 1267.347	1205.216
6	Product peak (triple Na^+)		1397.200	1397.527
	Product peak (double Na^+)		2084.311	2084.295
7	1 x core + 2 arms (double Na^+)		1536.571	1536.054
8	Cluster of 3 arms (double Na^+)	-	1664.182	1664.683
9	1 x core + 1 arm (single Na^+)		1955.688	1955.675
10	Cluster of 2 arms (single Na^+)	-	2211.925	2211.915

[a] core molecule is schematically represented by a black core with three blue functionalities attached, while the bifunctional arm is represented by the green color.
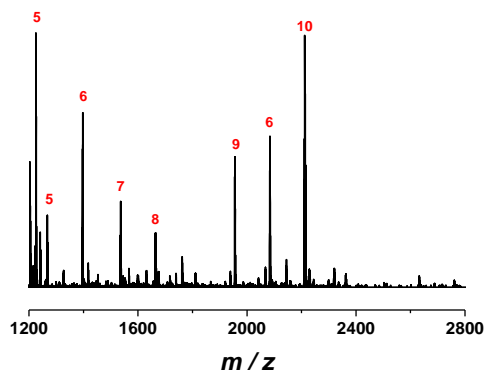
Figure 7-6: Zoom of the ESI–MS spectrum of 1st generation dendrimer synthesis **4** using a microreactor residence time of 1 minute and light intensity of 36 mW/cm^2

A zoom of the ESI-MS spectrum of product **4** as given in Figure 7-6 exhibits six main products, which correspond to different single sodium charged macromolecules. Only one of them corresponds to the product peak **6**, while the rest are side product or cluster formations of starting products. The signals denoted by **5** (m/z = 1225.510 and 1267.347) are aggregates, which after tandem mass spectroscopy (or better known as MS^2) is the result of a cluster between a fraction of the arm [C_7H_5O; m/z = 105.107], the core [$C_{10}H_{10}NO_6$; m/z = 240.207] and the deprotected core (m/z = 837.223), leading to a total mass of a 1205.216 (Na$^+$). Signal **7** (m/z = 1536.571) originates from a double sodium charged core molecule connected to two arms, while signal **8** (m/z = 1664.128) and **9** (m/z =1955.688) are related to a cluster of double sodium charged species of three arms or single charged product between the core molecule and the arm respectively. Signal **10** (m/z = 2211.925) is related to the last detectable cluster peak in the ESI-MS spectra originating from the signal of a single sodium charged

cluster of 2 arms. Although ESI-MS shows the presence of a variety of clusters and side products during the reaction, the double (m/z = 2084.311) and triple sodium charged (m/z = 1397.200) product peaks are clearly visible as well and marked in the ESI-MS spectrum **6**, indicating the partly successful photo-enol reaction. As ESI-MS is merely a qualitative and not a quantitative technique – due to the difference in ionization biases of the molecules – there is no direct correlation between the height of the peaks and the yield. Still, first results are really promising and successful detection of the product peaks was realized. However, more peaks than expected show up in the spectra, which can in fact be related to the chosen reaction conditions, as displayed in Figure 7-7 and 7-8.
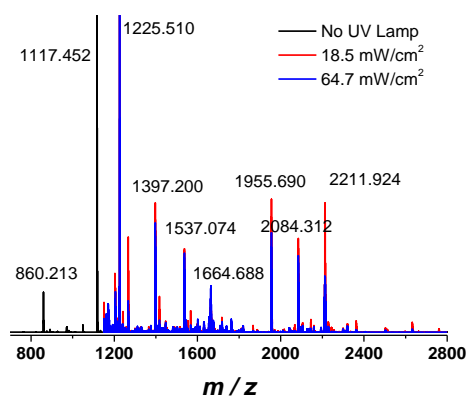
Figure 7-7: Comparison between ESI–MS spectrum of 1st generation dendrimer synthesis **4** using a microreactor residence time of 10 minutes and a light intensity of (a) no UV, (b) 18 mW/cm² or (c) 64.7 mW/cm²
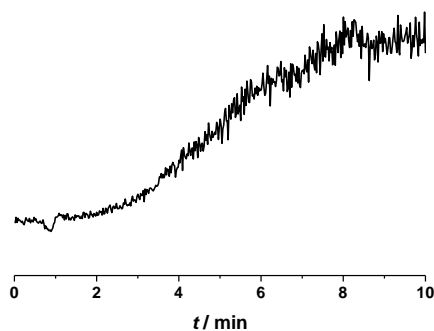
Figure 7-8: MS^2 results of the m/z = 1225.510 peak in time

In here, a comparison between the use of a light intensity of 18.5 mW/cm^2 and 64.7 mW/cm^2 for a photo-enol reaction with a microreactor residence time of 10 minutes is made. ESI-MS spectra of both light intensities were compared and show a clear difference in peak intensities. Although not used for quantitative purposes for single peaks, comparing the two spectra clearly shows the decreased yield of the product peaks upon increasing light intensity. In addition, time plays a crucial role as well, as an increase in microreactor residence time from 1 to 10 minutes clearly leads to an increase of some undesired side products (e.g. m/z = 1225.510; Figure 7-8).

This leads to the conclusion that the photo-enol reaction of the trisuccinate core **2** and disuccinate arm **3** does lead to the desired first generation dendrimer synthesis when screening the reaction for 2 min at 36 mW/cm^2. However, more research is needed to have a careful look at the full completion of the first generation of dendrimer species via the photo-enol reaction.

7.4. CONCLUSIONS

In conclusion it can be stated that continuous flow reactors open up a new way of synthesizing complex polymer architectures via light induced reaction pathways. Combined with the on-line ESI-MS/MRT coupling, new doors are opened and reactions are monitored on-line. A trifunctional 'core' with dienophile functionality (maleimides (MIs)) and a bifunctional 'arm' with photo-enol functionality are conjugated using a compact fluorescent lamp (wavelength (λ_{max}) = 365 nm), leading to a first generation dendrimer species. Therefore, first a complete screening of the core deprotection in flow was performed. A variety of microreactor residence times (1 to 40 minutes) as well as temperatures (120 °C to 195 °C) were screened on-line, leading to the conclusion that full deprotection of the three arms takes place in less than 5 minutes at 175 °C when a trapping agent is used. These results indicate the profound effect flow reactions have over batch reactions – due to batch limitations – as the reaction in batch takes 15 h at 110 °C to reach full completion. Next, the first generation of dendrimer species was targeted via photo-enol reaction. Although very promising results concerning deprotection of the furan protected MIs at first, dendrimer synthesis in flow is accompanied with incomplete conversions. ESI-MS spectra indicate the presence of multiple clusters as well as incomplete reaction products. Further research is needed to enable full conversion and the synthesis of higher order dendrimer species in microfluidic reactors.

7.5. REFERENCES

[1] O. Diels, K. Alder, *Justus Liebigs Ann. Chem.* **1928**, *460*, 98-122.

[2] K. Alder, *Neuere Methoden der preparativen organsichen Chemie*, Verlag Chemie, Weinheim, **1943**.

[3] S. M. Weinreb, R. R. Staib, *Tetrahedron* **1982**, *38*, 3087-3128.

[4] G. Desimoni, G. Tacconi, *Chem. Rev.* **1975**, *75*, 651-692.

[5] M. Conradi, *PhD Thesis*, Hasselt University, **2014**.

[6] C. Barner-Kowollik, F. E. Du Prez, P. Espeel, C. J. Hawker, T. Junkers, H. Schlaad, W. Van Camp, *Angew. Chem. Int. Ed.* **2011**, *50*, 60-62.

[7] T. Pauloehrl, G. Delaittre, V. Winkler, A. Welle, M. Bruns, H. G. Börner, A. M. Greiner, M. Bastmeyer, C. Barner-Kowollik, *Angew. Chem. Int. Ed.* **2012**, *51*, 1071-1074.

[8] M. Winkler, J. O. Mueller, K. K. Oehlenschlaeger, L. Montero de Espinosa, M. A. R. Meier, C. Barner-Kowollik, *Macromolecules* **2012**, *45*, 5012–5019.

[9] K. K. Oehlenschlaeger, J. O. Mueller, N. B. Heine, M. Glassner, N. K. Guimard, G. Delaittre, F. G. Schmidt, C. Barner-Kowollik, *Angew.Chem. Int. Ed.* **2013**, *52*, 762–766.

[10] K. Terao, Y. Nishiyama, H. Tanimoto, M. Tsumoru, M. Oelgemoller, K. Kakiuchi, *J. Flow Chem.* **2012**, *35*, 1144–1152.

[11] A. Sugimoto, T. Fukuyama, Y. Sumino, M. Takagi, I. Ryu, *Tetrahedron* **2009**, *65*, 1593–1598.

[12] O. Shvydkiv, A. Yavorskyy, S. B. Tan, K. Nolan, N. Hoffmann, A. Youssef, M. Oelgemoller, *Photochem. Photobiol. Sci.* **2011**, *10*, 1399–1404.

[13] G. Jas, A. Kirschning, *Chem. Eur. J.* **2003**, *9*, 5708-5723.

[14] K. Geyer, J. D. C. Codée, P. H. Seeberger, *Chem. Eur. J.* **2006**, *12*, 8434-8442.

[15] D. Wilms, J. Klos, H. Frey, *Macromol. Chem. Phys.* **2008**, *209*, 343-356.

[16] H. Seyler, D. J. Jones, A. B. Holmes, W. W. H. Wong, *Chem. Commun*. **2012**, *48*, 1598-1600.

[17] C. Wiles, P. Watts, *Eur. J. Org. Chem.* **2008**, 1655-1671.

[18] P. D. I. Fletcher, S. J. Haswell, E. Pombo-Villar, B. H. Warrington, P. Watts, S. Y. F. Wong, X. Zhang, *Tetrahedron* **2002**, *58*, 4735-4757.

[19] J. J. Haven, J. Vandenbergh, T. Junkers, *Chem. Comm*. **2015**, *51*, 4611-4614.

CHAPTER 8

Summary and Outlook
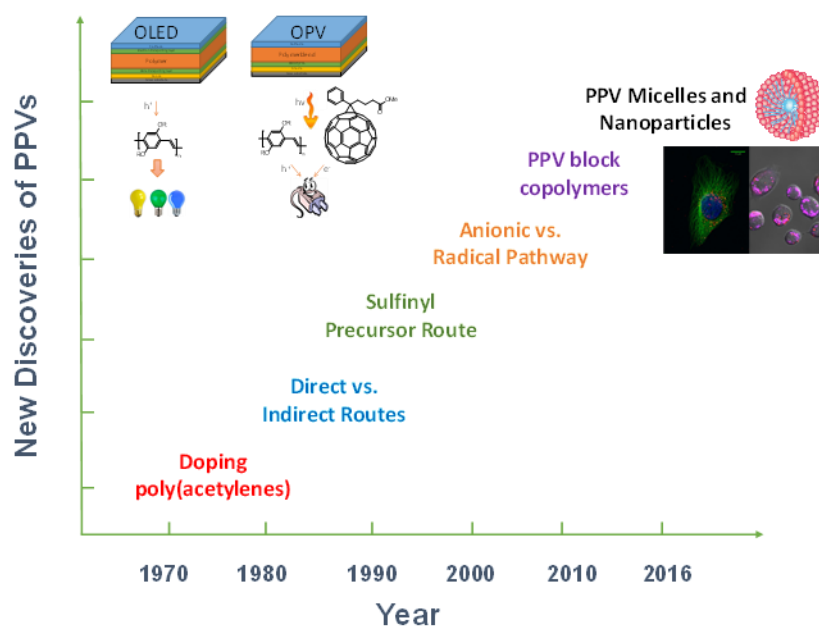
8.1. SUMMARY

Poly(*p*-phenylene vinylenes) (PPVs) and their derivatives are one of the most studied conjugated materials over the last decades. Although originally used in electronic applications, more recent developments opened a variety of application pathways for PPVs in the area of biosensors and biomedical research. The excellent fluorescent properties and low charge carrier mobility of PPVs make them ideal candidates to replace existing bioimaging agents such as organic fluorescent markers. In this thesis the mechanistic understanding of the PPV synthesis pathway, ultimately leading to the use of PPV materials in theranostic applications is presented.

In first instance, focus was placed on the controlled synthesis of (MDMO)-PPVs via the radical sulfinyl route through the use of a chain transfer agent (CTA). Polymerizations are characterized by systematic variation, leading to a negative activation energy upon the use of CBr_4 as CTA. High-end group fidelity of the CBr_4-derived PPVs via the sulfinyl route was proven via chain extension experiments using atom transfer radical polymerization (ATRP) reaction conditions. In addition, copper-catalyzed alkyne-azide cycloaddition (CuAAC) was used to successfully synthesize PPV (tri) block copolymer structures. Despite these achievements, the synthesis of complex macromolecular structures via the anionic sulfinyl route was investigated simultaneously, leading to an easy and more efficient way to synthesize PPV block copolymers via a 'living' method. Hence, focus was shifted towards the anionic route and amphiphilic PPV block copolymers were targeted by using post-polymerization methods or the use of a hydrophilic non-PPV block. One way to realize this was by combining (MDMO)-PPV with the ester functionalized

(CPM)-PPV, leading to copolymers with an ester in the side chain. Post-polymerization reactions on this side chain were easily realized by hydrolysis (water soluble) or functionalization into an alkyne (e.g. grafting reactions), alkene (e.g. thiol-ene reactions) or PEG (water soluble) thereby opening a broad range of new applications for PPVs outside the electronics field. One of those applications is the biomedical field and more specifically bioimaging or drug delivery. Synthesis of amphiphilic PPV block copolymers containing a PPV block and a (meth)acrylate or methacrylamide block was realized using SET-LRP reaction conditions. The block copolymers spontaneously self-assembled into micelles upon contact with water. The resulting non-cytotoxic micelles – by themselves non-fluorescent – showed excellent stability and payload retention for up to 1 year and were successfully loaded with anti-cancer drug (Curcumin or Doxorubicin). The micelles were taken up efficiently by the cells, which triggers spontaneous decomposition, releasing the encapsulated material. Hence, a first step for the use of PPVs in both bioimaging as well as drug delivery was taken.

As a result, the second part of the thesis is focused on the use of continuous flow reactors for the synthesis of complex (PPV) macromolecules. All results so far were obtained by performing batch reactions. However, the use of flow reactors has over the last years proven to be beneficial over batch reactions due to their excellent isothermal reaction conditions, efficient radial mixing as well as its easiness to scale up reactions from mg to kg. A general method for the continuous synthesis of the multi-step radical sulfinyl-route (MDMO)-PPV polymerizations was made available in this way by coupling two flow microreactors. Conjugated polymers could directly be obtained from the monomer which under batch conditions was not easily reached, especially for this type of polymerization. Next,

flow reactors were used as a way to systematically screen the very fast precursor polymerizations in time, thereby obtaining – for the very first time – reliable and time dependent data for different reaction times, temperatures and concentrations for the synthesis of (MDMO)-PPV precursor polymer via the radical sulfinyl route. Subsequently, this data was used for in-depth kinetic studies to get a better mechanistic and kinetic understanding of this specific polymerization by using Predici®. Two models were built in which chain transfer could lead to inhibition of the polymerization or that the transfer reaction is in line with classical free radical polymerization rules. Despite the differences between the radical precursor polymerization to conventional free radical copolymerization – mostly due to differences in initiation and biradical formation – the reaction followed similar driving forces as observed for most radical polymerizations and kinetic rate coefficients were in the same order of magnitude.

In the last part of the thesis, the use of continuous flow reactions is expanded to other polymerization methods and more specifically the synthesis of dendrimers via photo-enol reactions. In here, ESI-MS/Microreactor coupling was used, a technique recently developed in our group to on-line monitor reactions via ESI-MS. As a result the photo-enol reaction between a trifunctional trisuccinate core and bifunctional disuccinate arm was fully screened on-line. Despite product formation was clearly observed in ESI-MS, ^{1}H NMR as well as SEC, side product formation hindered the continuous synthesis of high order dendrimers. More research could elucidate on these side reactions to enable full conversions and the one-pot synthesis of dendrimers via photo-enol reactions.

8.2. OUTLOOK

In this work we have focused on two major aspects of high relevance in the PPV field, i.e. (i) the design of complex polymer structures for use in biomedical applications and (ii) in-depth kinetic studies to get a better mechanistic and kinetic understanding of the precursor polymerization of PPVs via the radical sulfinyl route. A third aspect is related to both the use of PPVs as well as the general design of new macromolecules by using continuous flow chemistry. In this section, some recommendations for further research are postulated.

8.2.1. PPVs in biomedical applications

In Chapters 2, 3 and 4 the positive influence of the incorporation of functional moieties in the side chain or in the backbone on the applicability of PPVs is demonstrated, ultimately leading to the synthesis of PPV micelles to be used as drug carrier vesicle. Most of the reactions were based on the synthesis of (tri) block copolymers using the well-known material (MDMO)-PPV. Over the last decades a lot of work has been done by using (MDMO)-PPV, leading to a very efficient way of synthesizing the monomer and its accompanying polymer in an easy and reproducible way of which all thermal, electrical as well as optical properties are reported in literature. As a result, new ideas, concepts or structures are always based on this polymer, even though much better materials – mostly with respect to optical properties – have been developed in the last years. After the first proof of concept has been established, it would be interesting to take this research one step further. At the moment nothing is known about the fate and transport of the micelles in and around the cell, as we only had a look if the micelles are able to penetrate into the cancer cell and release the encapsulated

material. The use of living cells in general could be tested, as well as a complete map of cell transport would give a lot of insight into the optimal way to target drug delivery. In addition, our block copolymers show fluorescence, however, when self-assembled the fluorescence is quenched. Upon cell uptake the fluorescence is clearly present again, thereby releasing the encapsulated materials as well. More information about this still unknown trigger would be of added value to enhance the current micellar system. Mimicking cell conditions on lab scale (e.g. addition of lipase or tripsin to micelles) could help in a better mechanistic understanding.

On the other side, we now used (MDMO)-PPV, a polymer which excites its photons in the range of 560 nm, leading to a red color. Variation in color in both the visible as well as (near / far) IR region as well as the use of materials with a higher quantum yield could be of added value to expand current applications even further into the biomedical field. In order to reach this goal, new PPV-like monomers need to be designed thereby varying the side chains into e.g. anthracene or fluorene like structures. Thanks to the ongoing collaboration with UNSW, even ideas for designing a PPV carrying a positive / negative charge along the backbone were mentioned, to be used in drug delivery systems for proteins. As a last step, we are not limited to bioimaging or drug delivery applications. We developed an easy and efficient way of encapsulating materials in general into PPV-micelles, which in theory could be used to load micelles with magnetic particles (e.g. used in photo-thermal therapy).

A new PhD student will start working on the use of PPVs in the biomedical field and will explore the possibilities as described above. First goal will be the synthesis of new phenylene vinylene like monomers and testing their polymerization

behavior with respect to livingness and end group fidelity at first and optical properties in a second stage. Once a novel material has been developed, micellization accompanied with cell tests will elucidate on the transport mechanism of the micelles into the cells as well as the fate of the micelles over a longer period of time. In addition, two master students will start working on this topic as well of which one will have a deeper look into the possibility of coupling proteins to the surface of the micelles. In that way targeted transport of the micelles is tested. Next, the use of continuous flow reactors for the actual micellization process will be explored by the other student.

Although the synthesis of PPV micelles is a new concept which was first explored in this thesis, another PhD student started working on the use of PPV polymer nanoparticles (NPs) for biomedical use two years ago. First trials using pure (MDMO)-PPV or (MDMO/CPM)-PPV NPs successfully led to the use of PPV-derivative based particles to be used as bioimaging probe. Limited by their optical properties – absorbance (500 nm) as well as emission (580 nm) – the use of PPV copolymers with different functional monomers was tested. As all PPV materials needed for this work was provided by me, an in-depth study towards the copolymerization behavior of (MDMO)-, (CPM),- and (CN)-PPV as well as the possibility to post-functionalize the PPV-polymers was taken, of which the results are described in chapter 3. Successful post-functionalization of the ester side chain of (MDMO/CPM)-PPV copolymers as well as copolymerization behavior of (MDMO/CPM)-, and (MDMO/CN)-PPV copolymers was shown. These results lead to new possibilities for the use of PPV NPs and hence the use of (CPM/CN)-PPV copolymers will be the next step in this research.

8.2.2. Mechanistic insight

Although PPVs are not being used in OPV applications anymore, their use in electronic devices (e.g. OLEDs) is still significant. Recent collaboration with MPI showed the extensive mechanistic work they performed on PPVs synthesized via the Gilch route. Although the Gilch route is classified as direct route (when using an excess of base) and the sulfinyl as indirect, both routes start their polymerization with a so-called premonomer, after which the real monomer is formed *in situ*. This monomer – better known as *p*-quinodimethane – spontaneously self-initiates into a biradical after which propagation of the reaction leads to the PPV polymer. So far, only online UV-Vis methods were able to detect the formation of the *p*-quinodimethane, due to the extremely fast reaction kinetics of this step. At MPI, they are able to perform *in situ* NMR experiments at low temperatures (-100 °C) thereby extremely slowing down the reaction and derive some of the kinetic parameters with respect to *p*-quinodimethane and subsequently its biradical formation. More information about these first steps in the polymerization would be of added value to get a better understanding of the kinetics.

In addition, a closer look into the electronic current in OLEDs can be taken as devices are negatively influenced by the presence of charge traps in the material. As a result, electrons are trapped and cannot be converted into light. At the moment, first trials for the design of trap-free plastic electronics by using PPV-*b*-PS block copolymers is conducted, which – combined with the mechanistic insights – could lead to materials with improved product properties. As we have general procedures of synthesizing PPV block copolymers, in theory any PPV block

copolymer could be synthesized (e.g. difference in optical properties, quantum yield).

8.2.3. Continuous Flow Chemistry

The use of flow reactors became part of the standard synthesis way in the lab over the last years. As a result, first step towards synthesis of conjugated polymers have been made but flow reactors can be used for so much more. A start was already made by trying to perform photo enol reactions in flow for the synthesis of higher order dendrimers. This knowledge can be expanded to the general synthesis of dendrimers by combining controlled living polymerization techniques (RAFT, ATRP, NMP) or 'click' reactions which – as shown in the past when using flow chemistry – would enhance synthesis procedures as well as product properties. In addition, a shift towards the use of dispersions (e.g. suspension, emulsion or precipitation polymerization) could greatly benefit from the use of flow reactors. Particle formation is of utmost importance in these reactions, hence PPV micelle formation targeted in flow reactors could lead to a variety of morphologies which are not available upon synthesizing micelles in batch conditions.

Next, flow reactors are a great tool to kinetically screen reaction conditions by using only a small amount of material. As shown in chapter 7, coupling the flow reactor to the ESI-MS setup allows the on-line monitoring of reactions, (side) product formation as well as determination of most abundant products. Although only preliminary results were shown for the deprotection of maleimides and the photo-enol reaction, a variety of reactions with respect to PPV synthesis would benefit from this ESI-MS/Microreactor coupling setup. As discussed, little is known about the p-quinodimethane and subsequent biradical formation, which – with the

help of the on-line setup – could greatly enhance our current knowledge. In addition, several side reactions take place during the polymerization of PPVs, leading to di -tri-and tetramers as well as cyclization (paracyclophane) products. Currently, identification of this 'rest' fraction after polymerization is performed off-line. However, using the online setup would give a complete overview of all side products formed and parameters needed (time, temperature, concentration), ultimately leading to suppression of these side reactions.

8.3. NEDERLANDSE SAMENVATTING

Poly(*p*-Phenylene Vinylenes) (PPVs) en zijn derivaten kunnen gezien worden als een van de meest bestudeerde geconjugeerde materialen van de afgelopen decennia. Ondanks dat dit materiaal voornamelijk werd gebruikt in fotovoltaïsche toepassing, hebben zich de laatste jaren steeds meer mogelijkheden voorgedaan voor het gebruik van PPVs in de biosensoren of het biomedische onderzoek. De uitstekende fluorescerende eigenschappen in combinatie met zijn lage ladingsmobiliteit maken PPVs de ideale kandidaat om huidige bioimaging materialen zoals organische fluorescerende markers te vervangen. Met het oog op deze doelstellingen hebben we ons in deze thesis gericht op het verkrijgen van meer en beter inzicht in het mechanisme dat gepaard gaat met de synthese van PPVs enerzijds, alsmede het toepassingsgebied uit te breiden door complexe PPV structuren te ontwikkelen met als einddoel theranostics.

In de eerste fase hebben we ons toegelegd op de gecontroleerde synthese van (MDMO)-PPV via de radicalaire sulfinyl route, door gebruik te maken van een ketenoverdrachtsreagens. Het karakteriseren van de verschillende polymerisaties verliep systematisch (variatie in temperatuur, concentratie, reactietijd) wat heeft geleid tot een negatieve activeringsenergie bij het gebuik van CBr_4 as ketenoverdrachtsreagens. Door het gebruik van CBr_4, werden de keteneindes voorzien van CBr_4 afgeleiden, welke in een volgende stap geïnitieerd werden. Gecombineerd met het gebruik van atom transfer radical polymerization (ATRP) reactie condities kon op deze manier de synthese van PPV blokcopolymeren gerealiseerd worden. Daarnaast werden de wel bekende CuAAC (copper-catalyzed alkyne-azide cycloaddition) reactie condities gebruikt voor de synthese van zowel

PPV blok als multi-blokcopolymeren. Ondanks de grote successen van de radicalaire sulfinyl route om eerst homopolymeren en volgens multi-blokcopolymeren te verkrijgen, vond er simultaan gelijksoortig onderzoek plaats voor de synthese van complexe structuren startende met PPVs gesynthetiseerd via de anionische sulfinyl route. Via deze route konden op een gemakkelijke, snelle en veel efficiëntere manier, verfijnde complexe polymeren via een levende polymerisatie verkregen worden. Er werd daarom besloten om de focus naar de anionische route te schuiven, waarbij amfifiele PPV blok copolymeren werden ontworpen door gebruik te maken van post-polymerisatie methodes enerzijds of het gebruik van een hydrofiel niet-PPV-blok. Wanneer (MDMO)-PPV wordt gecombineerd met een ester-gefunctionaliseerde (CPM)-PPV leidt dit tot copolymeren met een ester in de zijketen welke gemakkelijk gefuntionaliseerd kunnen worden. Hierbij valt te denken aan hydrolyse reacties om het polymeer wateroplosbaar te maken, maar eventuele functionalisatie met een alkyn – voor het gebruik van bijvoorbeeld oppervlakte reacties – of alkeen zijgroepen – te gebruiken in de welbekende Thiol-Ene reacties – openen hiermee een breed scala aan nieuwe toepassingen voor PPVs buiten het elektronische gebied. Een van die toepassingen is het gebruik in de biomedische wereld en meer specifiek als bioimaging reagens of voor drug delivery. Synthese van amfifiele PPV blokcopolymeren zelfassembleren in water spontaan tot micellen. Deze niet cytotoxische micellen – van zichzelf niet fluorescerend – vertonen uitstekende stabiliteit voor een periode van een jaar en kunnen succesvol geladen worden met anti-kanker medicijnen (Curcumin or Doxorubicin). Cel studies wijzen uit dat de micellen perfect kunnen worden opgenomen door de cel, waar de eventuele lading aanwezig in de micellen spontaan vrijgelaten wordt. Deze eerste studies laten de kracht van PPVs zien en het gebruik ervan in de biomedische wereld.

Het tweede deel van deze thesis handelt over het verkrijgen van meer inzicht in het mechanisme dat gepaard gaat met de polymerisatie van complexe PPV macromoleculen. Alle resultaten tot dusver zijn verkregen door gebruik te maken van batchreacties. De laatste jaren echter is het gebruik van flowreactoren enorm toegenomen en heeft dit geleid tot een nieuwe succesvolle manier om reacties uit te voeren, daar reacties in flow uitgevoerd kunnen worden met bijna perfect radiaal mixgedrag, isotherme reactiecondities en het gemak om van mg naar kg op te schalen. Een algemene methode voor de multi-stap synthese van geconjugeerde PPVs via de radicalaire sulfinyl route is opgesteld door twee reactoren aan elkaar te koppelen. Geconjugeerde polymeren kunnen op deze manier door toediening van het monomeer en de base direct verkregen worden, iets wat onder batchcondities niet haalbaar is. Daarnaast worden flowreactoren veelal gebruikt voor het screenen van reactiecondities, daar met een relatief kleine hoeveelheid materiaal een scala aan reactiecondities op een eenvoudige en continue manier getest kunnen worden. Op deze manier kan er voor de eerste keer betrouwbare tijdsafhankelijk data verkregen worden voor de synthese van (MDMO)-PPV via de radicalaire sulfinyl route. Deze data werd vervolgens gebruikt als input in een theoretisch model – opgesteld via Predici® – om op die manier een beter inzicht in de kinetiek van deze specifieke polymerisatie te krijgen. Twee modellen werden opgesteld, één waar ketenoverdracht leidt tot inhibitie terwijl de andere de regels van de klassieke vrije radicaalpolymerisatie volgt. Ondanks de verschillen tussen de radicalaire route om PPVs te verkrijgen en de klassieke manier – vooral door het verschil in initiatie van de reactie – lijken beide reactie dezelfde drijfkracht te bezitten. Daarnaast liggen de verkregen reactiesnelheidsconstantes in dezelfde orde van grootte als die voor klassieke vrije radicaal polymerisatie.

In het laatste deel van de thesis wordt het gebruik van flowreactoren verder uitgebreid naar de synthese van dendrimeren via foto-enol reacties. Hiervoor wordt gebruik gemaakt van een ESI-MS/flowreactorkoppeling, een techniek die het online volgen van reacties mogelijk maakt. Daardoor kan de reactie tussen een trifunctionele trisuccinaat en difunctionele disuccinaat volledig gevolgd worden met alle reacties en zijproduct vorming. Helaas bleek deze laatste de overhand te hebben. Om die reden was het nog niet mogelijk om hogere ordes dendrimeren in de flowreactor te synthetiseren, maar meer onderzoek zou het evenwicht van de reactie de juiste kant op kunnen drijven om zo op een simpele en efficiënte manier de continue synthese van dendrimeren via foto-enol reacties in flowreactoren te verwezenlijken.

CHAPTER 9

Materials and Characterization
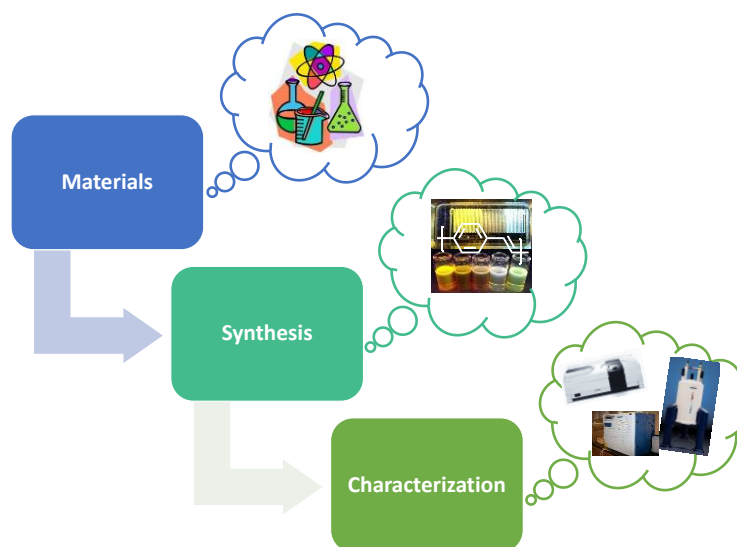
9.1. MATERIALS

All solvents and reagents were purchased from VWR, Acros, Ajax, or Aldrich and were used without further purification. Tetrahydrofurane (THF), dimethylformamide (DMF) and CH_2Cl_2 were dried on a MB-SPS 800 system (if indicated as dry solvent) in chapters 2, 3, 5, 6, 7 and 8. DMF, THF and toluene used in chapter 4 were bought at Ajax. The monomers *tert*-Butyl acrylate (*t*BuA), styrene, ethylene glycol methyl ether methacrylate (EGMA) and *2*-hydroxyethyl acrylate (HEA) used for the chain extension, were deinhibited over a column of basic alumina. *2*-hydroxypropyl methacrylate (HPMA) was synthesized according to literature procedure.

9.2. CHARACTERIZATION

9.2.1. Standard characterization techniques for monomers and initiators

^1H and ^{13}C NMR spectra as shown in chapters 2, 3, 5, 6, 7 and 8 were recorded in $CDCl_3$ or CD_2Cl_2 on a Varian Inova 300 spectrometer at 300 and 75 MHz respectively using a 5 mm probe. ^1H NMR spectra recorded in chapter 4 were obtained using a Bruker Avance Ш 300 spectrometer (300 MHz). All chemical shifts are recorded in ppm (δ) relative to tetramethylsilane (δ = 0 ppm), referenced to the chemical shifts of residual solvent resonances (^1H). The multiplicities were explained using the following abbreviations: s for singlet, d for doublet, t for triplet, m for multiplet and bs for broad signal.

Melting points were determined using a Electrothermal IA9000 series Digital Melting Point Apparatus.

Direct insertion probe/mass spectrometry (DIP MS) analyses were obtained with a Varian TSQ-70 and Voyager mass spectrometer (Thermoquest). The capillary column was a Chrompack Cpsil5CB or Cpsil8CB.

FT-IR and ATR FT-IR spectra as shown in chapters 2, 3, 5, 6, 7, and 8 were collected on a Brucker Tensor 27 FT-IR spectrophotometer (nominal resolution 4 cm^{-1}). Spectra recorded in chapter 4 were performed on a Bruker IFS 66/S Fourier transform spectrometer equipped with a tungsten halogen lamp, a CaF_2 beam splitter. Spectra were analyzed with OPUS software.

9.2.2. Spectroscopic techniques: UV-Vis and fluorescence spectroscopy

UV-Vis spectra as shown in chapters 2, 3, 5, 6, 7, and 8 were recorded on a Varian Cary 500 UV-Vis-NIR spectrophotometer (scan rate 600 nm·min^{-1}, continuous run from 200 to 800 nm). UV-Vis spectra as shown in chapter 4 were recorded on a Varian Cary 300 UV-Vis-NIR spectrophotometer (scan rate 600 nm·min^{-1}, continuous run from 200 to 800 nm) equipped with a temperature controller.

Fluorescence measurements as performed in chapters 2, 3, 5, 6, 7, and 8 were performed using a 'Fluorolog® Tau-3 Lifetime System' spectrofluorometer from Horiba Group, USA. The entire system was controlled by DataMax software. The absorption wavelength was depended on the type of PPV material (usually in a range between 400 and 500 nm) and the emission was scanned between respectively 400 (or higher) and 800 nm. The sample was placed at an angle of 22.5°, resulting in the highest fluorescence signal with a minimum of scattering and reflection coming from the glass. The slits of both monochromators were

adjusted to 5 nm. The fluorescence intensities of micelles as shown in chapter 4 were measured using a Cary Eclipse Fluorescence Spectrophotometer (Agilent Technologies). The absorption and emission wavelengths were 418 nm (PPV-*b*-P(EGMA)), 466 nm (PPV-*b*-P(HPMA)), 438 nm (PPV-*b*-P(HEA)), 552 nm (Nile Red), 431 nm (Curcumin) and 481 nm (Doxorubicin) respectively.

9.2.3. Size exclusion chromatography (SEC)

Analysis of the MWDs of the polymer samples described in Chapter 2, 3, 5, 6, 7 and 8 were performed on a Tosoh EcoSEC System, comprising an autosampler, a PSS guard column SDV (50 × 7.5 mm), followed by three PSS SDV analytical linear XL columns (5 μm, 300 × 7.5 mm) and a differential refractive index detector (Tosoh EcoSEC RI) using THF as the eluent at 40 °C with a flow rate of 1 mL·min^{-1}. The SEC system was calibrated using linear narrow polystyrene standards ranging from 474 to 7.5 x 10^6 g·mol^{-1} (PS (K = 14.1 x 10^{-5} dL·g^{-1} and α = 0.70)). Polymer concentrations were in the range of 3–5 mg·mL^{-1}. Although correct Mark Houwink parameters for plain precursor (α = 0.67605 and *k* = 0.000142 mL·g^{-1}) as well as conjugated (MDMO)–PPV (α = 0.809 and *k* = 0.00002 mL·g^{-1}) were used, differences in these parameters upon the formation of (tri) block copolymers (Chapter 2 and 3) were not taken into account. Therefore, only apparent values for these samples are discussed.

Analysis of the MWDs of the polymers with UV detection at λ$_{max}$ of the polymer was performed using a Spectra Series P100 (Spectra Physics) pump equipped with two mixed-B columns (10 μm, 2 cm x 30 cm, Polymer Laboratories) and an Agilent 1100 DAD UV detector at 60 °C. Chlorobenzene (CB) was used as the eluent at a

flow rate of 1.0 mL·min⁻¹. Molecular weights were determined relative to polystyrene standards.

Analysis of MWDs of the polymer samples described in chapter 4 were analyzed via size exclusion chromatography (SEC). A Shimadzu modular system comprising a SIL-10AD auto-injector, DGU-12A degasser, LC-10AT pump, CTO-10A column oven and a RID-10A refractive index detector was used. A 5.0-lm bead-size guard column (50 ×7.8 mm) followed by four 300 × 7.8 mm linear columns (500, 10³, 10⁴, and 10⁵ Å pore size, 5 μm particle size) were employed for analysis. *N*,*N*-Dimethylacetamide (DMAc; HPLC grade, 0.05% w/v 2,6-di-butyl-4-methylphenol (BHT) and 0.03% w/v LiBr) with a flow rate of 1 mL/min at 50 °C was used as mobile phase. 50 μL of polymer solution with a concentration of 2 mg/mL in DMAc was used for every injection. The calibration was performed using commercially available narrow polydispersity polystyrene standards (0.5-1000 kDa, Polymer Laboratories).

9.2.4. Recycle Size exclusion chromatography (Recycle-SEC)

Separation of polymers after selective precipitation were performed on a recycling preparative HPLC (high performance liquid chromatography) LC-9210 NEXT system in the recycle injection mode (3 mL) comprising a JAIGEL-2H and JAIGEL-3H column and a NEXT series UV detector using $CHCl_3$ as the eluent with a flow rate of 3.5 mL·min⁻¹.

9.2.5. Electrospray ionization – mass spectrometry (ESI–MS)

ESI–MS spectra were recorded on a LCQ Fleet mass spectrometer (ThermoFischer Scientific) equipped with an atmospheric pressure ionization source operating in

the nebulizer assisted electro spray mode. The instrument was calibrated in the *m/z* range 220–2000 using a standard solution containing caffeine, MRFA and Ultramark 1621. A constant spray voltage of 5 kV was used and nitrogen at a dimensionless auxiliary gas flow-rate of 10 and a dimensionless sheath gas flow-rate of 3 were applied. The capillary voltage, the tube lens offset voltage and the capillary temperature were set to 25 V, 120 V, and 275 °C respectively. A 250 µL aliquot of a polymer solution with concentration of 10 µg·mL^{-1} was injected. A mixture of CH_2Cl_2 and methanol (1/3), all HPLC grade, was used as the solvent.

9.2.6. Dynamic light scattering (DLS) for determination of hydrodynamic diameter of nanoparticles

The average hydrodynamic diameter and the polydispersity index of the nanoparticles were determined using a ZetaPALS equipment (Brookhaven Instruments Cooperation).

Zeta potential of all particles were determined using a Malvern Zataplus particle size analyzer (laser, 35mW, λ = 632 nm, angle = 90°) at a polymer concentration of 1 mg/mL. Samples were prepared in deionized water and purified from dust using a micro filter (0.45 µm) prior to the measurements.

9.2.7. Transmission Electron Microscopy (TEM) for the determination of particle morphology and diameter.

The TEM micrographs were obtained using a JEOL1400 transmission electron microscope comprising of a dispersive X-ray analyzer and a Gatan CCD facilitating the acquisition of digital images. The measurement was conducted at an accelerating voltage of 80 kV. The samples were prepared by casting the micellar

solution (1mg/mL) onto a copper grid. The grids were dried by air and then negatively stained with 2% phosphotungstic acid.

9.3. Cell work

9.3.1. In vitro cell culture

Human pancreatic carcinoma AsPC-1 cells were cultured in T25 cell culture flask with 5 % CO_2 at 37 °C. The culture medium was composed of RPMI1640 medium (Thermo Fisher Scientific, Australia) supplemented with 10% fetal bovine serum (Bovogen Biologicals, Australia), 100 U/mL penicillin (Sigma-aldrich, Australia), 100 µg/mL streptomycin (Sigma-aldrich, Australia) and 1× GlutaMAX^{TM} (Gibco, Thermo Fisher Scientific, Australia). After the cells reached confluence, the cells were washed with phosphate buffered saline (PBS) and detached by trypsin/EDTA treatment (Sigma-aldrich, Australia). The cells were collected, centrifuged and resuspended in the culture medium for the further experiments.

9.3.2. Cytotoxicity Analysis (SRB assay) for PPV-b-PEGMA micelles

AsPC-1 suspension was seeded in 96-well cell culture plates at a density of 4.000 cells per well and cultured with 100 µL cell culture medium at 37 °C for 1 day. The micelles were sterilised by passing through a sterile 0.45 µm membrane and serially diluted with sterile MilliQ water. Then the micelles were added into the plate at 100 µL per well along with 100 µL 2× concentrated cell culture medium. The cells were incubated with the micelles for 3 days and analyzed with a Sulforhodamine B Colorimetric Assay (SRB Assay). Cells were then fixed with 10% w/v cold trichloroacetic acid (Sigma-aldrich, Australia) and incubated at 4 °C for 30 min, and then washed five times with water and allowed to dry in the air for 2 h. TCA-fixed cells were stained for 20 min with 0.4% (w/v) SRB (Sigma-aldrich,

Australia) dissolved in 1% acetic acid. SRB was removed and rinsed five times with 1% acetic acid to remove unbounded dye. Then the cultures were air-dried until no conspicuous moisture was visible. The bound dye was solubilized with 200 µL 10mM Tris buffer. The absorbance at 490 nm of each well was measured using a Benchmark Microplate Reader (Bio-Rad). Sterile MilliQ water was used instead of micelle solution as a control. All cytotoxicity data are reported as mean ± standard deviation (n = 4).

9.3.3. Cytotoxicity Analysis (WST-1 assay) for PPV-b-P(HPMA), PPV-b-P(HEA) and PPV-b-PEGMA encapsulated with either curcumin or doxorubicin

The cell viability of these samples was measured using a WST-1 assay (Abam, Australia). AsPC-1 suspension was seeded in 96-well cell culture plates at a density of 4.000 cells per well and cultured with 100 µL cell culture medium at 37 °C for 1 day. The micelles were sterilised by passing through a sterile 0.45 µm membrane and serially diluted with sterile MilliQ water. Then the micelles were added into the plate at 100 µL per well along with 100 µL 2× concentrated cell culture medium. After incubation for 3 days with micelles, 10 µL WST-1 per well was added into the cell culture medium. The plates were then incubated for an additional 2 hours at 37 °C. After incubation, 100 µL of solution was taken out in a new 96-well plate and the absorbance of the samples against the background control on a Benchmark Microplate Reader (Bio-Rad) was obtained at a wavelength of 440 nm with a reference wavelength of 650 nm. Sterile MilliQ water was used instead of micelle solution as a control. All cytotoxicity data are reported as mean ± standard deviation (n = 4).

9.3.4. Micellar internalization observed with laser scanning confocal microscopy (LSCM)

AsPC-1 cells were seeded in 35 mm Fluoro-dishes (0.5×10^5 cells per dish) and incubated for 3 days at 37 °C and 5 % CO_2. The micelles were sterilised by passing through a sterile 0.45 μm membrane and loaded to the cells at a concentration of 100 μg/mL. After incubation for 2 h and 18 h, the cells were washed with Hanks' balanced salt solution (HBSS) thrice and stained with 100 nM LysoTracker Red DND-99 (Thermo Fisher Scientific, Australia) for 5 min. After rinsed with HBSS once, the cells were mounted in 1 mL HBSS and observed under a LSM780 laser scanning confocal microscope (Carl Zeiss). An incubation chamber was equipped on the LSM780 to provide the cells with an environment of 5 % CO_2 and 37 °C. The observation used a 100 × oil lense (1.4 N.A.), a Diode 405-30 and an argon lasers. ZEN2012 software (Zeiss) was used for image acquisition and processing.

9.3.5. Time lapse observation with laser scanning confocal microscopy

AsPC-1 cells were seeded in a 35 mm Fluoro-dishes (0.5×10^5 cells per dish) and incubated overnight. According to the manufacture's instruction, 15 μL of BacMam 2.0 CellLight® Lysosomes-GFP (Thermo Fisher Scientific, Australia) was added to the dish (approximately 30 particles per cell). The cells were then incubated at 37 °C and 5 % CO_2 for another 2 days before treatment with micelles. The micelles were sterilised by passing through a sterile 0.45 μm membrane and loaded to the cells at a concentration of 100 μg/mL. After incubation with micelles for 2h, the cells were washed with Hanks' balanced salt solution (HBSS) thrice and 1 mL phenol-red free RPMI 1640 (supplemented with 10% FBS) was added in the dish. The cells were then observed under a LSM780 laser scanning confocal microscope (Carl Zeiss) equipped with an incubation chamber providing an environment of 37

°C and 5 % CO_2. The observation used a 100 × oil lense (1.4 N.A.), a Diode 405-30 and an argon lasers. The images were taken every 10 min for duration of 16 h. ZEN2012 software (Zeiss) was used for image acquisition and processing.

9.3.6. Cellular uptake of the micelles with fluoro spectrometry

AsPC-1 cells were seeded in 24 well tissue culture plates at a density of 1.5×10^5 cells per well and incubated for 2 days at 37 °C and 5 % CO_2. The micelles were diluted with MilliQ water to 100 µg/mL and sterilised by passing through a sterile 0.45 µm membrane. 500 µL micelles were loaded to each well together with 500 µL 2 × concentrated cell culture medium (3 wells per time point). After incubation for 2 h and 18 h, the cell culture media were collected and freeze-dried. 1 mL dimethylformamide (DMF) was added to the lyophilised powder to dissolve the polymer. The mixture was sonicated for 30 min, shaken for 1h, and filtered through 0.45 µm membranes to remove the precipitations. The fluorescence intensity (FI) was measured with a Cary Eclipse fluorescence spectrophotometer (Agilent). The absorption and emission were 416 and 507 nm, respectively. The reading was zeroed with fresh cell culture medium. The micelles mixed with 2 × medium (1:1) was used as the control. The uptake ratio was calculated with the following equation:

Uptake ratio (%) $= \frac{FI\ (control) - FI(sample)}{FI\ (control)} \times 100\ \%$

LIST OF ABBREVIATIONS

° C	Degrees Celsius
ΔT	Elevated temperature
δ	Chemical shift
h	Plank constant
η	Yield
λ	Wavelength
λ_{max}	Wavelength at maximum absorbance
v	Frequency
φ	Quantum yield
$[\eta]$	Intrinsic viscosity
a	Mark-Houwink constant
AA	Acrylic acid
Ac_2O	Acetic anhydride
Ar	Phenyl
AsPC-1	Human pancreas cell culture
ATR	Attenuated total reflectance
ATRP	Atom transfer radical polymerization
-b-	*Block*
BB	Broad band
$[B]_i$	Initial base concentration
BEH-PPV	Poly[2,5-bis(2-ethylhexyloxy)-*p*-phenylene vinylene]
BPO	Benzoylperoxide
BuOAc	Butyl acetate
c	Speed of light
CB	Chlorobenzene
CBr_4	Carbon tetrabromide
CCl_4	Carbon tetrachloride
CD_2Cl_2	Deuterated dichloromethane
$CDCl_3$	Deuterated chloroform
CH_2Cl_2	Dichloromethane
$CHCl_3$	Chloroform
CI	Chemical impact ionization
C_i	Initiator concentration
C_m	Monomer concentration
CN	Cyano
CN-PPV	Poly[2,5-dicyano-*p*-phenylene vinylene]

CPM-PPV	Poly[2-methoxy-5-carboxypentyloxy)-*p*-phenylene vinylene]
CTA	Chain transfer agent
Cu	Copper
CuAAC	copper-catalyzed alkyne-azide cycloaddition
Cu(I)Br	Copper(I) bromide
CuCN	Copper cyanide
Cur	Curcumin
Đ	Polydispersity index
d	Doublet
D_2O	Deuterium oxide
Da	Dalton
DA	Diels Alder
DCC	N,N′-Dicyclohexylcarbodiimide
DIP MS	Direct insertion probe mass spectrometry
DLS	Dynamic light scattering
DMAc	Dimethylacetamide
DMAP	Dimethylaminopyridine
DMF	Dimethylformamide
DNA	Deoxyribonucleic acid
dn/dc	Specific refractive index increment for a change of solute concentration
Dox	Doxorubicin
DP_n	Degree of polymerization
DP_n^0	Degree of polymerization in an ideal case
DTC	Dithiocarbamate
E	Energy
E_a	Activation energy
E_g	Bandgap
EGMA	Ethylene glycol methyl ether methacrylte
EI	Electron impact ionization
EML	Emissive layer
eq	Equivalents
ESI-MS	Electrospray ionization – mass spectrometry
Et_2O	Diethylether
EtOAc	Ethylacetate
EtOH	Ethanol
eV	Electron volt
FET	Field effect transistor
FT-IR	Fourier transform infrared spectroscopy

GFP	Green fluorescent protein
h	Hour
H_2O	Water
H_2O_2	Hydrogen peroxide
HEA	*2*-hydroxyethyl acrylate
HPMA	*2*-hydroxypropyl methacrylate
HSC_8H_{17}	*n*-Octane thiol
H_2SO_4	Sulfuric acid
HCl	Hydrochloric acid
HOMO	Highest occupied molecular orbital
IC 50	Half maximum inhibitory concentration
I_{mean}	Intensity mean diameter
In	Initiator
[In]	Initiator concentration
J	Coupling constant
K	Mark-Houwink constant
k_{depr}	Deprotonation rate constant
k_i	Initiation rate constant
k_{na}	Base induced rate constant
KOH	Potassium hydroxide
k_p	Propagation rate constant
$k_{selfini}$	Selfinitiation rate constant
k_t	Termination rate constant
k_{tcycl}	Cyclization rate constant
k_{tr}	Transfer rate constant
K*t*BuO	Potassium *tert*-butoxide
L	Leaving group
LHMDS	Lithium hexamethyldisilazide
LUMO	Lowest unoccupied molecular orbital
m	Multiplet
M	Molar
$[M]_i$	Initial monomer concentration
m/z	Mass-to-charge ratio
M^+	Molecular ion
MADIX	Macromolecular design via the interchange of xanthates
MALLS	Multi-angle laser light scattering
MDMO-PPV	Poly[2-methoxy-5-(3,7-dimethyloctyloxy)-*p*-phenylene vinylene]
MEH-PPV	Poly[2-methoxy-5-(2-ethylhexyloxy)-*p*-phenylene vinylene]

Me$_6$TREN	Tris[2-(dimethylamino)ethyl]amine
MeOH	Methanol
MgSO$_4$	Magnesium sulfate
MHKS	Mark-Houwink Sakudara parameters
MHz	MegaHertz
MI	Maleimides
min	Minutes
MIP	Molecular imprinted polymer
MMA	Methyl methacrylate
M_n	Number-average molecular weight
M_n^{app}	Apparent number-average molecular weight
M$_p$	Meltingpoint
MRT	Microreactor Technology
MS	Mass spectrometry
$[M]_t$	Total concentration
M_w^{app}	Apparent weight-average molecular weight
MW, *M* or MWD	Molecular weight
N$_2$	Nitrogen
Na	Sodium
NaCl	Sodium chloride
NaHCO$_3$	Sodium bicarbonate
NaI	Sodium iodine
NaN$_3$	Sodium azide
NaOH	Sodium hydroxide
NaSMe	Sodium thiomethoxide
Na$_2$SO$_3$	Sodium sulfite
Na*t*BuO	Sodium *tert*-butoxide
NBE	Norbornene
NBS	N-bromosuccinimide
N_{mean}	Number mean diameter
NMP	Nitroxide mediated polymerization
NMR	Nuclear magnetic resonance
NR	Nile Red
OLED	Organic light emitting diode
OPV	Organic photovoltaic
P	Polarizer group
p-	*Para*
PBS	Phosphate buffer solution
p-CH$_2$O	*Para*-formaldehyde

P*t*BuA	Poly(*tert*-butyl acrylate)
PAA	Poly(acrylic acid)
PAR	Poly(arylene vinylene)
PEG	Poly(ethylene glycol)
PMA	Poly(methyl acrylate)
PMDETA	N,N,N',N'',N''-pentamethyldiethylenetriamine
PMMA	Poly(methyl methacrylate)
ppm	Parts per million
PPV	Poly(*p*-phenylene vinylene)
p-QM	*Para*-quinodimethane
PS	Polystyrene
q	Quadruplet
RAFT	Reversible addition-fragmentation radical polymerization
RI	Refractive index
RDRP	Reversible deactivation radical polymerization
ROMP	Ring opening metathesis polymerization
RT	Room temperature
s	Singulet
sec	Seconds
SEC	Size exclusion chromatography
sec-BuOH	*Sec*-butanol
SET-LRP	Single electron transfer – living radical polymerization
SiO$_2$	Silicon dioxide (Silica)
SRB	Sulforhodamine B
t	Triplet
T	Temperature
*t*BuA	*Tert*-butyl acrylate
TCE	Tetracyanoethylene
TEM	Transmission electron microscopy
TEMPO	2,2,6,6-tetramethylpiperidin-1-oxyl
TeO$_2$	Tellurium dioxide
TFA	Trifluoroacetic acid
THF	Tetrahydrofuran
THT	Tetrahydrothiophene
TLC	Thin layer chromatography
TMS	Tetramethylsilane
TosCl	*p*-Toluenesulfonyl chloride
UV	Ultraviolet
UV-Vis	Ultraviolet-visible

PUBLICATIONS AND PERSONAL CONTRIBUTION

PUBLICATIONS

PUBLICATIONS

N. Zaquen, B. Wenn, K. Ranieri, J. Vandenbergh, T. Junkers, *Facile Design of Biodegradable Poly(β-Thioester)s with Tunable Structure and Functionality*, *J. Pol. Science Part A: Pol. Chem*. **2014**, *52*, 178-187.

- Article writing

- Synthesis of linear poly(β-thioesters), characterization and analysis

- End-group Functionalization and ESI-MS studies: Kayte Ranieri

- Synthesis via RAFT polymerization: Benjamin Wenn

- Not presented in this thesis

N. Zaquen, J. Vandenbergh, L. Lutsen, D. Vanderzande, T. Junkers, *Synthesis of Well-defined (MDMO)-PPV Containing (tri)Block-Copolymers using Controlled Radical PPV Precursor Routes, Atom Transfer Radical Polymerization and Click Chemistry*, *Polymers* **2015**, *7*, 418-452.

- Article writing

- All synthetic work, characterization and analysis

N. Zaquen, E. Baeten, J. Vandenbergh, L. Lutsen, D. Vanderzande, T. Junkers, *Continuous Synthesis and Thermal Elimination of Sulfinyl-Route Poly(p-Phenylene*

Vinylene) in Consecutive Flow Reactors, Chem. Eng. Technol. **2015**, *38*, 1749-1757.

- Article writing
- All synthetic work, characterization and analysis

N. Zaquen, J. Vandenbergh, D. D'Hooge, M-F. Reyniers, P. Van Steenberge, G. Marin, L. Lutsen, D. Vanderzande, T. Junkers, *Improved Mechanistic Insights into Radical Sulfinyl Precursor (MDMO)-PPV Synthesis by Combining Microflow Technology and Computer Simulations*, *Macromolecules* **2015**, *48,* 8294-8306.

- Article writing
- All synthetic work, characterization and analysis
- All modeling work in cooperation with Ghent University

N. Zaquen, J. Vandenbergh, L. Lutsen, D. Vanderzande, T. Junkers, *Controlled / Living Polymerization towards Functional Poly(p-Phenylene Vinylene) Materials, Polym. Chem* **2016**, *7*, 1355-1367.

- Article writing

M. Peters, N. Zaquen, L. D'Olieslaeger, H. Bové, D. Vanderzande, N. Hellings, T. Junkers, A. Ethirajan, *PPV Based Conjugated Polymer Nanoparticles as a Versatile Bioimaging Probe: A Closer Look at the Inherent Optical Properties and Nanoparticle-Cell Interactions*, *Biomacromolecules* **2016**, in press.

- Synthesis, characterization and analysis of PPV materials
- Not presented in this thesis

N. Zaquen, L. Lutsen, D. Vanderzande, T. Junkers, *Modifiable Poly(p-Phenylene Vinylene) Copolymers Towards Functional Conjugated Materials, Polym. Chem*. **2016**, in press.

- Article writing
- All synthetic work, characterization and analysis

N. Zaquen, H. Lu, T. Chang, R. Mamdooh L. Lutsen, D. Vanderzande, M. Stenzel, T. Junkers, *Precision Design of Highly Fluorescent Amphiphilic Poly(p-Phenylene Vinylene) Micelles as a Versatile Theranostics Probe*, *Chem. Sci.* **2016**, submitted.

- Article writing
- All synthetic work, characterization and analysis
- All cell work in collabroration with UNSW (H. Lu and M. Mamdooh)
- All TEM in collaboration with UNSW (T. Chang)

N. Zaquen, H. Lu, L. Lutsen, D. Vanderzande, M. Stenzel, T. Junkers*, Patent*, **2016**, submitted.

- All synthetic work, characterization and analysis
- In collaboration with UNSW

CONFERENCES: oral presentations

N. Zaquen, J. Vandenbergh, T. Junkers, *Kinetic Modelling on Radical PPV Polymerizations based on Microreaction Molecular Weight*, Koninklijke Nederlandse Chemische Vereniging (KNCV) April 2014, Eindhoven, Netherlands.

N. Zaquen, J. Vandenbergh, L. Lutsen, D. Vanderzande, T. Junkers, *Precision Design of Highly Fluorescent Poly(Phenylene Vinylene) Block Copolymers from Batch and Microflow Synthesis,* 35 Australian Polymer Symposium (APS), July 2015, Gold Coast, Australia. *** *Best Presentation Award* ***

N. Zaquen, H. Lu, L. Lutsen, D. Vanderzande, M. Stenzel, T. Junkers, *Precision Design of Highly Fluorescent Poly(Phenylene Vinylene) Block Copolymers from Batch and Microflow Synthesis*, Belgian Polymer Group (BPG) annual meeting, May 2016, Hasselt, Belgium.

CONFERENCES: poster presentations

N. Zaquen, J. Vandenberg, L. Lutsen, D. Vanderzande, T. Junkers, *Controlled Synthesis of (MDMO)-PPV and Block Copolymers Obtained Therefrom*, Belgium German (BeGe) Macromolecular meeting, December 2012, Houffalize, Belgium.

N. Zaquen, J. Vandenberg, L. Lutsen, D. Vanderzande, T. Junkers, *Controlled Synthesis of Block Copolymers by Incorporating Semiconductive Segment Chains*, Belgian Polymer Group (BPG) annual meeting, May 2013, Houffalize, Belgium.

N. Zaquen, I. Cosemans, J. Vandenberg, L. Lutsen, D. Vanderzande, T. Junkers, *Controlled Synthesis of PPV via the Anionic and Radical Route and Block Copolymers Obtained Therefrom*, Precision Polymer Materials (P2M), August 2013, Ghent, Belgium.

N. Zaquen, J. Vandenbergh, D. D'Hooge, M-F. Reyniers, P. Van Steenberge, G. Marin, L. Lutsen, D. Vanderzande, T. Junkers, *Kinetic Study on the Radical PPV Polymerization using the Sulfinyl Precursor Route*, IAP P7/05 FS2, September 2013, Ghent, Belgium.

N. Zaquen, L. Lutsen, D. Vanderzande, T. Junkers, *Synthesis of Well-defined PPV Containing (tri)Block Copolymers*, Koninklijke Vlaamse Chemische Vereniging (KVCV), ChemCYS (Chemistry Conference for Young Scientists), February 2014, Blankenberge, Belgium.

N. Zaquen, J. Vamdembergh, L. Lutsen, D. Vanderzande, T. Junkers, *Synthesis of functionalized PPV copolymers for use in Boimedical Applications*, Belgian Polymer Group (BPG) annual meeting, May 2014, Ghent, Belgium.

N. Zaquen, J. Vandenbergh, D.R. D'Hooge, M-F. Reyniers, P.H.M. Van Steenberge, G.B. Marin, L. Lutsen, D. Vanderzande, T. Junkers, *Improved insights on the kinetics of the radical sulfinyl PPV polymerization*, IAP P7/05 FS2, September 2014, Louvan-la-Neuve, Belgium. *** ***Best Poster Award*** ***

N. Zaquen, J. Vandenbergh, D.R. D'Hooge, M-F. Reyniers, P.H.M. Van Steenberge, G.B. Marin, L. Lutsen, D. Vanderzande, T. Junkers, *Improved insights on the*

kinetics of the radical sulfinyl PPV polymerization, Flow Master Class, September 2014, Hasselt, Belgium.

N. Zaquen, J. Vandenbergh, L. Lutsen, D. Vanderzande, T. Junkers, *Precision design of highly fluorescent poly(phenylene vinylene) block copolymers from batch and microflow synthesis*, Belgian Polymer Group (BPG) annual meeting, May 2015, Houffalize, Belgium.

N. Zaquen, L. Lutsen, D. Vanderzande, T. Junkers, *Precision Design of Highly Fluorescent Poly(p-Phenyelen Vinylene) Materials from Micro Flow Synthesis,* Flow Master Class, January 2016, Hasselt, Belgium

DANKWOORD

Daar zijn we dan, 4 jaar verder en aan het einde van mijn doctoraat. Achteraf is het eigenlijk wel snel gegaan allemaal en voelt het vreemd om dit nu af te sluiten. Natuurlijk zijn de afgelopen jaren gepaard gegaan met ups en downs, maar gelukkig waren er maar weinig downs, mede dankzij de samenwerking en vele mensen die ik heb leren kennen. Daarom wil ik dit deel van de thesis toewijden aan het bedanken van een aantal mensen die zowel professioneel, maar zeker ook persoonlijk hebben bijgedragen aan de succesvolle afronding van mijn doctoraat. Natuurlijk wil ik niemand vergeten, maar dat zal vast wel gaan gebeuren, dus voor het geval dat: bedankt allemaal ☺

Allereerst zou ik mijn promotor, Thomas, willen bedanken. Super bedankt om mij niet alleen de kans te geven om hier te mogen doctoreren, maar ook voor je vertrouwen en motivatie door de jaren heen. Dankzij jou heb ik veel geweldige ervaringen in zowel binnen- als buitenland kunnen opdoen, die mij hebben gemaakt tot de persoon die ik nu ben. Bedankt voor alles! Mijn copromotor, Dirk, zou ik uiteraard ook willen bedanken. Onze eerste echte kennismaking was tijdens een congres (BPG) en daar werd ik toch wel verrast door je sociale karakter. Daarnaast hebben onze vele wandelgang-praatjes mij zeer veel geholpen in mijn onderzoek en daar wil ik je voor bedanken. Wouter, ook jou mag ik zeker niet vergeten toe te voegen aan dit lijstje. Ook al hadden we geen gezamenlijke projecten, ik heb toch vaker gebruik gemaakt van je kennis over geconjugeerde systemen, bedankt daarvoor! En natuurlijk niet te vergeten, alle gezellige praatjes tijdens de groepsuitjes. Laurence, thank you very much for all your help and input

over the last years, especially your knowledge when filing the patent was highly appreciated. Dagmar, bedankt voor de fijne week die ik heb mogen doorbrengen in jouw groep en de kennis die ik daar heb opgedaan. Jasper, bij toeval is Thomas met jou in contact gekomen, maar ik ben zeer blij met onze huidige samenwerking en ik kijk uit naar de voortzetting van onze gezamenlijke projecten. Last but not least, Martina, thank you for the 3 months I spend in your lab. It must not have been easy to accept a student without a biological background. I learned a lot and I am looking forward to the continuation of our collaboration.

Dit alles was niet mogelijk geweest zonder financiële steun, want 4 jaar onderzoek doen kost aardig wat geld. Daarom wil ik het IWT (Agentschap voor Innovatie door Wetenschap en Technologie) graag bedanken voor de financiering van mijn doctoraat. Het FWO (Fonds Wetenschappelijk Onderzoek) wil ik graag bedanken om mij de mogelijkheid te geven om gedurende 3 maanden naar Australië te gaan.

Voor al mijn collega's, zowel de 'nieuwe' als de 'oude', bedankt voor de fijne tijd in de labzaal. Ik ben altijd met plezier naar het werk gegaan en heb me er altijd thuis gevoeld. Joke (bedankt voor al je hulp op de labzaal, zeker in het begin van mijn doctoraat en de gezellige vrijdag middag biertjes), Jurgen ("zuurkastbuddy" die 24/7 naar mijn gezeur wilde luisteren ☺ en natuurlijk je hulp bij mijn FWO aanvraag, super bedankt!), Benjamin (the ultimate prank-master, I will never forget where my desk has been……), Stephan (de rustige Hollander die er altijd was als ik je nodig had), Evelien (talloze 'onnozele' gezellige kletsmomenten op het grote bureau totdat iedereen er gek van werd), Joachim (my krav maga partner, who's ass I can kick if I want to ☺), Joris (oh mijn god hoeveel projecten

hebben wij op een gegeven moment samen gehad, maar wel iedere keer gezellig, en vergeet de GPC niet ☺), Rebekka (geklets tot Tien er gek van werd), Svitlana (running budy, thanks for keeping me motivated), Ilona (Thanks for always being there for me and all the great moments we had either in Belgium, Denmark or Australia ☺)

Brecht, Yasmine, Jeroen B., Dries, Sanne, Monica, Roald, Mathias, Ruben, Luk, Erika, Martijn, Geert, Gijs, Jorne, Nok, Tien, Wouter, Pieter en Jeroen V. veel succes allemaal, zeker voor degene die nog maar net beginnen. De studenten die ik heb mogen begeleiden: Annelies, Kirsten, Steven, Christopher en Soren, bedankt voor jullie harde werk. Natuurlijk mag de oude 'garde' hier niet aan ontbreken, Inge (gelukkig hebben we onze gezellige kletsmomenten voortgezet ☺), Wouter V. (succes met jullie huisje), Tom (party beest, ik kom je ook overal tegen), Rafael (ga je de volgende in de rij zijn ☺).

Gunter en Koen, dank je wel voor het opnemen mijn vele NMRs. Gunter, een extra bedankje voor je hulp bij al mijn vragen. Huguette, bedankt voor je hulp bij de vele UV-Vis, FT-IR en fluorescentie metingen. Hilde, Gène, Iris en Rita van didactiek, ook jullie wil ik bedanken voor het lenen van materiaal en de hulp bij het geven van de labo's.

Next I would like to thank all the people I was able to collaborate with. Starting with the people from CAMD, a big thanks to all your help and measurements performed and off course the fun times we had after work ☺ A special thanks to Hongxu, I could not have finished the project without your help. Paul from UGhent,

thank you for your help during my stay in your group. I enjoyed our lunch breaks and the funny places we visited.

Tenslotte zou ik graag mijn ouders willen bedanken voor alle steun en kansen die ze me gedurende de afgelopen jaren hebben gegeven. Zonder jullie zou ik dit nooit gedaan hebben. Sabrina 'zussie' , bedankt voor al je steun. Ik kon altijd met alles bij je terecht en dat heeft me zeker door de soms moeilijke tijden geholpen.

DANK JE WEL ALLEMAAL!